THE UNFOLDED PROTEIN RESPONSE REGULATES HEPATOCELLULAR INJURY DURING THE PATHOGENESIS OF NONALCOHOLIC STEATOHEPATITIS

Jeffrey Allen Willy

Submitted to the faculty of the University Graduate School
in partial fulfillment of the requirements
for the degree
Doctor of Philosophy
in the Department of Biochemistry and Molecular Biology,
Indiana University

August 2016

Accepted by the Graduate Faculty, Indiana University, in partial fulfillment of the requirements for the degree of Doctor of Philosophy.

_____

Ronald C. Wek, Ph.D., Chair

_____

James L. Stevens, Ph.D.

Doctoral Committee

_____

Howard C. Masuoka, M.D., Ph.D.

June 17, 2016

_____

Lawrence A. Quilliam, Ph.D.

_____

Jeffrey S. Elmendorf, Ph.D.

_____

Sarath C. Janga, Ph.D.

ACKNOWLEDGEMENTS

I would collectively like to thank the entire faculty and staff of the Biochemistry and Molecular Biology Department at IUSM for their support and conversations. I would like to individually thank my thesis committee members for the time and dedication they have devoted to my scientific growth: Dr. Lawrence Quilliam, Dr. Jeffrey Elmendorf, and Dr. Howard Masuoka. I am especially grateful to Dr. Ronald Wek for his invaluable advice and encouragement during my graduate career, as I could not have asked for a more supportive and caring mentor. Additionally, I would like to thank the current and past members of the Wek lab for their continued support and conversations. Achieving this career milestone would not be feasible without the support of the LGRAD (Lilly Graduate Research Advanced Degrees) program at Eli Lilly, and especially the mentorship of Dr. James Stevens, who continually pushed me to grow from an excited young scientist with a lot of ideas to an independent research scientist with the ability to ask focused questions. I would also like to extend my gratitude to the excellent scientists, mentors, and colleagues that I have and the experience of interacting with at Eli Lilly, including Tom Baker, George Searfoss, Briana Paisley, and Dr. Anja Stauber.

Jeffrey Allen Willy

THE UNFOLDED PROTEIN RESPONSE REGULATES HEPATOCELLULAR INJURY DURING THE PATHOGENESIS OF NONALCOHOLIC STEATOHEPATITIS

Non-alcoholic steatohepatitis (NASH), which is characterized by the induction of hepatocellular death and inflammation, is associated with the activation of cellular stress pathways such as the Unfolded Protein Response (UPR), an adaptive response to disruptions in endoplasmic reticulum (ER) homeostasis. Because the role of the UPR in the progression of liver disease is not well understood, we established an in vitro model to evaluate the role of the UPR in NASH and translated results to clarify disease progression in human liver biopsy samples.

Treating HepG2 cells and primary human hepatocytes with saturated, but not unsaturated free fatty acids (FFAs), at physiologic concentrations induced hepatotoxicity by inhibiting autophagic flux. Saturated FFA treatment activated the UPR, including the transcription factors CHOP (GADD153/DDIT3) and NF-κB, leading to increased expression and secretion of cytokines such as TNFα and IL-8 that contributed to hepatic cell death and inflammation. Depletion of either CHOP or the RELA subunit of NF-κB in hepatocytes alleviated autophagy and cytokine secretion, resulting in enhanced cell viability and lowered inflammatory responses during exposure to saturated FFAs.

We carried out next generation sequencing on cells deleted for either CHOP or RELA and identified IBTKα as a novel UPR member directly regulated by CHOP and NF-κB. In response to saturated FFAs, loss of IBTKα increased cell survival through lowered phagophore formation and reduced cytokine secretion. We also identified binding partners of IBTKα by immunoprecipitation and LC/MS, indicating that that IBTKα

is part of a protein complex which functions at ER exit sites to facilitate initiation of autophagy and protein secretion. Furthermore, we discovered that CHOP and RELA coordinately regulate proteasome activity through NRF2 as an adaptive response to an inhibition of autophagic flux following palmitate exposure. To validate our model, we utilized human liver biopsy samples and demonstrated up-regulation of the UPR coincident with accumulation of autophagy markers, as well as secretion of cytokines IL-8 and TNFα in serum of NASH patients. Our study provides a mechanistic understanding of the roles of the UPR and autophagy in regulating saturated FFA-induced hepatotoxicity at the cellular level.

Ronald C. Wek, Ph.D., Chair

TABLE OF CONTENTS

APPENDICES

LIST OF TABLES

LIST OF FIGURES

CHAPTER 1. INTRODUCTION

CHAPTER 3. RESULTS: CHOP links ER stress to NF-κB activation

CHAPTER 4. RESULTS: IBTKα facilitates phagophore initiation and protein secretion

CHAPTER 5. RESULTS: CHOP and NF-κB activate coordinately regulate proteasome activity through NRF2

CHAPTER 6. DISCUSSION

ABBREVIATIONS

3-MA	3-Methyladenine
ALT	Alanine Aminotransferase
AST	Aspartate Transaminase
ATF	Activating Transcription Factor
ATG	Autophagy-Related Genes
BCL2	B-Cell Lymphoma 2
BiP/GRP78	Binding immunoglobulin Protein
BMI	Body Mass Index
BSA	Bovine Serum Albumin
BTB/POZ	Broad-complex Tramtrack and Bric-abrac/Pox Virus and Zinc Finger
ChIP	Chromatin Immunoprecipitation
CHOP	CCAAT/enhancer-binding protein Homologous Protein
CM	Conditioned Media
COPII	Coat Protein II
CUL3	Cullin 3
CXCL	Chemokine Motif Ligand
DNA	Deoxyribonucleic Acid
DR5	Death Receptor 5
eIF	eukaryotic Initiation Factor
ELISA	Enzyme-Linked Immunosorbent Assay
ER	Endoplasmic Reticulum
ERAD	Endoplasmic Reticulum Associated Degradation
ERES	Endoplasmic Reticulum Exit Sites
FFA	Free Fatty Acid
FIP200	Focal Adhesion Kinase-Family Interacting Protein of 200 kD

GADD34	Growth Arrest and DNA Damage-inducible protein
GAPDH	Glyceraldehyd 3-Posphate Dehydrogenase
GCLC	Glutamate-Cysteine Ligase Catalytic subunit
GCN2	General Control Nonderepressible 2
GDP	Guanine Diphosphate
GFP	Green Fluorescent Protein
GM-CSF	Granulocyte Macrophage Colony-Stimulating Factor
GO	Gene Ontology
GSR	Glutathione Reductase
GTP	Guanine Triphosphate
HbA1c	Glycated Hemoglobin
HCC	Hepatocellular Carcinoma
HepG2	Human Hepatocellular Carcinoma Cell Line
HMGB1	High Mobility Group Box 1
HPH	Human Primary Hepatocytes
HRI	Heme-Regulated eIF2α Kinase
IBTKα	Inhibitor of Bruton's Tyrosine Kinase alpha
IFNγ	Interferon Gamma
IgG	Immunoglobulin G
IKK	I Kappa B Kinase
IL	Interleukin
IRAK	Interleukin-1 Receptor-Associated Kinase
IRE1α	Inositol Requiring 1 alpha
IκB	Inhibitor of Kappa B
JNK	c-Jun-N-terminal Kinase
kb	kilobase

KC	Keratinocyte Chemoattractant
KEAP1	Kelch-like ECH-Associated Protein 1
KG1	Human Macrophage Cell Line
KO	Knock Out
LAMP	Lysosome-Associated Membrane Protein
LC/MS	Liquid Chromatography-Mass Spectrometry
LC3	Microtubule-Associated Protein Light Chain 3
LC50	Lethal Concentration at which 50% of Cells are Dead
LDH	Lactate Dehydrogenase
MAP	Mitogen-Activated Proteins
MIP-2	Macrophage Inflammatory Protein 2
miR	micro-RNA
MPH	Mouse Primary Hepatocytes
mTOR	Mammalian Target of Rapamycin
NAFLD	Non-alcoholic Fatty Liver Disease
NAS	Non-alcoholic Fatty Liver Disease Activity Score
NASH	Non-alcoholic Steatohepatitis
NFκB	Nuclear Factor κB
NQO1	NAD(P)H Dehydrogenase, Quinone 1
NRF	Nuclear Factor Erythroid-Derived 2-like
p62	62-kD Protein (see SQSTM1)
p65	65-kD Protein (see RELA)
PERK	PKR-like ER kinase or EIF2AK3/PEK
PKR	Protein Kinase RNA-activated
PUMA	p53-Upregulated Modulator of Apoptosis
qPCR	quantitative Polymerase Chain Reaction

RELA	V-Rel Avian Reticuloendotheliosis Viral Oncogene Homolog A
RIDD	Regulated IRE1 Dependent Decay of RNAs
RNA	Ribonucleic Acid
RPH	Rat Primary Hepatocytes
SQSTM1	Sequestosome 1
TChol	Total Cholesterol
TNF-R	Tumor Necrosis Factor-Receptor
TNFα	Tumor Necrosis alpha
TRAF2	Tumor Necrosis Factor Receptor-Associated Factor 2
TSS	Transcriptional Start Site
ULK	Unc-52-like Kinase
uORF	upstream Open Reading Frame
UPR	Unfolded Protein Response
UPS	Ubiquitin-Proteasome System
VPS34	Phosphatidylinositol 3-Kinase, Class 3 (PIK3C3)
WT	Wild Type
XBP1	X-box Binding Protein 1
ZVAD/FMK	Carbobenzoxy-valyl-alanyl-aspartyl-[O-methyl]-fluoromethylketone

CHAPTER 1. INTRODUCTION

1.1 The pathogenesis of nonalcoholic fatty liver disease.

Non-alcoholic fatty liver disease (NAFLD) includes a range of pathologies from simple hepatic steatosis to non-alcoholic steatohepatitis (NASH), which is characterized by fat accumulation in the liver, hepatic inflammation, and injury that can progress to cirrhosis [1, 2] (Fig 1-1). There is a strong correlation between body mass index (BMI) and the prevalence of NAFLD, and higher BMI has been associated with more severe liver disease; thus NAFLD is largely thought to be a result of over nutrition [3, 4]. Within the United States, approximately 1/3 of the population has some form of NAFLD, extending to over 3/4 of obese individuals [5]. Additionally, over half of patients with type 2 diabetes in both the United States and Europe also have some form of NAFLD, suggesting a strong correlation between liver disorders, obesity, and metabolic disease [6].

Although often thought to be relatively benign in the absence of inflammation, the manifestation of hepatic steatosis, or accumulation of fat in the liver, typically coincides with obesity, and excess fat in the adipose tissue has been suggested to lead to cellular dysfunction and the inability to properly store lipids [7]. During obese conditions, adipocytes containing excess fat secrete cytokines such as TNFα, which has been suggested to result in impaired insulin signaling [8]. Insulin resistance is a risk factor for NASH, contributing to excessive lipolysis within adipose tissues liberating free fatty acids (FFA) from triglycerides. Elevated serum FFAs play a key role in the pathogenesis of NASH, and therapies that enhance insulin sensitivity can ameliorate hepatic lipotoxicity, in part, by decreasing plasma FFAs. Saturated FFAs are more strongly implicated in hepatic lipotoxicity and are more potent inducers of hepatocyte death than unsaturated FFA [2, 9, 10]. Like other liver pathologies, inflammation due to cytokine activation and

release of alarmins from stressed and dying cells is considered to be central to disease progression, but the molecular pathways linking FFA lipotoxicity and inflammation in the progression of NASH are not yet well understood [11].

Current diagnosis and prognosis of NAFLD requires a combination of clinical assessment and invasive procedures to asses histopathology of the liver, which are combined into a scoring system referred to as the NAFLD Activity Score (NAS) [12, 13]. The current scoring system involves a combination of key parameters, such as steatosis, lobular inflammation, hepatocellular ballooning, and fibrosis, which are each evaluated on semi-quantitative scales that are integrated into a final NAS score ranging from in severity from 0 to 5. There is an urgent need to develop non-invasive approaches to monitor the progression of NAFLD towards NASH and fibrosis. Although sera-based biomarkers such as cleaved cytokeratin 18, TNFα, IL-8, and miR122 have been associated with NASH, these biomarkers are not accurate predictors of the severity of NASH, and liver biopsies are still relied upon for diagnosing disease progression of NAFLD [14-17].

There are currently no FDA-approved drugs to reverse the hepatotoxicity associated with NASH. Mild cases of NAFLD can normally be managed by lifestyle modifications, which feature caloric restriction and exercise that can reduce both liver enzymes and BMI. However, these lifestyle changes cannot reverse liver fibrosis [18, 19]. As a consequence, severe cases of NASH often require surgical intervention, such as bariatric surgery and even liver transplantation [20]. Importantly, it is not understood why only some NAFLD patients progress to more severe pathologies associated with NASH [21]. In order to improve diagnosis and treatment regimens, a better understanding of both the molecular mechanisms and etiology of pathogenesis of NAFLD/NASH is needed.

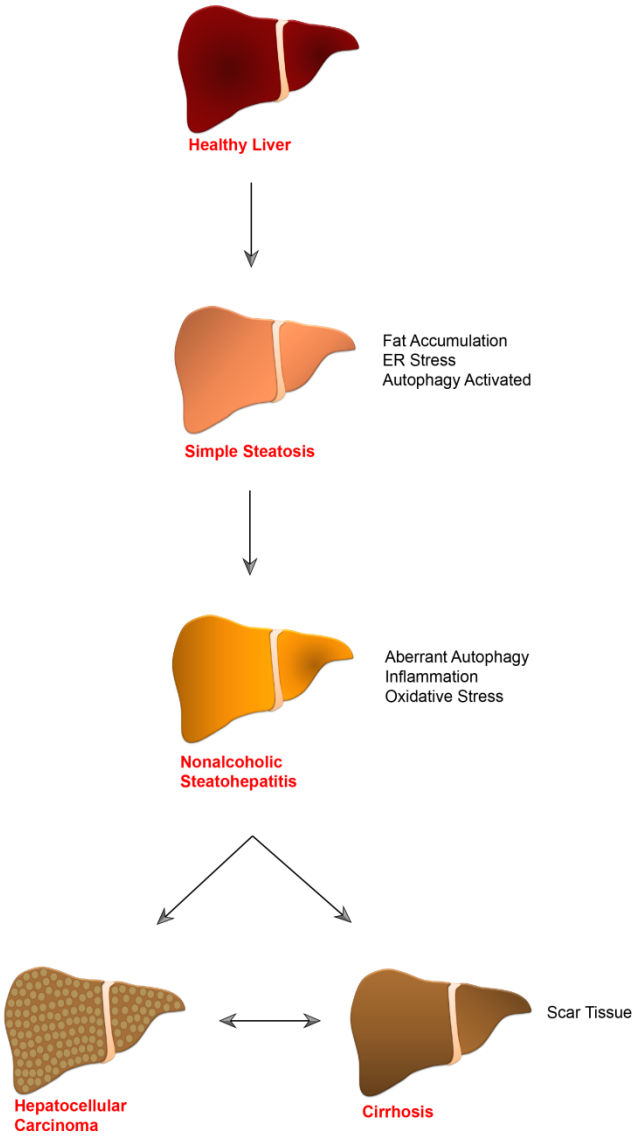

Figure 1-1. Pathogenesis of NAFLD. Nonalcoholic fatty liver disease begins with simple steatosis, or the presence of excessive fat in the liver. NAFLD can progress to nonalcoholic steatohepatitis, in which inflammation and scarring can begin to appear in addition to fat accumulation. Scar tissue can replace the hepatocytes during cirrhosis, and hepatocellular carcinoma can also arise either prior to or in the presence of cirrhotic tissue.

1.2 The Unfolded Protein Response in liver disease.

Recent studies suggest that excess saturated FFAs disrupt endoplasmic reticulum (ER) function, activating the Unfolded Protein Response (UPR) that features transcriptional and translational regulation of genes that serve to restore cell homeostasis [9, 22]. Newly synthesized proteins slated for the secretory pathway enter the ER to be folded and modified prior to transfer to the Golgi, for eventual placement into membranes or secretion. Perturbation of cell homeostasis, such as an excess of unfolded proteins in the ER or alterations in lipid metabolism, results in ER Stress and activation of the UPR.

The UPR is activated through three sensory proteins: Inositol Requiring 1α (IRE1α/ERN1), PKR-like ER kinase or PERK (EIF2AK3/PEK), and Activating Transcription Factor 6 (ATF6), which serve to sense perturbations in the ER [23]. Together these UPR sensors serve to induce gene expression networks to either alleviate stress damage and return the cell to homeostasis or alternatively proceed toward cell death (Fig 1-2). Each of these UPR sensors is a transmembrane protein embedded within the ER. During non-stressed conditions, the luminal portion of each sensory protein is bound to an ER chaperone protein called Binding immunoglobulin Protein (BiP/GRP78/HSPA5). However, upon ER stress, unfolded proteins are thought to titrate BiP from the luminal regulatory domains of UPR sensory proteins, contributing to their activation [24]. An alternative model for regulation of the UPR sensors suggests that unfolded proteins can bind directly to these luminal sequences, leading to sensor activation [25]. The consequent effect of either model is induction of the three branches of the UPR by disruptions of protein folding.

ATF6 is present in two isoforms from separate genes, ATF6α and ATF6β, with ATF6α being the dominant transcriptional activator of the UPR, which we will refer to as simply ATF6. ATF6 is a transmembrane protein that is localized in the ER and can

contains two Golgi localization sequences in its luminal domain normally concealed by BiP [26]. During ER stress, BiP dissociates and ATF6 is transported from the ER to the Golgi, where proteolytic cleavage by site-1 (S1P) and site-2 (S2P) proteases occurs. The 50 kDa N-terminal portion of ATF6 that is positioned in the cytosol is then released from the Golgi and translocated to the nucleus. ATF6 then binds to ER stress response elements (ERSE) with the consensus sequence CCAAT-N9-CCACG located in the promoters of UPR target genes [27]. These target genes function in protein folding and ER-associated degradation (ERAD), which serves to eliminate problematic and unfolded proteins from this organelle via ubiquitination and proteasome-mediated degradation. The remaining C-terminal peptide of ATF6 in the Golgi is thought to be secreted, and may serve as a biomarker for ER stress. While the gene targets of ATF6β are unclear, recent literature has suggested that following cleavage of ATF6β, the N-terminal peptide will translocate to the nucleus and compete with and inhibit the adaptive ER stress response by ATF6α [28].

There are also two gene isoforms of IRE1, designated IRE1α and IRE1β; however, only IRE1α is ubiquitously expressed [29]. The cytosolic portion of IRE1α (herein referred to as IRE1) has serine/threonine kinase and endoribonuclease domains. IRE1 is autophosphorylated following ER stress and BiP dissociation, and consequent IRE1 oligomerization activates the endoribonuclease functions [30, 31]. IRE1 endoribonuclease cleaves cytosolic splicing of X-box Binding Protein 1 *(XBP1*) mRNA, which is then ligated by the RTCB catalytic subunit of tRNA ligase, leading to synthesis of an active XBP1s transcription factor [32, 33]. XBP1 target genes have been shown to be important for the adaptive response involved in remediating ER stress, including enhanced vesicular trafficking, secretion, and protein folding [30]. While XBP1 is thought to be cytoprotective, IRE1 also induces cell death signals independent of *XBP1* splicing, such as the activation of c-Jun N-terminal kinase (JNK) through an interaction with

TRAF2 and the degradation of specific mRNAs, known as regulated IRE1-dependent decay (RIDD) [34, 35]

PERK phosphorylates the α subunit of eIF2 (eIF2α~P), which serves to deliver the aminoacylated initiator to ribosomes during the initiation phase of protein synthesis. The eIF2α~P serves to repress global translation initiation, which decreases the influx of nascent proteins into the ER. Additionally, eIF2α~P leads to preferential translation of key stress response gene transcripts via bypass of inhibitory upstream open reading frames (uORFs) in the 5'-leader of the targeted mRNAs [36]. Preferentially translated genes include *ATF4*, encoding a transcriptional activator that functions to alleviate stress damage [23]. ATF4 also induces transcription of *GADD34 (PPP1R15A)*, involved in feedback dephosphorylation of eIF2α~P, and CHOP (GADD153/DDIT3), a transcription factor that can trigger cell death during chronic stress. Both *GADD34* and *CHOP* are also subject to preferential translation during eIF2α~P through uORFs, which as a consequence tethers expression of these UPR genes to continued ER stress [36].

The three arms of the UPR do not act independently, but rather coordinately regulate transcriptional expression in response to ER stress. For example, ATF6 increases transcription of *XBP1*, resulting in increased *XBP1* mRNA substrate for IRE1α to process into the functional XBP1s transcription factor [37]. In a similar manner, deletion of *PERK* in the liver of mice results in loss of ATF6 cleavage, as well as reduced *XBP1* expression [38]. Furthermore, both ATF4 and ATF6 contribute to the transcriptional expression of *CHOP* in the liver during ER stress [39, 40]. Finally, although many of these transcription factors function as homodimers, they are also observed as heterodimers, such as ATF4-CHOP and ATF6α-XPB1s, allowing for the activation of quality control pathways, such as ERAD, to degrade of misfolded proteins [41-43].

Coordinated activation of the UPR activates biological pathways to expand the ER processing capacity, which as a consequence helps restore protein homeostasis. Key pathways that can assist with protein homeostasis include induction of autophagy, which transports damaged organelles and unfolded proteins to the lysosome for degradation, as well as ERAD to traffic problematic proteins to the proteasomes [43, 44]. Additionally, amino acid transporters and genes important for remediation of oxidative damage are upregulated to protect cells against negative metabolic events [45]. However, the UPR cannot always overcome the detrimental effects of cellular stresses, and continued induction of the UPR by chronic exposure to ER stress can instead activate cell death pathways and enhanced inflammation [46-48].

The UPR is activated in animal models of high fat diet and NASH, as well as liver biopsies from human patients of NAFLD [49, 50]. Because of the role of excess circulating FFAs in lipotoxicity in NAFLD, it has been suggested that FFAs play a role in activation of the UPR during the progression of simple steatosis to NASH [47]. Although the UPR is canonically activated during the accumulation of unfolded proteins, the liver plays a variety of roles in lipid metabolism and processing. Interestingly, both PERK and IRE1α can be activated by saturated FFAs even in the absence of their luminal domains, suggesting a non-canonical role for lipid-mediated activation within the trans-membrane domain of both kinases [51]. Additionally, saturated FFAs do not result in ATF6 cleavage and consequent downstream transcription regulation, indicating a discordant activation of the UPR [52]. While there is a strong correlation between activation of the UPR in progression of NAFLD, the direct role PERK and IRE1α pathways during the pathogenesis of simple steatosis to NASH remains unclear.

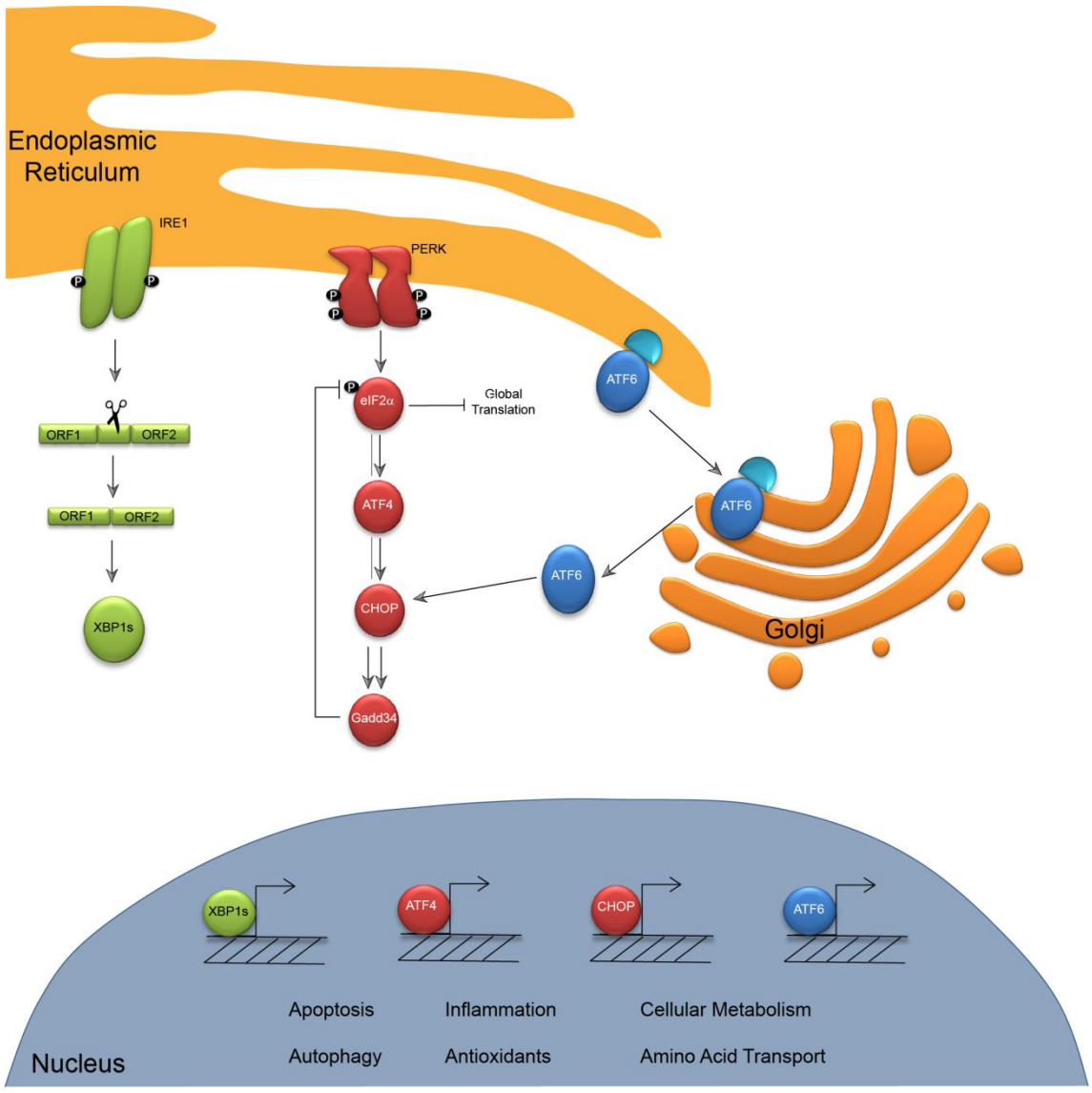

Figure 1-2. The Unfolded Protein Response. ER Stress activates PERK, ATF6, and IRE1 to elicit changes in gene expression. PERK phosphorylation of eIF2α results in a global inhibition of translation coincident with preferential translation of UPR-specific genes, *ATF4* and *CHOP*, which serve to accommodate ER stress and determine cell fate. ATF6 is released from the ER to the Golgi, where it is cleaved, and the N-terminal portion of ATF6 is subsequently translocated to the nucleus to induce gene expression. IRE1 acts as a riboendonuclease that facilitates cytoplasmic splicing of *XBP1* mRNA,

enhancing the synthesis of active XBP1 that increases transcription of UPR target genes. Together, these three branches of the UPR: PERK activation, ATF6 cleavage, and IRE1-directing splicing of XBP1 mRNA- comprise the transcriptional and translational gene expression encompassing the UPR.

1.3 CHOP regulates cell fate decisions.

While the main goal of UPR activation is to restore cell to homeostasis following onset of ER stress, chronic stress can trigger a sustained and heightened UPR that instead results in cell death. This dual nature of the UPR has been referred to as a binary switch [53]. During the initial stages of ER stress, eIF2α~P allows for the inhibition of global translation to conserve energy as well as the preferential translation of ATF4, which is involved in the transcriptional expression of many genes important for cell adaptation and survival, including those serving as amino acid transporters and those contributing as antioxidants [54, 55]. Chronic activation of the UPR will instead result in increasing levels of eIF2α~P over an extended period that will induce high levels of *CHOP* transcriptional expression [56]. *CHOP* mRNA is also preferentially translation by eIF2α~P, and induced expression of this transcription factor plays a major role in cell death upon chronic ER stress. CHOP is suggested to directly or indirectly regulate expression of genes involved in directing cell death during ER stress, including repression of pro-survival gene *BCL2* and activation of pro-death genes, such as *DR5* and *PUMA* [57]. While CHOP targeting of UPR gene transcription is generally thought to facilitate cell death, this can depend on cell type and the nature of the underlying ER stress.

The role that CHOP plays in liver disease during exposure to high levels of saturated FFA is not well understood. Prior studies linked activation of CHOP to cell death, an important pathophysiological feature of NASH and cirrhosis [46, 58]. However,

the notion that CHOP plays a direct role in the progression of NASH is quite controversial in the literature. Evidence arguing against the role of a protective effect of CHOP during the progression of NASH has emerged from studies utilizing whole body *CHOP* knock-out mouse models fed a methionine-choline deficient diet, in which it was demonstrated that the absence of CHOP enhanced liver injury and inflammation. [59]. However, this was coincident with decreased macrophage and T-cell apoptosis due to the absence of *CHOP* in a whole animal, thus making it hard to discern the role of CHOP in the hepatocyte. Interestingly, a different group found that mice with whole body knockout of C/EBPβ, a paralog of CHOP, led to decreased CHOP levels and attenuated inflammation and hepatocellular injury when animals were fed a high fat diet [60]. Because of technical reasons, liver specific CHOP knockout mice have not been created, resulting in controversial results utilizing whole animal knockout mice. Additionally, mouse models of NASH do not fully recapitulate the human disease state, making it increasingly difficult to understand the role of CHOP and inflammation at the level of hepatocyte during the progression of NASH.

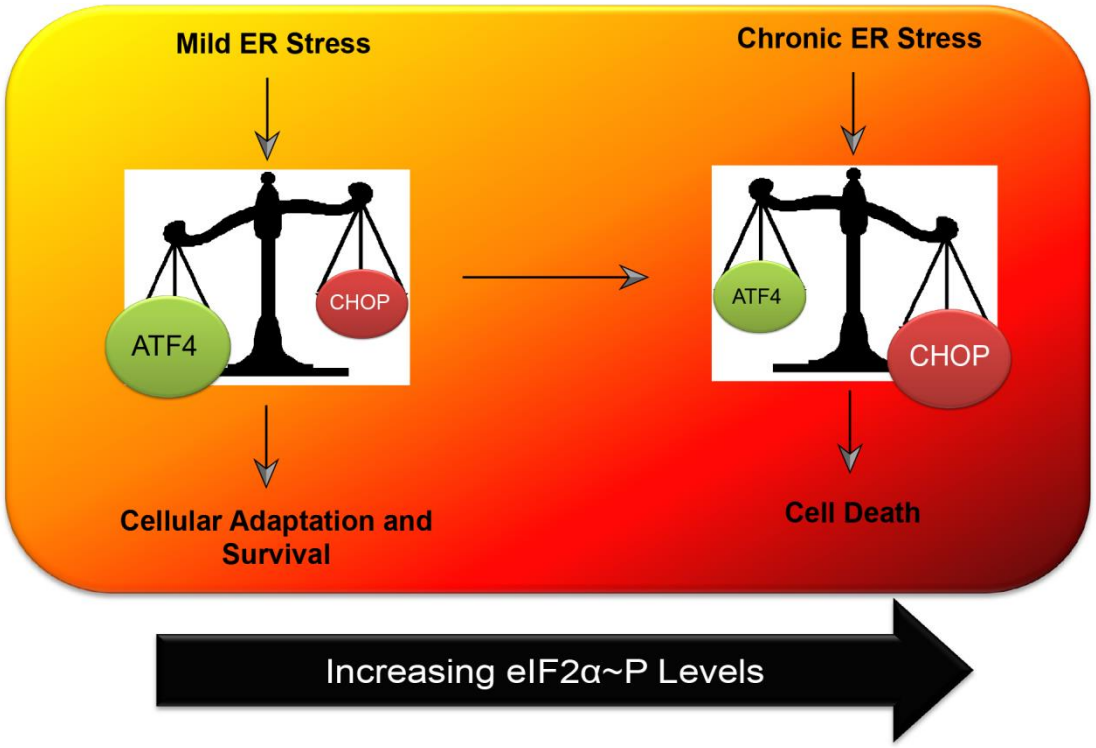

Figure 1-3. Binary switch model. During the early stages of ER stress, eIF2α~P induces the preferential translation of *ATF4*, which then activates the transcriptional expression of genes involved in cell survival. If the cell does not return to homeostasis and eIF2α~P levels become hyperactived in levels and duration, induced transcription factor CHOP will activate the transcription of genes involved in cell death.

1.4 Phosphorylation of eIF2α induces preferential translation of IBTKα

The central dogma of molecular biology features transcriptional expression of genes, followed by mRNA translation into protein. However, mRNA abundance does not necessarily correlate with protein expression, and recent literature has suggested that protein expression is primarily regulated by mechanisms of translational control [61]. A key protein involved in translational control is eIF2. During unstressed conditions, eIF2 is bound to GTP and amionacylated initiator tRNA, which then couples with the 40S ribosomal subunit. This 43S preinitiation complex associates with the 5'- "cap" of mRNAs, and then scans 5' to 3' along the mRNA until it couples the initiator tRNA to the start codon of the transcript. The large 60s ribosomal subunit will then join the initiation complex, allowing for translation elongation to ensue. During translation initiation, eIF2-GTP will be hydrolyzed to eIF2-GDP, and the released eIF2-GDP will be then recycled to the GTP-bound form through the action of a guanine nucleotide exchange factor called eIF2B [36, 62].

During cellular stresses, four different mammalian protein kinases, PERK, GCN2, PKR, and HRI can phosphorylate eIF2α at serine 51 [36, 63]. Once phosphorylated, eIF2α~P will act as an inhibitor for the eIF2-GDP to eIF2-GTP exchange by binding directly to eIF2B. The resulting lowered eIF2-GTP levels trigger a general reduction in translation initiation, coinciding with preferential translation of select mRNA transcripts, such as *ATF4* and *CHOP*. As noted earlier, this preferential translation during eIF2α~P occurs through the actions of uORFs embedded within 5'-leader of the gene transcript [64, 65].

We recently identified the α isoform of inhibitor of Bruton's tyrosine kinase (IBTKα) as being preferentially translated in response to and ER stress [66]. IBTKα contains four uORFs, of which uORF 1 and 2 are inhibitory and act to repress IBTKα protein expression. During ER stress, the inhibitory effects of uORFs 1 and 2 are

overcome and there is enhanced expression of IBTKα protein (Fig 1-4) [66]. While the biological functions of IBTKα are not yet understood, it is noted that IBTKα contains protein-protein interaction domains, including ankyrin repeats and the BTB/POZ domain, which is suggested to enable IBTKα to serve as a substrate adapter for the E3 ubiquitin ligase Cullin 3 [67, 68]. Furthermore, depletion of IBTKα from both mouse embryonic fibroblasts and HepG2 cells results in increased basal levels of cleaved caspase 3/7 without any changes in cell division, suggesting that IBTKα serves an essential role in cell survival; however, the exact mechanism and substrates by which IBTKα regulates cell fate remain yet to be elucidated [66].

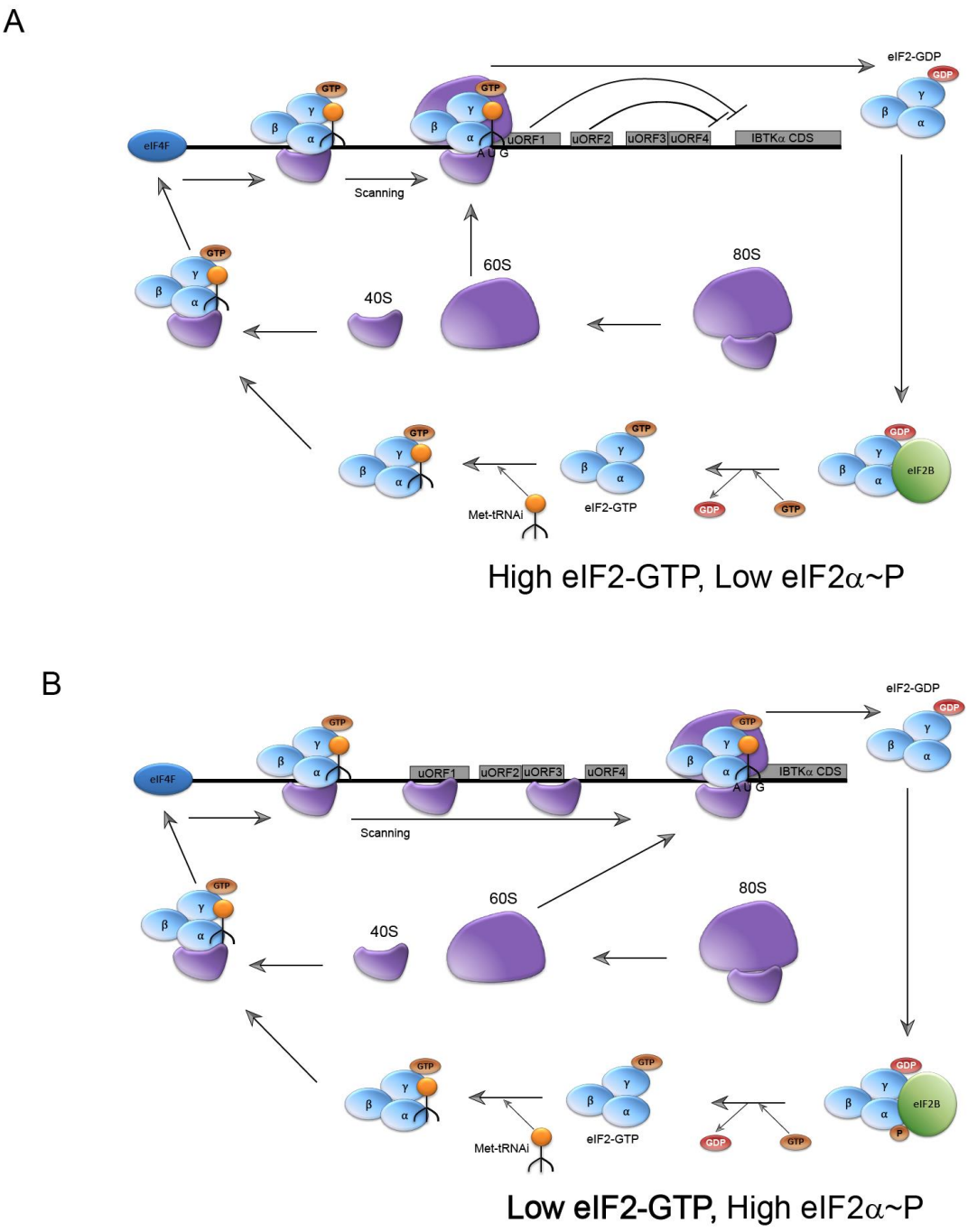

Figure 1-4. Mechanisms of translational control of IBTKα. (A) The 40S small ribosomal subunit couples with eIF2-GTP and initiator tRNA. Once the 43S preinitiation complex is loaded onto the 5'- "cap" containing the eIF4F complex, the ribosome complex scan until an initiation codon, typically an AUG, is recognized. The 60S

ribosomal subunit is recruited, culminating in the formation of the 80S ribosomes that mediates translation elongation. During the process of translation initiation, the GTP bound to eIF2 is hydrolyzed to GDP, and eIF2 must be recycled to the eIF2-GTP through the actions of the guanine exchange factor eIF2B. (A) During non-stressed conditions when eIF2-GTP levels are high, ribosomes will initiate translation at the inhibitory uORF1 and uORF2, preventing translation initiation of the lBTKα coding sequence. (B) During stress and levels of high eIF2α~P, there will be low levels of eIF2-GTP that aids bypass of uORF1 and uORF2. Scanning ribosomes instead initiate translation of the lBTKα coding sequence.

1.5 Mechanisms of inflammation during metabolic disease

During the course of cellular injury, inflammation is a key biological response in which the secretion of factors such as chemokines and cytokines coordinate the repair of damaged tissues [69]. Metabolic diseases, ranging from type 2 diabetes to NAFLD, are chronic disorders and result in a low grade inflammatory state. Increased expression of pro-inflammatory cytokine tumor necrosis factor alpha (TNFα) stemming from the adipocytes during both obesity and type 2 diabetes is a key feature of insulin resistance [8]. In addition to TNFα, a number of other cytokines, such as interleukins 6 and 1β (IL-6, IL-1β), are also induced during metabolic disorders such as obesity. These cytokines can bind to receptors on peripheral cells and activate key pathways: Nuclear Factor κB (NF-κB) and c-Jun N-terminal Kinase (JNK), acting as a cascade to further increase inflammation [70-72].

Early studies focused on adipose tissue, but it has been shown that an increasing number of cell types play a pro-inflammatory role during the progression of metabolic disease [47, 73, 74]. For example, Kupffer cells, or resident macrophages, which represent nearly 10% of the liver, were shown to have enhanced activation and

release of cytokines such as TNFα, IL-12, IL-18, and IFNγ during the progression of NAFLD [75-77]. However, it is unclear whether Kupffer cell activation is mediated directly by excess FFAs or by a secondary effect due to circulating of alarmins, also called damage associated molecular patterns, from injured hepatocytes during NASH [11].

Induction of inflammation is tightly regulated with the UPR during the progression of metabolic disease [22, 47, 78]. This is not entirely surprising, as both pathways are adaptive in nature. The UPR is initially activated to promote enhanced ERAD of mis-folded proteins, clearance of damaged organelles, and also plays an important role directing anti-oxidant effects against toxic xenobiotics and FFAs [79, 80]. Similarly, the immune system is activated to promote wound healing and rid the body of external threats [81]. However, during prolonged activation, both the UPR and inflammation can become adverse to the host cells resulting in tissue damage [8, 9]. As noted above, the UPR can function in conjunction with key pro-inflammatory pathways, such as those directed by JNK and NF-κB [35, 82].

The canonical JNK signal transduction pathway consists of induction of the activator protein-1 (AP-1) transcription factor via a cascade of protein kinases known as mitogen-activated proteins (MAPs). Environmental stresses, such as cytokines binding to cell surface receptors, activate the cascade of MAP kinases, eventually leading to nuclear localization of AP-1 and transcriptional expression of pro-apoptotic genes such as TNFα [83-85]. It has been shown that the UPR activates the JNK pathway through IRE1α association with TRAF2, an adapter protein for JNK. Hence, IRE1α is thought to be a critical mediator determining the balance between pro-survival, through downstream effects of XBP1s, and cell death responses, by activation of JNK and consequent TNFα expression (Fig 1-5) [35].

The canonical NF-κB signal transduction pathway consists of two transcription factors which dimerize, p50 and p65 (RELA), that are typically bound to the repressor

inhibitory kappa B alpha (IκBα) in the cytoplasm. When cytokines bind to specific cell surface receptors, such as tumor necrosis factor-receptor (TNF-R), the IKK complex will target IκBα for proteasomal degradation, allowing for NF-κB nuclear localization and transcriptional activation of target genes (Fig 1-5) [86-88]. It has been shown that the protein expression of IκBα is repressed by eIF2α~P during ER stress, allowing for nuclear localization of the p50/p65 dimer and consequent NF-κB pro-inflammatory response [82]. While NF-κB has been shown to be activated by saturated FFAs, it is unclear whether this regulatory scheme is due to canonical translational repression of IκBα [89]. Additionally, NF-κB activation is considered pro-survival for circulating B and T lymphotyctes [90], but the biological consequence of chronic NF-κB activation in hepatocytes has not yet been characterized during the progression of NAFLD.

NAFLD is a condition in which the liver must adapt to excess nutrient intake, and when unresolved this adaptation becomes a chronic metabolic disorder with the potential for cellular injury. It is known that both ER stress and inflammation are significant features during the progression of metabolic diseases such as NAFLD. However, how ER stress and mediators such as NF-κB, along with secreted factors such as TNFα, contribute to lipotoxicity, liver injury, inflammation and progression from simple steatosis to NASH are not yet resolved [22].

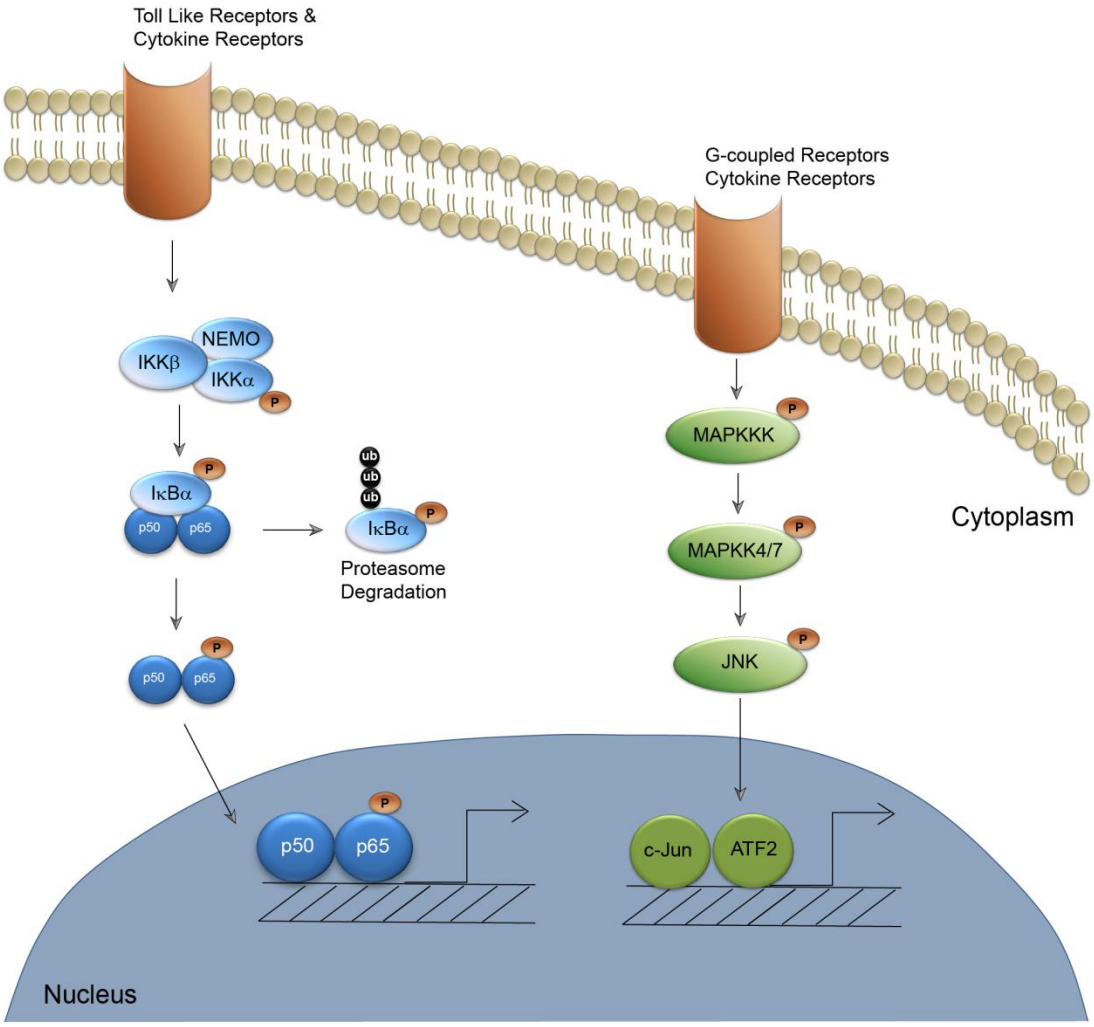

Figure 1-5. NF-κB and JNK signal transduction pathways. Model describing the signal transduction pathways of NF-κB and JNK during metabolic stress. The heterodimer p65 and p50 that comprise the canonical NF-κB, translocate to the nucleus when the IκBα repressor is phosphorylated by the IKK complex and targeted for proteasome degradation in the cytosol. c-JUN and ATF2 transcription factors translocate to the nucleus following activation of the MAP kinase cascade. Both pathways are activated by unique cellular stresses, including cytokine activation, and induce the transcription of cytokines and chemokines.

1.6 The role of the Unfolded Protein Response in autophagy

Autophagy is an essential pathway for the degradation and recycling of biological material within the cell, an important feature for establishing cellular homeostasis [91]. Upon induction of autophagy, double membrane vesicles called autophagosomes are responsible for trafficking damaged organelles and proteins to the lysosome for degradation by acid hydrolases, followed by release of degraded products into the cytosol, a process referred to as autophagic flux. Currently, 32 autophagy-related genes (ATG) have been identified in yeast, most of which have orthologues in higher eukaryotes with shared functions [92, 93]. These ATG proteins perform functions ranging from phagaphore initiation to facilitation of cargo loading into the lysosome (Fig 1-6).

Key proteins involved in formation of phagaphores are ATG1, for which there are two counterparts in higher eukaryotes: Unc-52-like kinase 1 (ULK1) and -2 (ULK2). Both ULK1 and ULK2 are known to associate with ATG13 and FIP200, and this complex localizes to and activates inducers of the initiating phagaphore such as the Beclin-1 (ATG6) in the VPS34 complex [94]. Once phagophores are formed, autophagosomes elongate and load cargo. During this process, the mammalian ATG8 homolog (LC3) is incorporated into the membrane of the forming phagaphores. LC3 initially exists as a cytoplasmic form (LC3b-I), and must be proteolytically cleaved at the C-terminal domain by ATG4, followed by the conjugation of phosphatidylethanolamine by ATG5-ATG12-ATG16L [95-97]. The lipidated form of LC3 (LC3b-II) facilitates loading of ubiquitinated cargo into autophagosomes through the interaction of proteins such as p62 [98, 99].

The location of autophagosome initiation has been suggested to occur at contact sites with the endoplasmic reticulum, designated ER exit sites (ERES), which are unique regions that are also central for assembly of COPII vesicles for secretion [100]. Formation of both autophagosomes and COPII vesicles at the ERES were shown to

require SEC proteins, such as SEC16, SEC31 and SEC13 [101, 102]. ER stress can alter SEC protein localization to the ERES, and disruptions in UPR signaling through liver specific PERK knockout lowers mRNA expression of multiple SEC family members [38]. While these results suggest a dynamic interplay between ER stress and SEC proteins, the biological implications have not been fully investigated.

The UPR is thought to play an essential role in the progression of autophagy, including phagophore initiation, elongation, and autophagolysosome fusion [44]. While the UPR transcription factors ATF4 and CHOP were reported to contribute to the induction of key autophagy genes, it is not clear how the most proximal consequence of UPR activation, acute eIF2α-P, is linked to induction of autophagy and subsequent hepatocellular injury upon saturated FFA exposure [103]. However the fact that substitutions in eIF2α that block phosphorylation by PERK result in defective lipidation of LC3b and a consequent block in phagophore initiation [103], suggests that an unknown direct translational target of eIF2α-P is essential for the induction of autophagy during stress.

It was shown that ER stress is a trigger for initiation of autophagy, and reclamation processes of autophagy are thought to be an important adaptation for cell survival [104, 105]. However, recent studies suggest that some ER stress agents induce an inhibition of autophagic flux, and this blockage in the autophagic process occurs coincident with cell death [106]. While the mechanisms of cell death are unclear, it has been suggested that induction of autophagy can thwart apoptosis, and inhibition of autophagic flux can instead contribute to necrotic phenotypes, such as necroptosis or autosis, which evokes an inflammatory response along with cell death [107-109]. Recent investigations have also shown an association with inhibition of autophagic flux and activation of ER stress in both mice fed high fat diets and liver biopsies of humans with

NASH, but it is not clear how this block in flux is occurring or if autophagy is playing an active role in cell death [50].

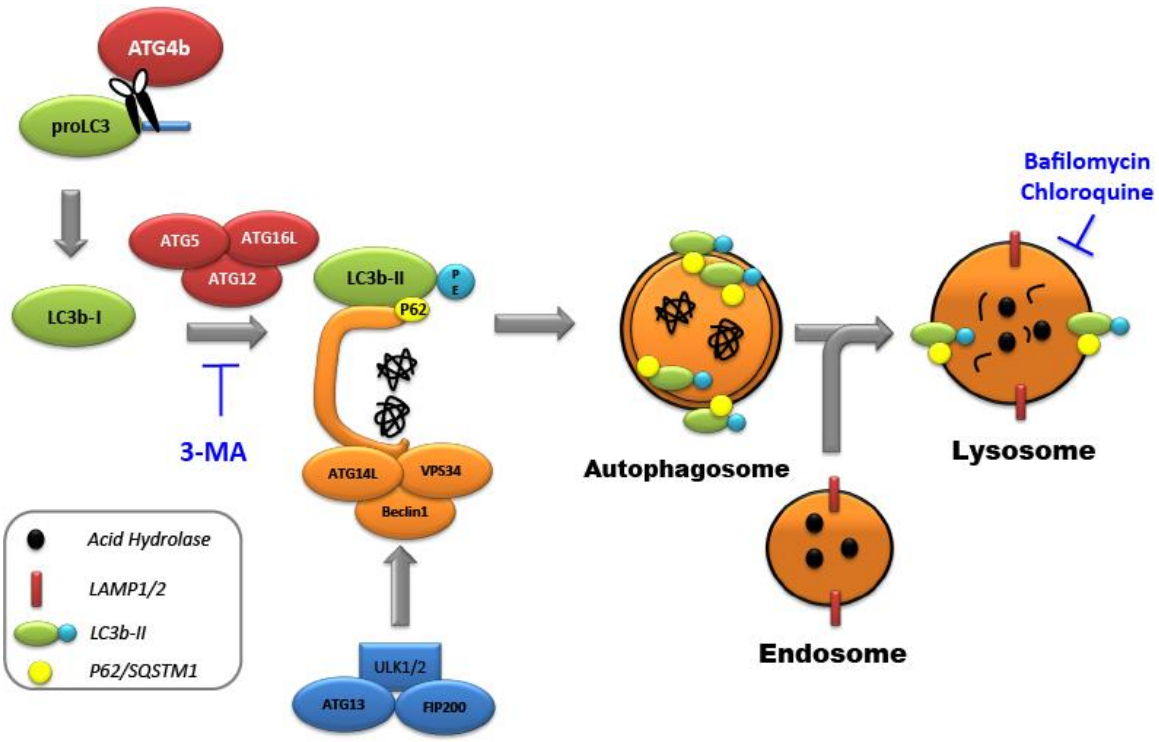

Figure 1-6. Steps in autophagy pathway. During autophagy initiation, a C-terminal peptide is cleaved by ATG4b, which results in formation of LC3b-I. The ATG5-ATG12-ATG16L complex acts as an E3 ligase-like enzyme to add phosphatidylethanolamine to the C-terminal domain of LC3b-1, resulting in LC3b-II. LC3b-II binds to p62 and integrates into the membranes of the emerging phagaphores to facilitate cargo loading. ULK1/2 forms a complex with ATG12 and FIP200, which activates the Beclin1-ATG14L-VPS34 complex, an essential step for initiation of phagaphores. Autophagosomes carry cargo to the lysosome and merge with endosomes, which carry acid hydrolases that are essential for degrading macromolecules. This pathway can be interrupted by pharmacological compounds, such as 3-methyladenine (3-MA), which blocks phagaphore initiation by inhibiting VPS34, or bafilomycin A1 or chloroquine, which blocks autophagic flux by collapse of the lysosomal pH gradient and preventing acid hydrolases from degrading material, respectively.

1.7 Proteasome functions in adaptive responses to injury

The half-live of proteins can range from minutes to days, and the degradation of proteins has been shown to be quite specific [110]. One of the main pathways for protein turnover within the cell is the ubiquitin-proteasome system (UPS). In the UPS, proteins are targeted to the proteasome for degradation through the addition of polyubiquitination on lysine 48 by specific enzymes called E1 ubiquitin-activating enzymes, E2 ubiquitin-conjugating enzymes, and E3 ubiquitin-protein ligases [111]. While most proteins degraded through the proteasome require polyubiquitination, it is important to note that some proteins have been shown to be directed to the proteasome for degradation without the addition of ubiquitin [112].

The proteasome is a multisubunit complex consisting of a 20S core subunit and a 19S regulatory particle designed to break down cytosolic proteins into short peptides. Recognition of polyubiquitinated proteins is mediated by distinct subunits containing ubiquitin-like and ubiquitin-associated domains in the 19S regulatory particle [113]. Following substrate recognition, proteins are deubiquitinated in an ATP-dependent manner and translocated into the 20S core subunit for degradation [114]. The core subunit is comprised of two catalytic β-rings encoded by gene products PSMB1-7, as well as a side chain on either side called an α-ring encoded by genes PSMA1-7. The β rings 1, 2, and 5 possess proteolytic activity consisting of three key enzymatic features that cleave proteins, allowing for their breakdown to smaller peptide fragments. These enzymatic activities are (1) caspase-like, which cleaves after acidic residues, (2) trypsin-like that cleaves after basic residues, (3) and chymotrypsin-like, which cleaves after hydrophobic residues, respectively [115, 116].

Because the proteasome degrades mostly short-lived proteins, it is an important pathway for the rapid degradation of regulatory proteins such as IκB to facilitate the activation of NF-κB (Fig 1-5). Another key regulatory pathway controlled by the

proteasome is nuclear factor erythroid-derived 2-like 2 (NRF2), which is activated in response to oxidative damage. Under nonstressed conditions, NRF2 is targeted for proteasome degradation by kelch-like ECH-associated protein 1 (KEAP1); however, during certain cellular stresses, the KEAP1-NRF2 interaction is disrupted and NRF2 localizes to the nucleus to promote transcriptional activation of stress response genes to alleviate oxidative damage, such as *NQO1*, *GCLC* and *GSR*. (Fig 1-7) [117]. Although the regulation of NRF2 by proteasome degradation is well understood, recent studies have shown that NRF2 also has an effect on proteasome activity and gene expression of proteasome subunits, such as *PSMB5*, in some but not all cell types [118, 119]. Furthermore, it was suggested that NRF2-dependent activation of genes encoding proteasome subunits plays a protective role, allowing for enhanced cell survival during the progression of ER stress [118].

To understand the role of NRF2 in the progression of NASH, mice lacking *NRF2* ($NRF2^{-/-}$) have been fed a long-term high fat diet. While these mice observed greater insulin sensitivity than WT counterparts fed a high fat diet, the $NRF2^{-/-}$ mice displayed increased liver damage and inflammation. Interestingly, this phenotype was associated with enhanced activation of the UPR [120]. During ER stress and consequent activation of the UPR, the proteasome acts as a key degradation pathway to compensate for the accumulation of misfolded proteins through ERAD. During ERAD, chaperone proteins such as heat-shock protein 70 (HSP70) facilitate the substrate targeting and polyubiquitination of misfolded proteins through E3 ligases, allowing for proteasome targeting and degradation [121, 122]. NRF2 has been suggested to function as a downstream effector in the PERK pathway, in which NRF2 mutant cells exhibit decreased viability in response to ER stress agents [123]. While it has been suggested that PERK regulates phosphorylation of NRF2 and nuclear localization, other

mechanisms that involve alteration of KEAP1 regulation of NRF2 have not been explored [123].

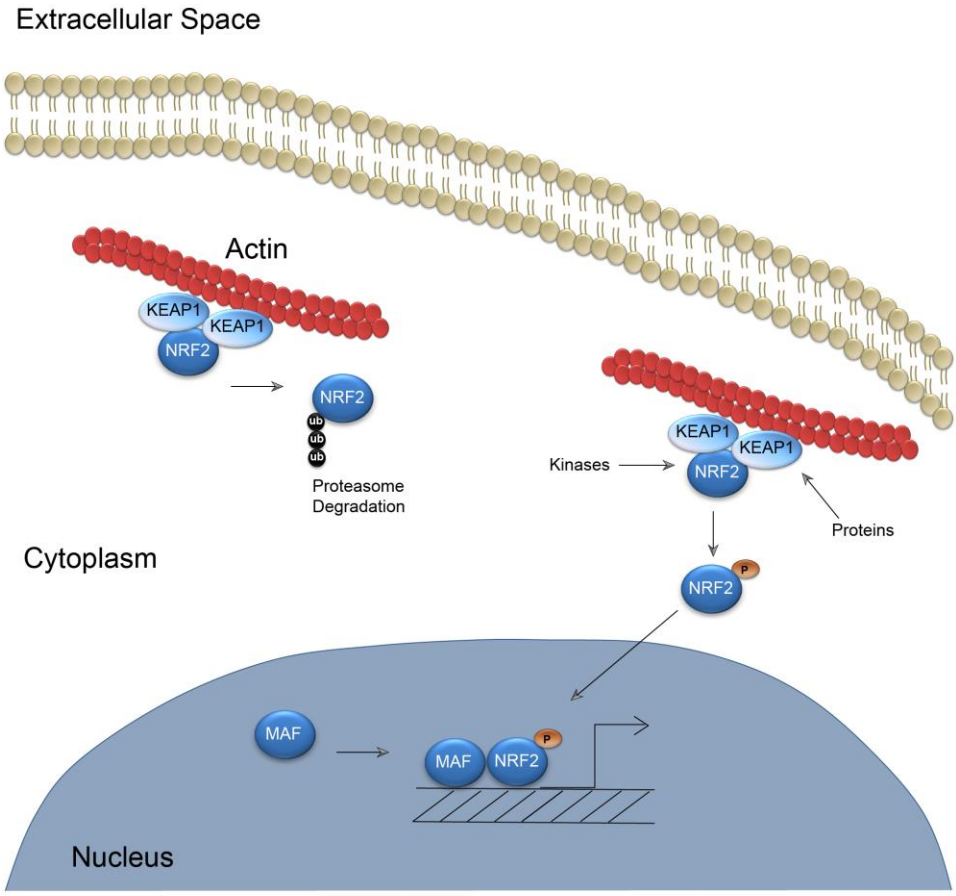

Figure 1-7. NRF2 signaling pathway. Under normal conditions, NRF2 is targeted for proteasome degradation by KEAP1, a cytoplasmic protein bound to actin. The KEAP1-NRF2 interaction can be disrupted by either induction of protein kinases that phosphorylate NRF2 or proteins interacting with KEAP1. Both scenarios result in nuclear localization of NRF2 to allow it to bind with MAF proteins and transcriptional activation of target genes involved in antioxidant responses and enhanced proteasome activities.

1.8 The role of NAFLD in hepatocellular carcinoma

Liver cancer, of which hepatocellular carcinoma (HCC) represents 70-85% of all subtypes, is the third leading cause of death due to cancer [124, 125]. While most cases of HCC are a result of chronic viral infection or alcoholic injury, the epidemiology of nearly half of all cases are unclear. Recent large scale studies have associated both obesity and NAFLD with an increased risk for HCC [126]. Interestingly, while fibrosis with progression to cirrhosis is often a key feature of HCC, recent literature has suggested that NAFLD might contribute to a small percentage (<20%) of non-cirrhotic HCC. This finding suggests that HCC might compromise the progression of NAFLD from simple steatosis to NASH, although the pathobiology and molecular mechanism remains unclear [127].

While the molecular mechanisms describing the progression of NAFLD to HCC are not well understood, obesity and NAFLD are characterized as chronic inflammatory diseases. During obesity, TNFα is released from the adipose tissue and acts as a potent activator of both NF-κB and JNK, pathways that have both been implicated as pro-oncogenic in multiple cancers [128]. Additionally, dysregulation of the mTOR pathway coincident with induction of autophagy has been observed in NAFLD [129]. Autophagy is upregulated in HCC, and inhibition of autophagy initiation enhances the efficacy of standard of care drugs [130]. Additionally, it was shown that the UPR is activated not only in NAFLD, but also in HCC, concurrent with increased *CHOP* expression in tumors. Deletion of *CHOP* in mice resulted in reduced tumor size and decreased pro-inflammatory cytokines coincident with reduced macrophages [131]. While there is currently no direct evidence connecting the progression of NAFLD to HCC, the correlation between molecular pathways perturbed in the two disease states is significant.

1.9 CHOP regulates a biological network in the pathogenesis of NASH

Recent studies have highlighted the importance of UPR activation and aberrant autophagy in the pathogenesis of NASH, but these reports rely on broad associations and lack mechanistic understanding regarding the roles of the UPR in the progression of simple steatosis to NASH [132, 133]. Chronic ER stress has long been associated with induction of cell death, but we propose that CHOP plays a direct role in both the hepatotoxicity and expression of secreted factors that induce death in the context of NASH. In this thesis, we will address the hypothesis that CHOP regulates NF-κB activation and consequent expression and TNFα, a cytokine shown to drive insulin resistance in metabolic disease. Additionally, we provide insight into why rodent models of NASH can be inadequate for recapitulating human liver disease. Determining the biological pathways and secreted factors directed by CHOP and the UPR will also help identify biomarkers and prognostic tools for liver disease and open new lines for research of therapies for NASH. Furthermore, whereas it has been suggested that FFAs are associated with an inhibition of autophagic flux, we propose a new mechanistic link between induction of ER stress, autophagy, and the resulting pathology associated with NASH [49, 134]. Together this line of investigation addresses a critical gap in our knowledge of NASH and the UPR by determining the mechanisms of hepatocyte death during saturated FFA exposure. We also explored the role of a novel UPR protein IBTKα in autophagy and provide a better understanding of the mode of death triggered by the UPR during metabolic stress. Finally, we explored the gene networks co-regulated by CHOP and NF-κB through next generation sequencing technology, and discovered that these two transcription factors coordinately regulate a biological network of activities, including proteasome activation through NRF2 as an adaptive response to a block in autophagic flux. Overall, these studies reveal new biological roles for both the UPR and CHOP in the hepatocyte during the pathogenesis of NAFLD.

CHAPTER 2. EXPERIMENTAL METHODS

2.1 Cell Culture and Measurements of Cell Viability

HepG2 cells were purchased from ATCC and cultured in Minimum Essential Media from Life Technologies (Grand Island, NY) supplemented with 1 mM non-essential amino acids, 1 mM sodium pyruvate, 2 mM glutaMAX, and 10% (v/v) fetal bovine serum at 37°C. Cells were seeded at 15,000 cells per 96-well plate or $3.7x10^6$ cells per 10 cm dish and treated with FFA in 1% BSA for the indicated times. FAAs were reconstituted first using warm isopropanol at 80 mM and then diluted to desired concentrations using media containing 10% FBS and 1% BSA. Following cell treatment with FFA for the indicated times, media was collected from cells and lactate dehydrogenase (LDH) [135]. Data was normalized to total LDH release by 10% triton X-100. Conditioned media experiments was collected and subjected to centrifugation at 200XG for 10 min prior to adding to recipient cells. Comparison of LDH activity in the donor conditioned medium before and after recipient cell incubation for 12 or 24 hours indicated that there was minimal contribution of LDH activity carried over from the conditioned medium. Furthermore, independent measurements of cell death were also carried out by imaging with calcein-AM, and these results supported key findings using LDH release. For inactivation studies, conditioned media supernatants were treated at 1 hour using heat inactivation at 56°C, 10 µg/mL RNase A at 37°C, or 50 µg/mL Proteinase K at 37°C [136, 137]. Caspase 3/7 activity was measured using the Apo-ONE homogenous caspase 3/7 assay from Promega (Madison, WI). Proteasome measurements were carried out using the chymotrypsin-like, trypsin-like, and caspase-like promteasome-glo assays from Promega.

2.2 Generation of Stable Gene Knockdowns and Knockouts

Stable knockdown and control cells were generated by transducing HepG2 cells with lentivirus carrying shRNA from Sigma-Aldrich (St. Louis, MO) against shCHOP (TRCN0000364393 and TRCN0000007263), shATF4 (TRCN0000013574 and TRCN0000013575), shCXCL8 (IL-8) (TRCN0000058029 and TRCN0000058030), shTNFA (TNFα) (TRCN0000355911 and TRCN0000003757), shRELA (p65)(TRCN0000014687), shIRAK2 (TRCN0000431467 and TRCN0000418461), shIBTKα (TRCN0000082575 and TRCN0000082577), shATG5 (TRCN0000151963 and TRCN0000151474), shSEC16A (TRCN0000246017), shSEC31A (TRCN0000436177), shNFE2L2 (TRCN0000281950), shPSMB5 (TRCN0000003917), or control (SCH001). Cells transduced with lentivirus particles were selected for by resistance to 5 µg/mL puromycin and maintained for at least one week in the absence of puromycin prior to conducting experiments. Stable knockouts were constructed by using a plasmid from Sigma-Aldrich expressing the guide RNA, Cas9, long terminal repeats, and puromycin for CHOP (HS0000185403, GGAAATCGAGCGCCTGACCAGG), PERK (Hs0000302986, AATTATCAGCACTTTAGATGGG), or IBTKα (HS0000392536, GCTTTGGATCTTGTAATGAAGG). Stable N-terminal GFP-LC3b cells were constructed using a plasmid (EX-T0824-Lv103) from GeneCopoepia (Rockville, MD). Following transduction, cells taking up virus were selected using 10 µg/mL puromycin and knockout cells were sorted for single cells using flow cytometry. For the *Gaussia* luciferase assay, PSV40-gluc control plasmid from New Englad Biolabs (Ipswich, MA,) was transfected to cells and supernatant was used to measure secreted luciferase.

2.3 Immunoblot Analysis and ELISAs

Protein lysates were collected, quantified using Pierce BCA Protein Assay Kit from Thermo Scientific (Waltham, MA), and separated by SDS-PAGE using 4-12% Bis-

Tris gels. Following electrophoresis, proteins were transferred to nitrocellulose filters and blocked for 1 hr at room temperature with BLOTTO (Pierce). Filters were incubated overnight with antibodies that are listed in the supplement. Antibody preparations used in the immunoblot analyses include the following: Cell Signaling Technologies (Beverly, MA): eIF2α~P (#9721), eIF2α from (#5324), ATF4 (#11815S), GAPDH (# 2118S), TNFα (#6945), IκBα (#4812), p65 (#8242), p65~P (#3033), IRAK1 (#4504), IRAK2 (#4367), IRAKM (#4369), IRAK4 (#4363) CUL3 (2759S), ULK1 (8054S), PERK (5683), ATG5 (2630S), S6K (9202S), P~S6K (9208S), calnexin (26795), cleaved caspase 3 (9664L), K48 (8081), K63 (5621), NRF1 (12381), NRF2 (12721); from Santa Cruz Biotechnology (Dallas, TX), CHOP (sc-7351) and LAMP2 (sc-18822); from Sigma-Aldrich, β-actin (A5441); from Novus, IL-8 (#H00003576-M05), LC3b (NB1002220), SEC16A (NB183016), IBTKα (NBP15033 & NBP188512), p62/SQSTM1 (H00008878-M01), ULK2 (NBP133136), PSMB5 (NBP219983), and KEAP1 (NBP237431); from Thermo Scientific, calnexin (MA3-027); from Abcam (Cambridge, MA), SEC31A (AB8660), and Cathepsin D (AB97499); and from Abnova IRAK2 (#H00003656-M04). A 45-biomarker Multi-Analyte Profile- Human InflammationMAP v 1.0 from Myriad RBM was used to measure cytokines, chemokines and acute-phase reactants, in conditioned media from HepG2 cells treated with palmitate, oleate, or vehicle for 12 hours as well as human serum samples. Conditioned media experiments was collected and subjected to centrifugation at 200XG for 10 minutes. The fold change for the indicated cytokine in response to either FFA was normalized to vehicle. Human IL-8 and TNFα in the conditioned media were measured by using the R&D systems Quantikine ELISA kit D8000C and DTA00C, respectively.

2.4 Immunoprecipitation

For immunoprecipitation analyses, cells were trypsinized, washed once with PBS, and flash frozen following a five min incubation on ice in a hypotonic lysis buffer containing 20 mM Hepes, 2 mM MgCl2, and 10% Glycerol. Following a rapid thaw in a pre-warmed water bath, NaCl (150 mM final concentration) was added to cell suspensions on ice for five min, followed by a 15 min spin in a microfuge at 10,000xg. Supernatant was transferred to Protein G Dynabeads coated with the following primary antibodies: from Abcam, SEC16A (ab70722) and SEC31A (AB8660), from Novus, IBTKα (NBP188512), KEAP1 (NBP237431) and IgG rabbit and mouse control (3900 and 5415). After an overnight incubation in a cold room with continual rotation, beads were washed with a buffer solution containing 20 mM Hepes, 2 mM $MgCl_2$, 10% glycerol, and 150 mM NaCl. Supernatant was removed and proteins associated with beads were eluted with either urea for LC/MS analysis, or with 1X SDS-PAGE buffer for immunoblot analysis.

2.5 Cell Imaging

For neutral lipid accumulation, cells were fixed with 1X Prefer from Anatech (San Diego, CA) this then stained with 1X LipidTOX™ Deep Red Neutral Lipid Stain and 10 µg/mL Hoechst 33342, both from Life Technologies. For immunofluorescence, cells were fixed, permeabilized with 0.1% triton X-100 for 10 minutes, followed by overnight incubations with primary antibody in PBS containing 0.1% BSA, and finally a two hour incubation with the corresponding secondary Alexa Fluor conjugates and 10 µg/mL Hoechst (33342) from Life Technologies. For CLICK-IT reactions, 5 µM alexa-fluor 488 alkyne was utilized from Life Technologies. To monitor viability, live cells were stained with 2.5 µM calcein-AM and 10 µg/mL Hoechst for 30 minutes prior to imaging. All images were acquired via spinning disk confocal microscopy using Perkin Elmer's Opera

and quantified using Columbus (Waltham, MA). Three dimensional rendering of z-stack images was performed and quantified using Perkin Elmer's Volocity. For electron microscopy, cells were concentrated by centrifugation, fixed in modified Karnovsky's fixative, embedded in agar, post-fixed with 1% osmium tetroxide, dehydrated through an ascending series of ethanol, and processed and embedded in epoxy resin. Approximately one-micron thick toluidine blue stained sections, collected on glass slides, were prepared for ultrathin area selection. Ultrathin sections were collected on 200 mesh copper grids, counterstained with uranyl acetate and Sato's Lead stain, and examined in a CM100 Philips transmission electron microscope (TEM). Digital images of representative tissue areas were captured for evaluation.

2.6 Isolation of Primary Hepatocytes

C57BL/6 female mouse and Sprague Dawley male rat primary hepatocytes were isolated by anesthetizing rodents with sodium-pentobarbital and perfusing the liver through the portal vein for 12-14 minutes with Perfusion Buffer (Gibco) followed by 10 minutes L15 Buffer (Corning) containing collagenase and trypsin inhibitor (Worthington) at 42°C. Following digestion, livers were extracted from animals; digested cells were scraped and shaken from liver, followed by filtration and two spins at 50xG for 4.5 minutes as described [138, 139]. Primary human hepatocytes were purchased from Life Technologies (lots Hu8203, Hu1743, and Hu1745).

2.7 Polysome Profiling

HepG2 cells were treated for indicated times in the presence of vehicle, palmitate, thapsigargin, or oleate. Following incubations, MEM containing 50 µg/mL cycloheximide was added for 10 minutes at 37°C prior to harvesting. Cells were washed with ice cold PBS containing 50 µg/mL cycloheximide and lysed, lysates were added to

10-50% sucrose gradient, subjected to centrifugation in a Beckman SW41Ti rotor for 2 hours at 4°C at 40,000 rpm, and monitored by absorbance at 254 nm as described [140]. *ATF4*, *CHOP*, and *IBTKα* mRNA levels were measured by qPCR in each of the seven collected fractions as described [66]. Firefly luciferase mRNA was spiked into to each fraction to facilitate normalization in the cDNA and qPCR analysis for the transcript measurements as described. Data is represented as the percentage of transcript found in each fraction relative to the total for each mRNA, and a percentage change in large polysomes (fractions 5-7) with treatment relative to vehicle was measured.

2.8 Measurements of mRNA by qPCR and Luciferase Activities

RNA was isolated from cells using TRizol reagent (Invitrogen) and cDNA synthesis was carried out using TaqMan RT kit (Applied Biosystems) according to manufacturer's instructions. Primers used in the study are listed in Table 2-1. Transcript measurements were normalized to *GAPDH* for HepG2 and human primary hepatocytes or *ACTB* (β-actin) for mouse primary hepatocytes. HepG2 cells were transiently transfected using fugene 6 with the NF-κB reporter plasmid p5XIP10κB [141] and Renilla luciferase reporter plasmid for 24 hours, and the transfected cells were treated with palmitate or vehicle 12 hours, as indicated. Luciferase assays were carried out using the Dual-Luciferase reporter assay system (Promega) following the manufacturer's instructions.

2.9 RNA-seq and ChIP-seq analysis

For RNA-seq, wild type, CHOP-KO, and RELA-KO HepG2 cells were treated for 12 hours with either vehicle or 600μM palmitate. RNA was isolated using TRizol reagent and sequencing was carried out on the Illumina platform at Covance Genomics. Sequencing reads were aligned to the hg19 human genome from UCSC using Tophat2,

and mapped reads were assembled and merged using the Cufflinks and Cuffmerge packages, followed by differential gene expression using Cuffdiff. For ChIP-seq experiments, wild type HepG2 cells were treated with 600µM palmitate for 12 hours and fixed using formaldehyde. DNA was isolated, pulled down with either CHOP or P~p65, and sequenced at Covance Genomics. Sequencing reads were aligned to the human genome from UCSC (hg19) using Homer, and peaks were called by comparing palmitate treated cells to untreated for each respective pull-down.

2.10 Cell Migration Assay

Cell Migration assays were carried out using transwell boyden chambers with 5 µM pores from Cell BioLabs (#CBA-105). Macrophage murine RAW 264.7 and human KG-1 cells were plated at 50,000 cells per insert in serum-free DMEM. Conditioned media from either control or knockdown cells was added to the lower wells and cells were allowed to migrate for six hours at 37°C.

2.11 Statistical Analysis

Data are depicted as mean +/- standard deviation. Differences between multiple groups were analyzed using a one-way ANOVA followed by a post hoc Tukey HSD test to compare multiple groups. P values less than 0.05 were considered statistically significant and were indicated by "*", and treatment groups considered statistically significant from shCTRL treatment were indicated by the "#" sign unless otherwise noted.

Table 2-1: Human Primers for quantitative RT-PCR

GENE_ID	Species	Primer	Sequence
GAPDH	Homo sapien	Forward	5'-AGGGCTGCTTTTAACTCTGGT-3'
		Reverse	5'-CCCCACTTGATTTTGGAGGGA-3'
ATF4	Homo sapien	Forward	5'-TCAAACCTCATGGGTTCTCC-3'
		Reverse	5'-GTGTCATCCAACGTGGTCAG-3'
ATF6	Homo sapien	Forward	5'-CAATTGGAAGCAGCAAATGA-3'
		Reverse	5'-ACCGAGGAGACGAGACTGAA-3'
GRP78	Homo sapien	Forward	5'-TAGCGTATGGTGCTGCTGTC-3'
		Reverse	5'-TTTGTCAGGGGTCTTTCACC-3'
CHOP/DDIT3	Homo sapien	Forward	5'-AGGAACCAGGAAACGGAAACAGA-3'
		Reverse	5'-TCTCCTTCATGCGCTGCTT-3'
XBP1 total	Homo sapien	Forward	5'-GGAGTTAAGACAGCGCTTGG-3'
		Reverse	5'- ACTGGGTCCAAGTTGTCCAG-3'
XBP1 spliced	Homo sapien	Forward	5'-CTGAGTCCGCAGCAGGTG-3'
		Reverse	5'- ACTGGGTCCAAGTTGTCCAG-3'
CXCL1	Homo sapien	Forward	5'-AGGGAATTCACCCCAAGAAC-3'
		Reverse	5'-CACCAGTGAGCTTCCTCCTC-3'
CXCL2	Homo sapien	Forward	5'-CTCAAGAATGGGCAGAAAGC-3'
		Reverse	5'-AAACACATTAGGCGCAATCC-3'
CXCL3	Homo sapien	Forward	5'-GCAGGGAATTCACCTCAAGA-3'
		Reverse	5'-GGTGCTCCCCTTGTTCAGTA-3'
CXCL8	Homo sapien	Forward	5'-CTGCGCCAACACAGAAATTA-3'
		Reverse	5'-ATTGCATCTGGCAACCCTAC-3'
TNFA	Homo sapien	Forward	5'-CTCTCTCCCCTGGAAAGGAC-3'
		Reverse	5'-GCCAGAGGGCTGATTAGAGA-3'
IRAK1	Homo sapien	Forward	5'-TGCTAGAGACCTTGGCTGGT-3'
		Reverse	5'-GGGTCCAGGTGCTTCTTGTA-3'
IRAK2	Homo sapien	Forward	5'-AGAAGATGCCCCTCATTCCT-3'
		Reverse	5'-GCTGATTTTGCGGTTTTGAT-3'
IRAKM	Homo sapien	Forward	5'-CTGGCTGGATGTTCGTCATA-3'
		Reverse	5'-TTTGGAAATCCACCTTCCTG-3'
IRAK4	Homo sapien	Forward	5'-GCCACCTGACTCCTCAAGTC-3'
		Reverse	5'-CAAATCCTCCCTCTCCCATT-3'
IBTKα	Homo sapien	Forward	5'-CCGCCTTCCAGTTGTAATG-3'
		Reverse	5'-AGCAAACAACCCAGTTGTCC-3'
SQSMT1	Homo sapien	Forward	5'-CACCTGTCTGAGGGCTTCTC-3'
		Reverse	5'-CACACTCTCCCCAACGTTCT-3'
MAP1LC3B	Homo sapien	Forward	5'-ATTCGAGAGCAGCATCCAAC-3'
		Reverse	5'-CTGTGTCCGTTCACCAACAG-3'
NFE2L2	Homo sapien	Forward	5'-AAACCAGTGGATCTGCCAAC-3'
		Reverse	5'-GCAATGAAGACTGGCTCTC-3'
NQO1	Homo sapien	Forward	5'-AAAGGACCCTTCCGGAGTAA-3'
		Reverse	5'-CCATCCTTCCAGGATTTGAA-3'
GCLC	Homo sapien	Forward	5'-AGAGAAGGGGGAAAACAA-3'
		Reverse	5'-GTGAACCCAGGACAGCCTAA-3'
GSR	Homo sapien	Forward	5'-CAGTGGGACTCACGGAAGAT-3'
		Reverse	5'-AAACCCTGCAGCATTTCATC-3'
PSMB2	Homo sapien	Forward	5'-AAGGCCCCGACTATGTTCTT-3'
		Reverse	5'-GCGTGTGAAGTTAGCTGCTG-3'
PSMB5	Homo sapien	Forward	5'-CCATACCTGCATGGCACCAT-3'
		Reverse	5'-CCTCTCTTATCCCAGCCACA-3'
PSMD2	Homo sapien	Forward	5'-TTGCTGCTGACATCATCTCC-3'
		Reverse	5'-GGACGATTTCCTTCACCAGA-3'
PSMA1	Homo sapien	Forward	5'-GCGTCAGGAGTGTTTGGATT-3'
		Reverse	5'-GACATGGCTCTGCAGTCAAA-3'
PSMA5	Homo sapien	Forward	5'-CCATGAGTGGGCTAATTGCT-3'
		Reverse	5'-GTGGGGTCCTTTCTCATCAA-3'

Table 2-2: Mouse Primers for quantitative RT-PCR

GENE_ID	Species	Primer	Sequence
ACTB	Mus musculus	Forward	5'-CAGCTTCTTTGCAGCTCCTT-3'
		Reverse	5'-CACGATGGAGGGGAATACAG-3'
ATF4	Mus musculus	Forward	5'-GCCGGTTTAAGTTGTGTGCT-3'
		Reverse	5'-CTGGATTCGAGGAATGTGCT-3'
CHOP/DDIT3	Mus musculus	Forward	5'-CACCACACCTGAAAGCAGAA-3'
		Reverse	5'-CGTTTCCTGGGGATGAGATA-3'
IRAK2	Mus musculus	Forward	5'-GGCACCTTTGCCGATATCTA-3'
		Reverse	5'-GGGTAGATGAGGCTGTGGAA-3'
TNFA	Mus musculus	Forward	5'-GAACTGGCAGAAGAGGCACT-3'
		Reverse	5'-AGGGTCTGGGCCATAGAACT-3'
CXCL1	Mus musculus	Forward	5'-GCTGGGATTCACCTCAAGAA-3'
		Reverse	5'-TGGGGACACCTTTTAGCATC-3'
CXCL2	Mus musculus	Forward	5'-AAGTTTGCCTTGACCCTGAA-3'
		Reverse	5'-AGGCACATCAGGTACGATCC-3'

CHAPTER 3. RESULTS: CHOP links ER stress to NF-κB activation

3.0 Introduction

Free fatty acid induction of inflammation and cell death is an important feature of nonalcoholic steatohepatitis (NASH) and has been associated with disruption of the ER and activation of the Unfolded Protein Response (UPR). Following chronic UPR activation, the transcription factor CHOP triggers cell death; however, the mechanisms linking the UPR or CHOP to hepatoceullular injury and inflammation in the pathogenesis of NASH are not well understood. Using HepG2 and primary human hepatocytes, we found that CHOP induces cell death and inflammatory responses following exposure to saturated FFA by activating NF-κB through IRAK2 expression, resulting in secretion of cytokines IL-8 and TNFα directly from hepatocytes. Interestingly, CHOP/NF-κB signaling is not conserved in primary rodent hepatocytes. Our studies suggest that CHOP plays a vital role in the pathophysiology of NASH through induction of secreted factors that trigger inflammation and hepatocellular death via a signaling pathway specific to human hepatocytes.

3.1 Saturated FFAs induce the UPR before lipotoxicity in hepatocytes

Rodents are less sensitive to FFA-induced liver injury compared to humans [142-144]. To determine if this species dependence is a property of hepatocytes, we measured the sensitivity of human hepatoma HepG2 cells and primary human, mouse, and rat hepatocytes to 24 hours of exposure to increasing concentrations of saturated FFA palmitate or stearate and unsaturated FFA oleate (Fig 3-1 A-C). Both saturated FFA triggered significant cell death in HepG2 and primary human hepatocytes (LC50 <600 μM), whereas oleate did not induce cell death at concentrations up to 1000 μM (Fig 3-1 D). By contrast, mouse and rat primary hepatocytes were less sensitive to palmitate and

completely resistant to cytotoxic effects of stearate (Fig 3-1 A-D). These results suggest that the species sensitivity to lipotoxic effects of saturated FFA is a property of the hepatocytes.

Because HepG2 cells exhibited similar sensitivity to human primary hepatocytes following saturated FFA exposure, we used HepG2 cells to further explore the role of the UPR in hepatocellular stress responses to saturate FFA. As will be discussed later in the study, primary human hepatocytes also share many of the key features of UPR signaling that we discovered in the HepG2 cells. Hepatic steatosis characterized by intracellular accumulation of neutral lipid in hepatoctyes is a quintessential pathophysiologic feature of non-alcoholic fatty liver disease [1]. To determine if HepG2 cells accumulate neutral lipid in response to FFA exposure, we stained HepG2 cells with LipidTox™. Both saturated and unsaturated FFA resulted in significant neutral lipid accumulation in HepG2 cells; however, the morphology was dissimilar (Fig 3-1 E). Palmitate and stearate resulted in diffuse cytoplasmic lipid staining, whereas cells treated with oleate formed polarized neutral lipid droplets without demonstrable toxicity. These results suggest that despite neutral lipid accumulation within cells, the inability of HepG2 cells to properly store neutral lipid upon exposure to saturated FFA is correlated with lipotoxicity, an idea supported by an earlier study [145].

To determine whether the UPR is activated prior to saturated FFA-induced cell death, we measured markers of the UPR during a time course of exposure to physiological concentrations of free fatty acids (600 μM) [146, 147]. Cell death first occurred from 12 to 24 hours after treatment with either palmitate or stearate (Fig 3-2 A-B), which was preceded by activation of the UPR, with increased eIF2α~P and ATF4 expression after just 3 hours of saturated FFA exposure and robust expression of CHOP at 12 hours (Fig 3-2 E-F). By comparison, oleate had a minimal effect on the UPR, with only modest transient induction of eIF2α~P and ATF4 levels, minimal CHOP expression,

and full cell viability (Figs 3-2 C and F). As a control, we also measured activation of the PERK pathway in response to tunicamycin, a well-characterized inducer of ER stress and the UPR. Tunicamycin activated the UPR in a manner similar to saturated FFA, but without any adverse effect on cell viability (Fig 3-2 D and F). To confirm that palmitate indeed activated the UPR, as opposed to cytosolic stresses that induce eIF2α~P, we measured IRE1-mediated splicing of *XBP1* mRNA as well as *GRP78* (BiP) levels by qPCR. There were significantly elevated spliced *XBP1* and *GRP78* mRNAs upon palmitate treatment of HepG2 cells, which were absent during oleate exposure (Fig 3-3 A-B). The timing of the splicing of *XBP1* mRNA mirrored that for increased *CHOP* mRNA levels, both of which followed a modest increase in *ATF4* mRNA levels (Fig 3-3 C-D). However, there was no increase of *ATF6* mRNA during treatment with palmitate (Fig 3-3 E), supporting a previously reported discordant induction of the canonical branches of the UPR by saturated FFAs [52]. Oleate did induce *ATF4* mRNA, consistent with the transient induction of this cytoprotective transcription factor (Fig 3-3 D). We conclude that saturated FFAs are potent inducers of the UPR in human hepatocytes prior to lipotoxicity.

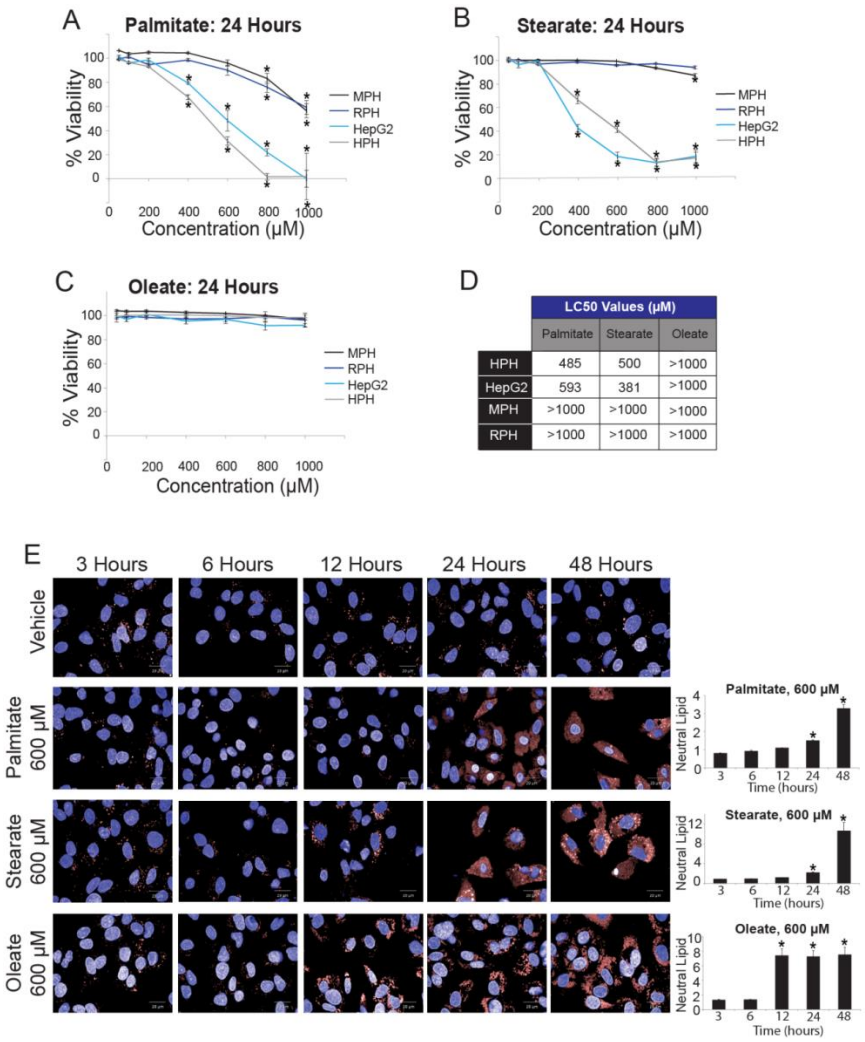

Figure 3-1. Human hepatocytes are more sensitive to lipotoxicity than rodent hepatocytes. (A-C) Mouse primary hepatocytes (MPH), rat primary hepatocytes (RPH), HepG2 cells, and primary human hepatocytes (HPH) were treated with the indicated concentrations of palmitate, stearate, or oleate for 24 hours. Cell death was measured by LDH release. (D) LC50 values (μM) from LDH release assay were calculated in XLfit using four parameter curve fits. (E) HepG2 cells stained for neutral lipid accumulation using LipidTox Deep Red imaging, for up to 24 hours. Accumulation of neutral lipid in response to saturated FFAs was quantified by counting total spot counts in Perkin Elmer's Columbus software package and normalized to vehicle.

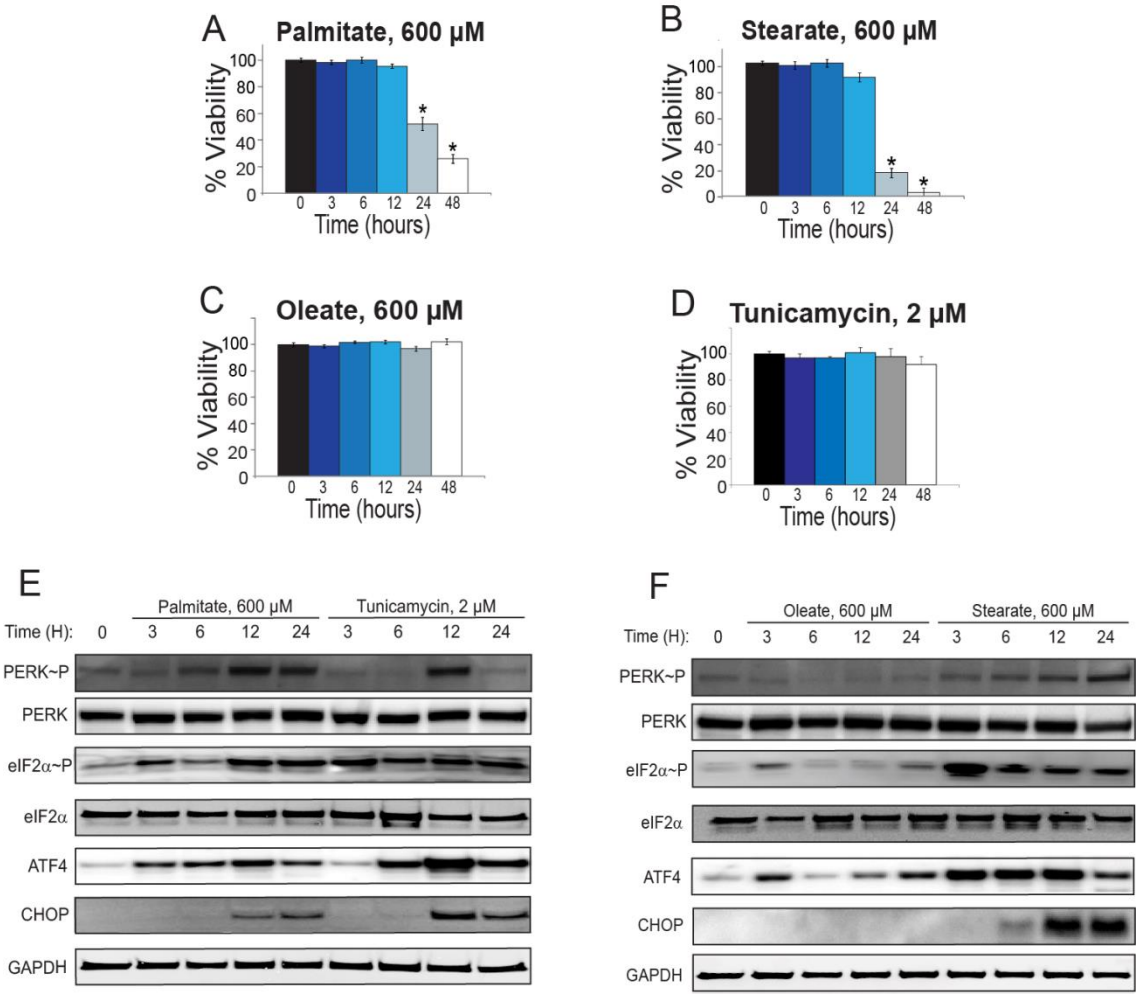

Figure 3-2. Saturated but not unsaturated free fatty acids induce the UPR prior to lipotoxicity in human hepatocytes. (A-C) Cell death was measured by LDH release in HepG2 cells incubated with 600 µM palmitate, stearate, or oleate, for the indicated times. (D) Cell death was measured by LDH release in HepG2 cells incubated with 2 µM tunicamycin for the indicated times. (E-F) Immunoblot analysis of HepG2 lysates treated with 600 µM palmitate, 2 µM tunicamycin, 600 µM stearate, or 600 µM oleate for up to 24 hours, as indicated.

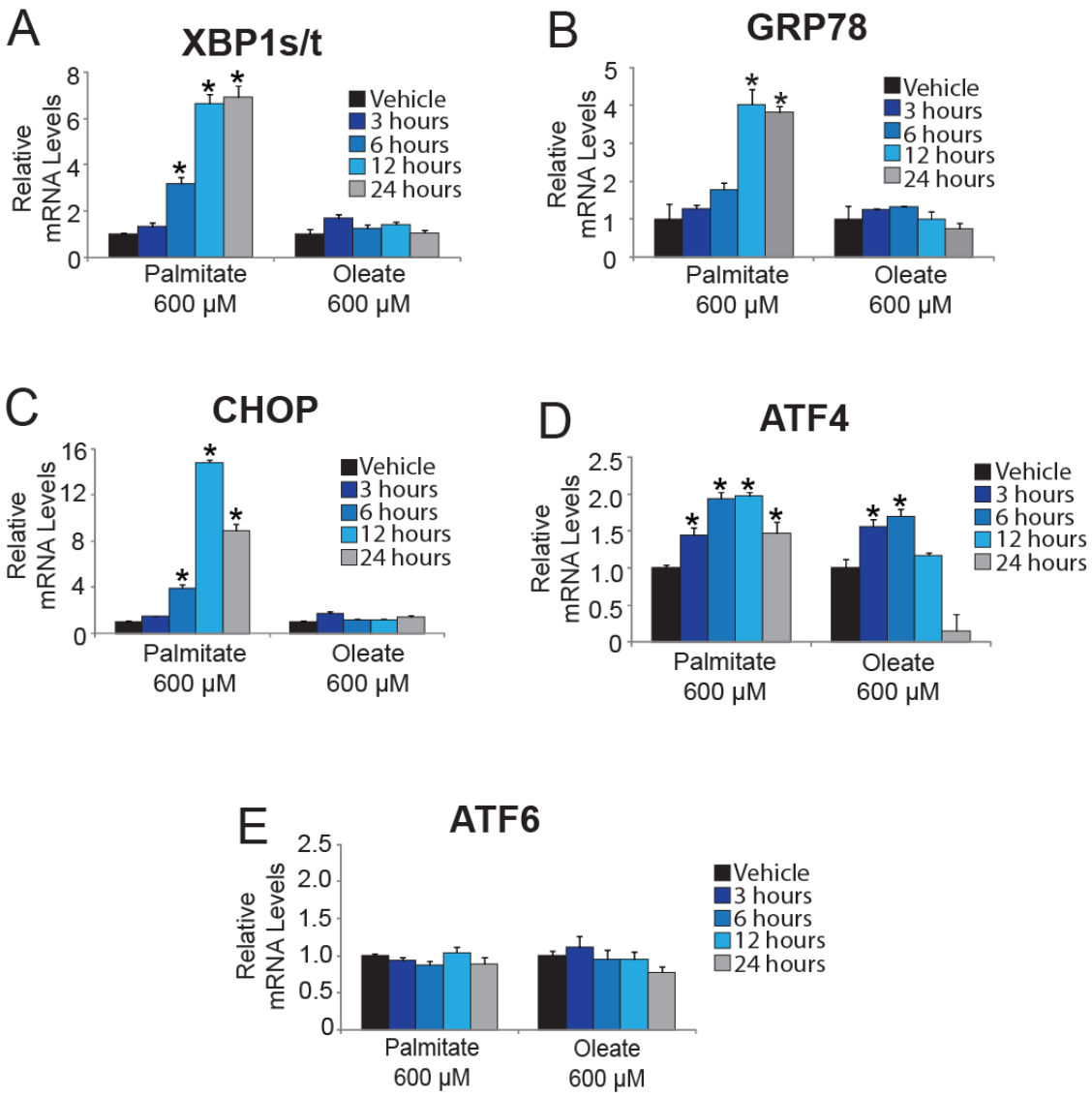

Figure 3-3. The UPR is discordantly activated by saturated FFAs. (A-E) Changes in gene transcripts from HepG2 cells incubated with 600 µM palmitate or oleate for up to 24 hours, as indicated. The XBP1s/t is a ratio of the spliced *XBP1* mRNA relative to total *XBP1* transcript.

3.2 Palmitate disrupts neutral lipid formation by localizing directly to the ER

Because both saturated FFA, but not oleate, induced ER stress along with aberrant and diffuse neutral lipid staining proceeding cell death, we evaluated the ultrastructural features of HepG2 cells treated with FFA. HepG2 cells were treated with vehicle, palmitate, or oleate and observed by transmission electron microscopy (Fig 3-4). Similar to previous neutral lipid staining (Fig 3-1 E), ulltrastructural examination revealed that oleate treatment produced large neutral lipid droplets with a polarized cellular distribution. However, palmitate treatment led to crystalline structures in HepG2 cells without the appearance of polarized neutral lipid droplets (Fig 3-4). Finally, to address the intracellular localization of palmitate, HepG2 cells were treated with CLICK-IT® palmitic acid, azide. There was significant co-localization of the tagged palmitate with ER-associated proteins, PERK (27%) and calnexin (40%), which were visualized by immunofluorescence (Fig 3-5 A-B). These findings indicate that palmitate can localize directly to the ER in hepatocytes and that the neutral lipid droplets accumulating from palmitate have marked differences in character and distribution relative to neutral lipid accumulation after treatment with the non-toxic oleate.

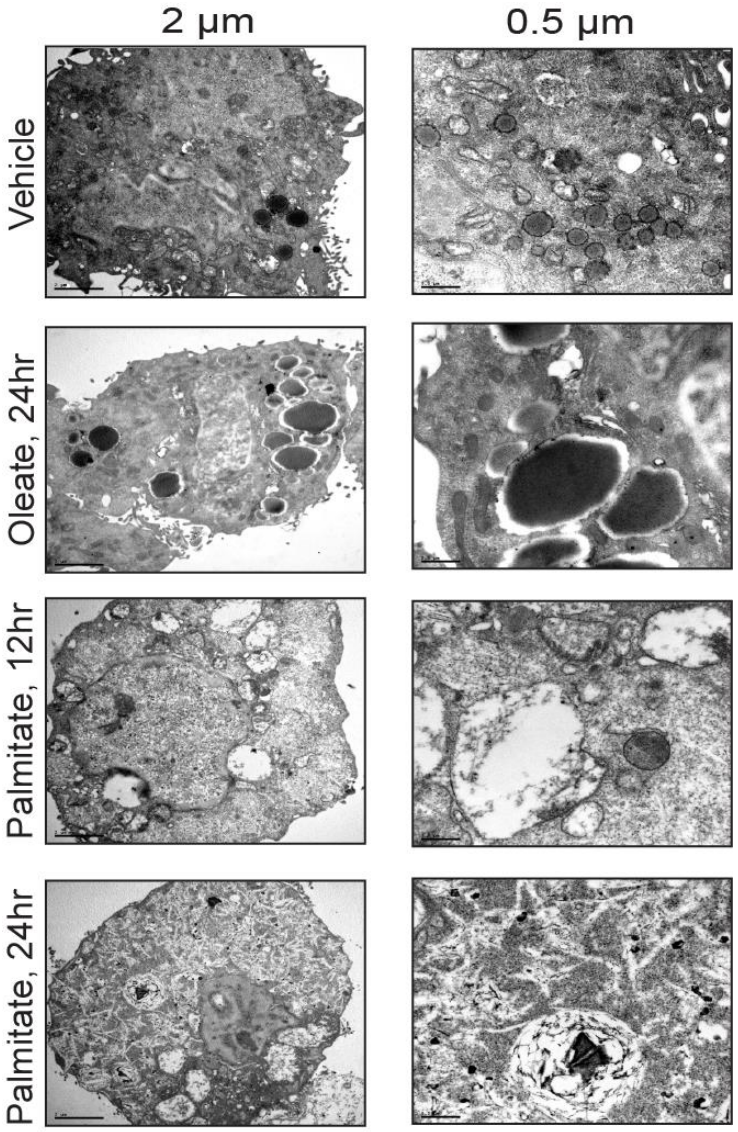

Figure 3-4. Electron microscopy of HepG2 cells treated with FFAs. Electron microscopy showing ultrastructures of HepG2 cells treated with vehicle, oleate, or palmitate for the indicated times.

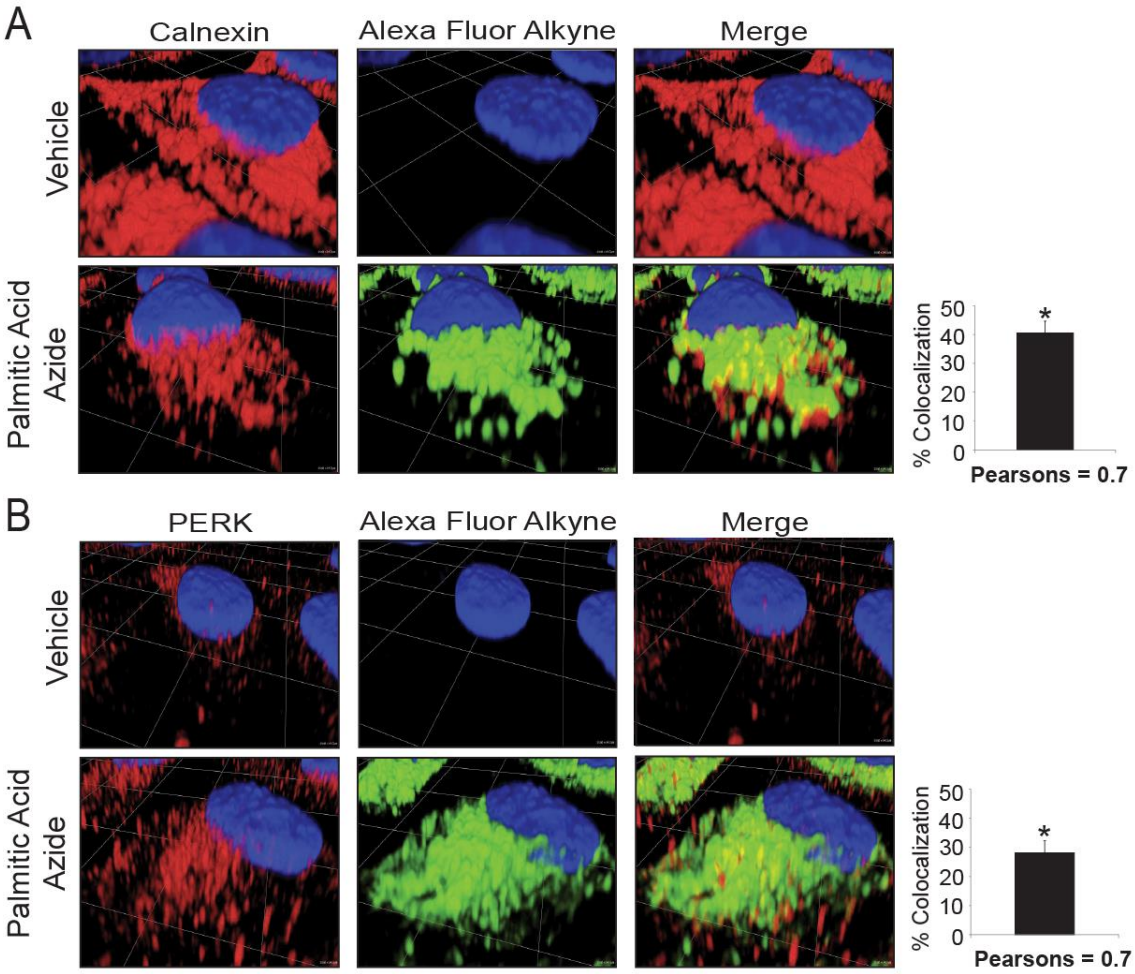

Figure 3-5. Palmitate localizes directly to the ER and PERK. (A-B) Spinning disk confocal images of CLICK-IT labeled palmitic acid azide tagged with alexa-fluor 488 alklyne showing colocalization with the ER (calnexin) or PERK. The percent co-localization of palmitate with calnexin and PERK are illustrated to the right of the images.

3.3 Palmitate inhibits initiation of global translation by PERK

Activation of PERK and downstream eIF2α~P results in a global reduction in translation initiation. To address the effects of palmitate on translation, we performed polysome profiling using lysates prepared from HepG2 cells treated with vehicle, palmitate, oleate, or tunicamycin as a control for ER stress (Fig 3-6 A-C). Both palmitate and tunicamycin reduced large polysomes coincident with accumulation of monosomes, indicative of lowered global translation initiation. Oleate did not alter polysome profiles, consistent with its minimal effects on the UPR. To understand the role of PERK during translational repression following palmitate exposure, we treated HepG2 cells deleted for PERK by using CRISPR (PERK-KO) with palmitate and found that there was no reduction in large polysomes relative to vehicle, although there was some accumulation of monosomes (Fig 3-6 D). Additionally, PERK-KO cells were resistant to palmitate-induced lipotoxicity coincident with decreased ATF4 and CHOP levels (Fig 3-6 E-F). These results suggest that activation of PERK due to saturated FFA palmitate is detrimental to hepatocyte survival.

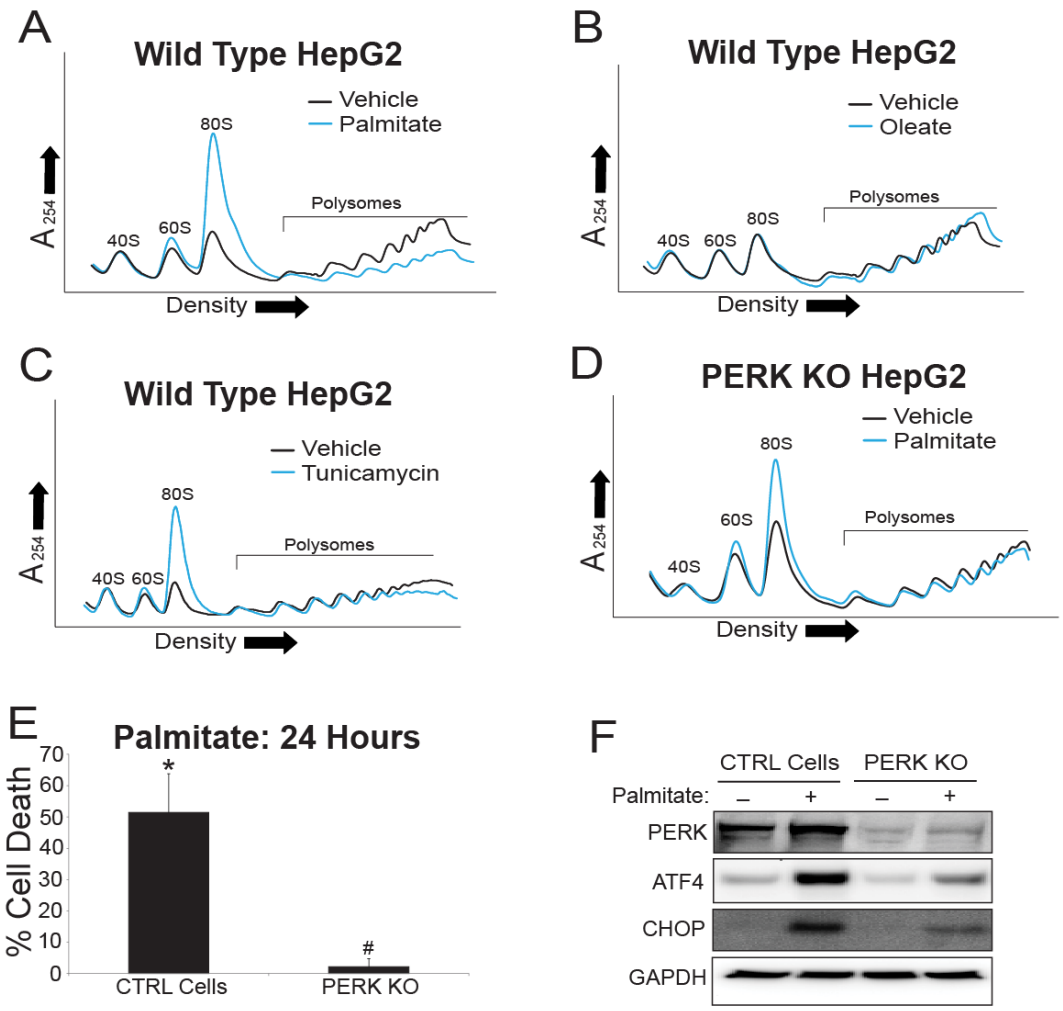

Figure 3-6. Palmitate exposure results in an inhibition of global translation in a PERK-dependent manner. (A-C) Polysome profiles of lysates prepared from HepG2 cells treated with vehicle, palmitate, oleate, or tunicamyicin for 12 hours. (D) Polysome profile of PERK KO HepG2 cells treated with either vehicle or palmitate for 12 hours. (E) Cell death of PERK KO HepG2 cells treated in the presence or absence of palmitate, as measured by LDH release,. (F) Immunoblot analysis of control and PERK KO HepG2 cells after 12 h treatment of either vehicle or palmitate.

3.4 Knockdown of CHOP protects hepatocytes from lipotoxicity

Elevated levels of CHOP are suggested to play a role in cell death during extended periods of ER stress [46, 58]. We addressed the role of CHOP in lipotoxicity by shRNA knockdown (shCHOP) in HepG2 cells. Control (shCTRL) and shCHOP cells were then measured for cell viability following exposure to palmitate for 24 hours. Palmitate treatment led to a modest loss of shCTRL cell viability as measured by LDH release after 12 hours of treatment, with about 50% lethality after 24 hours of palmitate exposure (Fig 3-7 A-B). By comparison, knockdown of *CHOP* provided for resistance to palmitate, as well as stearate treatment (Fig 3-7 C). Additionally, knockdown of *ATF4* (shATF4) in HepG2 cells did not alleviate saturated FFA induced cell death (Fig 3-7 D and Fig E). This finding is consistent with the notion that ATF4 has protective functions, whereas elevated CHOP levels facilitate cell death.

During liver injury and NASH, release of both autocrine and paracrine factors is thought to play a role in disease progression [11]. We wished to address whether the sensitivity of human hepatocytes to saturated FFA can occur by release of paracrine factors. As illustrated in Fig 3-8 A, conditioned media prepared from shCTRL HepG2 cells treated with palmitate for 3, 6, 12, or 24 hours was then applied to recipient shCHOP cells, which were incubated for an additional 24 hours and assayed for viability. The 12 hour conditioned medium led to over 20% death of the shCHOP cells, with approximately 40% of the cells succumbing to death following incubation with 24 hour conditioned medium (Fig 3-8 B). By comparison, conditioned medium from donor shCTRL cells treated with oleate or vehicle did not have a deleterious effect on survival of the recipient shCHOP cells (Fig 3-8 C). Additionally, we used another cell survival assay- calcein-AM, a cell-permeant dye that measures cell viability, to confirm that there was elevated death of the shCHOP cells treated with conditioned medium prepared from donor shCTRL cells incubated with palmitate for 24 hours (Fig 3-8 D). By comparison,

direct palmitate treatment of shCHOP showed robust calcein-AM conversion, consistent with full viability.

To address whether the secreted factor(s) in the conditioned medium that triggered death of recipient shCHOP cells is a polypeptide(s), the 12 and 24 hour conditioned media was treated with proteinase K, heat inactivation, or RNase A prior to incubation with the shCHOP cells for an additional 24 hours (Fig 3-8 E-F). Both proteinase K and heat treatments enhanced survival of the shCHOP cells, suggesting that CHOP induces expression and/or subsequent secretion of polypeptide(s) released from hepatocytes that can facilitate cell death during exposure to saturated FFA.

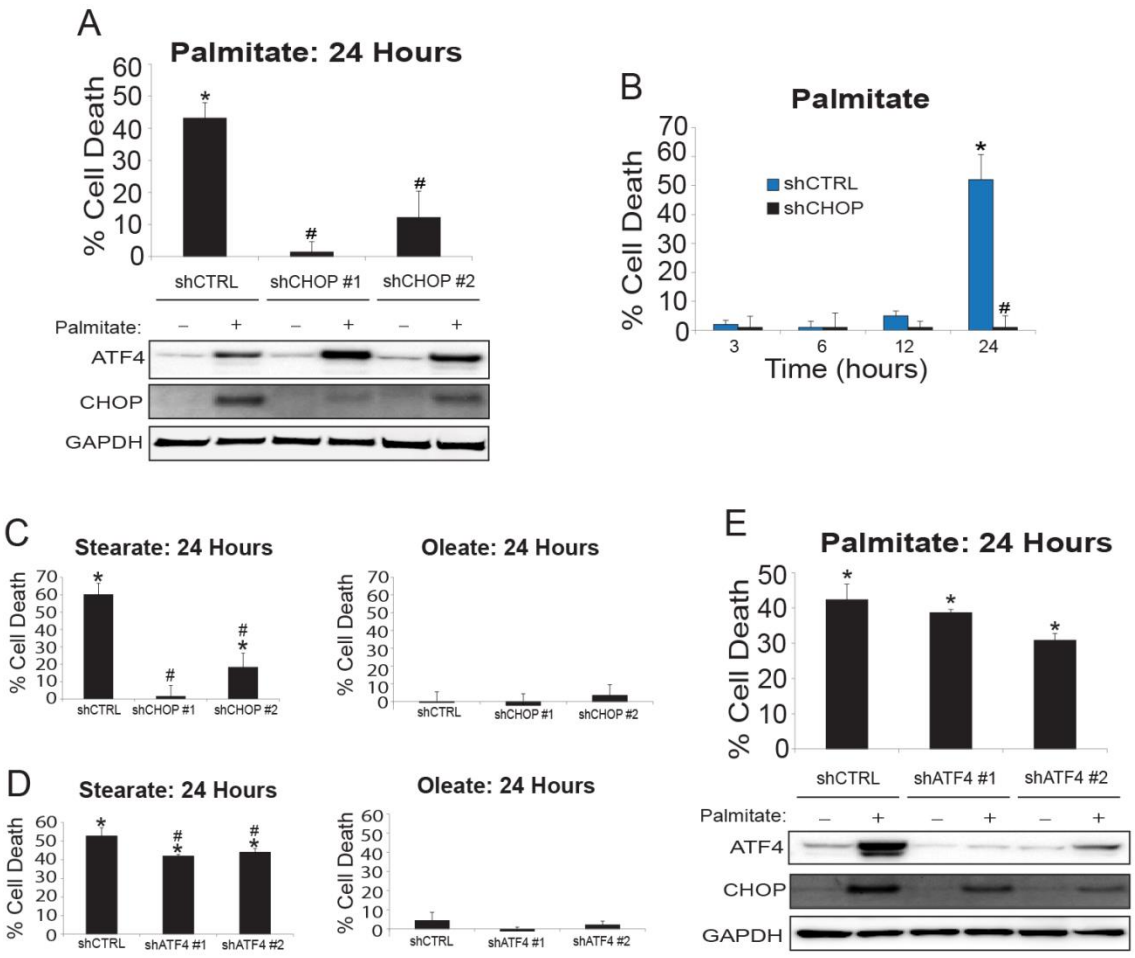

Figure 3-7. CHOP but not ATF4 is required for saturated FFA-induced hepatocellular death. (A) Control (shCTRL) HepG2 cells, or those knocked down for CHOP (shCHOP #1 and shCHOP #2), were treated with palmitate for 24 hours and cell death was measured by LDH release (top). The control and shCHOP cells were incubated for 12 hours in the presence (+) or absence (-) of 600 µM palmitate and the indicated proteins were measured by immunoblot (bottom). (B) shCTRL and shCHOP HepG2 cells treated with palmitate for indicated times and cell death was measured by LDH release. (C) Control (shCTRL) HepG2 cells, or those knocked down for CHOP (shCHOP #1 and shCHOP #2), were treated with stearate or oleate for 24 hours and cell death was measured by LDH release. (D) Control (shCTRL) HepG2 cells, or those

knocked down for ATF4 (shATF4 #1 and shATF4 #2), were treated with stearate or oleate for 24 hours and cell death was measured by LDH release. (E) Control (shCTRL) HepG2 cells, or those knocked down for ATF4 (shATF4 #1 and shATF4 #2), were treated with palmitate for 24 hours and cell death was measured by LDH release (top). Control and shATF4 cells were treated for 12 hours in the presence (+) or absence (-) of 600 μM palmitate and the indicated proteins were visualized by immunoblot (bottom).

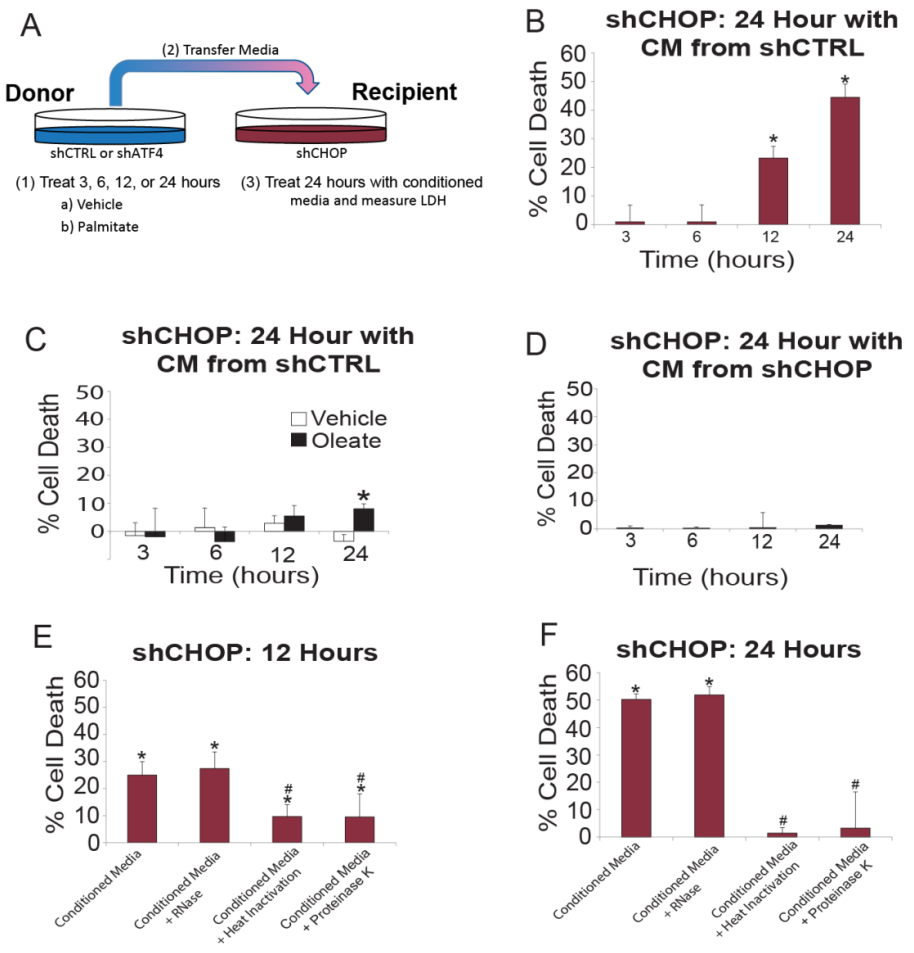

Figure 3-8. CHOP induces secretion of factors involved in hepatocyte death. (A) Diagram depicting conditioned media experiment. Donor shCTRL HepG2 cells were incubated with for 600 µM palmitate or control vehicle for up to 24 hours, as indicated. The conditioned medium was then transferred to recipient shCHOP HepG2 cells for 24 hours, and cell death was measured by LDH release. (B) Conditioned media was prepared from shCTRL HepG2 donor cells incubated for 3, 6, 12, or 24 hours in the presence of palmitate. Conditioned medium was then transferred to recipient shCHOP HepG2, and following incubation for 24 hour cell death was measured by LDH release. (C) Conditioned media was prepared from donor shCTRL HepG2 cells incubated for 3, 6, 12, or 24 hours in the presence of vehicle or oleate. Conditioned medium was then

transferred to recipient shCHOP HepG2 cells, and following a 24 hour incubation cell death was measured by LDH release. (D) Conditioned media was prepared from donor shCTRL HepG2 cells incubated for 3, 6, 12, or 24 hours in the presence of vehicle. Conditioned medium was then transferred to recipient shCHOP HepG2 cells, and following a 24 hour incubation cell death was measured by LDH release. (E-F) Conditioned medium prepared from donor shCTRL cells cultured with palmitate for 12 or 24 hours was treated with RNase A, heat inactivation, or proteinase K, and the treated conditioned medium was then incubated with recipient shCHOP cells for 24 hours. Cell death was measured by LDH release.

3.5 CHOP induces an inflammatory response in hepatocytes in response to palmitate

To determine the identity of the secreted factor(s), we profiled the conditioned media from Hep2G cells treated with vehicle, palmitate, or oleate by using an inflammatory biomarker screen (Myriad RBM). Secretion of several cytokines was induced in hepatocytes upon palmitate exposure, including IL-8, IL-7, TNFα, IL-4, and TNFR2 (Fig 3-9 A). To address the role of CHOP in the secretion of these factors, we carried out individual sandwich ELISAs in both control and shCHOP cells for IL-8 and TNFα, both of which have been shown to be increased in patients with NASH [17]. There were significant increases in the secretion of both IL-8 and TNFα in HepG2 cells treated with palmitate, which were sharply lowered in shCHOP cells (Fig 3-9 B-E). These results indicate that CHOP is required for secretion of pro-inflammatory factors from hepatocytes following exposure to saturated FFA.

To determine the biological implications of the CHOP-dependent secreted factors, we knocked down IL-8 (*CXCL8*) and TNFα (*TNFA*) in HepG2 cells using shRNA (Fig 3-10 A-B). These knockdowns sharply reduced IL-8 and TNFα secreted

polypeptides (Fig 3-10 C-D). Whereas depletion of IL-8 did not rescue hepatocytes from palmitate-induced cell death relative to control cells (Fig 3-10 A), there was a sharp reduction in macrophage recruitment as measured by trans-well chemotaxis (Fig 3-10 E). Depletion of TNFα rescued both the HepG2 cells from palmitate-induced cell death and prevented macrophage recruitment (Fig 3-10 B and F). These results indicate that CHOP is essential for secretion of factors involved in both hepatocyte cell death and pro-inflammatory signals. To further address whether TNFα is a secreted factor by which CHOP signaling can drive cell death, 12 hour conditioned media from palmitate treated donor control or shTNFA cells was added to recipient shCHOP cells. Whereas conditioned media from the palmitate-treated control cells triggered almost 30% death of recipient shCHOP cells, conditioned media from the palmitate treated shTNFA cells only caused about 5% death (Fig 3-11 A). These results indicate that TNFα is a major CHOP-dependent secreted factor responsible for hepatocyte cell death during exposure to saturated FFAs.

Is TNFα sufficient to trigger death of shCHOP hepatocytes? To address this question, we added recombinant TNFα to the cultured medium of these cells in the presence or absence of palmitate. There was significant death of the shCHOP cells upon TNFα treatment only when added in combination with palmitate (Fig 3-11 B). By comparison, addition of recombinant IL-8 to the shCHOP cells did not have any adverse effect on cell viability. We conclude that induced secretion of TNFα is an important reason for the CHOP pathway eliciting hepatocyte death upon exposure to saturated FFAs. Furthermore, treatment of shCHOP cells with the combination of TNFα and IL-8, but neither alone, signaled macrophage migration, as judged by transwell chemotaxis (Fig 3-11 C). The requirement for both TNFα and IL-8 for the inflammatory response is consistent with our finding that knockdown of either was sufficient to thwart macrophage migration.

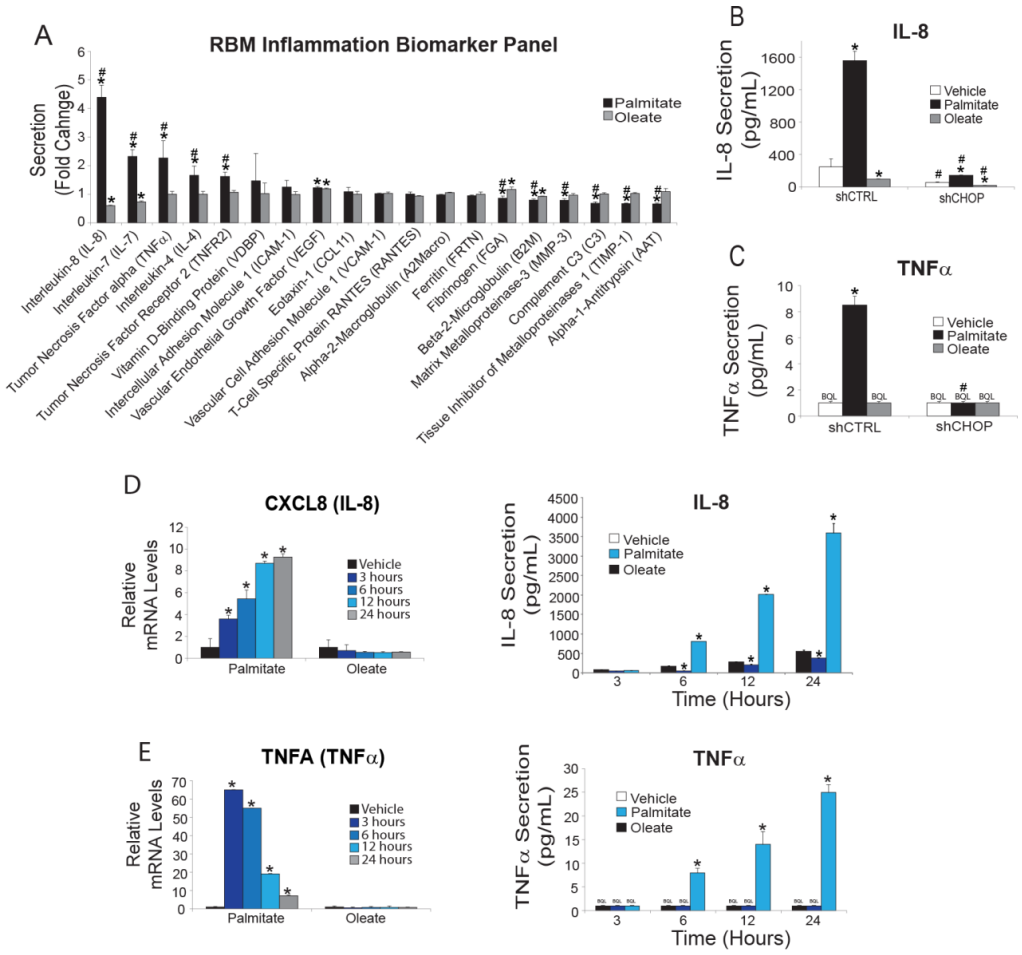

Figure 3-9. CHOP directs hepatocyte secretion of TNFα and IL-8 upon exposure to palmitate. (A) RBM Myriad biomarker panel measuring the indicated secreted factors from HepG2 cells treated with either palmitate or oleate for 12 hours. Values are normalized to vehicle treatment, and "#" indicates biomarkers were statistically significant relative to the oleate treatment group. (B-C) Sandwich ELISAs measuring IL-8 and TNFα from conditioned media of shCTRL or shCHOP HepG2 cells treated with 600 μM palmitate or oleate for 12 hours, or vehicle control. (D-E) HepG2 cells were treated with palmitate, oleate, or vehicle for the indicated numbers of hours. From these cells, levels of *CXCL8* (IL-8) and TNFA (TNFα) mRNAs were measured by qPCR (left) and TNFα and IL-8 were measured by sandwich ELISA (right).

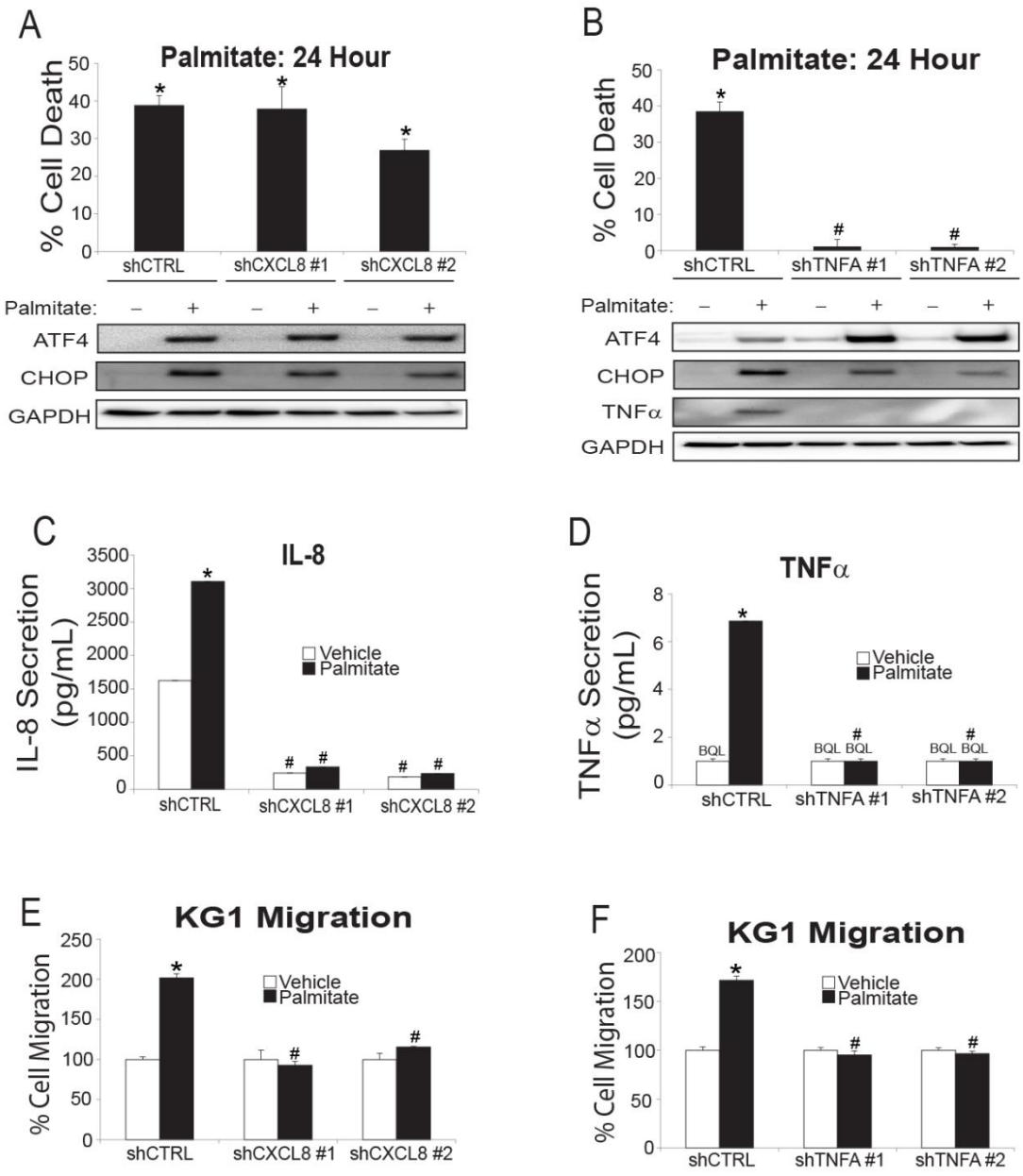

Figure 3-10. TNFα and IL-8 recruit inflammatory cells while only TNFα plays a role in hepatocellular viability. (A) Control (shCTRL) HepG2 cells, or those knocked down for IL-8 expression (shCXCL8 #1 and shCXCL8 #2), were treated with palmitate for 24 hours and cell death was measured by LDH release (top). The indicated proteins were measured by immunoblot using lysates prepared from control and shCXCL8 cells

incubated for 12 hours in the presence (+) or absence (-) of 600 μM palmitate (bottom). (B) Control HepG2 and those depleted for TNFα (shTNFA #1 and shTNFA #2) were treated with palmitate for 24 hours and cell death was measured by LDH release (top). Immunoblot analyses were also carried out to measure the indicated proteins in the shCTRL and shTNFA cells treated with palmitate for 12 hours (+) or vehicle (-) (bottom). (C-D) Sandwich ELISAs for shCXCL8 and shTNFA cells depicting repressed secreted polypeptides. (E-F) Cell migration assay for KG-1 cells using conditioned media prepared from shCTRL, shCXCL8, or shTNFA cells treated with either vehicle or palmitate for 12 hours.

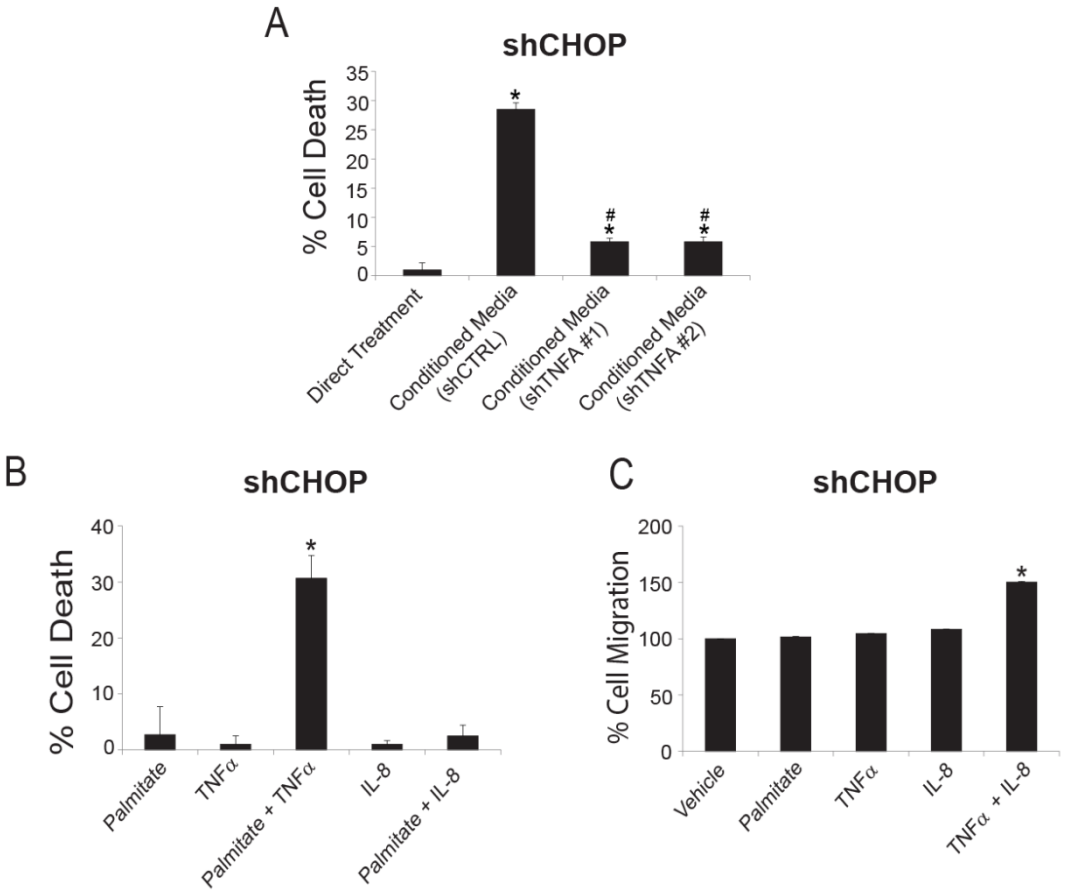

Figure 3-11. Palmitate requires TNFα for hepatocellular death. (A) Direct treatment indicates cell death of shCHOP cells incubated with palmitate for 24 hours. Alternatively, donor shCTRL or shTNFA HepG2 cells were incubated with palmitate for 12 hours. Conditioned medium was then applied to recipient shCHOP cells for 24 hours, and cell death was measured by LDH release. (K) The shCHOP HepG2 cells were treated with vehicle, 600 μM palmitate, 10 ng/ml TNFα, 1000 ng/ml IL-8, or a combination of the recombinant proteins and palmitate for 24 h, as indicated. Cell death was measured by LDH release. (L) Conditioned medium was prepared from donor shCHOP HepG2 cells after 12-h treatment with vehicle or palmitate, and 10 ng/ml TNFα and/or 1000 ng/ml IL-8 was added to indicated conditioned medium before performing the KG1 cell migration assay.

3.6 CHOP activates NF-κB during palmitate exposure

Transcriptional expression of *CXCL8 (*IL-8*)* and *TNFA* (TNFα) are known targets of NF-κB, so we determined whether CHOP serves to activate NF-κB in response to saturated FFA. Elevated eIF2α~P can reduce synthesis of the IκBα, which can contribute to NF-κB activation [148]. Indeed IκBα levels were reduced after treatment with the saturated FFA, which were undeterred in the *CHOP*-deficient cells (Fig 3-12 A). In fact, IκBα levels were lowered basally in shCHOP cells, contributing to further reductions in IκBα during treatment with palmitate. Next we measured phosphorylation of the p65 subunit of NF-κB at serine 536, which facilitates NF-κB targeting to the nucleus and transcriptional activation [87]. Phosphorylation of p65 was induced in shCTRL HepG2 cells by palmitate, but not in shCHOP cells (Fig 3-12 A). Furthermore, phosphorylated p65 localized to the nucleus upon palmitate treatment (Fig 3-12 B). Finally, transcriptional activity of a NF-κB-responsive reporter was induced 3-fold upon treatment of HepG2 cells with palmitate (Fig 3-12 C). By comparison, shCHOP cells showed minimal NF-κB activity. Collectively these results indicate that CHOP is required for induced NF-κB transcriptional activation in response to saturated FFA.

We next investigated the requirement for CHOP in activation of canonical NF-κB target genes *CXCL1*, *CXCL2,* and *CXCL3*, as well as *CXCL8*, and *TNFA* (Fig 3-13). For each of these NF-κB-target genes, *CHOP*-depletion blocked increased mRNA levels in response to palmitate to the same or greater extent as knockdown of *RELA*, encoding the p65 subunit of NF-κB. These results suggest that *CHOP* is not only required for NF-κB activation, but also plays a central role in secretion of pro-inflammatory cytokines following palmitate exposure.

To address whether the decrease in cytokine gene expression in shCHOP and shRELA cells affects inflammation, we measured macrophage chemotaxis using 12 hour conditioned media from HepG2 cells treated with palmitate (Fig 3-14 A). Whereas,

conditioned medium prepared from shCTRL HepG2 cells enhanced migration of human KG-1 cells, there was a marked reduction in macrophage migration when the conditioned medium was prepared from cells depleted for either CHOP or p65. Knockdown of p65 (shRELA) in HepG2 cells also prevented cell death following palmitate exposure (Fig 3-14 B-C). However, conditioned media from donor shCTRL HepG2 cells triggered death of recipient shCHOP and shRELA cells (Fig 3-14 D), supporting the idea that both CHOP and p65 are required for the activation and secretion of TNFα, but are not the downstream effector pathway resulting in cell death. These results indicate that CHOP is required for the activation of NF-κB-dependent secreted factors that play a role in both cell death and inflammation.

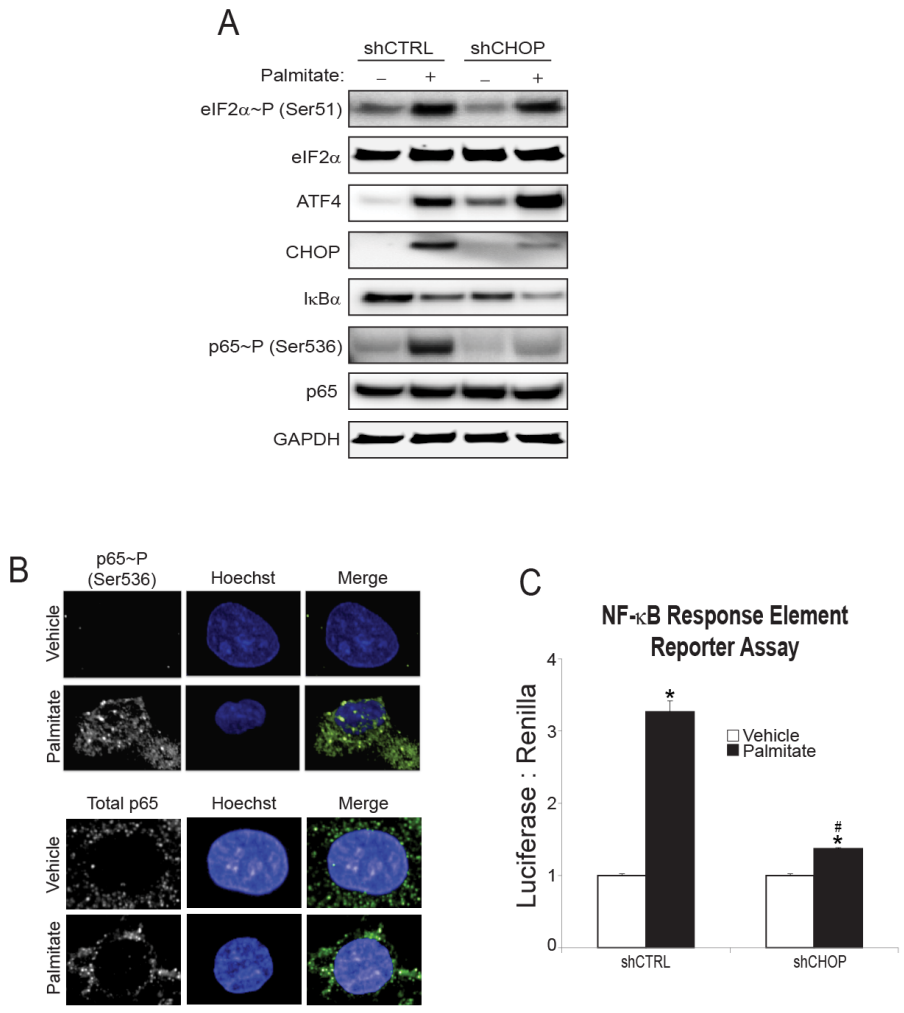

Figure 3-12. CHOP is required for activation of NF-κB in hepatocytes treated with palmitate. (A) shCTRL or shCHOP HepG2 cells were treated with either vehicle (-) or palmitate (+) for 12 hours, followed by immunoblot analyses that measured the indicated proteins. (B) Nuclear localization of total and phospho-p65 was measured by Immunofluorescence microscopy in HepG2 cells that were treated with palmitate or vehicle. In parallel, Hoeschst staining was used to visualize nuclei, and the nuclear staining and p65 imaging was merged. (C) An NF-κB reporter plasmid was transiently transfected into shCTRL and shCHOP HepG2 cells, which were then treated with either vehicle or palmitate for 12 hours and reporter firefly luciferase activity was measured and normalized to Renilla luciferase.

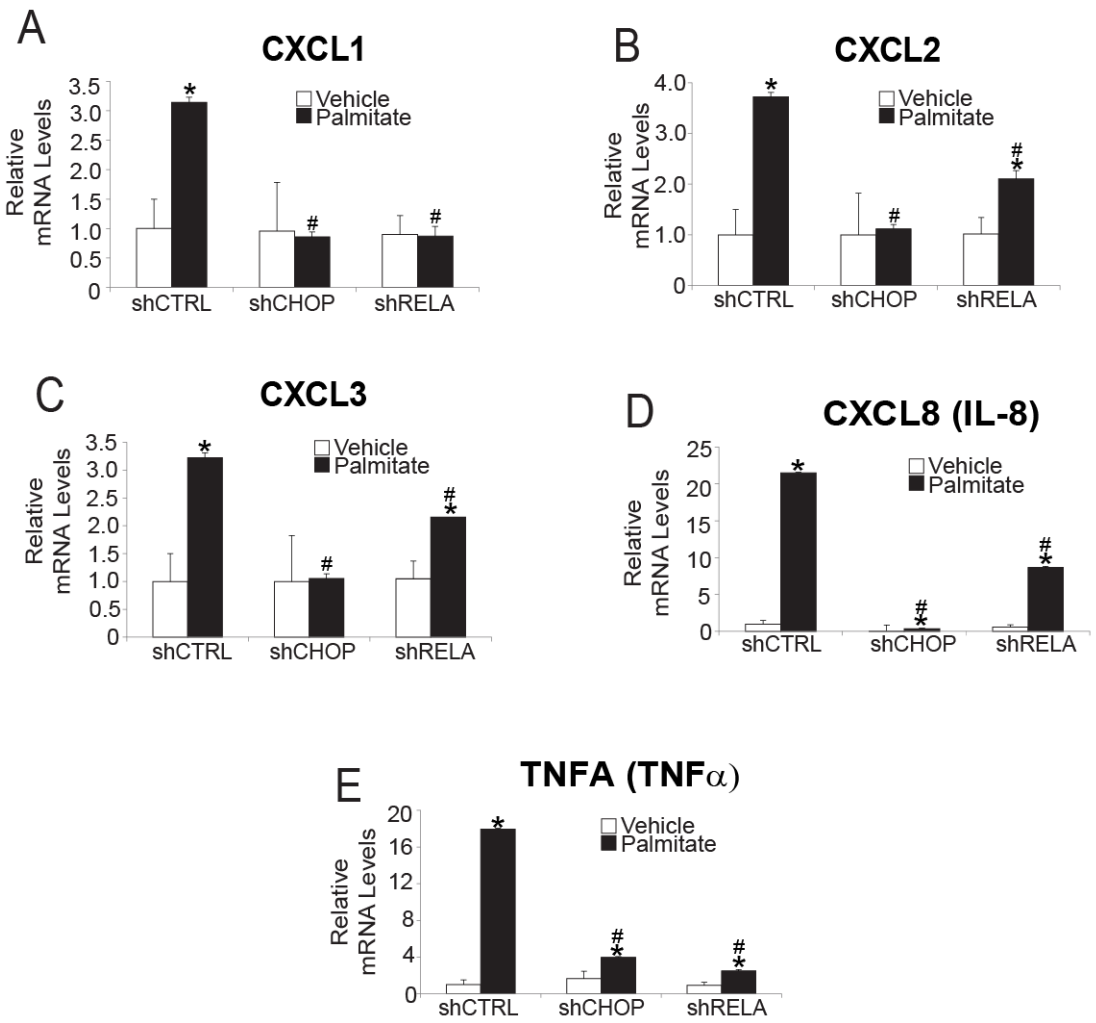

Figure 3-13. CHOP and NF-κB are both required for a subset of cytokine and chemokine gene expression. (A-E) Levels of the indicated gene transcripts were measured by qPCR in HepG2 cells that were treated with palmitate for 12 hours, or vehicle.

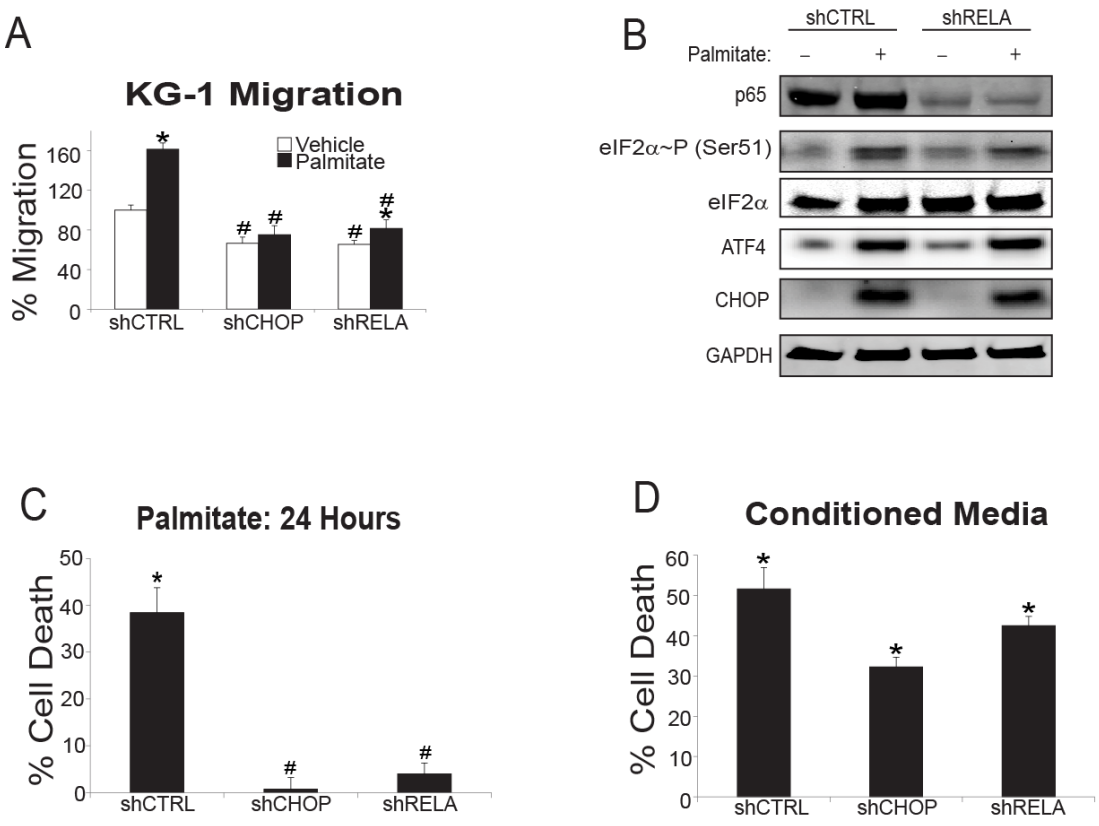

Figure 3-14. CHOP and NF-κB are both required for cell death and macrophage recruitment. (A) Cell migration assays were carried out for 6 hours using KG-1 cells incubated with conditioned media prepared from HepG2 cells expressing shCTRL, shCHOP, or shRELA that were treated with palmitate for 12 hours, or vehicle. (B) The shCTRL and shRELA HepG2 cells were treated with either vehicle (-) or palmitate (+) for 12 hours, and the indicated proteins were measured by immunoblot analyses. (C) HepG2 cells expressing shCTRL, shCHOP, or shRELA were cultured in palmitate for 24 hours and cell death was measured by LDH release. (D) Conditioned medium was prepared from donor shCTRL cultured in palmitate for 12 hours and applied to recipient shCTRL, shCHOP, or shRELA HepG2, and following a 24 incubation cell death was measured by LDH release.

3.7 CHOP activates NF-κB in part through IRAK2 signaling

CHOP protein is fully induced in shRELA cells in response to palmitate, further supporting the idea that CHOP functions upstream of NF-κB (Fig 3-14 B). We proposed that an IRAK protein, previously linked to NF-κB signaling [149], may function downstream of CHOP in its activation of NF-κB. There are four human IRAK isoforms, IRAK1, IRAK2, IRAKM, and IRAK4, and we measured the mRNA and protein for each in the shCTRL and shCHOP HepG2 cells treated with palmitate. *IRAK2* mRNA was the only isoform induced following exposure to palmitate, and was also the only isoform for which the mRNA and protein was substantially lowered by shCHOP (Fig 3-15 A-B). It is noted that the IRAK2 protein was not significantly induced in response to palmitate, despite the robust increase in *IRAK2* mRNA. This suggests that CHOP serves to enhance *IRAK2* mRNA, which is required to maintain IRAK2 protein levels during the saturated FFA stress. By contrast, knockdown of ATF4 did not affect induction of *IRAK2* mRNA in response to palmitate (Fig 3-15 B). These results suggest that CHOP, but not ATF4, is required for *IRAK2* expression following UPR activation by saturated FFA.

To determine the effects of IRAK2 on NF-κB following palmitate exposure, we knocked down IRAK2 in HepG2 with two different shRNAs and treated the cells with palmitate (Fig 3-16 A). Depletion of IRAK2 significantly lowered phosphorylation of p65 at serine 536 following palmitate exposure despite elevated CHOP levels, suggesting that IRAK2 is a CHOP-dependent protein kinase essential for NF-κB activation in hepatocytes following exposure to palmitate. Next we carried out a chemotaxis assay with the KG-1 cells utilizing the conditioned media from either shCTRL or shIRAK2 cells, and determined that depletion of IRAK2 impaired macrophage migration (Fig 3-16 B). Because we previously showed that IL-8 and TNFα are both required for macrophage chemotaxis following palmitate treatment, we measured their mRNA levels by qPCR in shCTRL and shIRAK2 cells (Fig 3-16 C-D). There was a sharp reduction in *CXL8* (IL-8)

and *TNFA* (TNFα) transcripts in shIRAK2 cells, consistent with lowered NF-κB activity. These results indicate that IRAK2 contributes to the initiation of an inflammatory response stemming from hepatocytes through activation of NF-κB.

To address the role of IRAK2 depletion on hepatocyte lipotoxicity, we evaluated cell death by LDH release in shIRAK2 cells following exposure to palmitate. Knockdown of IRAK2 rescued HepG2 cells from palmitate-induced cell death (Fig 3-16 E). Furthermore, to explore whether IRAK2 is required for the secretion of factors involved in hepatocyte cell death, we measured the viability of recipient shCHOP cells treated with conditioned media prepared from donor shIRAK2 cells exposed to palmitate (Fig 3-16 F). Knockdown of IRAK2 thwarted the ability of the conditioned medium to trigger death of the recipient shCHOP cells, supporting the idea that IRAK2 facilitates NF-κB-directed secretion that can trigger hepatocyte death.

CHOP is directly or indirectly required for induction of *IRAK2* mRNA in response to palmitate treatment, as well as for sustained IRAK2 protein levels (Fig 3-15 A-B and 3-16 A). However, there was no reproducible increase in the levels of IRAK2 protein in response to saturated FFAs. There was a sharp reduction in global translation in HepG2 cells treated with palmitate for 12 h (Fig 3-6 A). Lowered global initiation of protein synthesis, as judged by diminished polysomes coincident with increased monosomes, was also observed after 6 h of treatment with saturated FFAs (Fig 3-17 A). *ATF4* and *CHOP* mRNAs are preferentially translated in response to eIF2α~P, which can be visualized by the shift of either transcript from monosome to polysome fractions upon palmitate treatment (Fig 3-17 B-C). By contrast, in HepG2 cells treated with palmitate for either 6 or 12 h, the distribution of *IRAK2* mRNA was largely unchanged between the monosome and polysome fractions compared with nonstressed conditions (Fig 3-17 D-E). Note that in nonstressed conditions, the majority of *IRAK2* transcripts were in the largest polysome fraction, fraction 7, whereas upon exposure to palmitate for either 6 or

12 h, there was a shift of IRAK2 mRNA toward smaller polysome fractions. This distribution of *IRAK2* mRNA within polysome fractions suggests that there is lowered *IRAK2* mRNA translation in response to eIF2α~P and exposure to saturated FFAs, which provides an explanation for why IRAK2 protein was not significantly enhanced during palmitate treatment despite there being increased *IRAK2* mRNA. Together these results indicate that CHOP is required for hepatocytes to sustain elevated levels of IRAK2 protein upon exposure to saturated FFAs. Elevated levels of IRAK2 proteins are suggested to be required for activation of NF-κB and subsequent increased expression and secretion of cytokines, such as TNFα and IL-8, which are involved in cell death and inflammation. However, high levels of IRAK2 protein are not sufficient to induce NF-κB, suggesting that additional signals emanating from hepatocyte stress induced by saturated FFAs also contribute to the observed activation of NF-κB.

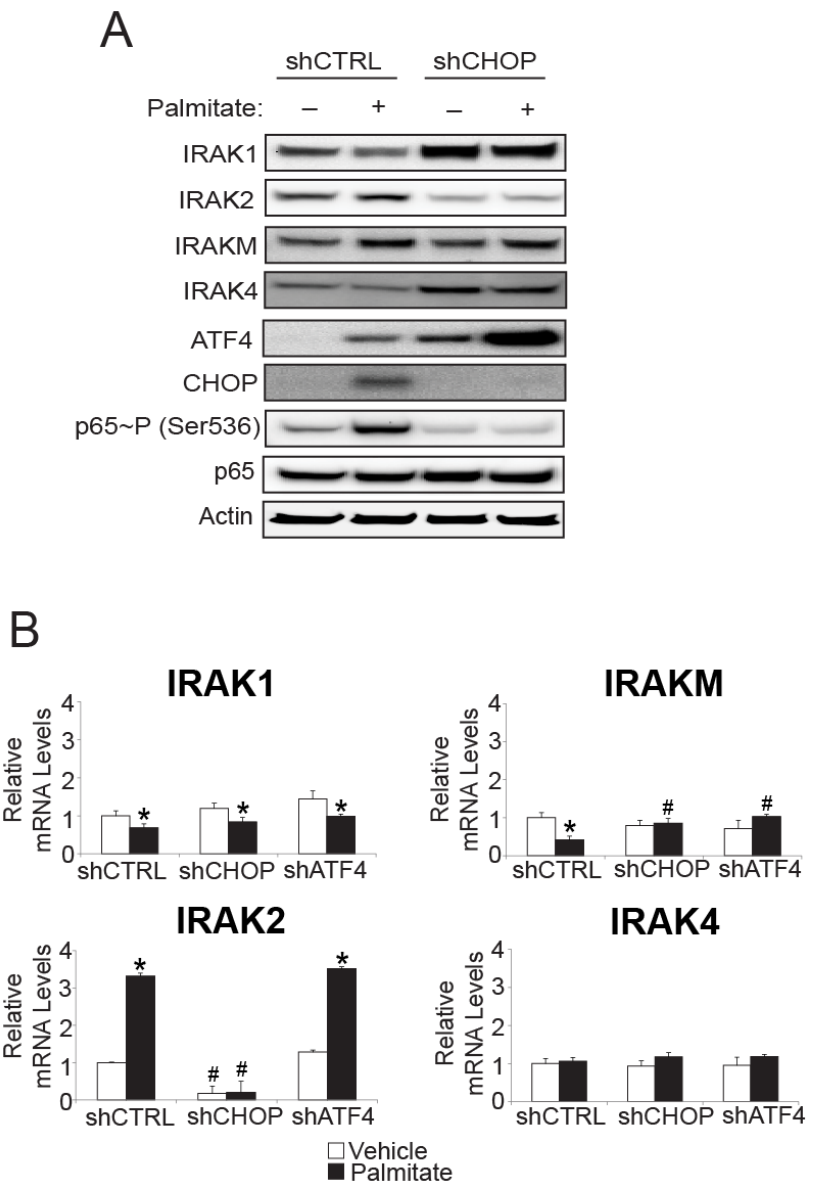

Figure 3-15. CHOP is required for *IRAK2* expression. HepG2 cells expressing shCTRL or shCHOP were cultured in the presence (+) or absence (-) of palmitate. (A) The indicated proteins from these cells were then measured by immunoblot analyses. (B) Levels of the indicated isoforms of *IRAK* mRNAs expressed in these cells were measured by qPCR.

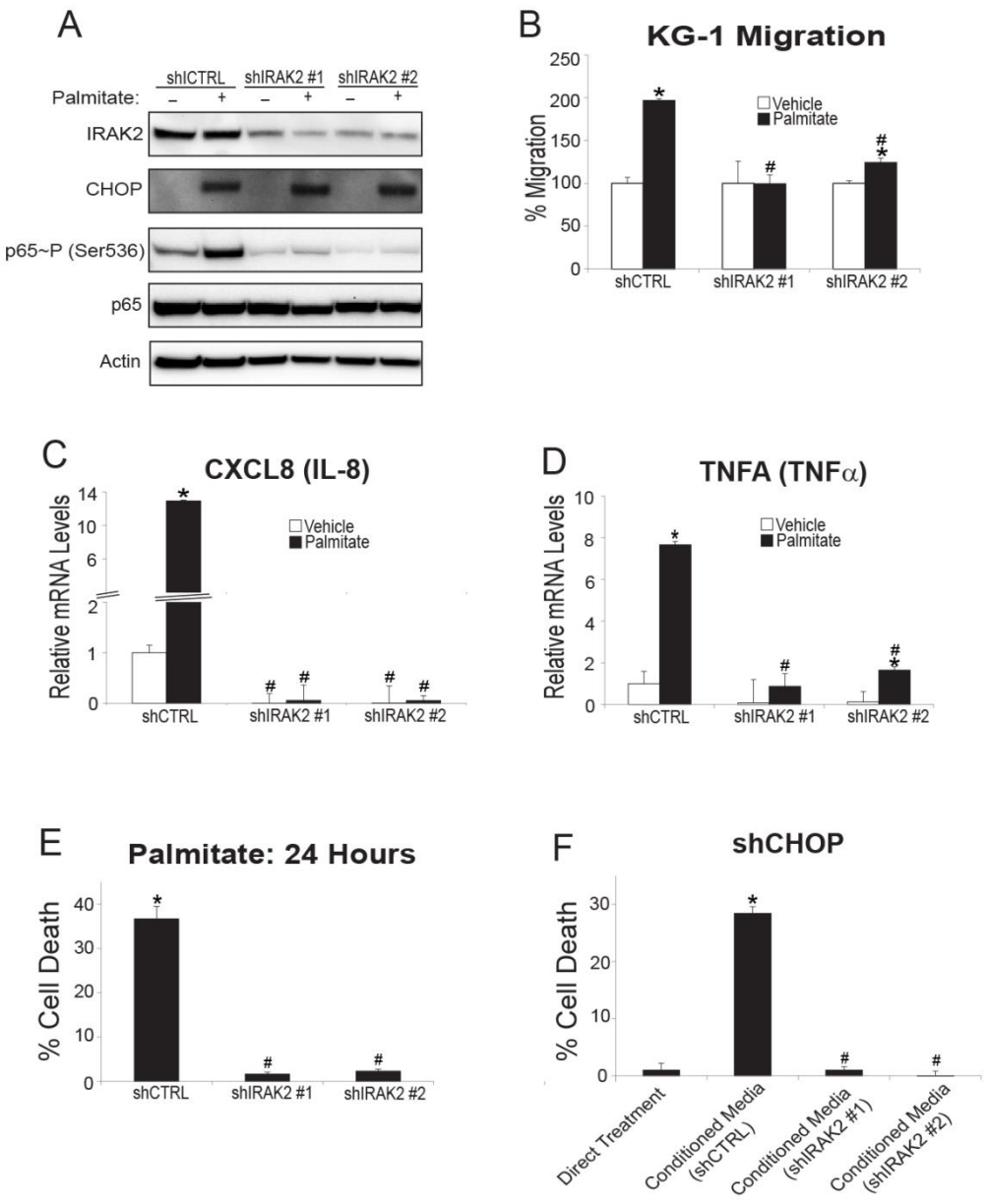

Figure 3-16. IRAK2 is required for palmitate-induced hepatotoxicity and cell migration. (A) The shCTRL HepG2 cells, or those expressing shIRAK2 were treated with either vehicle (-) or palmitate (+) for 12 hours, and the indicated proteins were measured by immunoblot analyses. (B) Cell migration assay for KG-1 cells using conditioned media prepared from shCTRL or shIRAK2 HepG2 cells that were treated with either vehicle or palmitate for 12 hrs. (C-D) The mRNA levels of *CXCL8* (IL-8) and *TNFA* (TNFα) were measured by qPCR in shCTRL and shIRAK2 HepG2 cells treated

with palmitate for 12 hours or vehicle. (E) HepG2 cell expressing shCTRL or shIRAK2 were cultured in the presence of palmitate for 24 hours and cell death was measured by LDH release. (F) Direct treatment indicates cell death as measured by LDH release of shCHOP cells incubated with palmitate for 24 hours. Alternatively, donor shCTRL or shIRAK2 HepG2 cells were incubated with palmitate for 12 hours. The conditioned medium was then applied to recipient shCHOP cells for 24 hours, and cell death was measured by LDH release.

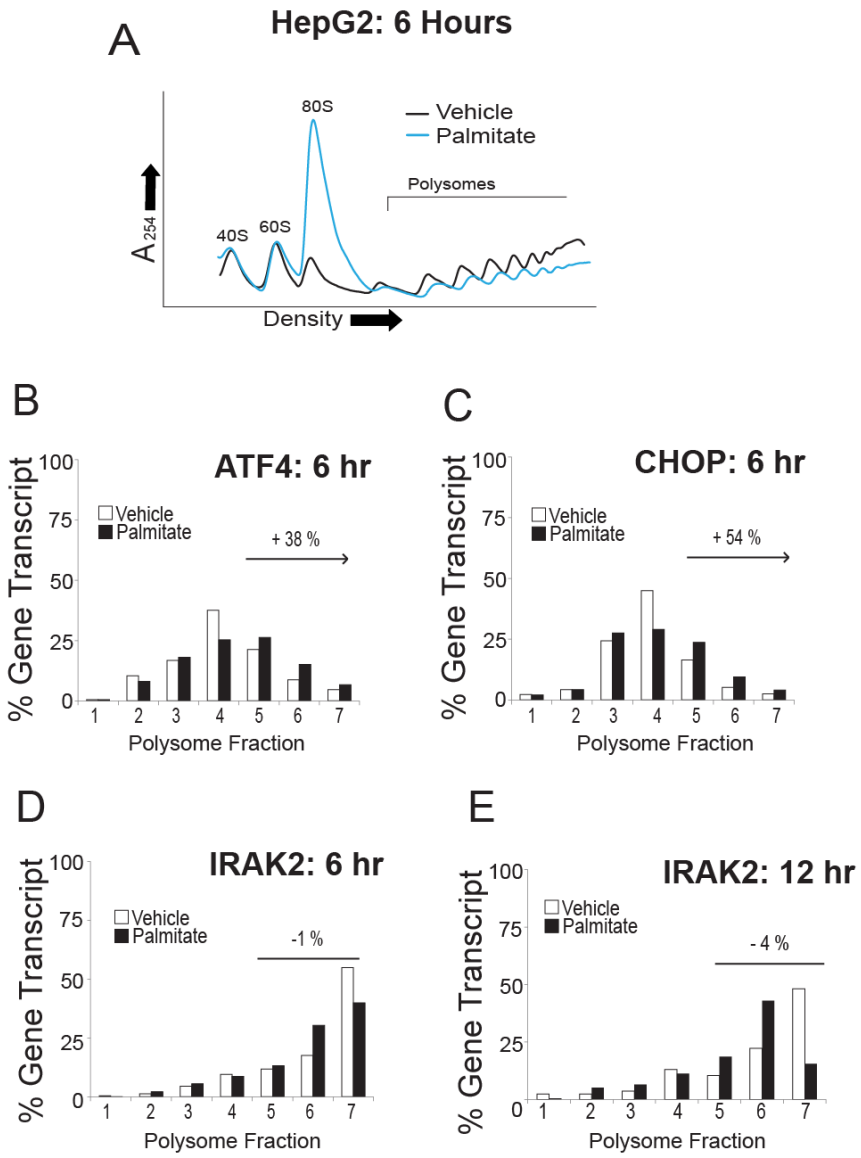

Figure 3-17. *IRAK2* exhibits reduced translation following eIF2α~P. (I) Polysome profiles of lysates prepared from HepG2 cells treated with palmitate or vehicle for 6 h. (J–L) Fractions were collected by the sucrose gradient analyses prepared from the HepG2 cells treated with palmitate or vehicle for 6 h, and the relative levels of the *ATF4*, *CHOP*, and *IRAK2* mRNA were then determined by qPCR for each fraction. The percentage of the total levels for the indicated gene transcript in each of the seven fractions is illustrated. The percentage change in the indicated mRNA association with

large polysomes (fractions 5–7) in response to palmitate is indicated above the polysome. For example, *ATF4* showed a 38% increase in transcript levels into fractions 5–7 during palmitate treatment. (M) A similar analysis was carried out for changes in *IRAK2* mRNA in polysome fractions in HepG2 cells treated with palmitate or vehicle for 12 h.

3.8 CHOP activates NF-κB in human but not mouse primary hepatocytes

Rodent models of NASH are often lacking in their ability to mimic the human disease [142, 143]. Earlier we showed differential affects between rodent and human hepatocytes with regards to lipotoxicity, suggesting a cell autonomous component for the species difference (Fig 3-1 A-D). Next we determined if there were also differences in NF-κB signaling and expression of cytokines following exposure to saturated FFA. Following 12 hours treatment with palmitate, mouse primary hepatocytes lacked the ability to activate NF-κB as judged by p65 phosphorylation of serine 536 (Fig 3-18 A). There was no induction of *IRAK2* mRNA in the mouse primary hepatocytes upon palmitate exposure and minimal IRAK2 protein expression (Fig 3-18 A). Although the UPR was activated in the mouse primary hepatocytes, as indicated by elevated CHOP levels, the inability of primary mouse hepatocytes to activate NF-κB resulted in no induction of *TNFA* mRNA (Fig 3-18 B). Because mice do not express *CXCL8*, we measured mRNA levels for *CXCL1* (KC) and *CXCL2* (MIP-2), murine paralogs for IL-8, and found that only MIP-2 was modestly induced following palmitate exposure (Fig 3-18 B). These results indicate that although the UPR can be activated in mouse hepatocytes exposed to palmitate, downstream NF-κB signaling appears to be unaffected by saturated FFA.

In contrast to primary mouse hepatocytes, we found that palmitate treatment of primary human hepatocytes led to activation of NF-κB, in combination with induction of

the UPR as supported by induction of CHOP mRNA and protein (Fig 3-19 A-B). Importantly, palmitate treatment of human primary hepatocytes increased p65 phosphorylation of serine 536 (Fig 3-19 A), along with increases in *IRAK2*, *TNFA* (TNFα) and *CXCL8* (IL-8) mRNAs (Fig 3-19 B). To understand the functional consequence of NF-κB activation in the primary cells, we carried out a chemotaxis assay with both human KG-1 and murine RAW cells utilizing conditioned media from HepG2, human primary hepatocytes, and mouse primary hepatocytes. We found that only HepG2 and human primary hepatocytes elicited migratory effects on the macrophage cell lines (Fig 3-20 A). Finally as noted earlier, saturated FFA triggered death of human primary hepatocytes, but not rodent hepatocytes (Fig 3-1 A-B). Together these results support the model that in human hepatocytes both CHOP and NF-κB are activated by palmitate, leading to production of TNFα and IL-8 that facilitate cell death and/or inflammatory responses.

Because there were such significant differences between NF-κB activation in cell death and inflammation in human primary hepatocytes compared to murine hepatocytes, we wanted to determine if secreted factors from human hepatocytes could trigger death of mouse hepatocytes. Conditioned media was prepared from donor shCTRL HepG2 cells treated with either vehicle or palmitate and applied to recipient mouse primary hepatocytes (Fig 3-20 B). There was only a modest increase, albeit significant, in mouse hepatocyte death with the palmitate containing conditioned media relative to control. Consistent with our earlier findings, palmitate treatment alone did not appreciably affect the viability of mouse hepatocytes. Finally, we prepared conditioned medium from donor mouse hepatocytes treated with palmitate, which was applied to shCTRL and shCHOP HepG2 cells. There was less death of these human hepatocytes than when palmitate alone was applied to the media (Fig 3-20 B). These results suggest that in addition to not

inducing NF-κB activity and secretion of target cytokines upon exposure to saturated FFA, mouse hepatocytes lack sensitivity to respond to these regulatory signals.

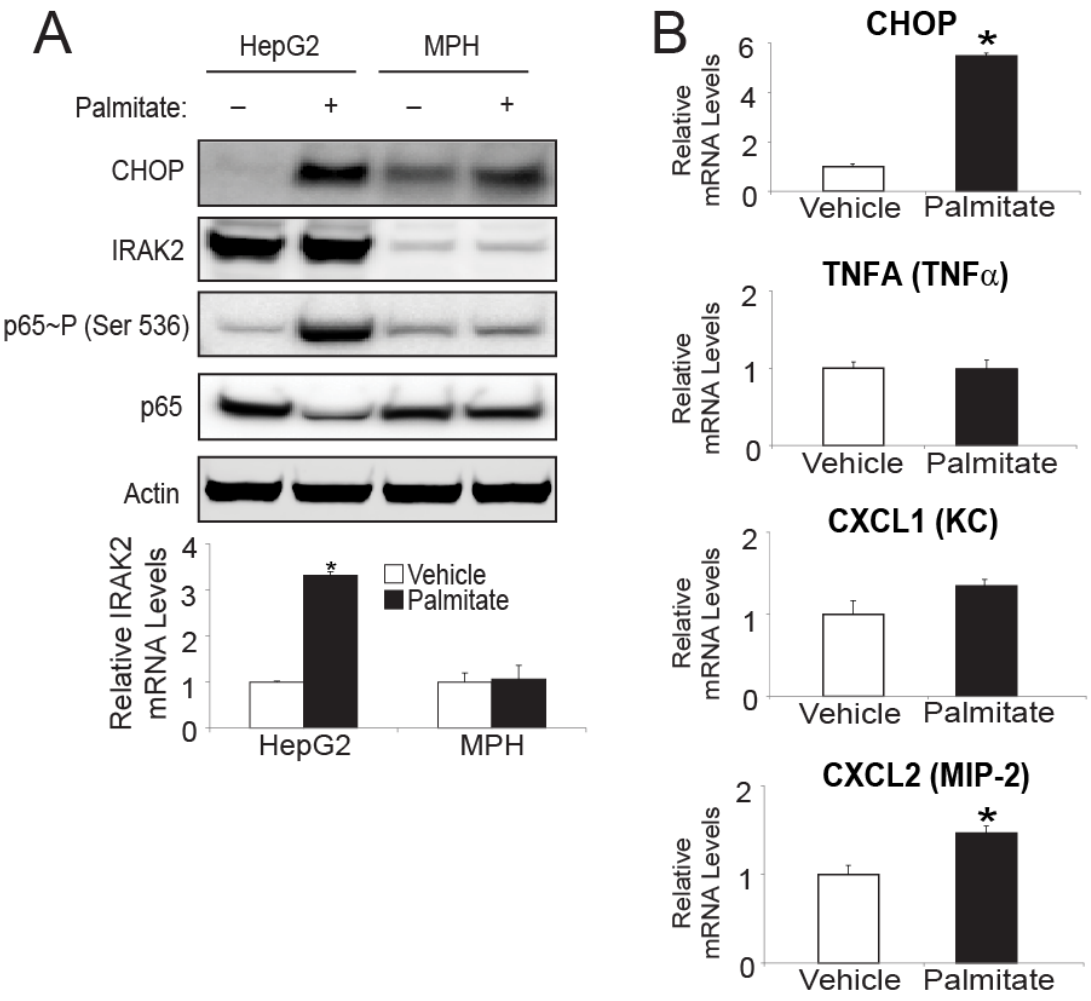

Figure 3-18. NF-κB is activated in HepG2 cells but not mouse primary hepatocytes following palmitate exposure. (A) Human HepG2 cells and mouse primary hepatocytes (MPH) were treated with palmitate for 12 hours, or vehicle, and the indicated proteins were measured by immunoblot analyses (Top). IRAK2 antibody from Abnova was used in the immunoblot analysis (see Fig S3A). In parallel, *IRAK2* mRNA was measured by qPCR in the HepG2 and mouse hepatocytes treated with palmitate for 12 hours (Bottom). (B) Levels of the indicated mRNAs were measured in mouse primary hepatocytes treated with palmitate for 12 hours.

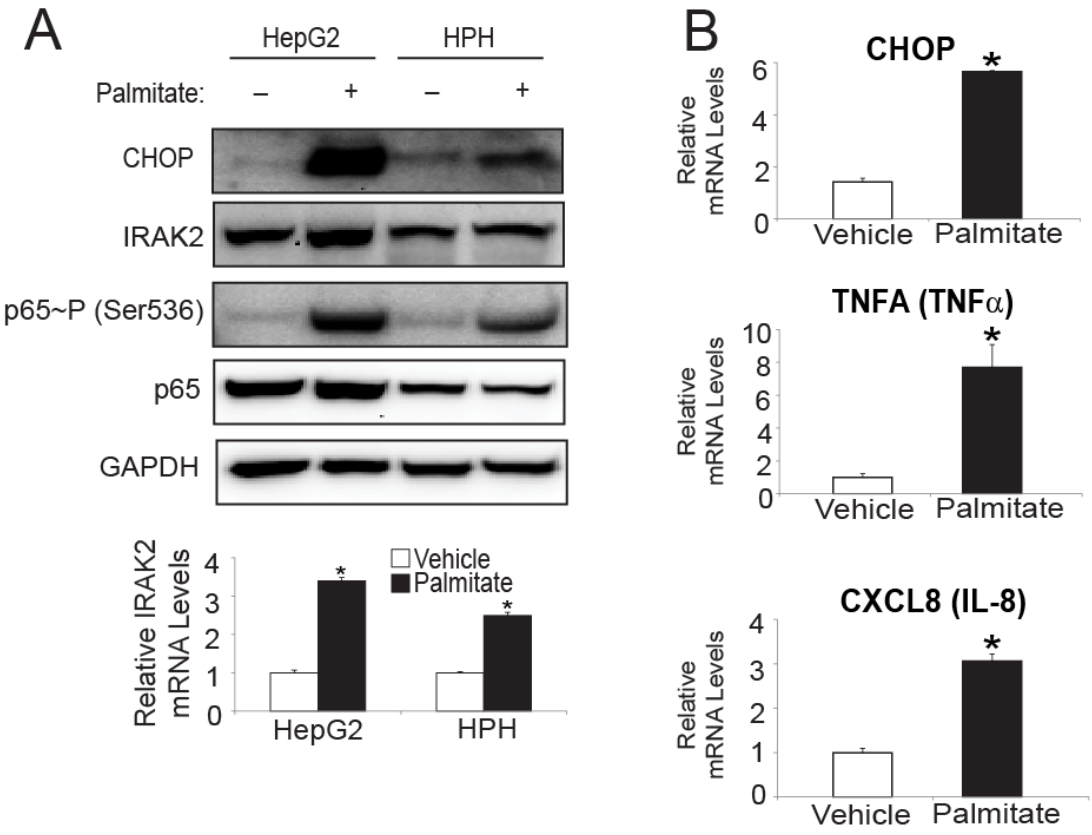

Figure 3-19. NF-κB is activated in primary human hepatocytes following palmitate exposure. (C) Human HepG2 cells and human primary hepatocytes (HPH) were treated with palmitate for 12 hours, or vehicle, and the indicated proteins were measured by immunoblot analyses (Top). Furthermore, *IRAK2* mRNA was measured by qPCR in the HepG2 and human hepatocytes (HPH) treated with palmitate for 12 hours (Bottom). (D) The indicated mRNA levels were measured in human primary hepatocytes treated with palmitate for 12 hours.

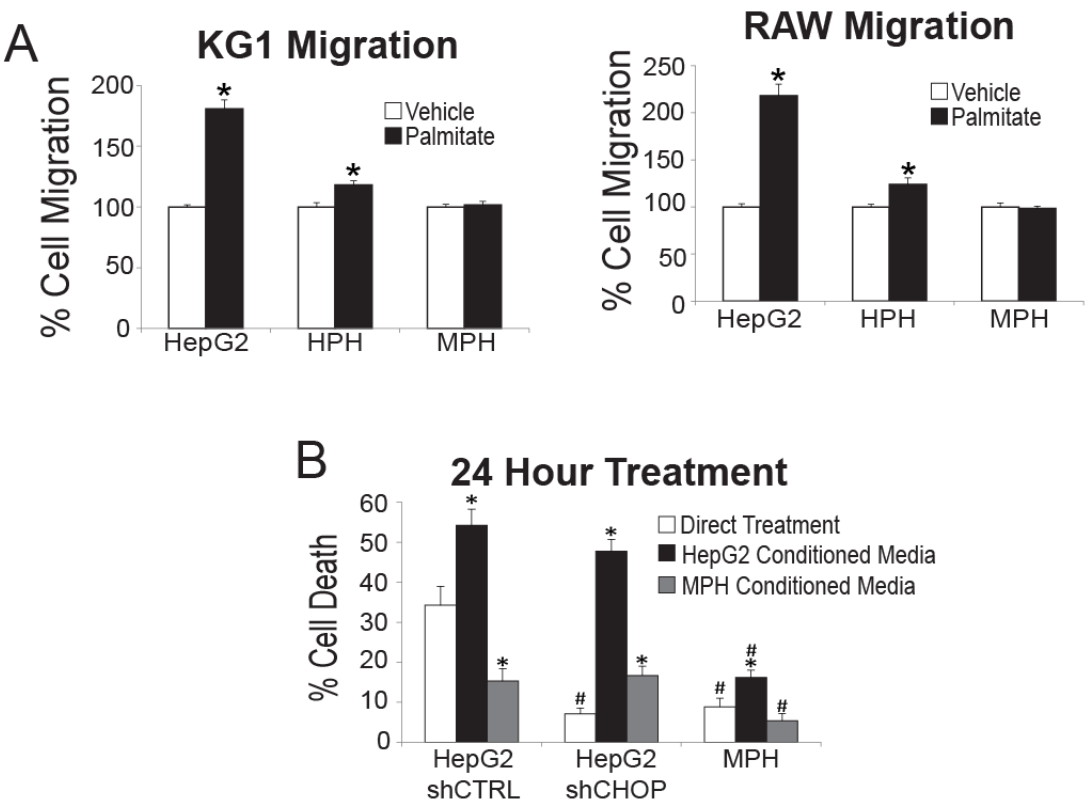

Figure 3-20. Mouse primary hepatocytes lack sensitivity to respond to cell death and cell migration signals following palmitate exposure. (A) Cell migration assay for human KG-1 and murine RAW cells using conditioned media prepared from HepG2, human primary hepatocytes (HPH), or mouse primary hepatocytes (MPH) treated with either vehicle or palmitate for 12 hours. (B) Direct treatment indicates cell death as measured by LDH release of shCTRL HepG2, shCHOP HepG2, or mouse primary hepatocytes (MPH) incubated with palmitate for 24 hours. Alternatively, conditioned medium was prepared from donor shCTRL HepG2 or MPH cells that were incubated with palmitate for 24 hours. The conditioned medium was then applied to recipient of shCTRL HepG2, shCHOP HepG2, or mouse primary hepatocytes for 24 hours, as indicated, and cell death was measured by LDH release.

3.9 Summary

Excess lipid accumulation is a hallmark of obesity, and lipotoxicity associated with saturated FFA has been suggested to result from activation of the UPR observed in hepatic steatosis [9]. This study suggests that activation of the UPR plays a pivotal role in the pathophysiology of NASH through elevated levels of the UPR and CHOP expression (Fig 3-21). Depletion of CHOP in human hepatocytes enhanced survival in response to saturated FFA (Fig 3-7 A-B), and CHOP-dependent secretion of key cytokines, including IL-8 and TNFα, have central roles in macrophage recruitment and hepatocyte lipotoxicity (Fig 3-10 and 3-11). CHOP is suggested to facilitate secretion of these factors in hepatocytes exposed to saturated FFA by enhancing phosphorylation of p65 at serine 536, triggering NF-κB entry into the nucleus and transcriptional expression of a collection of cytokines (Fig 3-12 and 3-21). CHOP induction of NF-κB involves in part signaling through IRAK2 protein (Fig 3-15, 3-16, and 3-17). IRAK2 has been linked with phosphorylation and activation of NF-κB [150-153], and CHOP is suggested to contribute to increased *IRAK2* mRNA in hepatocytes exposed to saturated FFAs; however, palmitate treatment is suggested to diminish *IRAK2* mRNA translation, which, as a consequence, leads to no significant change in IRAK2 protein compared with nonstressed conditions (Fig 3-15, 3-16, and 3-17). Depletion of either IRAK2 or RELA blocked induction of *CXCL8* (IL-8) and *TNFA* (TNFα) expression in response to palmitate, protecting hepatocytes against death and macrophage infiltration (Fig 3-16, and 3-21). These results suggest that whereas IRAK2 is required for CHOP activation of NF- κB in response to saturated FFA, increased levels of IRAK2 are not sufficient to induce NF-κB. Instead, other signals triggered by saturated FFAs contribute in conjunction with IRAK2 to induce NF-κB and secreted cytokines.

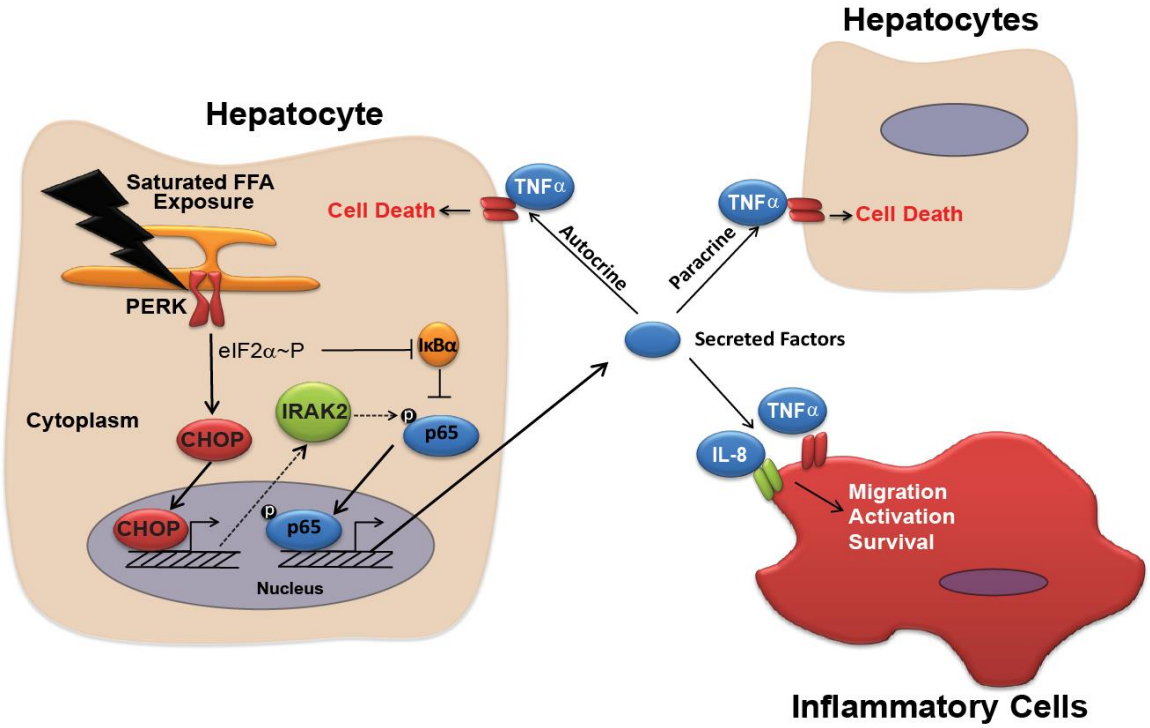

Figure 3-21. Model for UPR regulation during metabolic stress. (G) Model for CHOP and UPR regulation of hepatocyte inflammation and death signaling during metabolic stress. CHOP regulation of key secreted factors, including TNFα and IL-8, occurs by signaling through IRAK2 and NF-κB.

CHAPTER 4. RESULTS: IBTKα facilitates phagophore initiation and protein secretion

4.0 Introduction

NASH is associated with induction of the UPR and disruption of autophagic flux, but the mechanisms by which these processes contribute to the pathogenesis of human diseases are unclear. Herein we identify IBTKα as a novel member of the UPR, which associates with LC3b, SEC16A, and SEC31A, and plays a previously unrecognized role in phagophore initiation and protein secretion from endoplasmic reticulum exit sites. Depletion of IBTKα helped prevent accumulation of autophagosome intermediates stemming from exposure to saturated free fatty acids and rescued hepatocytes from death. Induction of IBTKα and the UPR, along with inhibition of autophagic flux, are associated with progression from steatosis to NASH in liver biopsies. These results demonstrate a novel function for IBTKα in NASH that links autophagy to the early secretory pathway through activation of the UPR.

4.1 IBTKα is a novel UPR member induced by saturated FFAs

To determine whether IBTKα is preferentially translated in human hepatocytes following metabolic stress, we treated human hepatoma HepG2 cells with the saturated FFA palmitate or thapsigargin, a pharmacological agent that potently induces ER stress. Following 6 hours of treatment, we performed polysome profiling (Figure 4-1 A). Both thapsigargin and palmitate resulted in a reduction of heavy polysomes coincident with accumulation of monosomes, indicative of lowered global translation initiation compared to vehicle treatment. *IBTK*α mRNA, as well as those encoding preferentially translated controls *ATF4* and *CHOP*, were then measured by comparing the percent of each gene transcript in each gradient fraction (Figure 4-1 B-C). After either stress treatment, there was a significant shift of *IBTK*α mRNA toward large polysomes compared to vehicle,

similar to the expected increase in the *ATF4* and *CHOP* transcripts. Interestingly, *IBTK*α was present in the heaviest polysome fractions 6 and 7 after either thapsigargin or palmitate treatment, whereas *ATF4* and *CHOP* were predominantly in polysome fractions 4, 5, and 6. This shift of the *IBTK*α mRNA to the heaviest polysome fractions is consistent with the fact that *IBTK*α has a longer coding sequence that can accommodate more translating ribosomes compared to *ATF4* and *CHOP*. HepG2 cells deleted for *PERK* (PERK-KO) by using CRISPR/Cas9 retained high levels of translation as viewed by heavy polysomes independent of stress (Figure 4-2 A-B) and showed only modest changes in fraction distributions of *IBTK*α, *ATF4*, or *CHOP* mRNAs (Figure 4-2 C-D). We conclude that PERK is required for repression of global protein synthesis, coincident with preferential translation of *IBTK*α and UPR members in human hepatocytes in response to ER stress triggered by lipotoxicity.

PERK and its downstream effector CHOP also trigger transcriptional expression of UPR target genes to alleviate stress or activate inflammation [23, 154]. To determine whether *IBTK*α expression was also regulated at the transcriptional level during treatment with palmitate, we generated *CHOP* knockout (CHOP-KO) HepG2 cells and exposed these cells along with WT to saturated FFAs or vehicle (Figure 4-3 A-B). *IBTK*α mRNA and protein were induced only in WT HepG2 cells treated with palmitate, whereas basal levels remained unchanged between WT and CHOP-KO cells. These results indicate that PERK activation and its downstream effector CHOP are also required for induced *IBTK*α mRNA expression in the UPR.

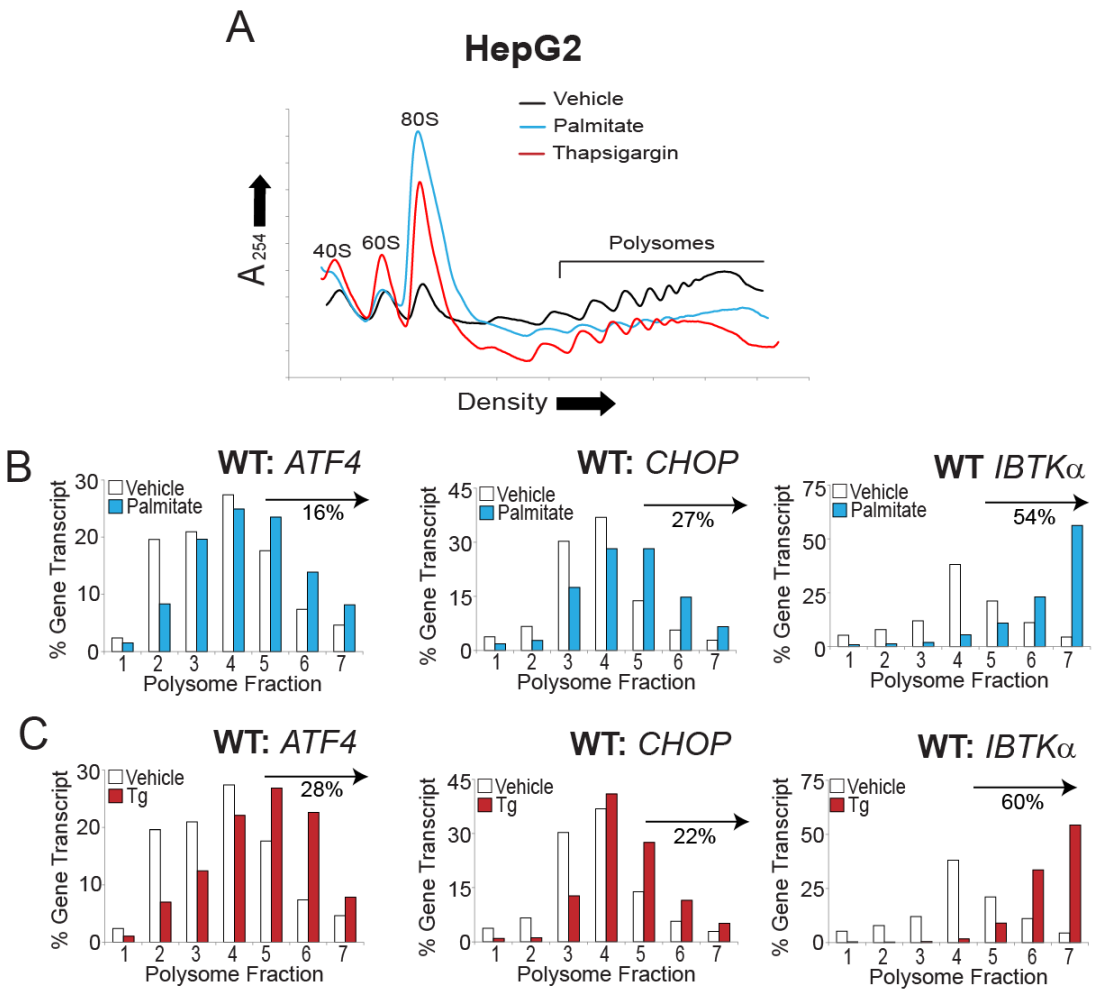

Figure 4-1. *IBTKα* is preferentially translated following palmitate exposure. (A) Polysome profiles of lysates prepared from HepG2 cells treated with palmitate, thapsigargin, or vehicle for 6 hours. (B-C) Following polysome analysis, fractions 1 through 7 were collected and the percentage of *ATF4*, *CHOP*, and *IBTK*α mRNA in each were quantified by qPCR and shown as a histogram. The percentage of the total gene transcripts in the heavy polysomes (fractions 5-7) for HepG2 treated with either palmitate or thapsigargin versus vehicle is indicated for each polysome profile.

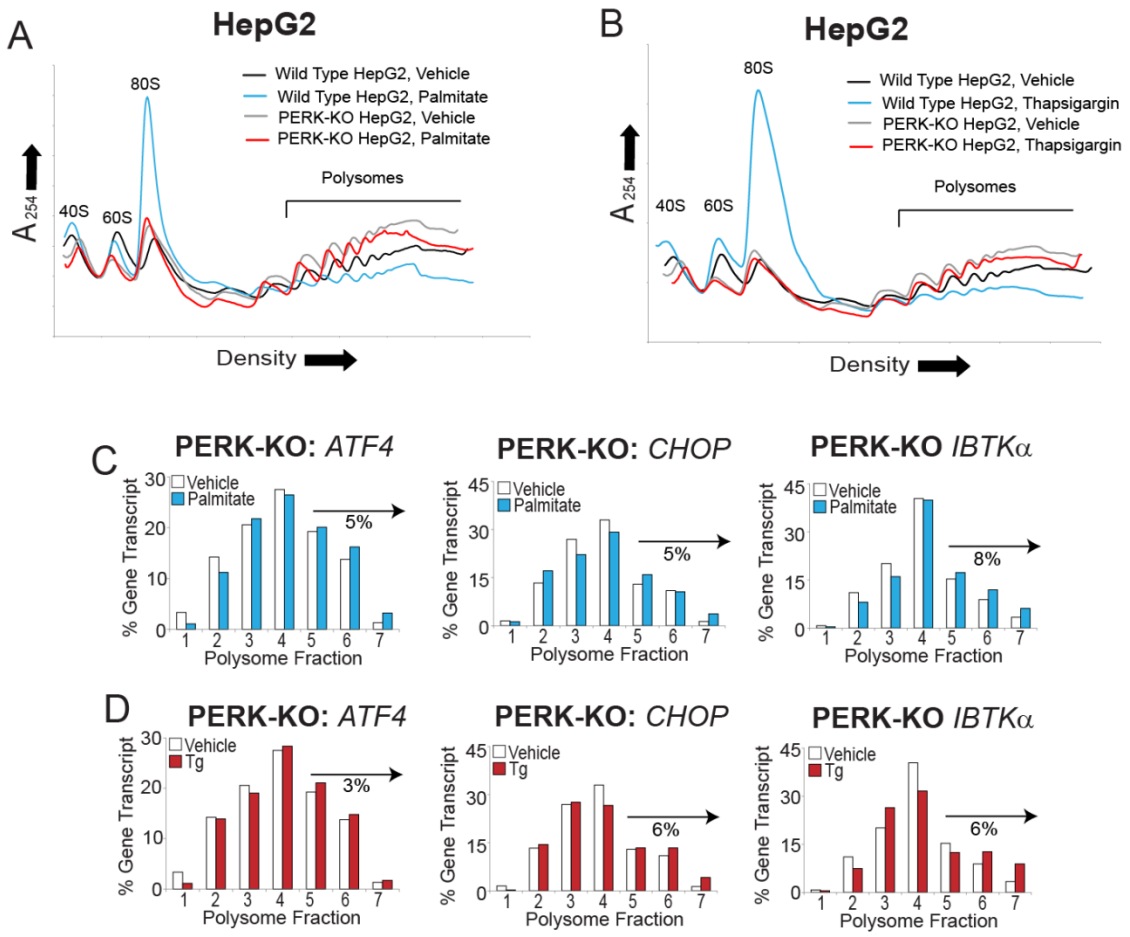

Figure 4-2. PERK induces preferential translation of *IBTKα* in response to ER stress. (A-B) Polysome profiles of lysates prepared from either HepG2 or PERK-KO HepG2 cells treated for 6 hours with palmitate, thapsigargin, or vehicle, as indicated. (C-D) Following polysome analysis, the percentage of *ATF4, CHOP, and IBTKα* mRNA distributed in fractions 1-7 were quantified by qPCR and are illustrated as histograms. The change in the percentage of each gene transcript in the heavy polysomes (fractions 5-7) for HepG2 treated with either palmitate or thapsigargin versus vehicle is indicated.

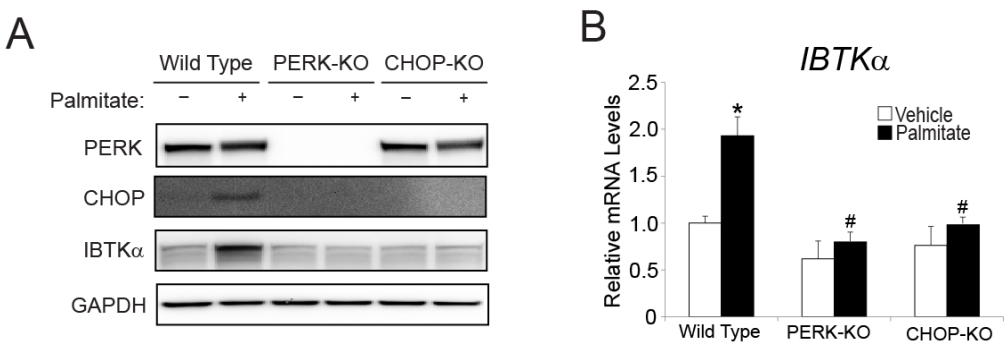

Figure 4-3. PERK and CHOP are required for induced IBTKα expression during ER stress. (A) WT, PERK-KO, or CHOP-KO HepG2 cells were treated with either vehicle (-) or palmitate (+) for 12 hours, followed by immunoblot analysis for the indicated proteins. (B) WT, PERK-KO, or CHOP-KO HepG2 cells were treated with either vehicle (-) or palmitate (+) for 12 hours, followed by qPCR measurements of *IBTKα* mRNA.

4.2 Saturated FFAs induce cell death through inhibition of autophagic flux

While it has been suggested that both apoptosis and autophagy are associated with lipotoxicity during NASH [2, 155], it is unclear whether either of these pathways play a direct role in hepatocyte death. To determine whether apoptotic pathways are involved, we investigated the role of capases in hepatocyte death during lipotoxicity by treating HepG2 cells with saturated and unsaturated FFAs, along with staurosporine and tunicamycin controls, either alone or in the presence of pan-caspase inhibitor ZVAD/FMK (Fig 4-4 A-E). Treatment with saturated FFAs palmitate and stearate produced a modest increase in caspase activity, but the addition of ZVAD/FMK did not rescue cell death. By contrast, ZVAD/FMK blocked both staurosporine-induced cell death and caspase 3/7 activation. Neither the unsaturated FFA oleate nor the canonical UPR activator tunicamycin resulted in appreciable cell death after 24 hours. During apoptosis, nuclear localization of cleaved caspase 3 is essential for breakdown of the

nuclear lamina and DNA fragmentation [156]. Whereas cleaved caspase 3 was localized predominantly to the nucleus after staurosporine treatment as judged by immunocytochemistry, total cleaved caspase 3 was reduced and retained in the cytoplasm with the addition of ZVAD/FMK (Fig 4-5). By contrast, the low levels of caspase 3 activation determined during treatment with saturated FFAs were coincident with caspase 3 being retained in the cytoplasm. These results indicate that apoptosis is not the predominant mode of hepatocyte death following exposure to saturated FFAs.

Inhibition of autophagic flux is linked with NASH in human patients [50, 134]. To determine if autophagy was associated with activation of the UPR, induction of IBTKα, and cell death, we treated HepG2 cells with saturated or unsaturated FFAs for up to 24 hours and measured key markers of UPR activation as well as LC3b and p62/SQSTM1 to assess changes in autophagy (Fig 4-6). Increased levels of ATF4 and IBTKα proteins were noted by 3 hours after treatment with palmitate and 6 hours of tunicamycin, prior to induction of CHOP. Furthermore, palmitate and stearate triggered accumulation of lipidated LC3b-II and p62, suggesting that saturated FFAs either induced autophagy or, alternatively blocked autophagic flux. Oleate had only a modest effect on the UPR and did not alter the autophagic markers, whereas treatment with tunicamycin led to potent induction of the UPR and increased LC3b-II but produced only a transient increase in p62.

To determine whether saturated FFAs induce the UPR and interfere with autophagic flux, we expressed N-terminal GFP-LC3b in HepG2 cells and assessed its co-localization with lysosomes by staining with LAMP2 (Fig 4-7 A). First we treated the HepG2 cells with chloroquine, which inhibits proteolysis in the lysosome and hence stabilizes LC3b; 75% of GFP-LC3b was colocalized with the lysosomal marker LAMP2, indicating that autophagosomes were properly trafficked to the lysosomes. By contrast, treatment with palmitate disrupted autophagosome trafficking to the lysosome, with only

10% of GFP-LC3b being co-localized with LAMP2 despite a robust induction of autophagy. These results clearly indicate that treatment with palmitate leads to a block in autophagic flux, which would impair proper trafficking of damaged macromolecules and organelles to the lysosome for degradation.

Does disruption in the autophagic process play an active role in hepatocyte death upon exposure to saturated FFAs? We treated HepG2 cells with palmitate alone or in combination with agents that disrupt either autophagy initiation (3-methyladenine) or lysosomal function (chloroquine or bafilomycin A1) and measured cell death (Fig 4-7 B-C). To determine if this mechanism was relevant to human hepatocytes, we also repeated the experiment with primary human hepatocytes. Addition of 3-methyladenine, which prevents induction of autophagy by inhibiting PI3K, increased the survival of both HepG2 cells and primary human hepatocytes, whereas the lysosome inhibitors resulted in increased death of HepG2 cells. Human primary hepatocytes were more sensitive to palmitate induced cell death (>80% compared to 30% in HepG2), therefore adding chloroquine and bafilomycin A1 did not increase cell death further. These results suggest that inhibition of autophagic flux, rather than inhibition of phagophore formation per se plays an important role in palmitate-induced hepatotoxicity (Fig 4-8).

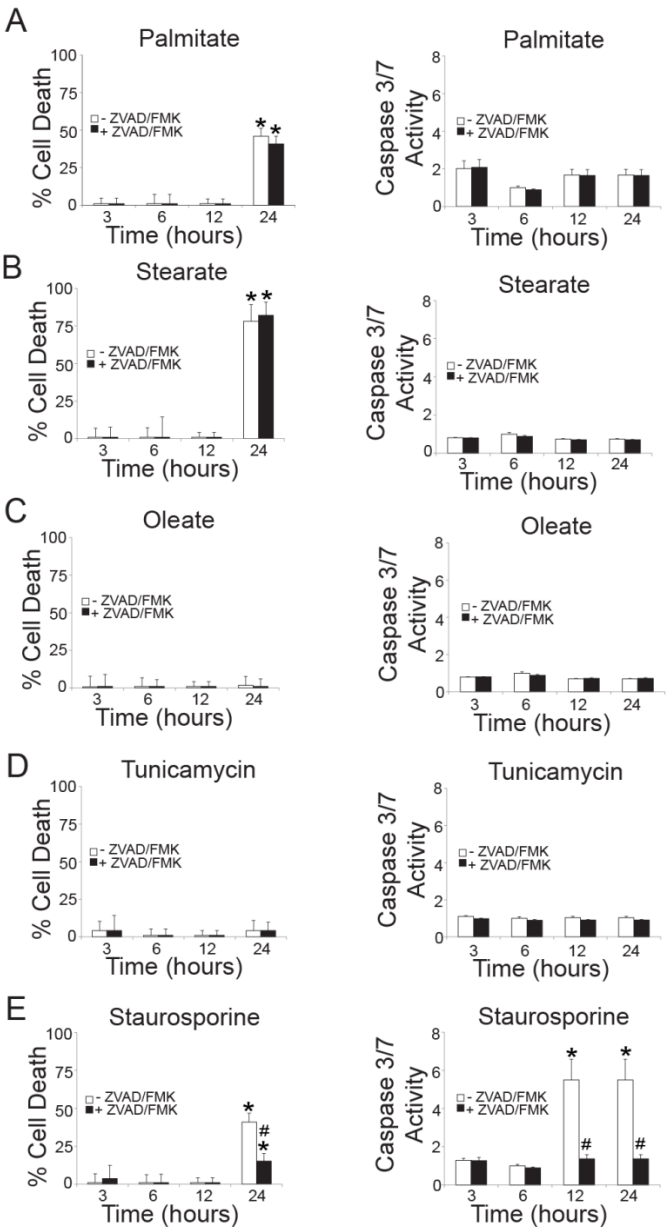

Figure 4-4. Saturated FFAs induce cell death in a caspase-independent manner. (A-B) HepG2 cells were treated palmitate, stearate, oleate, tunicamycin, or staurosporine in the presence or absence of 20 μM ZVAD/FMK for up to 24 hours and cell viability was determined by LDH release and caspase 3/7 activity was measured using Apo-ONE biochemical assay.

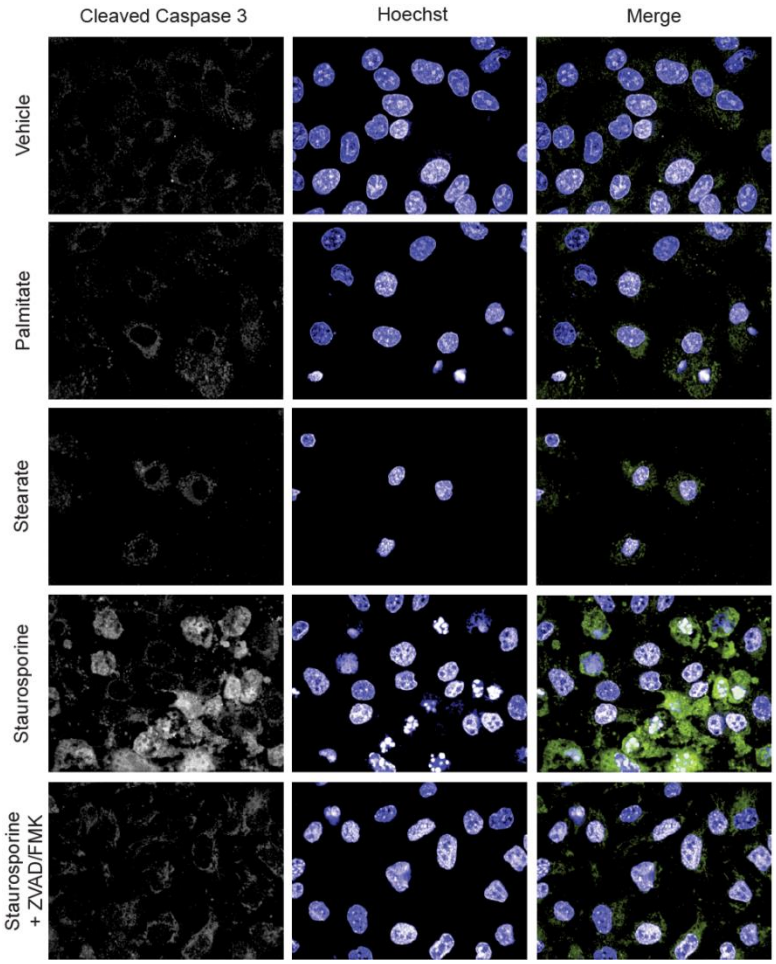

Figure 4-5. Cleaved caspase 3 is not localized to the nucleus by saturated FFAs. Sub-cellular localization of cleaved caspase 3 and DNA integrity was visualized using immunofluorescence microscopy in HepG2 cells treated with vehicle, palmitate, staurosporine, or staurosporine + ZVAD/FMK for 24 hours.

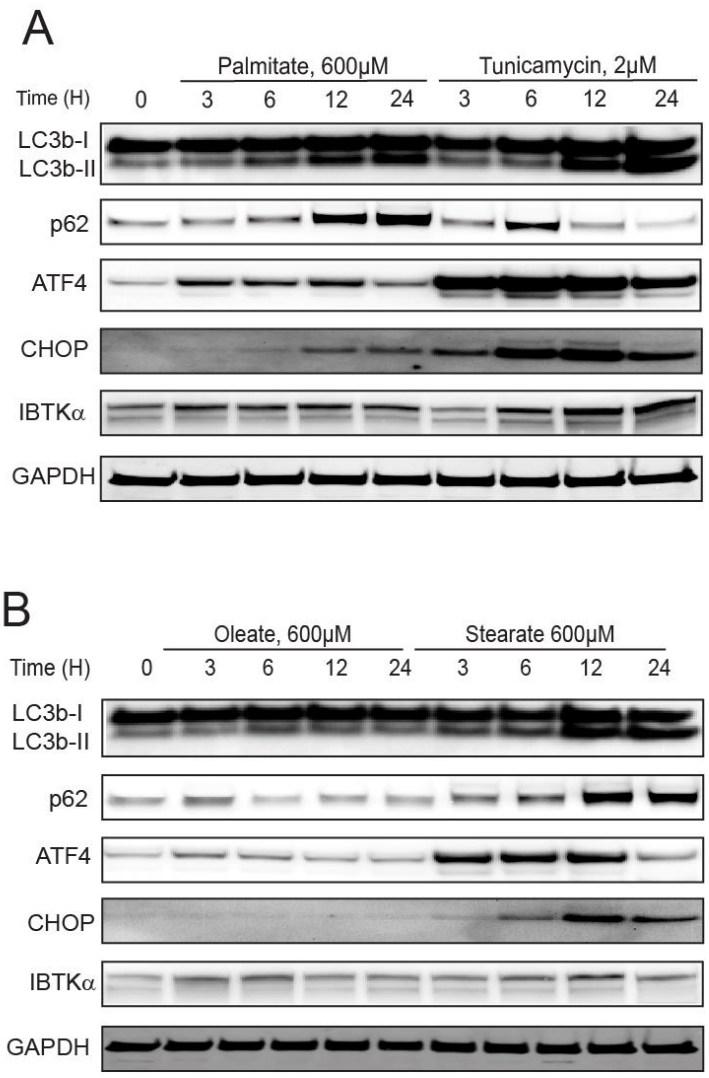

Figure 4-6. Saturated FFAs but not unsaturated FFAs induce inhibition of autophagic flux. (A-B) HepG2 cells were treated for 24 hours with palmitate, tunicamycin, oleate, or stearate and the indicated proteins were measured by immunoblot analyses.

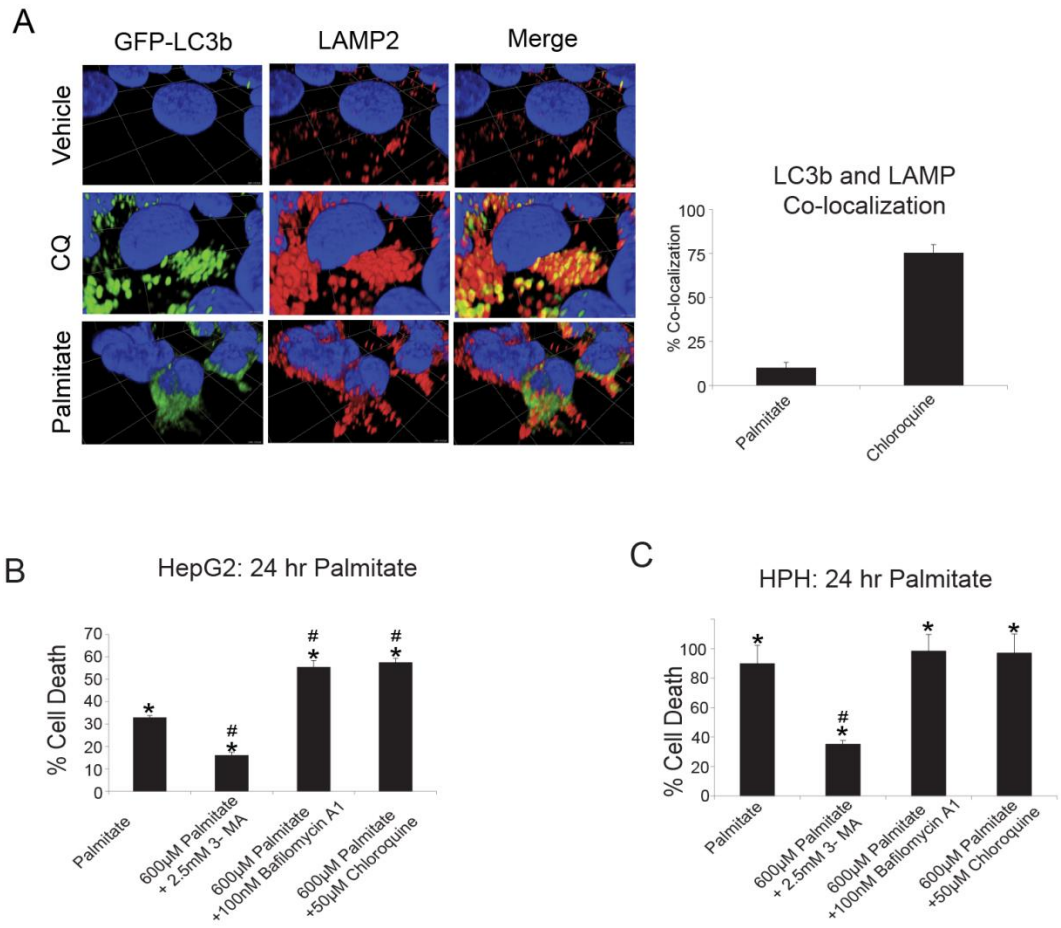

Figure 4-7. Saturated FFAs cause hepatocyte cell death through an autophagy-dependent mechanism. (A) HepG2 cells stably transduced with GFP-LC3b were treated with vehicle, chloroquine (CQ), or palmitate, and co-localization with LAMP2 was visualized using immunofluorescence microscopy and quantified at the pixel level. (B-C) HepG2 and primary human hepatocytes (HPH) were treated for 24 hours and viability was assessed using LDH release.

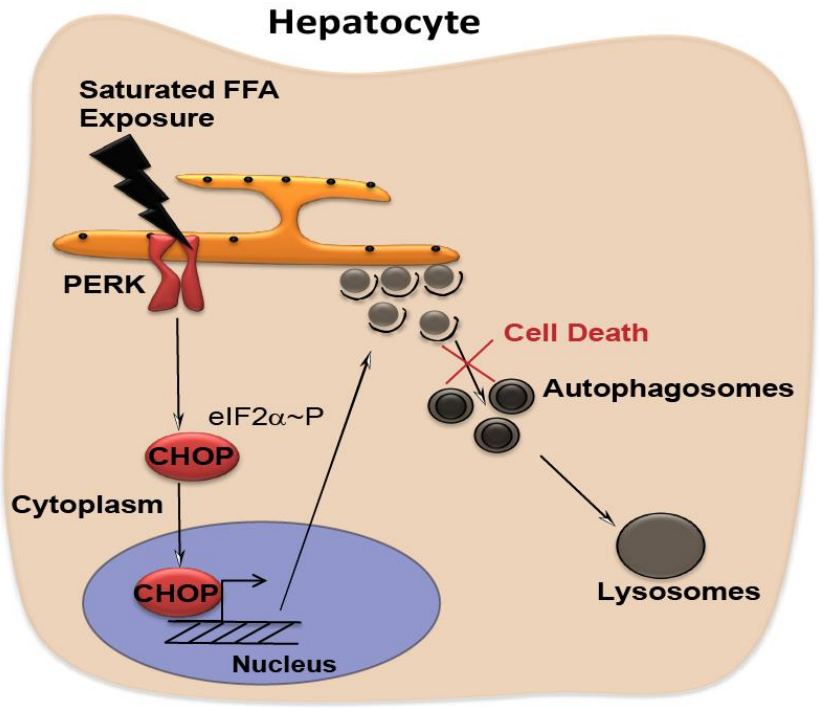

Figure 4-8. Model for saturated FFA-induced cell death. Model detailing the mechanisms for how a block in autophagic flux by palmitate can lead to hepatocyte death.

4.3. IBTKα is required for autophagosome formation and sensitizes hepatocytes to lipotoxicity

To address the hypothesis that IBTKα regulates cell survival by induction of autophagy, we generated IBTKα knockdown (shIBTKα) HepG2 cells using shRNA. Both shIBTKα and control (shCTRL) cells were assayed for accumulation of LC3b in the presence or absence of bafilomycin A1 or chloroquine (Fig 4-9 A). Depletion of IBTKα resulted in a loss of conversion of LC3b-I to LC3b-II, as well as a lack of accumulation of p62 upon treatment with either bafilomycin A1 and chloroquine. These results suggest that IBTKα is not only a downstream UPR target but is also an essential effector in a pathway leading to the induction of autophagy prior to LC3b lipidation.

Because we previously showed that inhibition of phagophore initiation rescued hepatocytes from lipotoxicity (Fig 4-7 B-C), we asked whether depletion of IBTKα would also rescue hepatocytes from palmitate induced cell death. To test this idea, we depleted HepG2 cells for *IBTK*α or *CHOP* using shRNA and measured key stress and autophagy protein levels in addition to cell death following palmitate treatment (Fig 4-9 B-C). As a control, we also characterized HepG2 cells depleted for ATG5, a factor known to be required for formation of autophagosomes. Following palmitate exposure, each of the three knockdowns resulted in decreased conversion of LC3b-I to LC3b-II, coincident with rescue from cell death. Corresponding mRNA measurements of the *IBTK*α-depleted cells indicated that while *IBTK*α mRNA was reduced as expected, *CHOP* and its known transcriptional target genes *MAP1LC3B* and *SQSTM1* were not affected, suggesting that IBTKα is a unique downstream effector in the UPR (Fig 4-10). Of note, mTORC1 remained repressed in all knockdowns following palmitate treatment, as measured by phospho-S6K, yet autophagy was not induced. These findings indicate that IBTKα is required for the induction of autophagy during activation of the UPR by lipotoxicity, and depletion of IBTKα or its upstream regulator CHOP rescue hepatocytes from exposure to saturated FFAs.

We next investigated effects at the ultrastructural level by electron microscopic evaluation of WT, CHOP-KO, and IBTKα-KO HepG2 cells treated with bafilomycin A1, palmitate, or vehicle (Fig 4-11). Deletion of *IBTK*α in cells in the absence of stress resulted in loss of ER organization and an accumulation of damaged mitochondria (Fig 4-11 C). Bafilomycin A1 or palmitate treatment of IBTKα-KO cells, but not control cells, led to dilation of the ER, suggesting that IBTKα is important for ER organization and general trafficking in the adaptive response to ER stress. WT HepG2 cells treated with bafilomycin A1 showed accumulation of large autophagolysosomes (Fig 4-11 A); however, no autophagosomes were present in either CHOP-KO or IBTKα-KO HepG2

cells treated with bafilomycin A1 (Fig 4-11 B-C). Exposure of WT HepG2 cells to palmitate also resulted in the appearance of lipid vacuoles throughout the cytoplasm, but a lack of autophagolysosomes, consistent with the observation that there was aberrant LC3b trafficking to the lysosome (Figure 3H). By comparison, treatment of CHOP-KO and IBTKα-KO cells with palmitate resulted in decreased amounts of neutral lipid accumulation, still without the appearance of autophagosomes (Fig 4-11 B-C). These results support the idea that the UPR plays a direct role in phagophore formation through a signaling pathway involving CHOP and IBTKα.

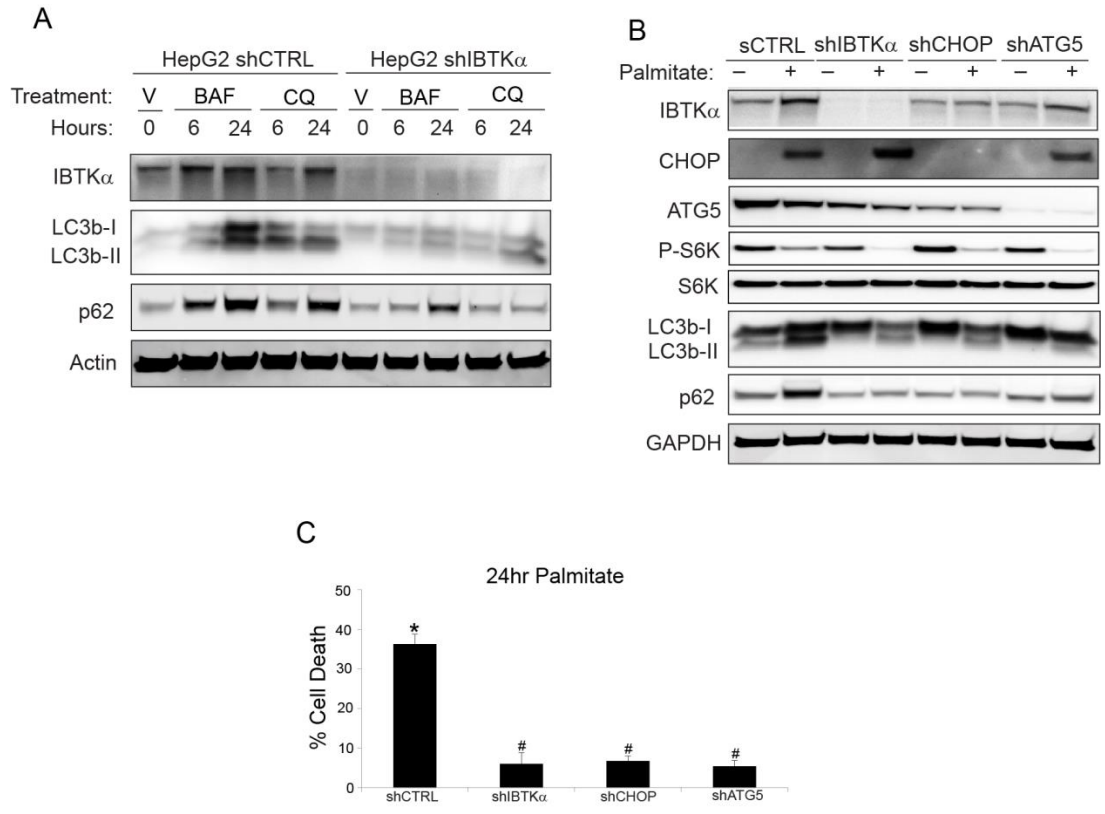

Figure 4-9. IBTKα facilitates phagophore induction. (A) shCTRL and shIBTKα HepG2 cells were treated with vehicle (V), bafilomycin A1 (BAF), or chloroquine (CQ) for up to 24 h and the indicated proteins were measured by immunoblot analyses. (B) shCTRL, shIBTKα, shCHOP, and shATG5 HepG2 cells were treated with either vehicle (-) or palmitate (+) for 12 hours, and the indicated proteins were measured by immunoblots. (C) shCTRL, shIBTKα, shCHOP, and shATG5 HepG2 cells were treated with palmitate or vehicle for 24 h and viability was measured by LDH release.

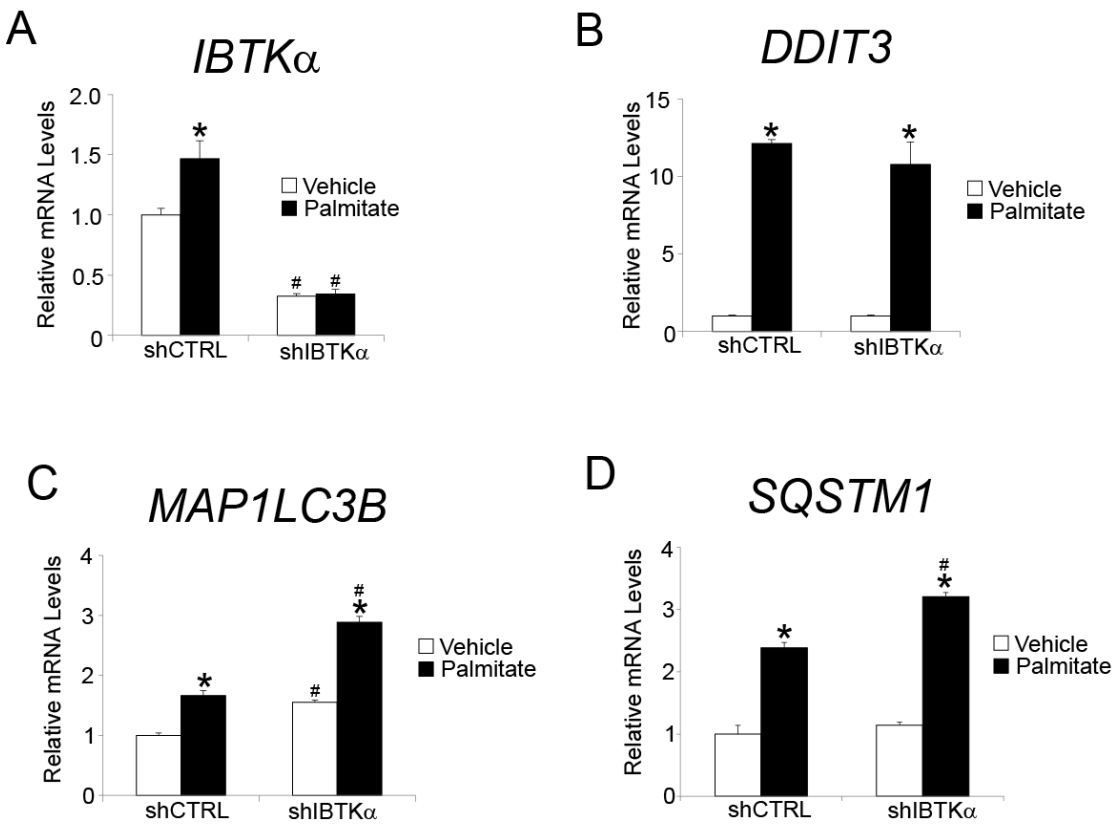

Figure 4-10. IBTKα does not prevent expression of *MAP1LC3B* or *SQSTM1.* (A-D) shCTRL and shIBTKα HepG2 cells were treated with palmitate or vehicle for 12 hours and the indicated gene transcripts were measured by qPCR.

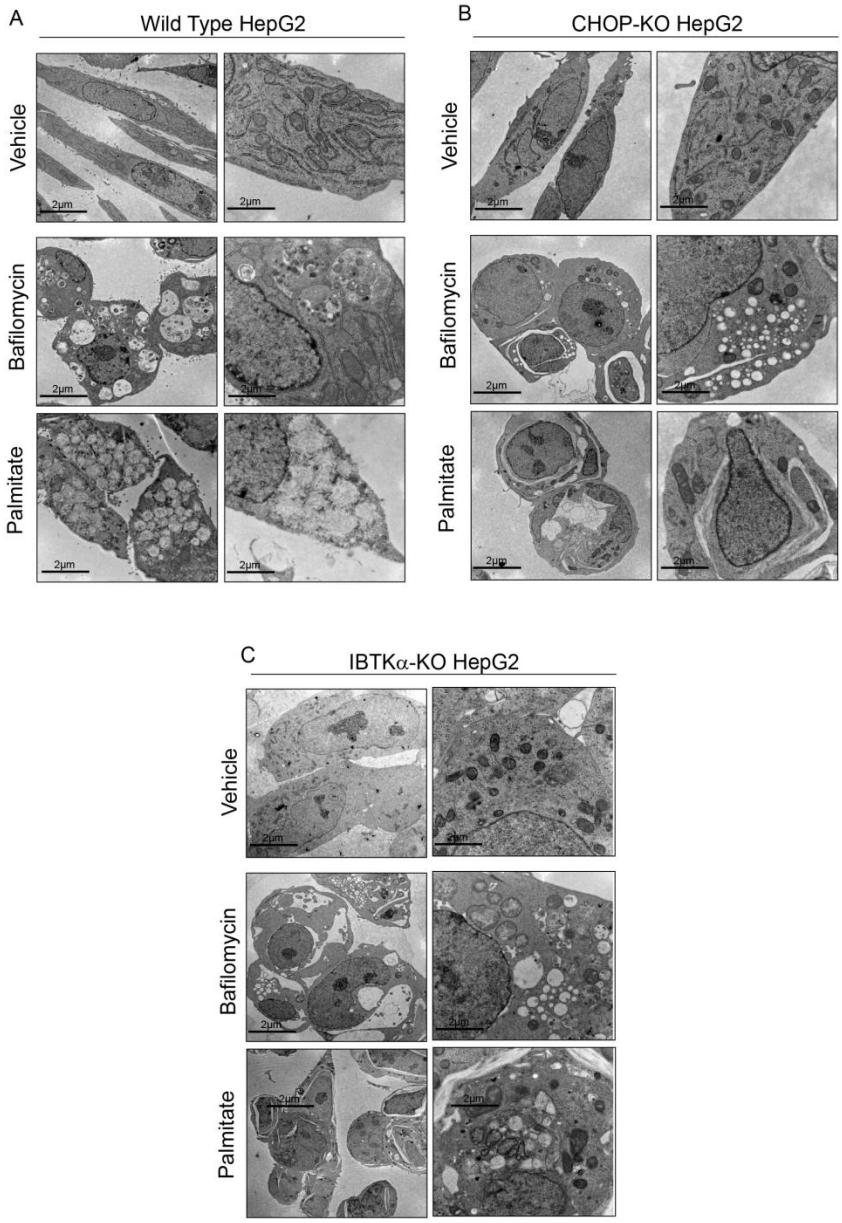

Figure 4-11. Deletion of CHOP and IBTKα prevents induction of autophagy at the ultrastructural level. (A-C) Electron microscopy showing ultrastructural features of WT, CHOP-KO, and IBTKα-KO HepG2 cells treated with vehicle, bafilomycin A1, or palmitate for 12 hours.

4.4 IBTKα induces autophagy by binding to a multisubunit protein complex including LC3b at the ERES

Phagophores have been suggested to form at the ER [157]. Because both phagophore induction and ER morphology are dependent upon IBTKα (Fig 4-9 and 4-11), we wanted to test the hypothesis that IBTKα is central for phagophore formation at the ER. We first utilized immunocytochemistry to determine the cellular location of IBTKα in WT HepG2 cells treated with chloroquine, palmitate, or vehicle, by staining for endogenous IBTKα (Fig 4-12 A). IBTKα was primarily co-localized with the ER marker calenxin independent of stress. To assess whether IBTKα is also located at the site of autophagosome formation, we used GFP-LC3b HepG2 cells and followed a similar experimental design. IBTKα co-localized with only 5% of LC3b in both the vehicle and chloroquine treated cells (Fig 4-12 B). However upon treatment with palmitate, which would block autophagic flux, IBTKα co-localized with 90% of LC3b. These findings indicate that IBTKα co-localizes with phagophores initiating while resident at the ER, but not with mature autophagosomes at the lysosome.

To better understand the mechanism by which IBTKα is involved in phagophore initiation at the ER membrane, we treated WT HepG2 cells with palmitate, thapsigargin, chloroquine, or vehicle and carried out an immunoprecipitations using antibody specific for endogenous IBTKα. Isolated proteins were then digested with trypsin, followed by mass spectrometry using multidimensional protein identification technology (MudPIT) (Fig 4-12 C-D & Appendix 1). Technical replicate RAW data files were pooled for FASTA database searching using SEQUEST, and the resulting dataset was filtered to require a false discovery rate of ≤1%. SAINT analysis was performed using the SAINT-express algorithm to identify proteins that displayed significant association with IBTKα prepared from WT cells compared to affinity carried out using IgG control pull-downs. A total of 73 proteins were identified that met the SAINT probability score of ≥0.8. Of interest among

proteins pulled-down with IBTKα with the greatest degree of confidence were SEC16A and SEC31A, two essential proteins situated in the ERES, with functions in COPII-vesicle trafficking and proposed roles in phagophore initiation [100]. The pull-down results were consistent with the notion that IBTKα is part of a larger complex that plays a role in phagophore formation at the ERES.

To determine if the IBTKα binding partner SEC16A also plays a direct role in phagophore formation and lipotoxicity, we treated HepG2 cells depleted for *SEC16A* expression with either palmitate or vehicle and measured changes in conversion of LC3b-I to LC3b-II as well as cell death (Fig 4-13 A-B). Depletion of SEC16A decreased initiation of autophagy coincident with enhanced resistance to lipotoxicity. Additionally, immunocytochemical analyses of the SEC16A-depleted cells HepG2 cells revealed an altered ER morphology and consequent changes in the pattern of IBTKα localization (Fig 4-13 C). These results indicate that SEC16A is important for ER organization, IBTKα localization, and induction of autophagy.

To further confirm whether IBTKα associates with SEC16A and LC3b, we treated WT HepG2 cells with thapsigargin, chloroquine, or palmitate, and then immunoprecipated IBTKα, followed by immunoblot analyses of associated proteins (Fig 4-14 A). We found that independent of stress, IBTKα was complexed with LC3b, along with SEC16A, and ULK1/2, which has been suggested to interact directly with LC3b at the ERES and be essential for phagophore formation [100, 101, 158]. These same protein interactions were observed using reciprocal SEC16A pull-downs, and loss of *SEC16A* expression resulted in disruption of the IBTKα complex (Fig 4-14 B-C). These findings suggest that IBTKα associates with a complex including SEC16A, and that this complex is essential for recruitment of a key phagophore inducing complex involving LC3b and ULK1/2. While IBTKα can be bound to this multisubunit complex independent

of stress as judged by pull-down experiments, exposure to saturated FFAs enhance expression of IBTKα and the localization of this complex to ERES.

To further test whether IBTKα associates with SEC31A and to identify additional members of the complex, we immunoprecipitated IBTKα from HepG2 cells treated with palmitate or vehicle, followed by immunoblot analyses of the bound proteins. IBTKα associated with SEC31A, CUL3, along with LC3b independent of treatment with saturated FFAs (Fig 4-14 D-F). However, reciprocal pull down of SEC31A indicated that LC3b is not part of this complex, suggesting that IBTKα can associate with distinct complexes at the ERES that participate in phagophore initiation.

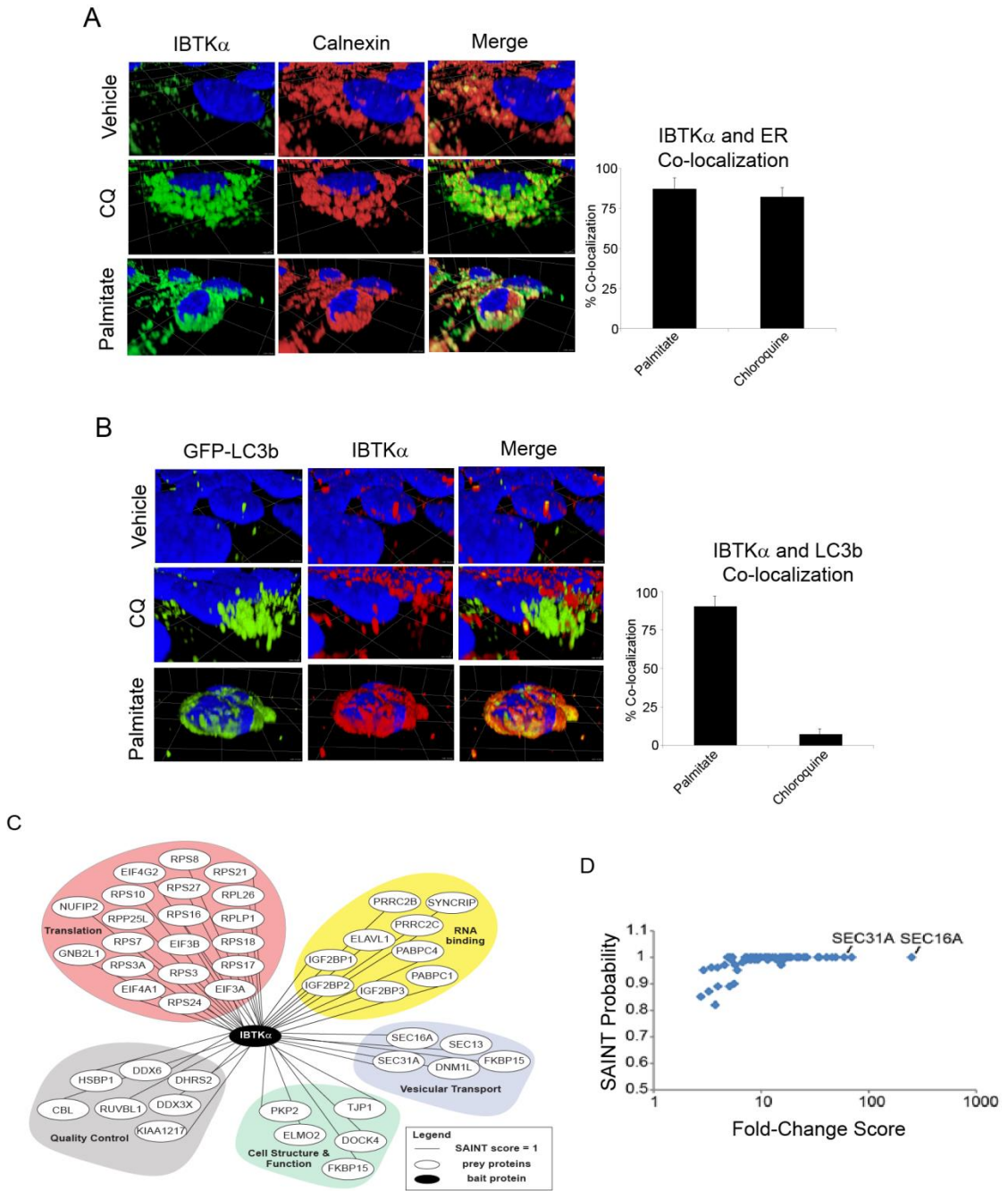

Figure 4-12. IBTKα localizes to the endoplasmic reticulum and interacts with a variety of biological networks. (A) HepG2 cells were treated with vehicle, chloroquine (CQ), or palmitate, and IBTKα and the ER marker calnexin were visualized using immunofluorescence microscopy. Co-localization of IBTKα and ER were quantified at

the pixel level. (B) HepG2 cells stably expressing GFP-LC3b were treated with vehicle, chloroquine (CQ), or palmitate, and co-localization with IBTKα was visualized using immunofluorescence microscopy and quantified. (C) HepG2 cells were treated with vehicle, chloroquine (CQ), thapsigargin (Tg) or palmitate (PA). Cell lysates were used in immunoprecipitation experiments with endogenous IBTKα as bait. The network represents proteins, and their functional classes, pulled down following LC/MS analysis of eluents. (D) Diagram showing SAINT score against fold change spectral abundance for proteins identified in LC/MS analysis of IBTKα immunoprecipitation experiment.

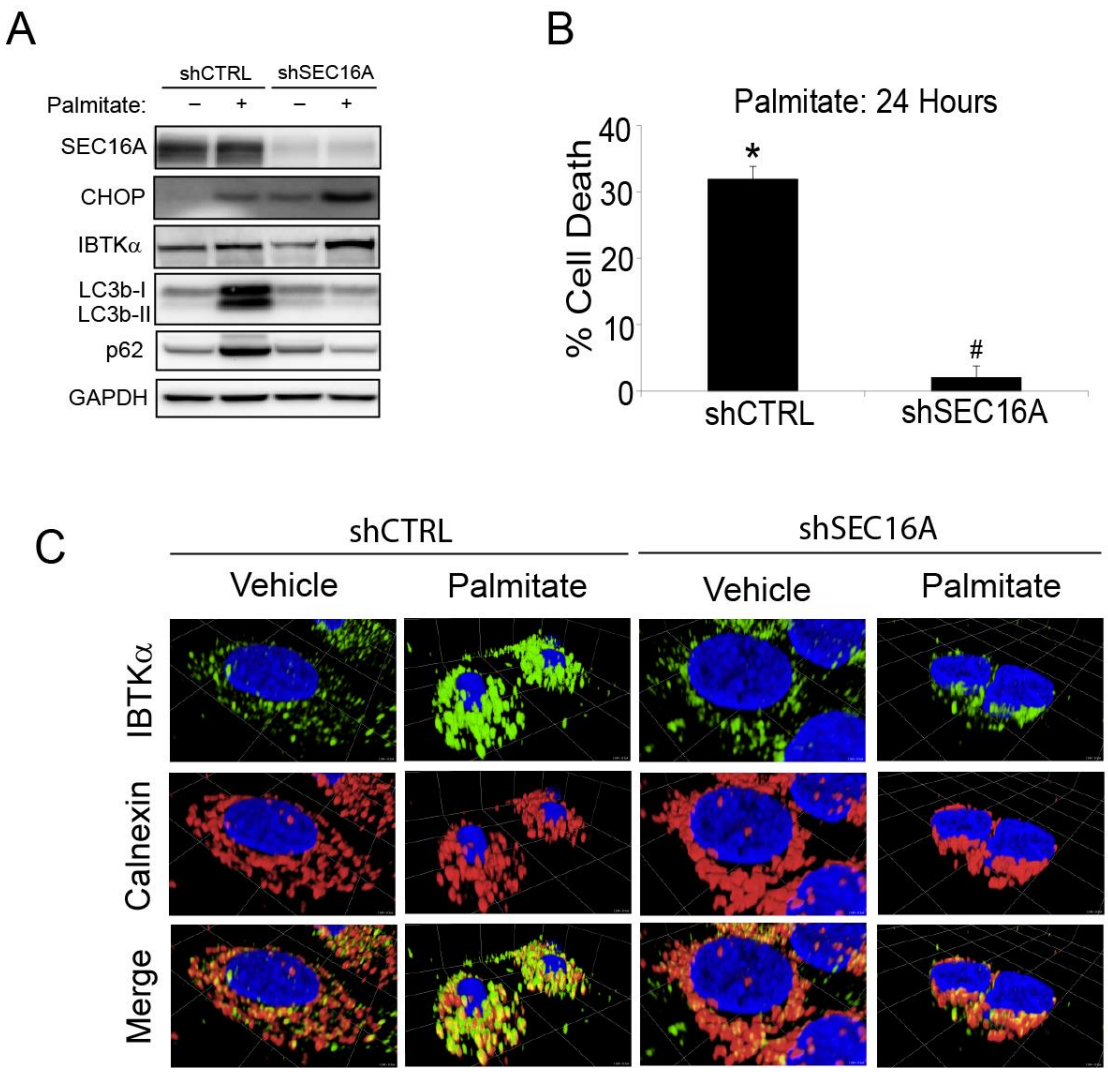

Figure 4-13. SEC16A is required for autophagy induction. (A) shCTRL and shSEC16A HepG2 cells were treated with either vehicle (-) or palmitate (+) for 12 hours and the indicated proteins were measured by immunoblot analyses. (B) shCTRL and shSEC16A HepG2 cells were treated for 24 hours and viability was measured by LDH release. (C) shCTRL and shSEC16A HepG2 cells were treated with palmitate or vehicle for 12h and co-localization of IBTKα and canexin was visualized using immunofluorescence microscopy.

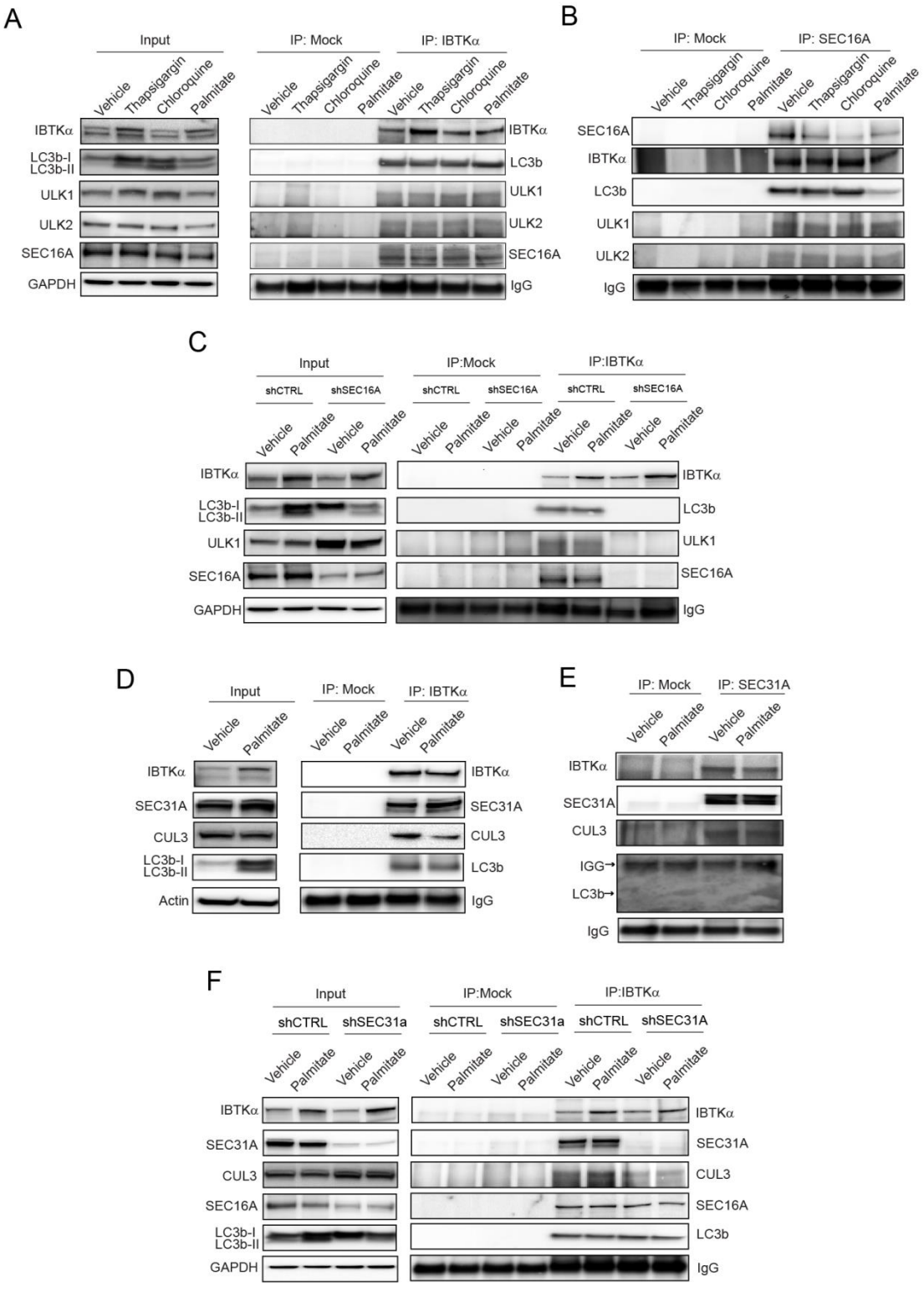

Figure 4-14. IBTKα associates with protein complex at the ERES and induces formation of phagophores. (A-B) HepG2 cells were treated for 12 hours with the

indicated stress compound and cell lysates were used for immunoprecipitation with IgG control (mock), IBTKα, or SEC16A followed by immunoblot analysis. On the left of panel H, input indicates the immunoblot analyses of total lysates. (C) shCTRL and shSEC16A HepG2 cells were treated for 12 hours with vehicle or palmitate and cell lysates were used for immunoprecipitation with IgG control (mock) or IBTKα followed by immunoblot analysis. On the left of panel J, input indicates the immunoblot analyses of total lysates. (D-E) HepG2 cells were treated with palmitate or vehicle for 12 hours and cell lysates were used for immunoprecipitation with IgG control (mock), IBTKα, or SEC16A followed by immunoblot analysis to measure the indicated proteins. On the left of panel A, input indicates immunoblot analyses carried out using total lysates. (F) shCTRL and shSEC31A HepG2 cells were treated with vehicle or palmitate for 12 hours, and cell lysates were used for immunoprecipitation with IgG control (mock) or IBTKα, followed by immunoblot analyses to measure the indicated proteins.

4.5 IBTKα and the UPR activate NF-κB and secretion of cytokines triggering lipotoxicity

We previously determined that treatment of hepatocytes with saturated FFAs induces a PERK/CHOP pathway in the UPR, leading to activation of NF-κB by a process involving phosphorylation of the subunit p65/RelA at serine 536 and consequent induced secretion of many cytokines [47]. Lowered NF-κB activity subsequently blocked induced expression and secretion of TNFα and IL-8 [47]. Deletion of *CHOP* in HepG2 cells, which would thwart initiation of autophagy and therefore alleviate accumulation of suggested toxic autophagosome intermediates during exposure to saturated FFAs, prevented p65 phosphorylation at serine-536 (Fig 4-9 B). Because phosphorylation of p65 is linked with induction of NF-κB transcriptional activity [87], we wanted to determine if depletion of IBTKα, or its interacting partner SEC31A, also prevented induction of NF-

κB-directed expression of TNFα, and IL-8 in response to palmitate treatment. SEC31A is not only critical for formation of COPII vesicles at the ERES [159], but is also suggested to be positioned in phagophores during assembly [100]. Depletion of either IBTKα or SEC31A in the HepG2 cells significantly lowered phosphorylation of p65 at serine 536 and LC3b-II conversion in response to palmitate exposure, as well as reduced lipotoxicity (Fig 4-15 A- B). Additionally, depletion of SEC16A or ATG5 prevented phosphorylation of p65, suggesting that NF-κB activation during lipotoxicity is dependent upon the induction of autophagy (Fig 4-15 C). Levels of secreted IL-8 and TNFα were measured by sandwich ELISA and both cytokines were lowered by >100-fold in the vehicle and palmitate treated shCHOP, shIBTKα, and shSEC31A cells (Fig 4-16 A-B). Additionally, CHOP and IBTKα were required for expression of *CXCL8* (IL-8) and *TNFA* (TNFα) mRNAs (Fig 4-16 C-D). These findings indicate that lowered secretion of TNFα and IL-8 in the IBTKα-depleted cells was not merely a consequence of loss of COPII-directed secretion, which may occur with disruption of the protein complexes featuring SEC16A and SEC31A at the ERES [159].

To address whether general secretion also involves the IBTKα and associated proteins at the ERES that facilitate initiation of autophagy, we transfected control and HepG2 cells depleted for IBTKα, CHOP, SEC16A, or SEC31A with a *Gaussia* luciferase reporter construct and measured secreted luciferase activity in the cell culture media following treatment with either vehicle of palmitate (Fig 4-17 A). Depletion of each of the four gene targets resulted in a reduction of *Gaussia* luciferase secretion. These findings suggest that the assembled multisubunit protein complexes containing IBTKα at the ERES are integral to secretion emanating from the ER, as well as the formation of autophagosomes.

We previously showed that secreted TNFα is central for hepatocellular death upon exposure to saturated FFAs [47]. We addressed this idea by adding recombinant TNFα to WT, shCHOP, and shIBTKα HepG2 cells in the presence or absence of palmitate treatment. There was significant death of shCHOP and shIBTKα cells only after treatment with TNFα in combination with palmitate (Fig 4-17 B), which was accompanied by increased phosphorylation of p65 (Fig 4-17 C). These results indicate that IBTKα is essential for cytokine expression and secretion and consequent inhibition of autophagic flux during metabolic stress.

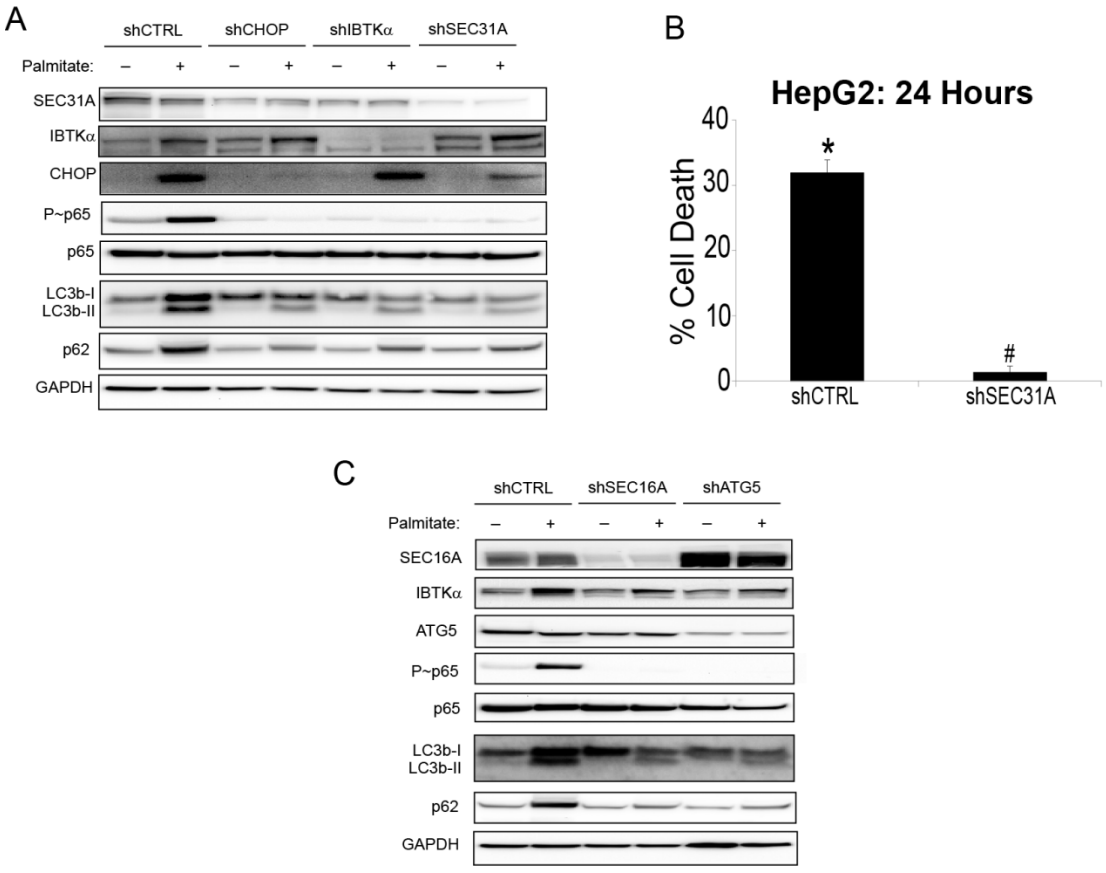

Figure 4-15. IBTKα is required for NF-κB activation during exposure to saturated FFAs. (A) shCTRL, shCHOP, shIBTKα, and shSEC31A HepG2 cells were treated with vehicle (-) or palmitate (+) for 12 hours and cell lysates were used for immunoblot analyses to determine the levels of the indicated proteins. (B) shCTRL and shSEC31A HepG2 cells were treated with palmitate for 24 hours and cell viability was measured by LDH release. (C) shCTRL, shSEC16A, and shATG5 HepG2 cells were treated with either vehicle (-) or palmitate (+) for 12 hours and cell lysates were used for immunoblot analyses to determine the levels of the indicated proteins.

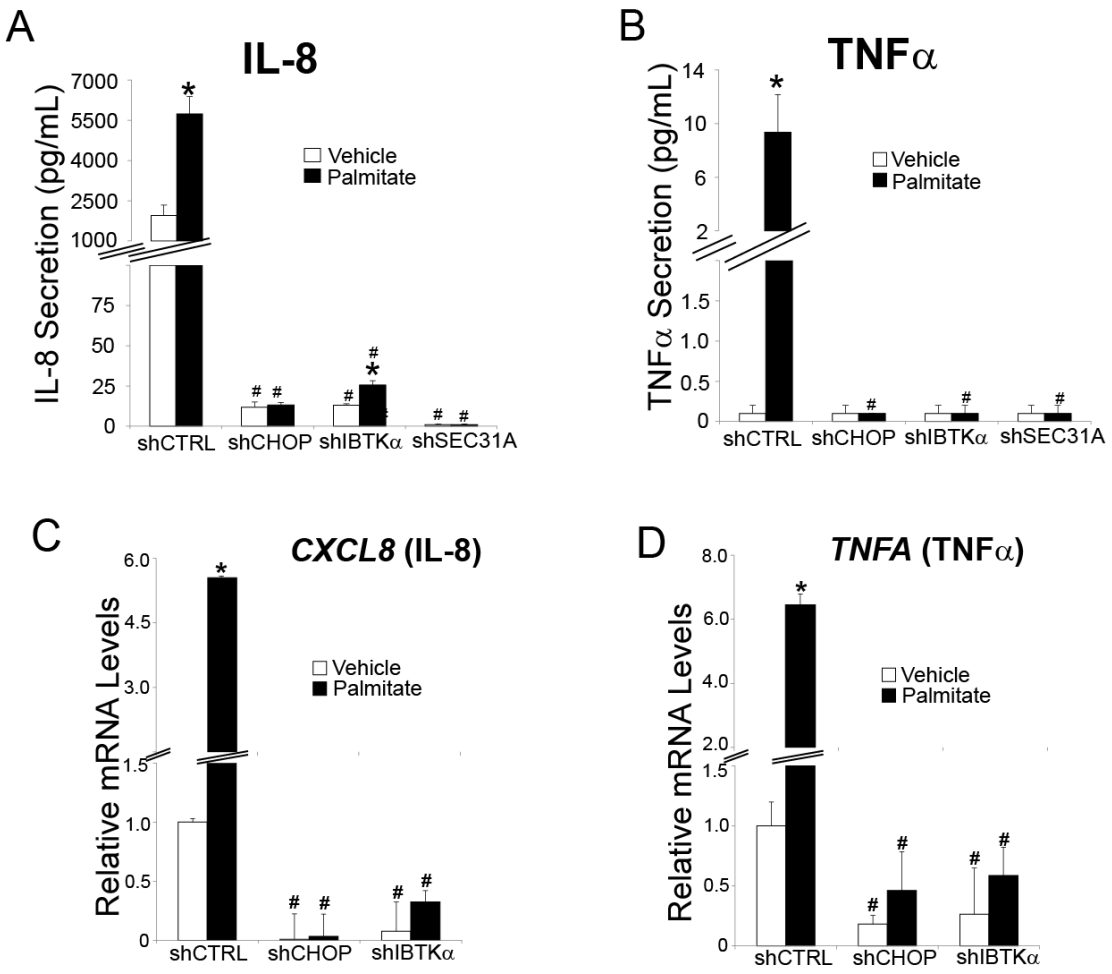

Figure 4-16. IBTKα and the UPR are required for secretion of cytokines. (A-B) shCTRL, shCHOP, shIBTKα, and shSEC31A HepG2 cells were treated with vehicle or palmitate for 12h and IL-8 and TNFα release was measured by sandwich ELISA. (C-D) shCTRL, shCHOP, and shIBTKα HepG2 cells were treated with vehicle or palmitate for 12 hours and the levels of *CXCL8* (IL-8) and *TNFA* (TNFα) mRNAs were measure by qPCR.

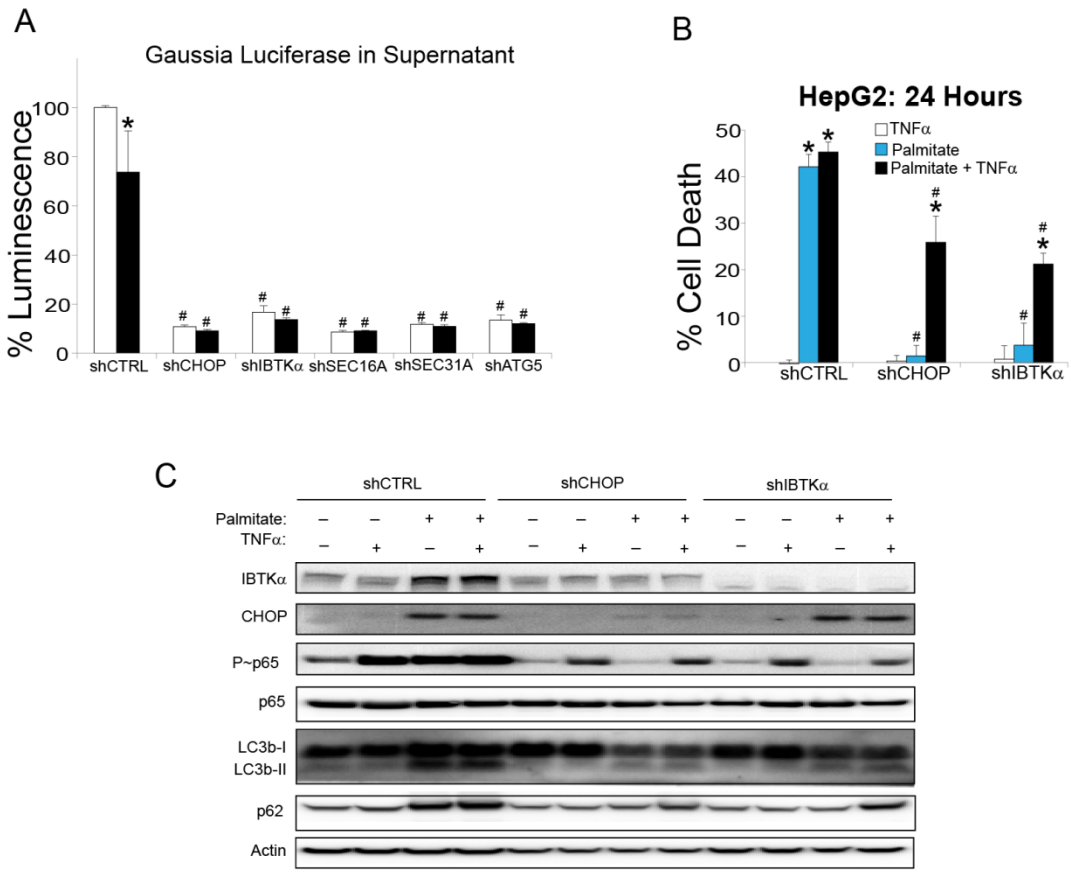

Figure 4-17. IBTKα and the UPR activate NF-κB triggering lipotoxicity. (A) shCTRL, shCHOP, shIBTKα, shSEC16A, and shSEC31A HepG2 cells were transfected with a *Gaussia* luciferase reporter and treated with vehicle or palmitate for 12 hours. Luciferase activity was measured in the supernatant. (B) Cultured shCTRL, shCHOP, and shIBTKα HepG2 cells were treated for 24 hours with recombinant TNFα, and palmitate, alone or in combination, as indicated, and cell viability was measured by LDH release. (C) shCTRL, shCHOP, and shIBTKα HepG2 cells were treated for 24 hours with recombinant TNFα and/or and palmitate, as indicated, and the indicated proteins were measured by immunoblot analyses.

4.6 The UPR and NF-κB are induced in human liver biopsies of NASH patients

To determine if the mechanism proposed from the HepG2 and primary human hepatocyte studies are truly relevant to disease progression in human liver, we investigated induction of the UPR and autophagy in a set of liver biopsy samples from patients matched for BMI and age following bariatric surgery (Table 4-1). Patients were categorized after histological evaluation and standard scoring for NASH, comprising of steatosis grade, degree of fibrosis, and presence of hepatocellular ballooning and lobular inflammation. Levels of CHOP, p65, phosphorylated p65, and IBTKα were increased in the livers of patients with simple steatosis and NASH relative to normal control (Fig 4-18 A-E). Additionally, inhibition of autophagic flux was observed in NASH patients as measured by LC3b-II conversion and p62 (Fig 4-18 F-G), consistent with severe hepatocellular injury markers such as ballooning (Fig 4-18 H-I). These findings indicate that the UPR, including CHOP and IBTKα, and NF-κB are activated in patients with NAFLD, and as the disease progresses from simple steatosis to NASH, there is a strong correlation with inhibition of autophagic flux.

To address whether UPR and NF-κB activation are associated with increased cytokine secretion, we performed a cytokine panel on serum from patients (Fig 4-19 A-C and Table 4-2). Levels of IL-6, IL-8, and TNFα were elevated in NASH patients, whereas only IL-6 and TNFα were elevated in those with simple steatosis. These results, along with all other metadata collected on the human samples, were utilized to carry out a principle component analysis (Fig 4-20 A-B). From this analysis, we identified a mixture of cell based and serum biomarkers that are closely related to NASH, steatosis, or both NAFLD states. For example, CHOP, IL-8, AST, LC3b, and p62 correlate strongly with NASH, whereas IBTKα, phosphorylated p65, and TNFα correlate with both NAFLD states.

Features	Control (n = 10)	Simple Steatosis (n = 10)	NASH (n = 10)
Age (mean, std)	42 +/- 12	40 +/- 10	43 +/- 9
Gender (male/female)	1/9	2/8	2/8
BMI (kg/m2)	48 +/- 7	51 +/- 5	49 +/- 6
Weight (lbs)	305 +/- 62	317 +/- 34	308 +/- 56
AST (IU/L)	22 +/- 7	26+/- 21	33 +/- 16
ALT (IU/L)	20 +/- 12	26 +/- 9	35 +/- 20*
Glucose (mg/dL)	110 +/- 26	115 +/- 45	143 +/- 38
Insulin	22 +/- 10	24 +/- 8	59 +/- 57
Triglycerides (mg/dL)	126 +/- 46	128 +/- 35	342 +/- 312*
Steatosis			
Grade 0	10 (100%)		
Grade 1		6 (60%)	4 (40%)
Grade 2		3 (30%)	6 (50%)
Grade 3		1 (10%)	
Fibrosis			
Absent	10 (100%)	10 (100%)	5 (50%)
Present			5 (50%)
Ballooning and Lobular Inflammation			
Absent	10 (100%)	10 (100%)	2 (20%)
Present			8 (80%)

Table 4-1. Clinical features and histological evaluation and scoring for NASH from patients that provide liver biopsy samples. Summary of histological and clinical chemical parameters from liver biopsies and matched sera of patients.

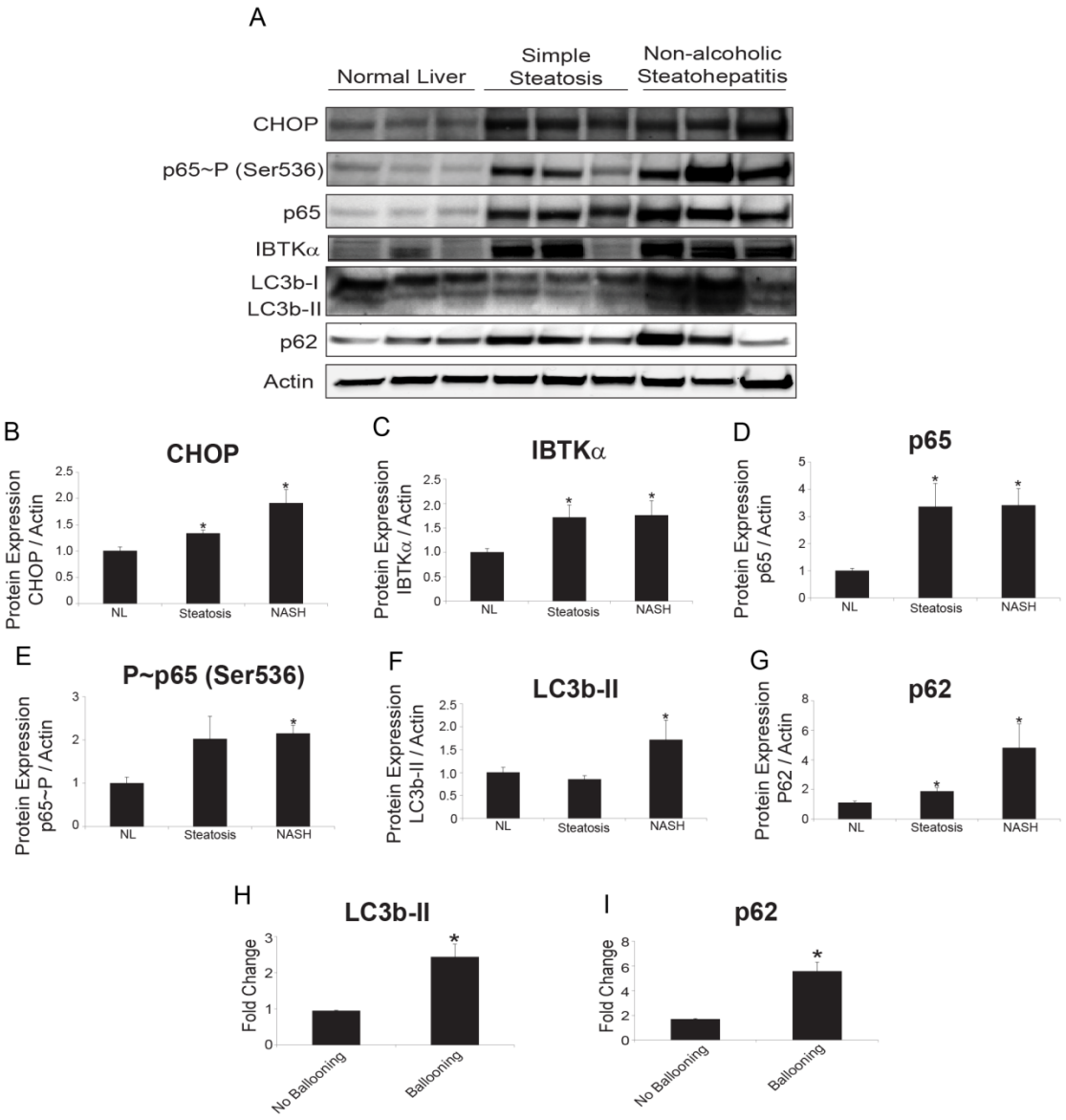

Figure 4-18. The UPR and NF-κB are upregulated in simple steatosis and NASH.

(A) Representative immunoblot measurements for the indicated proteins in lysates prepared human liver biopsy samples of patients with normal liver, simple steatosis, or NASH. (B-G) Protein quantification of immunoblots from lysates of human liver biopsy samples (n=10 per group). Data is shown as mean +/- standard error of the mean (SEM). (H-I) Protein quantification of immunoblots for LC3b-II and SQSMT1 from

lysates prepared from human liver biopsy samples of patients grouped by histological presence of ballooning. Data is shown as mean +/- SEM.

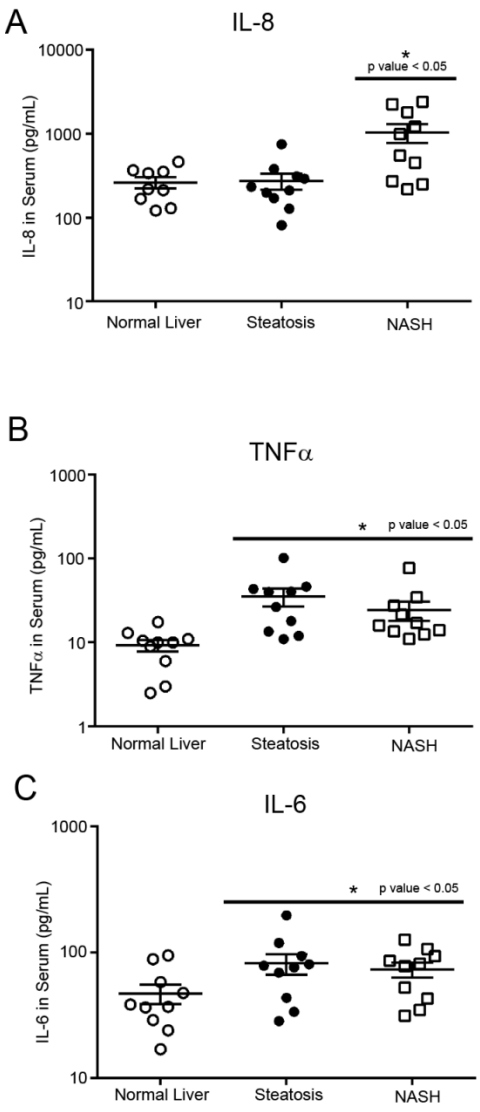

Figure 4-19. IL-8, TNFα, and IL-6 are present in serum of NASH patients. (A-C) Circulating levels of IL-8, TNFα, and IL-6 from serum of patients to matched liver biopsy samples.

Cytokine	Control (n = 9)	Simple Steatosis (n = 10)	NASH (n = 10)
IL-8	281 +/- 126	276 +/- 188	1039 +/- 840*
TNFa	10.45 +/- 6	35 +/- 27*	24 +/- 20*
IL-6	47 +/- 26	82 +/- 49*	73 +/- 32*
IL-2	29 +/- 18	62 +/- 71	51 +/- 72
IL-4	27 +/- 14	44 +/- 45	18 +/- 5
IL-5	16 +/- 9	20 +/- 19	15 +/- 7
IL-1b	67 +/- 43	120 +/- 81	84 +/- 53
IL-10	35 +/- 20	49 +/- 44	44 +/- 22
GM-CSF	16 +/- 15	100 +/- 223	15 +/- 10
INF-y	48 +/- 19	55 +/- 29	45 +/- 27
HMGB1	2 +/- 1.5	2 +/- 1.3	3 +/- 2

Table 4-2. Cytokine panel on serum from patients providing liver biopsy samples.

Cytokine, chemokine, and DAMP measurements of biomarkers from serum of patients to matched liver biopsy samples.

A

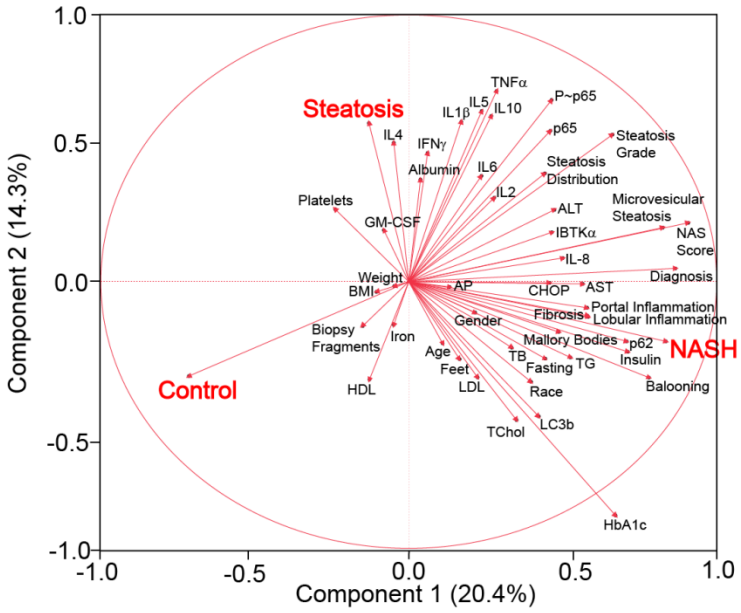

B

Parameter	Control	Simple Steatosis	NASH
Balooning	-0.3901	-0.3901	0.7802
HbA1c	-0.3597	-0.5351	0.7243
Microvesicular Steatosis	0.0703	0.0000`	0.7071
IL-8	-0.2972	-0.3034	0.6006
CHOP	-0.4788	-0.0931	0.5719
Lobular Inflammation	-0.2774	-0.2774	0.5547
LC3b	-0.1998	-0.3291	0.5364
Fibrosis	-0.2552	-0.2552	0.5104
Triglycerides	-0.2555	-0.2477	0.5032
Portal Inflamation	-0.4661	-0.0359	0.5019
Insulin	-0.2701	-0.1949	0.4795
p62	-0.3217	-0.1565	0.4781
Steatosis Grade	-0.8351	0.3771	0.4580
AST	-0.2053	-0.2485	0.4538
P65	-0.4972	-0.0872	0.4100
ALT	-0.3147	-0.0559	0.3707
TChol	0.0216	-0.3845	0.3629
P~p65	-0.4579	0.1892	0.2686
IBTKα	-0.4450	0.2028	0.2422

Figure 4-20. Principal component analysis correlates biomarkers with simple steatosis and NASH. (A) Principal component analysis combining all cytokine data, histological and clinical chemistry findings, as well as protein quantification from liver biopsy samples. (B) Abridged correlation table from principal component analysis.

4.7 Summary

Accumulation of saturated FFAs and activation of the UPR activation are common features associated with NAFLD; however, how the UPR contributes to the progression from simple steatosis to NASH is not clear [9]. Our study indicates that activation of the UPR and IBTKα, in combination with inhibition of autophagic flux during exposure to saturated FFAs, is as a key driver of hepatocellular death and the pathophysiology of NASH (Fig 4-21 a). *IBTK*α expression was induced as part of the UPR by both translational and transcriptional control mechanisms (Fig 4-1, 4-2, and 4-3), and loss of IBTKα in human hepatocytes thwarted induction of autophagy and enhanced survival of hepatocytes exposed to saturated FFAs (Fig 4-9). Translational control during ER stress allows for rapid enhanced expression of *IBTK*α and consequent assembly of a multisubunit complex at the ERES that included key factors, such as LC3b, ULK1/2, SEC16A, and SEC31A that served to promote phagophore initiation (Fig 4-14). In response to saturated FFAs, the UPR and CHOP trigger a signaling pathway involving NF-κB, which induces transcriptional expression of key cytokines that contribute to inflammation and cell death (Fig 4-15, 4-16, and 4-21 B). Among these cytokines, TNFα is suggested to function as an autocrine and paracrine factor that contributes to cell death and amplifies NF-κB-directed gene expression (Fig 4-21 B). Enhanced levels of IBTKα can also promote formation of vesicles from the ER that facilitate secretion of these cytokines (Fig 4-16). IBTKα may function as a multidomain adaptor protein in the assembly of the protein complex at the ERES and/or help direct E3 ubiquitin ligase CUL3 ubiquitylation of proteins required for assembly or function of the complex. Importantly, loss of SEC31A did not disrupt IBTKα association with SEC16A or LC3b, suggesting that there are distinct complexes including IBTKα that are situated at the ERES (Fig 4-21). The coupled effect of autophagy initiation and secretion through

interaction with key proteins at the ER places IBTKα at a pivotal intersect between cell survival pathways, which given metabolic stress can result in adverse consequences.

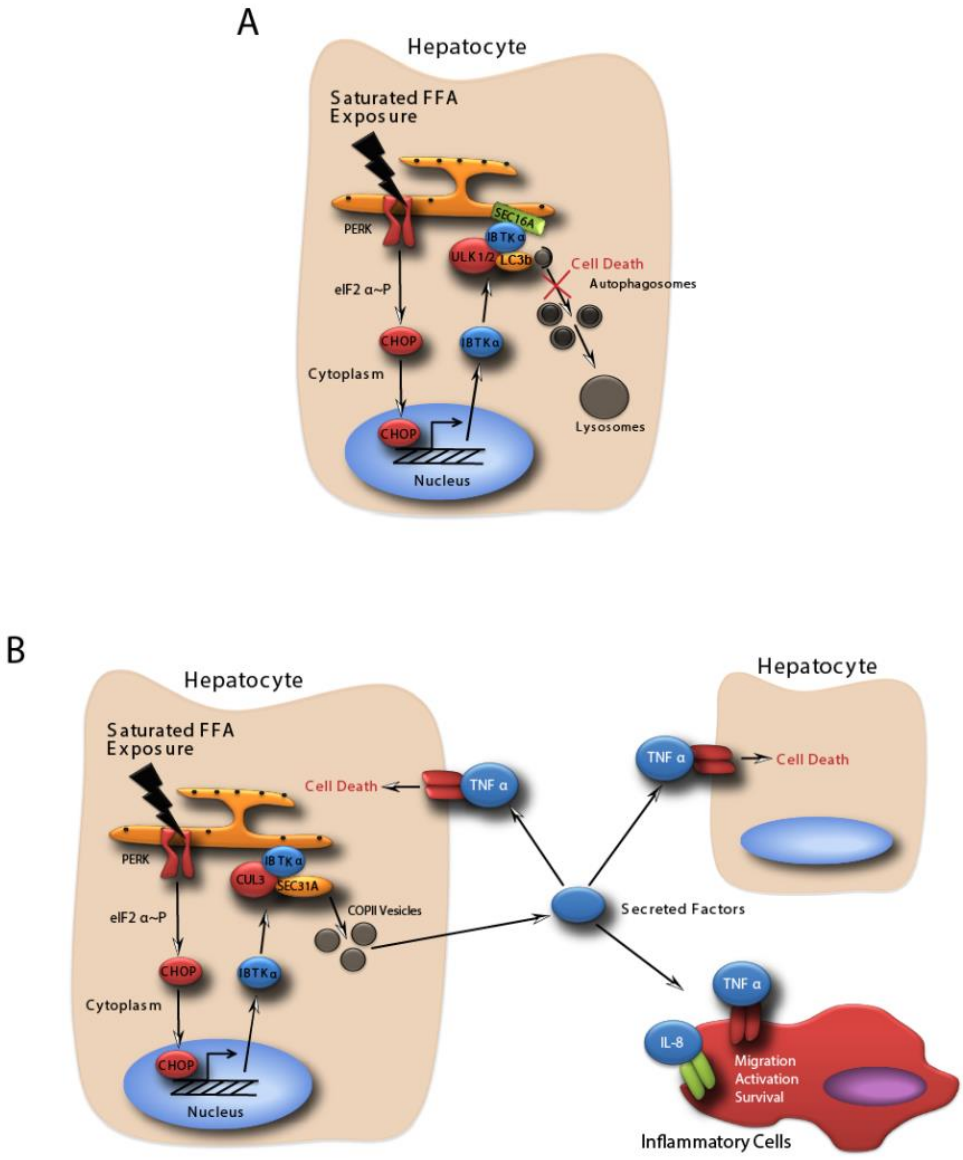

Figure 4-21. Model for Role of IBTKα in the Pathogenesis of NASH. (A) Model for the UPR and IBTKα regulation of autophagy induction at the ERES during metabolic stress. Saturated FFAs induce the UPR, featuring induced transcriptional expression of IBTKα by CHOP and preferential translation by eIF2α-P. IBTKα assembles in a multi-subunit complex with SEC16A, ULK1/2, and LC3b at the ERES, culminating in induction

of phagophores. Saturated FFAs also block the autophagic flux, contributing to hepatocyte death. (B) Model for the UPR and IBTKα regulation of secretion through COPII vesicles during metabolic stress. Induced secretion of key cytokines, including TNFα and IL-8, play a key role in hepatocyte cell death and inflammation during lipotoxicity.

CHAPTER 5. RESULTS: CHOP and NF-κB coordinately regulate proteasome activity through NRF2 following a block in autophagic flux

5.0 Introduction

NASH is associated with activation of CHOP and NF-κB, but the biological networks that these transcription factors regulate during the progression of hepatocellular injury have not been fully elucidated. In this study, we carried out ChIP-seq and RNA-seq analyses on hepatocytes deleted for either *CHOP* or the p65 (*RELA*) subunit of NF-κB and determined how these transcription factors coordinately regulate global gene expression patterns following exposure to palmitate. Additionally, we found that inhibition of autophagic flux, a key driver of hepatocellular death during the progression of NASH, results in activation of the proteasome. Induction of proteasomes occurs via a signaling pathway featuring the transcription factor NRF2, which is suggested to serve as an adaptive response to hepatocyte injury. These results provide mechanistic insight into global transcriptional networks co-regulating autophagy and proteasome pathways and their roles in both hepatocellular injury and adaptive responses during the pathogenesis of NASH.

5.1 CHOP and NF-κB mediate palmitate-induced hepatocellular injury

In Chapter 4, we showed that CHOP regulates hepatocellular injury through inhibition of phagophore formation and secretion of cytokines, such as TNFα. We also addressed the underlying CHOP signaling networks and showed that CHOP is required for the secretion of cytokines such as TNFα through activation of the p65 subunit of NF-κB (Fig 3-21), and that CHOP mediates both phagophore induction and COPII vesicle mediated secretion through IBTKα (Fig 4-21). To address whether CHOP and NF-κB activation are required for IBTKα protein expression, we treated WT HepG2 cells

depleted for either CHOP (CHOP-KO) or p65 (RELA-KO) with vehicle or palmitate. In WT cells there was a sharp increase in *IBTK*α mRNA after palmitate treatment, which was largely absent with loss of CHOP or NF-κB functions (Fig 5-1 A). To be certain that the induction of *IBTK*α mRNA was a consequence of transcriptional regulation, a reporter was constructed that fused the *IBTK*α promoter to GFP, and this reporter was introduced into the HepG2 cells. Whereas GFP expression was increased in WT cells following palmitate exposure, there was minimal change in the CHOP-KO and RELA-KO cells (Fig 5-1 B). Finally we determined that IBTKα protein expression was only induced in WT cells exposed to palmitate but not in RELA-KO or CHOP-KO cells (Fig 5-1 C). We conclude that expression of *IBTK*α is induced in hepatocytes following treatment with saturated FFAs by a mechanism requiring CHOP and NF-κB-directed transcription of *IBTK*α. Coincident with decreased IBTKα protein expression, LC3b-II lipidation and p62 accumulation were reduced in both the CHOP-KO and RELA-KO cells treated with palmitate (Fig 5-1 C). To determine if lowered induction of autophagy resulted in increased cell viability, we measured cell death by LDH release (Fig 5-1 D). After palmitate exposure, both CHOP-KO and RELA-KO cells resulted in reduced cell death compared with WT. These results, combined with those in Chapter 4, indicate that both CHOP and NF-κB are required for autophagic cell death through a mechanism involving induced IBTKα expression.

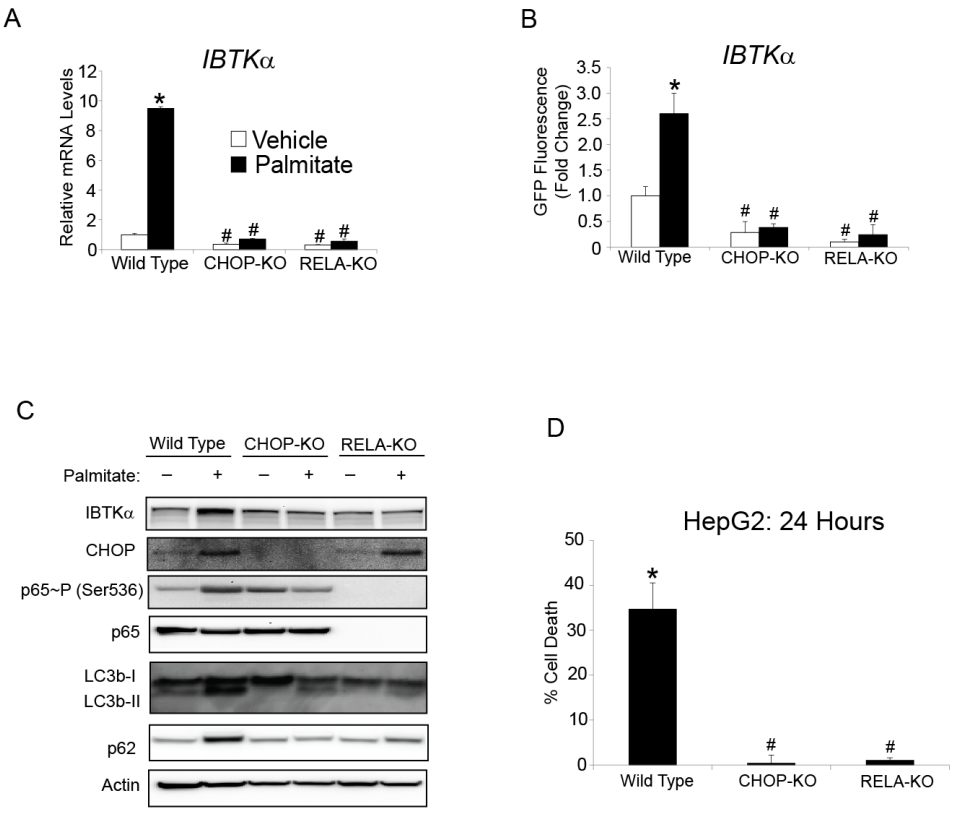

Figure 5-1. CHOP and NF-κB are required for palmitate-induced lipotoxicity. (A) WT, CHOP-KO, and RELA-KO HepG2 cells were treated with either vehicle or palmitate for 12 hours, followed by qPCR measurements for *IBTKα* mRNA. (B) Wild type, CHOP-KO, and RELA-KO HepG2 cells were transfected with a construct containing the promoter of the *IBTKα* gene that was fused with the GFP coding sequence, followed by treatment with either vehicle or palmitate for 12 hours. Results are shown as the fold change in GFP signal intensity relative to WT treated with only vehicle. (C) WT, CHOP-KO, and RELA-KO HepG2 cells were treated with either vehicle (-) or palmitate (+) for 12 hours, followed by immunoblot analysis for the indicated proteins. (D) WT, CHOP-KO, and RELA-KO HepG2 cells were treated with palmitate for 24 hours and cell death was measured by LDH release.

5.2 CHOP and NF-κB share target genes

In Chapter 3, we showed that CHOP is required for the phosphorylation of p65 at serine 536 and consequent nuclear localization following palmitate exposure, resulting in increased expression of pro-inflammatory cytokines and chemokines, such as TNFα and IL-8 [47]. In addition to *IBTK*α gene expression, CHOP has been reported to contribute to induction of autophagy genes such as *BECLN1*, *MAP1LC3B*, *SQSTM1*, and several ATG family members [56, 160]; however, it is not known whether CHOP or NF-κB are direct regulators of these genes and others induced by saturated FFAs. To identify genes directly regulated by CHOP and phosphorylated p65 (P~p65), we carried out genome-wide chromatin immunoprecipitation sequencing (ChIP-seq) on WT HepG2 cells treated with either vehicle or palmitate for 12 hours (Fig 5-2 and Appendix 2). We identified 1499 unique peaks for CHOP and 542 unique peaks for P~p65 binding to DNA, which were assigned to the nearest transcription start sites (TSSs) of known human genes using USCS gene annotation (hg19). 8.8% of the CHOP and 2.1% of the P~p65 binding sites were <3 kilobases (kb) from the TSSs, whereas 35% of the CHOP- and 50.4% of the P~p65 binding sites were >3kb from the TSSs (Fig 5-2 A). Interestingly, a total of 61 genes <3kb from the TSS and 1728 genes >3kb from the TSS were bound by both CHOP and P~p65 (Fig 5-2 B and Appendix 2). This finding suggests that a small, but significant, portion of the CHOP and NF-κB –targeted genes are bound by both transcription factors.

A DNA binding motif for CHOP was found to be similar to that of p50, the canonical binding partner to p65 in NF-κB (Fig 5-2 C). Additionally, the p65 subunit of NF-κB has been shown to associate with several isoforms of C/EPB, a family of bZIP transcription factors to which CHOP also belongs [161]. To address whether CHOP and

P~p65 proteins can associate with each other, we carried out CHOP pull-down using CHOP-specific antibodies, and then carried out an immunoblot analyses of proteins in the immunopreciptation. P~p65 was present in the CHOP pull-down, along with ATF4, which was previously reported to complex with CHOP in HepG2 cells (Fig 5-2 D). These findings suggest that CHOP can indeed associate with P~p65 in human hepatocytes.

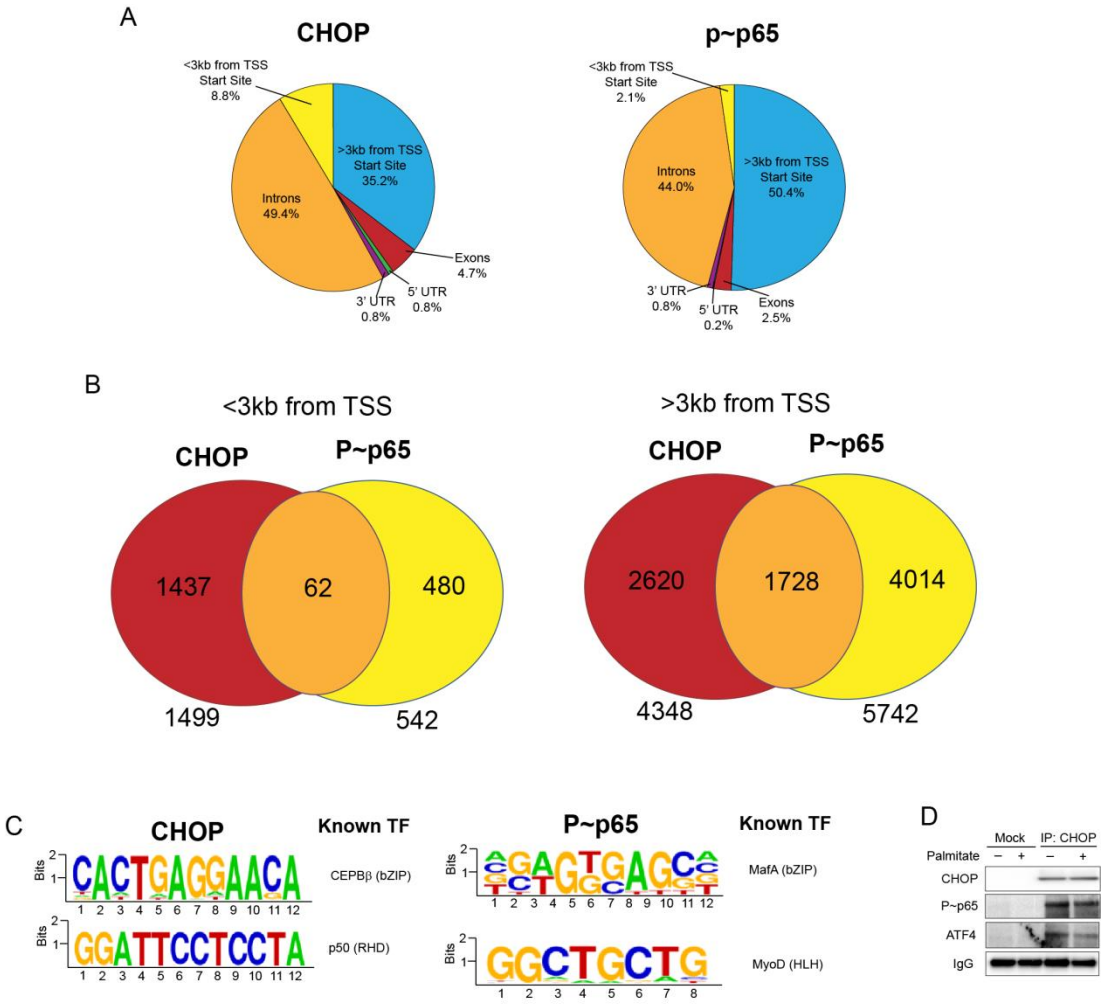

Figure 5-2. CHOP and NF-κB bind to the promoters of a collection of genes. (A) Distribution of CHOP and P~p65 ChIP-seq peaks across the human genome. The percentages indicate the representative peaks called for each segment of the genome: Introns, <3kb from the TSS, >3kb from the TSS, Exons, 5'-untranslated region, and 3'-untranslated region. (B) Total number of peaks called for CHOP, P~p65, or both CHOP and P~p65 binding for either <3 kb and >3 kb from the TSS. (C) Binding motifs identified from CHOP and P~p65 ChIP-seq peaks as well as known proteins which bind the same motif. (D) Immunoprecipitation of CHOP in wild type HepG2 cells treated with either

vehicle (-) or palmitate (+) for 12 hours, followed by immunoblot analysis of the indicated proteins.

5.3 RNA-seq reveals CHOP and NF-κB coordinately regulate global gene expression

Do CHOP and NF-κB coordinate changes in mRNA expression during the pathogenesis of NASH? The genes expression networks regulated by CHOP and NF-κB have been well studied in *in vitro* murine models, but it is not known how these transcription factors regulate gene expression in hepatocytes with regards to the pathogenesis of simple steatosis to NASH. Hence, we chose to carry out RNA-seq analyses on WT, CHOP-KO, and RELA-KO HepG2 cells treated with either vehicle or palmitate for 12 hours to understand the gene regulatory networks control by CHOP and NF-κB. Following palmitate treatment, we found that the mRNA levels for 2327 genes were significantly induced and 1237 genes were significantly repressed using a false discovery rate of 0.05 as a cutoff. We compared these genes to the ChIP-seq binding peaks to address whether any of these genes were directly regulated by CHOP or P~p65 (Fig 5-3 A-B). We found that 244 out of the 2327 (10%) genes induced following palmitate exposure also showed direct binding by CHOP and P~p65 individually, or both Fig 5-3 A), whereas 141 of the 1237 (11%) genes repressed following palmitate exposure had direct binding by CHOP, P~p65, or both (Fig 5-3 B). These findings suggest that among all genes showing significant changes upon loss of either CHOP and NF-κB, these transcription factors bind directly to a subset, and that other gene regulation might be either indirect or through the regulation of additional control mechanisms.

In order to understand how CHOP and NF-κB are regulating gene expression at a more global level, we compared statistically significant genes from the RNA-seq data

set across wild type, CHOP-KO, and RELA-KO HepG2 cells (Fig 5-4 A). We found that both CHOP and P-p65 coordinately regulate gene expression at a global level. To further understand the biological pathways that the transcription factors were regulating, we performed a gene ontology analysis using DAVID, and found that depletion of either CHOP and P~p65 suggest their involvement in the upregulation of biological pathways such as DNA replication, electron transport chain, and cell cycle, as well as downregulation of biological pathways such as inflammation, cell death, and proteasome degradation (Fig 5-4 B). Collectively, this indicates that CHOP and NF-κB coordinately regulate both global gene expression as well as distinct biological networks involved in cellular injury following treatment with palmitate, but only a small percentage (10-11%) is through direct promoter binding.

Of the genes suggested to be directly regulated by CHOP and/or NF-κB, functional annotation clustering was performed using the DAVID Bioinformatics Database to identify GO ontology terms associated with both up- and down-regulated gene sets following palmitate treatment (Fig 5-5 A and B). A large portion of the upregulated genes directly bound by CHOP and NF-κB were involved in cell cycle control and transcriptional regulation, with the later providing a rationale for the expression of the large number of regulated genes that were not directly bound by either CHOP or NF-κB. CHOP and NF-κB also induced genes involved in proteolysis. Additionally, genes involved in regulation of cell size, lipid metabolism, and kinase activity were repressed. Additionally, we found that CHOP and P~p65 bound to promoters of pro-inflammatory genes that are upregulated following palmitate exposure (5-5 A and 5-6 A-B).

In addition to increased inflammation, we also observed GO ontology terms associated with decreased lysosome function, including TFEB and SORT1, which are

important for genes involved in lysosomal function and trafficking, respectively (Fig 5-5 A-B). This may help explain some of our findings from Chapter 4, where we showed that palmitate results in a block in autophagic flux which prevents the trafficking of autophagosomes to lysosomes resulting in increased cell death (Fig 4-7 and 5-1). Additionally, to determine whether CHOP and NF-κB directly regulates genes involved in the induction of autophagy after treatment with palmitate in addition to IBTKα, we identified known genes essential for the induction of autophagosomes from the ChIP-seq dataset and compared the RNA-seq expression profile in WT, CHOP-KO, and RELA-KO for the corresponding genes (Fig 5-6 C-D). We found that CHOP and P~p65 bound to the promoters of many genes that were essential for the induction and maintenance of autophagy, including SEC16A, which we previously found to associate in a protein complex with IBTKα to induce phagophores (Fig 4-12 and 4-14). Many of the proteins identified as regulated directly by CHOP and P~p65 are involved in the early stages of phagophore initiation and trafficking, including ATG12, ARF6, and RAB32. While both CHOP and P~p65 associated to the promoter of IBTKα, the preferential binding to gene promoters coincident with repressed gene expression in the CRISPR-KO cells indicates that CHOP and P~p65 directly regulate a set of genes to control the activation of autophagy, and that defective trafficking of autophagosomes to the lysosome is a key feature of hepatocellular injury during NASH (Fig 4-7 and 5-6 C-D).

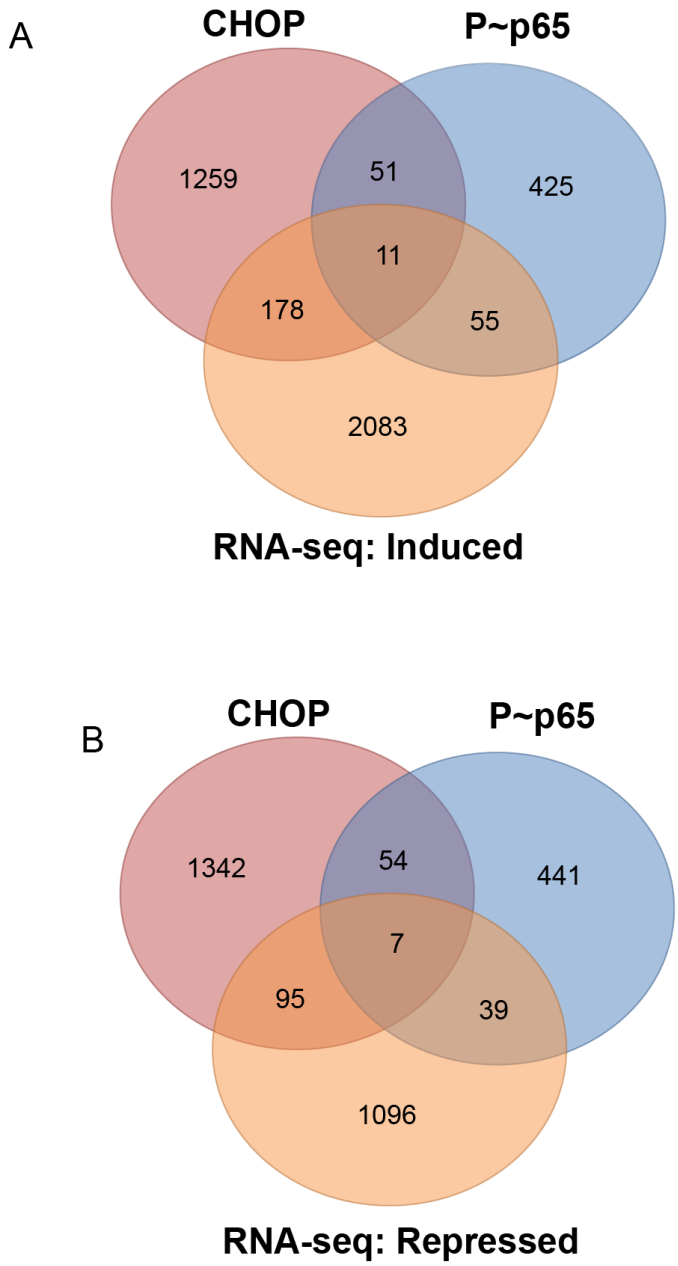

Figure 5-3. CHOP and NF-κB regulate unique genes sets. (A) Transcription factor binding sites from CHOP and P~p65 ChIP-seq are illustrated in the red and yellow in the Venn diagram. These binding sites are overlayed with induced genes (orange) following palmitate exposure as identified by RNA-seq. (B) Transcription factor binding sites from CHOP and P~p65 ChIP-seq were overlayed with the repressed genes following palmitate exposure as identified by the RNA-seq analysis.

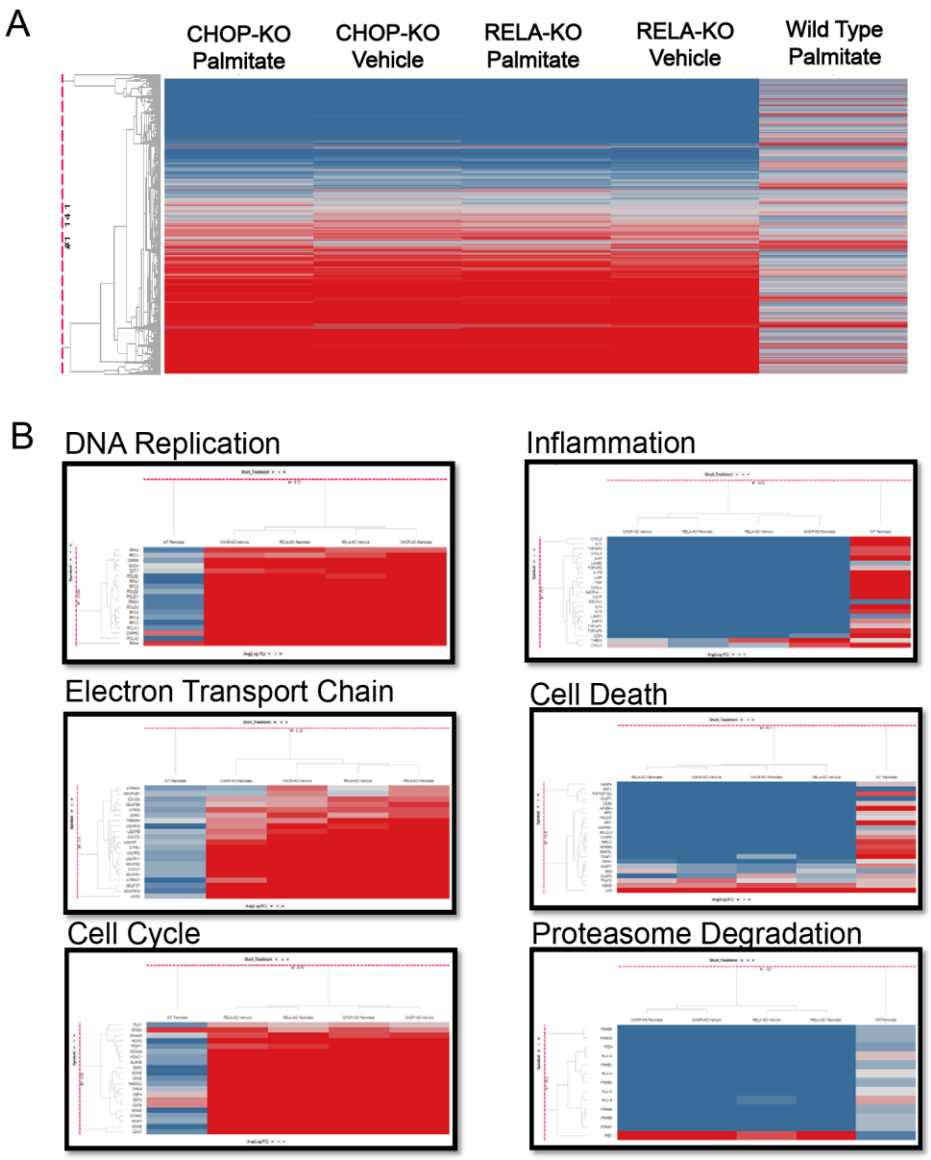

Figure 5-4. CHOP and NF-κB co-regulate multiple biological pathways. (A) Global gene expression profile from RNA-seq data set of wile type, CHOP-KO, and RELA-KO HepG2 cells treated with either vehicle or palmitate for 12 hours. Genes are clustered using Euclidean clustering. (B) Heat maps from RNA-seq analysis depicting biological pathways co-regulated by CHOP and NF-κB. Red depicts induced genes and blue depicts repressed genes. Pathways were identified using DAVID gene ontology. Genes are clustered using Euclidean clustering.

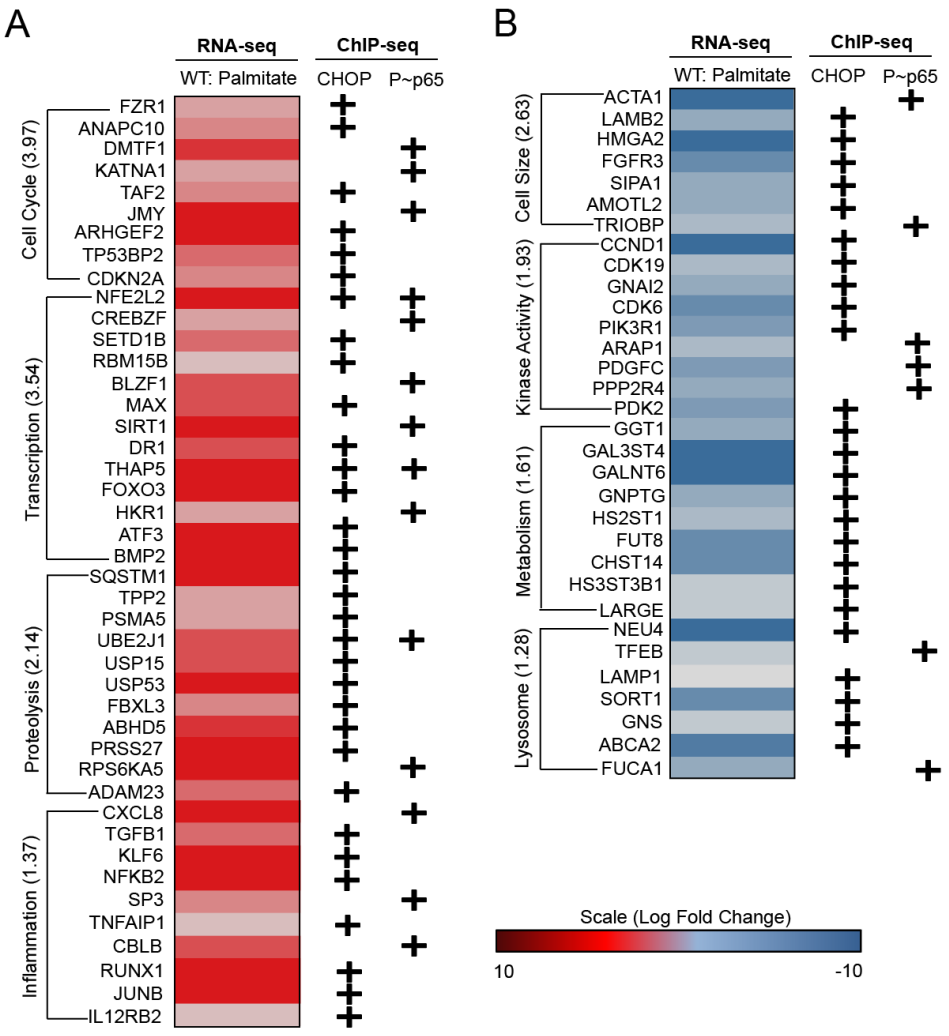

Figure 5-5. CHOP and NF-κB regulate unique genes to control overlapping biological pathways. DAVID analysis followed by a functional annotation clustering of the top induced genes (A) and repressed genes (B) following palmitate treatment was performed. Associated go ontology terms along with the enrichment scores are located on the left, and the corresponding transcription factor which binds to the promoter is indicated by a "+" on the right.

A

Pro-Inflammatory Genes

Gene	WT: Palmitate Fold Change	CHOP-KO Fold Change	RELA-KO Fold Change	Transcription Factor(s)
IL4I1	-1.2	1.2	1.3	CHOP / P~p65
IL1RAP	1.0	-3.0	-2.0	CHOP / P~p65
IL12RB1	3.6	-2.0	-2.0	CHOP
IL32	1.0	-478	-549	CHOP
TNFAIP1	1.1	-2.0	-1.9	CHOP
ADAM10	1.0	-4.0	-3.2	CHOP
JUNB	2.6	-1.9	1.0	CHOP
TGFB1	1.3	-11.3	-12.1	CHOP
NFKB2	2.3	-3.5	-1.6	CHOP
RUNX1	1.9	-2.1	-1.3	CHOP
IRAK1BP1	-1.1	4.0	4.0	P~p65
CXCL8	7.5	-338	-478	P~p65
FASLG	1.0	-1.0	-1.0	P~p65
TLR1	1.1	-4.0	-2.6	P~p65
SP3	1.2	-1.6	-1.9	P~p65
CBLB	1.4	-2.0	-1.3	P~p65

B

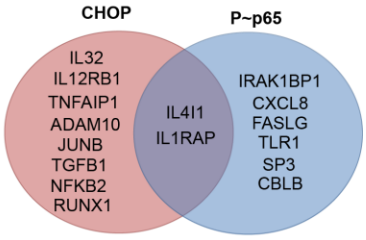

C

Autophagy Regulated Genes

Gene	WT: Palmitate Fold Change	CHOP-KO Fold Change	RELA-KO Fold Change	Transcription Factor(s)
IBTKα	1.7	-1.7	-3.0	CHOP / P~p65
SEC16A	1.3	-1.0	-1.0	CHOP
SQSTM1	4.6	-3.7	-1.9	CHOP
ATG9B	-1.1	-13.9	-13.0	CHOP
ATG12	1.2	1.0	-1.0	CHOP
ARF6	1.0	-1.2	-1.2	CHOP
ATG13	1.3	-1.5	1.0	P~p65
ATG14	1.3	-1.1	-1.5	P~p65
RAB32	1.3	-5.7	-3.7	P~p65

D

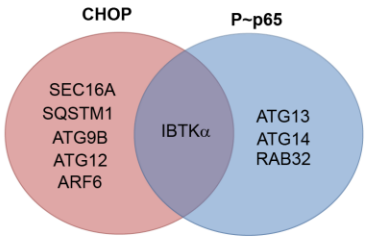

Figure 5-6. CHOP and NF-κB regulate unique genes to control inflammation and autophagy. (A) Genes involved in inflammation directly bound by either CHOP, P~p65, or both CHOP and P~p65 as identified through ChIP-seq analysis. RNA-seq data is shown as fold change from wild type untreated. (B) Venn diagram depicting genes directly bound by CHOP and/or P~p65 involved in inflammation. (C) Genes involved in the induction of autophagy directly bound by either CHOP, P~p65, or both CHOP and P~p65 as identified through ChIP-seq analysis. RNA-seq data is shown as fold change from wild type untreated. (D) Venn diagram depicting genes directly bound by CHOP and/or P~p65 involved in the induction of autophagy.

5.4 CHOP and NF-κB activate the proteasome through NRF2

Global gene expression analysis by RNA-seq revealed that although CHOP and NF-κB were involved in reduced lysosome function, they coordinately contribute to the activation of genes involved in proteasome activity (Fig 5-4 and 5-6), suggesting that there is a compensatory process to insure a certain level of proteolysis capacity in cells. To test this idea biochemically, we treated WT, CHOP-KO, and RELA-KO HepG2 cells with either vehicle or palmitate for 24 hours and measured proteasome activity using the chymotrypsin-like proteasome-glo assay (Fig 5-7 A). Whereas palmitate resulted in a 10-fold increase in proteasome activity in WT cells, lowered activity was observed in both vehicle and palmitate-treated CHOP-KO and RELA-KO cells.

NRF2 (NFE2L2) has been shown to transcriptionally regulate proteasome subunits such as the chymotrypsin-like β5 ring PSMB5 in response to DNA damaging agents such as 3-methylcholanthrene and antioxidants such as sulforaphane [162-164]. We identified the NRF2 transcription factor to be directly regulated by both CHOP and P~p65 in our ChIP-seq and RNA-seq data sets (Appendix 2). To further validate these findings, we transfected WT, CHOP-KO, and RELA-KO HepG2 cells with a construct containing the promoter region of *NFE2L2* fused to the GFP reporter, followed by treatment with either vehicle or palmitate for 12 hours. Expression of the GFP reporter was increased over 4-fold in WT cells after treatment with palmitate, with minimal induction in the CHOP-KO and RELA-KO cells (Fig 5-7 B). Additionally, we observed increased NRF2 mRNA and protein in palmitate-treated WT cells, as measured by qPCR and immunoblot analyses, respectively (Fig 5-7 C-D). There was minimal expression of either NRF2 mRNA or protein in either CHOP-KO or RELA-KO cells. Furthermore, NRF2 localized to the nucleus upon palmitate treatment (Fig 5-7 E).

Collectively, these results indicate that CHOP and NF-κB are required for transcriptional induction of *NFE2L2* (NRF2) mRNA and protein levels in response to palmitate.

Following nuclear localization, NRF2 binds to the promoter of genes encoding subunits of proteasomes, including PSMB5 that is critical for chymotrypsin-like activity, as well as antioxidant genes *NQO1*, *GCLC*, and *GSR* [165, 166]. Both CHOP and NF-κB were required for induction of these NRF2 target genes in response to palmitate (Fig 5-8 A-D). Additionally, we identified several proteasome subunits in the ChIP-seq analysis that were suggested to be directly regulated by CHOP and/or P~p65, and each of these were confirmed by qPCR (Fig 5-8 E-H). These results suggest that CHOP and P~p65 coordinately regulate proteasome expression following palmitate treatment through both NRF2, as well as suggested direct regulation of genes encoding selected proteasome subunits (Fig 5-8 I).

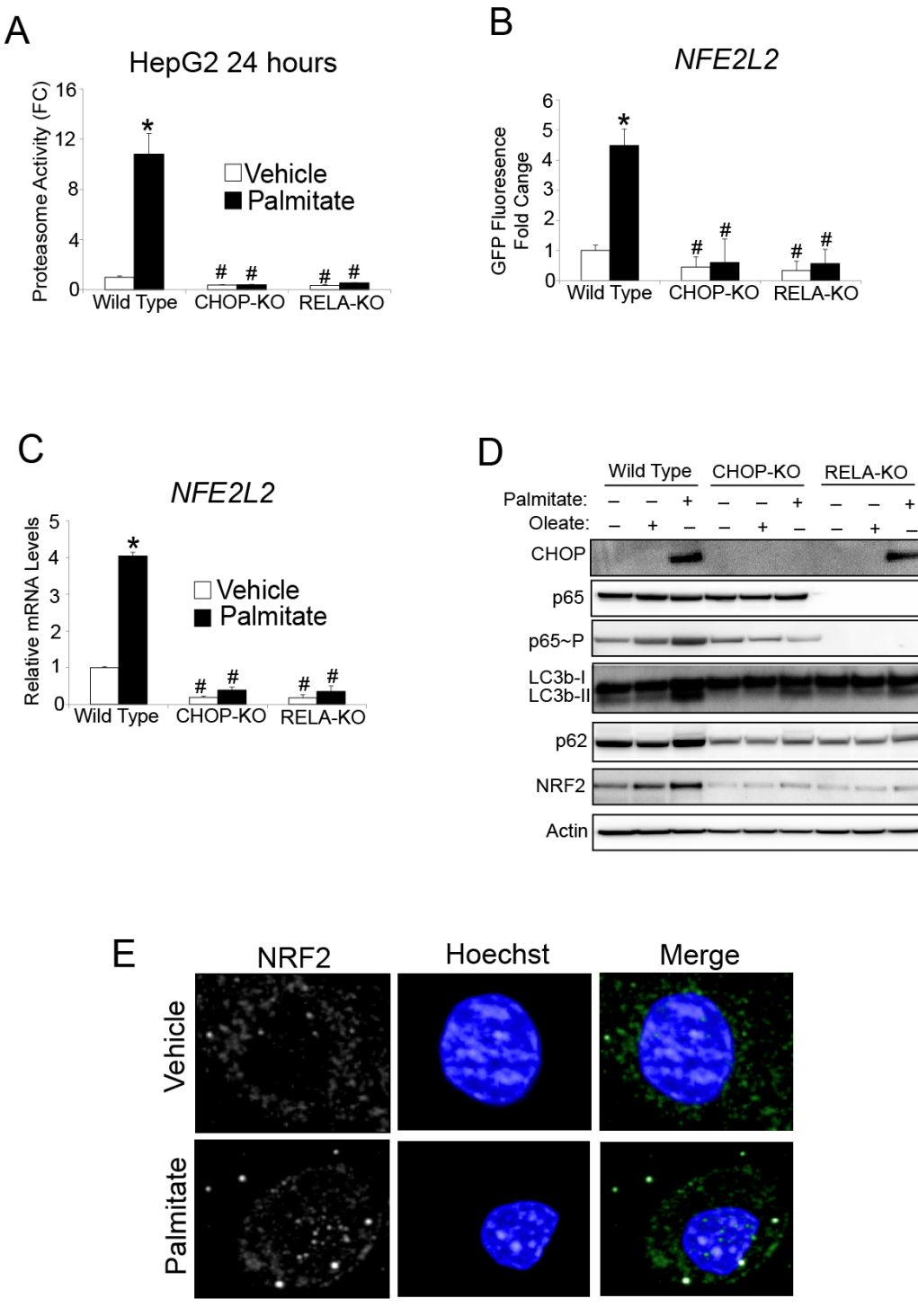

Figure 5-7. CHOP and NF-κB regulate proteasome activation through NRF2. (A) WT HepG2, CHOP-KO, and RELA-KO cells were treated with palmitate or vehicle for 24

hours and proteasome activity was measured by the chymotrypsin proteasome-glo assay. (B) WT, CHOP-KO and RELA-KO cells were transiently transfected with a reporter containing the *NFE2L2* promoter fused to the GFP reporter, followed by treatment with vehicle or palmitate for 12 hours. (C) WT, CHOP-KO, and RELA-KO cells were treated with palmitate or vehicle for 12 hours and *NFE2L2* mRNA levels were measured by qPCR. (D) WT, CHOP-KO, or RELA-KO cells were treated with vehicle (-) or palmitate or oleate (+) for 12 hours and immunoblot analyses were carried out to measure the indicated proteins. (E) Nuclear localization of NRF2 protein was measured by Immunofluorescence microscopy in HepG2 cells that were treated with palmitate or vehicle. In parallel, Hoeschst staining was used to visualize nuclei, and the nuclear staining and NRF2 imaging was merged.

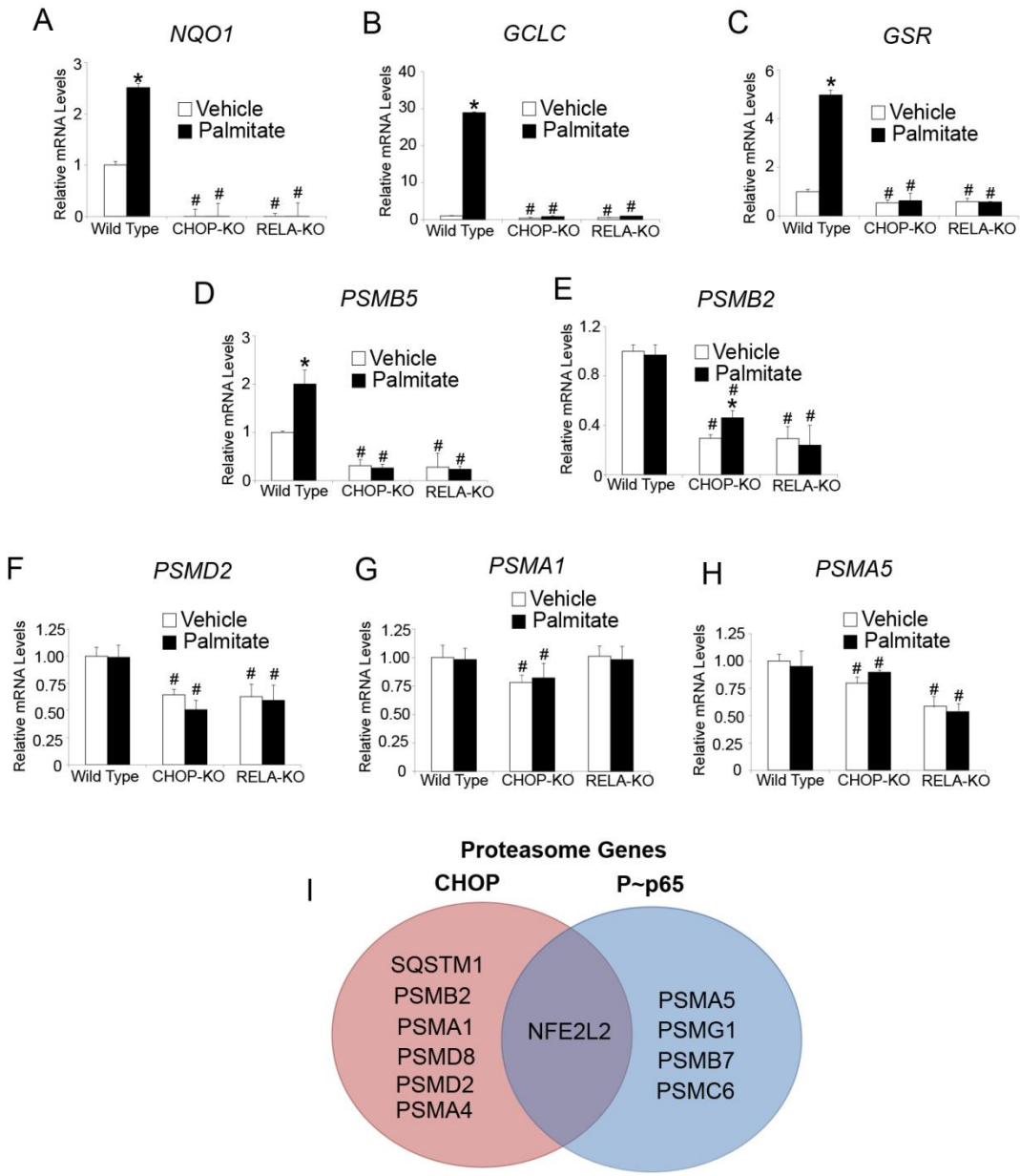

Figure 5-8. Palmitate exposure induces NRF2 targets and proteasome subunits. (A-H) WT, CHOP-KO, and RELA-KO cells were treated with palmitate or vehicle for 12 hours and and the indicated mRNAs were measured by aPCR. (I) Venn diagram indicating CHOP and P~p65 regulation of genes involved in proteasome function. Genes were identified by ChIP-seq as being bound by CHOP and P~p65, individually or in combination.

5.5 Inhibition of autophagic flux enhances NRF2 transcriptional activity

Does NRF2-mediated proteasome activation require autophagy? Recent literature has suggested a high degree of crosstalk between autophagy and the ubiquitin/proteasome system [167]. Because both CHOP and NF-κB are required for the initiation of autophagy as well as NRF2 expression (Fig 5-1, 5-6 and 5-7), we address whether the induction of autophagy itself was also required for proteasome activation. To explore this concept, we treated cells depleted for *IBTK*α or *ATG5*, a well-established factor required for formation of phagophores, with palmitate and did not observe an increase in chymotrypsin-like and caspase-like proteasome activity coincident with decreased initiation of autophagy (Fig 5-9 A-B). These results suggest that induction of autophagy is important for enhanced proteasome activation following palmitate exposure. We suggest that cell changes occurring with accumulating autophagosomes that are blocked in flux are critical for the NRF2 induction.

Inhibition of autophagic flux results in an accumulation of macromolecules and proteins, including an up-regulation of LC3b-II and p62, crucial regulatory proteins involved in trafficking autophagic cargo to the lysosome for degradation [98, 99]. Recent reports suggested that p62 aggregates can directly inhibit the KEAP1-NRF2 complex, resulting in activation of NRF2 [168]. To explore the idea that inhibition of autophagic flux and consequent accumulation of p62 can lead to NRF2 activation, we treated a variety of autophagy inducers and blockers of autophagic flux and measured NRF2 protein levels (Fig 5-10 A). Compounds which inhibited autophagic flux, including palmitate, choroquine, bafilomycin A1, and thapsigargin, resulted in both an accumulation of p62 and NRF2, as well as enhanced proteasome activity (Fig 5-10 A-B). Because NRF1 has also been reported to enhance proteasome activity through elevating expression levels of proteasome subunits [20], we evaluated NRF1 protein levels but observed no change with response to compound treatment (Fig 5-10 A). These results suggest that with

inhibition of autophagic flux there is increased NRF2 protein levels that can trigger enhanced proteasome activity.

During inhibition of autophagic flux there are accumulating amounts of p62, and it was suggested that increased levels of p62 can bind to KEAP1 and disrupt the KEAP1-NRF2 complex, preventing NRF2 proteasome degradation and allowing for NRF2 nuclear localization [168]. To determine whether p62 forms a complex with KEAP1 following inhibition of autophagic flux in human hepatocytes, we treated WT HepG2 cells with vehicle, palmitate, choroquine, or thapsigargin and carried out an immunoprecipitation using an antibody specific for KEAP1 and IgG as a control, followed by immunoblot analysis for KEAP1 and associated p62 protein (Fig 5-11 A). There were increased levels of p62 complexed with KEAP1 when cells were treated with palmitate, chloroquine, and thapsigargin, all inhibitors of autophagic flux. Next, to understand if the increased levels of p62 and consequent nuclear localization of NRF2 directly affected proteasome activation, we transfected HepG2 cells with a plasmid expressing p62 (Fig 5-11 B-C). Overexpression of p62 resulted in increased NRF2 levels, as well as enhanced proteasome activity. Collectively, these results indicate that inhibition of autophagic flux leads to an association of p62 with KEAP1, and increased p62 levels result in enhanced proteasome activity consequent with induced NRF2 protein expression.

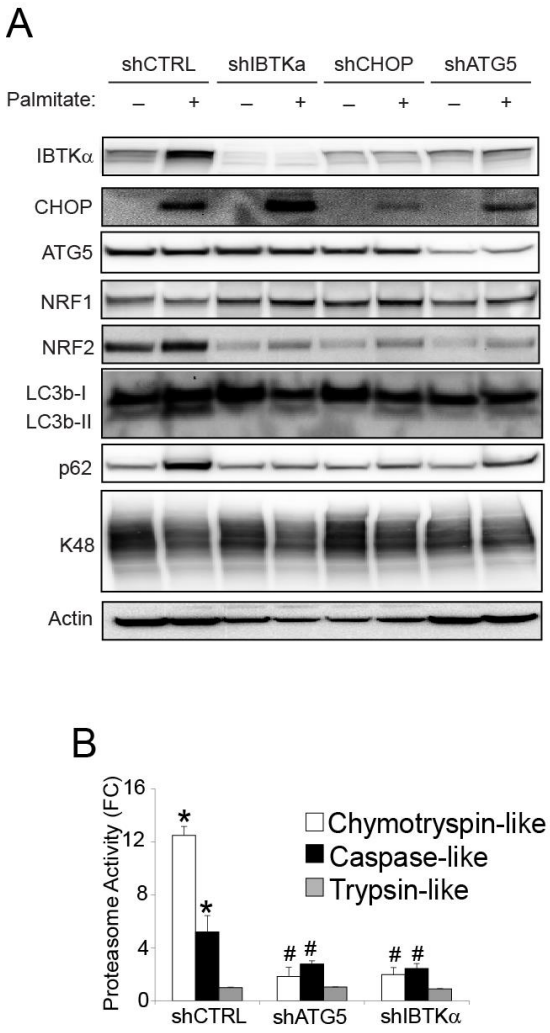

Figure 5-9. Autophagy is required for NR2-mediated proteasome activation. (A) shCTRL, shATG5, and shIBTKα HepG2 cells were treated with vehicle (-) or palmitate (+) for 12 hours and immunoblot analyses were carried out indicated proteins. (B) shCTRL, shATG5, and shIBTKα HepG2 cells were treated with palmitate for 24 hours and proteasome activity was measured by the chymotrypsin, caspase-like, and trypsin-like proteasome-glo assays.

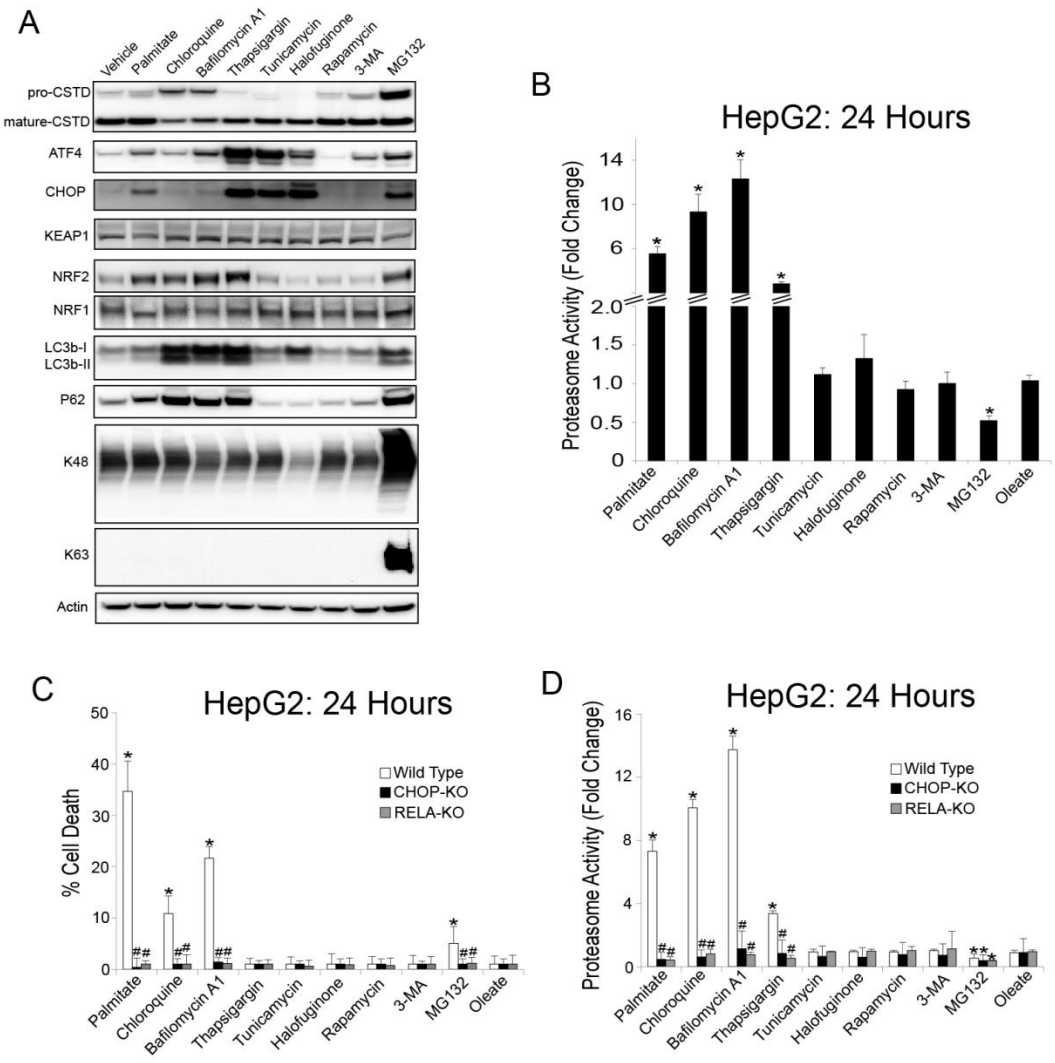

Figure 5-10. Inhibitors of autophagic flux induce proteasome activation through CHOP and NF-κB. (A) HepG2 cells were treated with indicated compounds for 24 hours and immunoblot analyses were carried out for indicated proteins. (B) HepG2 cells were treated for indicated compounds for 24 hours and proteasome activity was measured by the chymotrypsin proteasome-glo assay. (C) WT, CHOP-KO, and RELA-KO cells were treated with indicated compounds for 24 hours and cell death was measured by LDH release. (D) Wild type, CHOP-KO, and RELA-KO HepG2 cells were treated with indicated compounds for 24 hours and proteasome activity was measured by the chymotrypsin-like proteasome-glo assay.

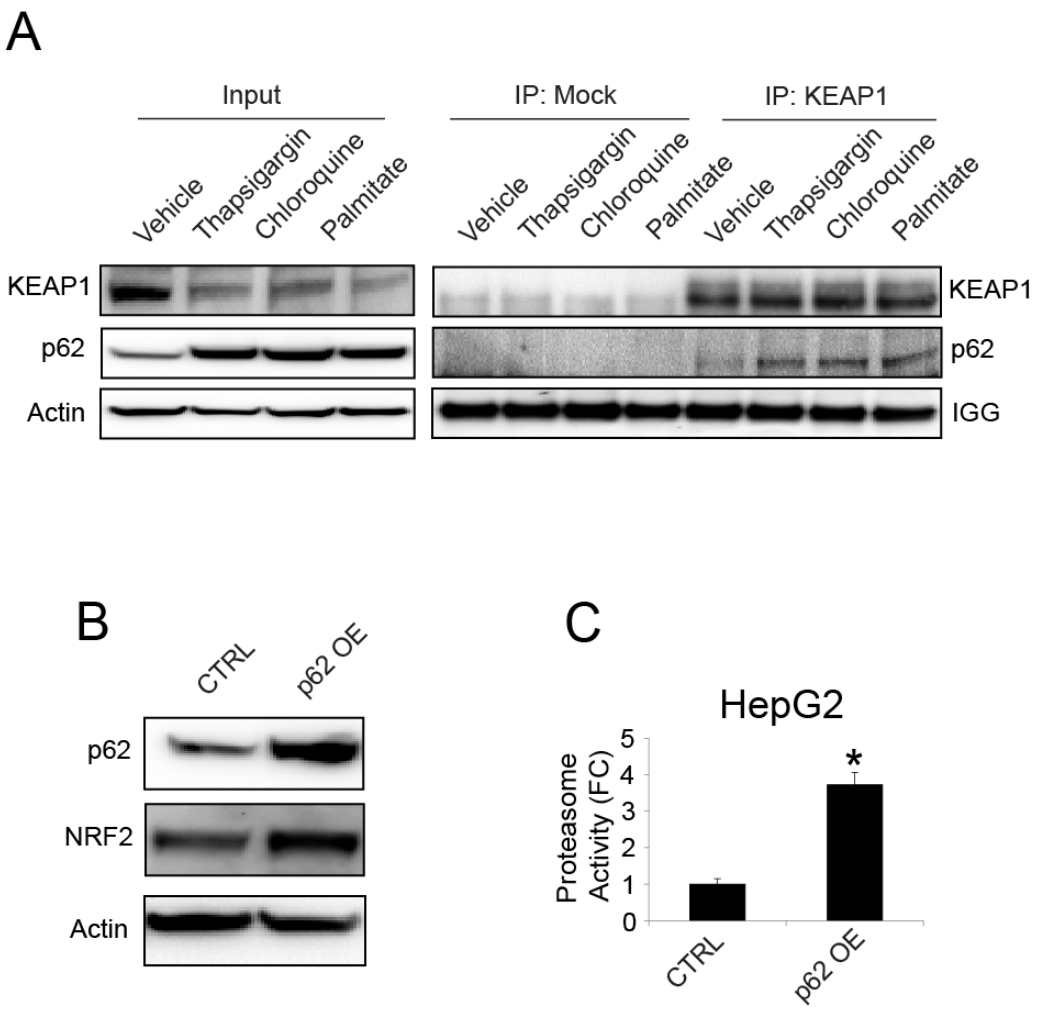

Figure 5-11. p62 interacts with KEAP1 upon stress treatment that block autophagic flux. (A) HepG2 cells were treated for 12 hours with the indicated stress compound and cell lysates were used for immunoprecipitation with IGG control (mock) or KEAP1, followed by immunoblot analysis. The left panel measures the indicated proteins in total lysates. (B) HepG2 cells were transiently transfected with a plasmid containing the coding sequence for p62 and lysates were collected for immunoblot analysis for the indicated proteins. (C) HepG2 cells were transiently transfected with a plasmid containing the coding sequence for p62 and proteasome activity was measured by chymotrypsin proteasome-glo assay.

5.6 NRF2 enhances cell viability in response to palmitate through proteasome activation

Activation of NRF2 is thought to be a major regulatory mechanism against cellular perturbations by inducing gene expression to overcome oxidative damage and enhance cellular detoxification [165, 166]. To address the idea the NRF2 is playing a protective role due to a block in autophagic flux, we treated both control cells (shCTRL) and cells depleted for NRF2 (shNRF2) with vehicle, palmitate, or chloroquine for 24 hours (Fig 5-12 A-B). Following exposure to palmitate, increased cell death was observed in shNRF2 HepG2 cells relative to shCTRL (Fig 5-12 B). Interestingly, p62 and LC3b-II were still induced in the NRF2-depleted cells following both treatment regimes, whereas proteasome activity was decreased (Fig 5-12 A and E).

Does NRF2 enhance cell survival through enhanced proteasome activity alone? To determine whether the antioxidant potential of NRF2 was playing a protective role during palmitate-induced lipotoxicity, we treated shCTRL and shNRF2 cells with palmintate alone or in combination with the antioxidant N-acetyl cysteine (NAC), but did not observe a significant decrease in cell death in either the shCTRL or shNRF2 cells with the addition of NAC (Fig 5-13 A). To investigate the role of the NRF2-mediated proteasome response in cell survival, we treated shCTRL and cells depleted for PSMB5 (shPSMB5), a proteasomal subunit regulated by NRF2 (Fig 5-13 B). Following treatment with palmitate for 24 hours, the shPSMB5 HepG2 cells showed increased cell death relative to the shCTRL cells (Fig 5-13 B-C). These results suggest that NRF2 is mediating cell survival in response to a block in autophagic flux through increased proteasome activity as a compensatory mechanism to degrade damaged proteins.

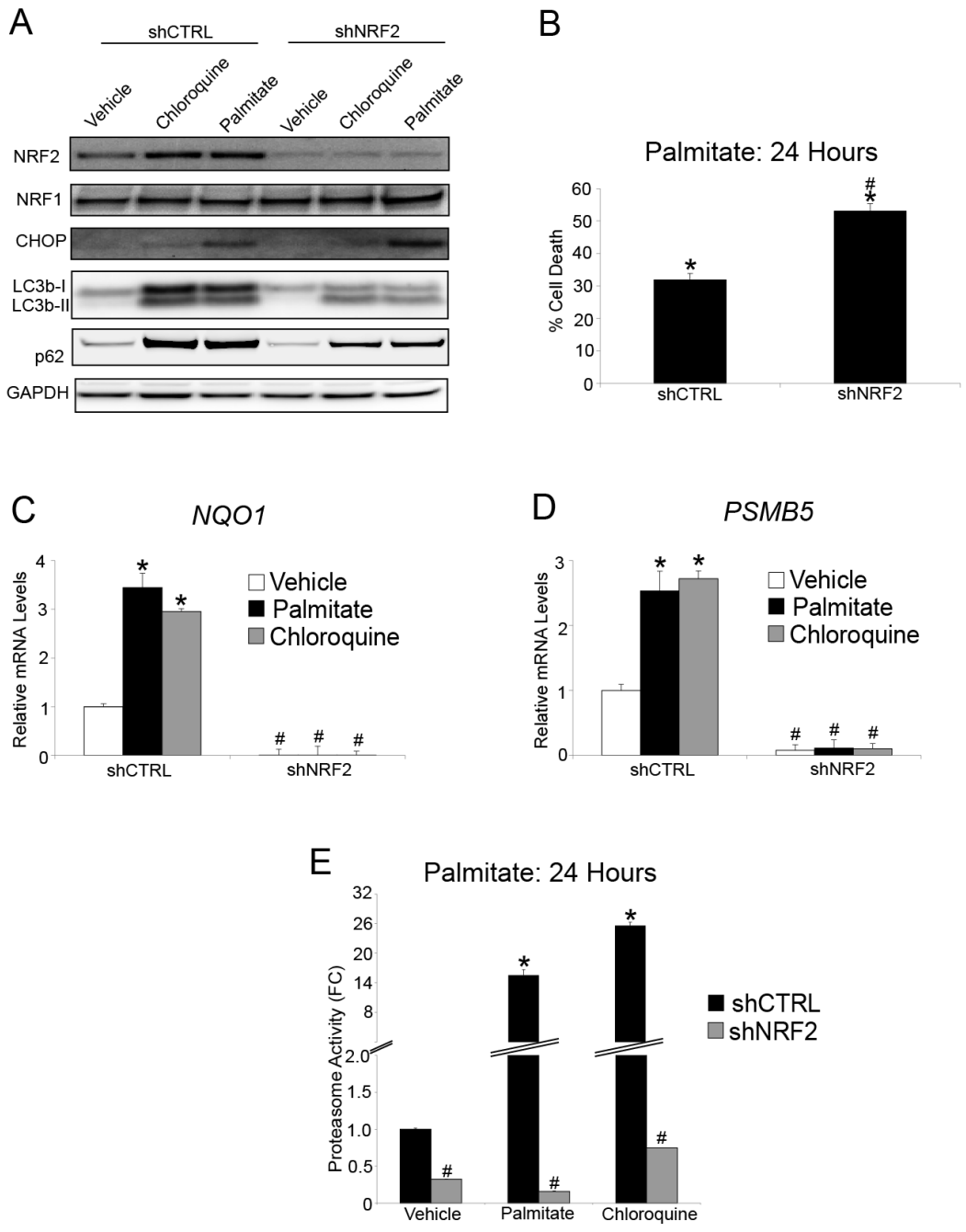

Figure 5-12. NRF2 activation is protective from inhibitors of autophagic flux. (A) shCTRL and shNRF2 HepG2 cells were treated with vehicle, chloroquine, or palmitate for 12 hours and immunoblots were carried out for indicated proteins. (B) shCTRL and shNRF2 cells were treated with palmitate for 24 hours and viability was measure by LDH release. (C-D) shCTRL and shNRF2 cells were treated with vehicle, palmitate, or

chloroquine for 12 hours and qPCR was carried out on the indicated mRNAs. (E) shCTRL and shNRF2 HepG2 cells were treated with vehicle, palmitate, or chloroquine for 24 hours and proteasome activity was measured using the chymotrypsin proteo-glo assay.

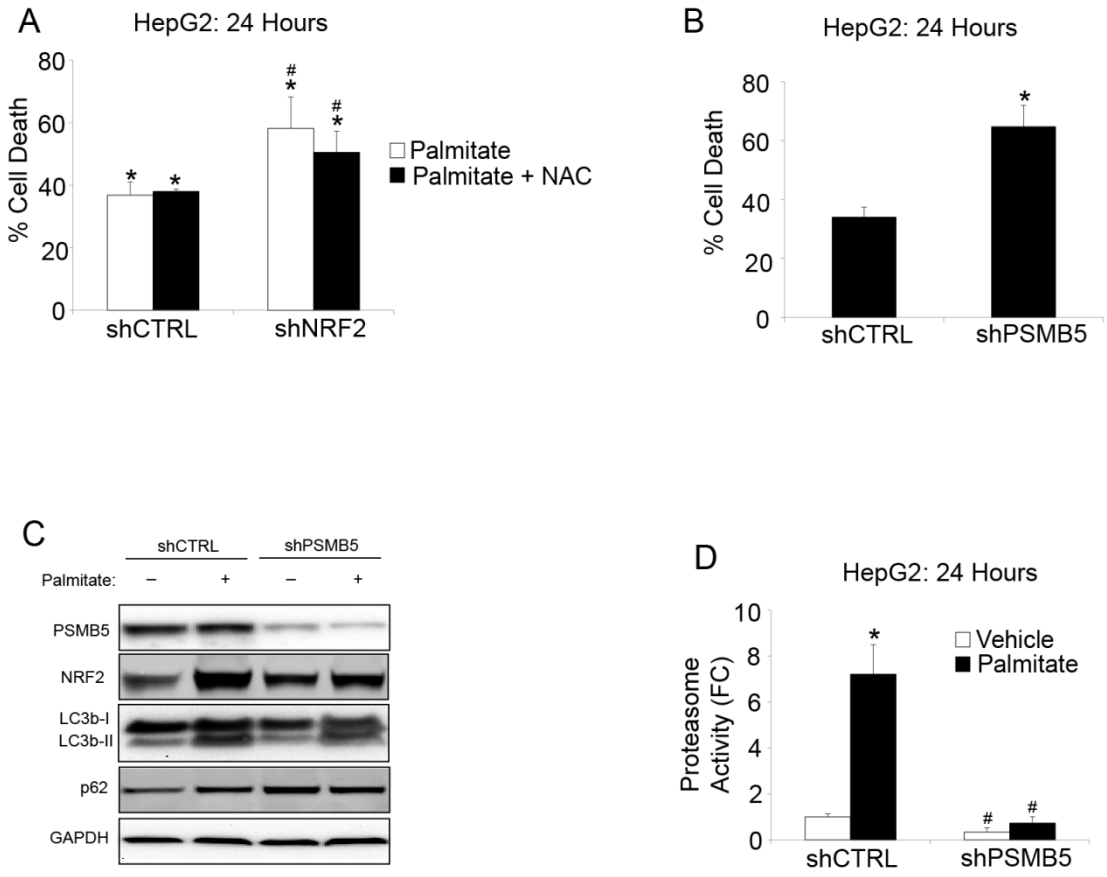

Figure 5-13. Proteasome activation is an adaptive response to inhibition of autophagic flux by palmitate. (A) shCTRL and shNRF2 HepG2 cells were treated with palmitate alone or in the presence of 10mM NAC for 24 hours and cell viability was measured by LDH release. (B) shCTRL and shPSMB5 cells were treated with palmitate for 24 hours and cell viability was measured by LDH release. (C) shCTRL and shPSMB5 cells were treated with palmitate or vehicle for 12 hours and immunoblot analyses were carried out to measure the levels of the indicated proteins. (D) shCTRL and shPSMB5 HepG2 cells were treated with either vehicle or palmitate for 24 hours and proteasome activity was measured using the chymotrypsin proteasome-glo assay.

5.7 Summary

Both CHOP and NF-κB have been associated with the progression of NASH, but the full extent of biologic pathways which they regulate both hepatocellular injury and adaptive responses are not clear [47]. Our study indicates that both CHOP and NF-κB regulate the induction of autophagy coordinately through direct promoter binding and expression of IBTKα, as well as through the unique binding of essential genes needed to form the phagaphore and properly traffic the autophagosome to the lysosome (Fig 5-1 and 5-5). Additionally, global gene expression analysis revealed that CHOP and NF-κB coordinately regulate diverse biological processes in response to palmitate, ranging from cell cycle to hepatoceullar survival and inflammation, with approximately 10% of these genes being regulated by the transcription factor by their direct binding at the promoters of the target genes (Fig 5-4, 5-5, and 5-6). Additionally, CHOP has been shown to be essential for phosphorylation of the p65 subunit of NF-κB, which could explain the majority of co-regulated gene expression changes observed. A unique biological response identified in this study was that both CHOP and NF-κB coordinately regulate the proteasome in response to an inhibition of autophagic flux both through NRF2 activity, which is mediated both by p62 binding to KEAP1. Additionally, CHOP and NF-κB direct transcriptional expression of NRF2 in response to palmitate treatment, as well as through direct binding at genes encoding proteasome subunits (Fig 5-7 and 5-8). Further investigations suggest that both the enhanced proteasome activity and NRF2-mediated response acts as a compensatory mechanism that provides for resistance to a block in autophagic flux (Fig 5-10, 5-12, 5-13, and 5-14). These ideas suggest that the efficacy of the degradative machinery in the cells and their upstream regulatory networks involved are central to the pathogenesis of NASH and progression of hepatocellular injury.

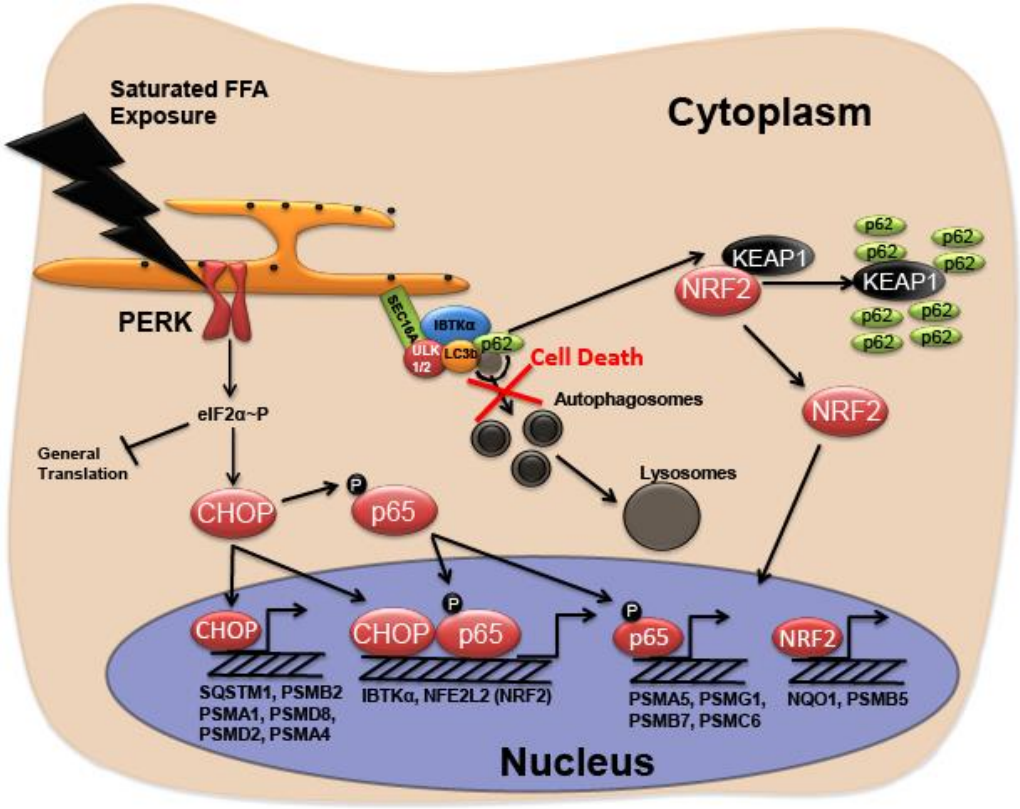

Figure 5-14. Model for UPR regulation of proteasome activation. Saturated FFAs activate PERK and eIF2α~P, which results in preferential translation of CHOP, which is required for the phosphorylation of p65 (P~p65). CHOP and P~p65 bind to genes involved in both the induction of autophagy, such as IBTKα, as well as the proteasome, such as NRF2. Palmitate results in a block in autophagic flux, which causes an accumulation of p62. P62 will bind to KEAP1 and prevent KEAP1 from targeting NRF2 for degradation, allowing for NRF2 to activate proteasome genes such as *PSMB5*.

CHAPTER 6: DISCUSSION

6.1 Saturated FFAs are potent activators of the UPR

Saturated FFAs, but not unsaturated FFAs, activate UPR sensory proteins PERK and IRE1 prior to lipotoxicity (Fig 3-2) [2, 9, 10]. In fact, unsaturated FFAs can help prevent ER stress elicited by palmitate by supporting adaptive mechanisms, including activating triglyceride synthesis that can contribute to growth of lipid droplets. There are many models for how saturated FFAs can trigger ER stress [9]. We found that a portion of palmitate is co-localized to the ER (Fig 3-5), and that saturated FFAs can alter the distribution of the lipid droplets (Fig 3-1 and 3-4), which is predominantly synthesized at the ER [169]. This suggests that saturated FFAs modify the ER membrane, which stresses this organelle [170]. This idea is supported by a study that showed that PERK and IRE1 mutants that lacked their ER luminal sensing domains retained their ability to be activated upon by increased lipid saturation by a mechanism involving increased oligomerization of these UPR sensory proteins [51]. It is curious that expression of the UPR sensor ATF6 was not altered in HepG2 cells in response to palmitate (Fig 3-3), and it was reported that ATF6 is not activated by cleavage to the mature transcription activator [52]. The apparent lack of ATF6 activation may be a consequence of differences in the mechanisms by which ER stress is triggered by saturated FFA, as well as palmitate alteration of vesicular trafficking required for ATF6 passage to the Golgi for cleavage and release to the nucleus.

6.2 CHOP induces secretion of cytokines involved in hepatocyte death and inflammation

Inflammation plays a critical role in a variety of liver pathologies and activation of chronic inflammation may be an important tipping point in the progression from simple

hepatic steatosis to NASH [11, 22]. Secretion of inflammatory cytokines by resident or invading immune cells or release of pro-inflammatory and chemotactic alarmins from stressed and dying hepatocytes is suggested to be central to progressive inflammation in liver pathology. We propose a novel mechanism through which chronically stressed hepatocytes produce cytokines that are part of the cell death and pro-inflammatory responses (Fig 3-21). In this model, elevated and sustained *CHOP* expression is considered to be a potent trigger for the UPR to switch from an adaptive function to death response [46, 58].

These experiments suggest that the signaling pathway by which CHOP activates NF-κB involves enhanced phosphorylation of p65 phosphorylation at serine 536, which is suggested to facilitate nuclear localization and transcriptional activation of NF-κB (Fig 3-12 and 3-21) [87]. Whereas knockdown of CHOP substantially reduced phosphorylation of NF-κB, loss of CHOP function did not deter lowered IκBα levels during treatment with palmitate. Translational expression of IκBα is substantially reduced upon PERK phosphorylation of eIF2α~P [148]; therefore there are multiple modes of UPR regulation of NF-κB. It is noteworthy than knockdown of RELA (p65) did not diminish enhanced *CHOP* expression by palmitate (Fig 3-14), which supports the idea that CHOP functions upstream of NF-κB to induce expression of cytokines. Part of CHOP activation of NF-κB involves the IRAK2 protein kinase, which directly or indirectly enhances p65 phosphorylation at serine 536 (Fig 3-15). It was reported that both CHOP and NF-κB can bind to the *CXCL8* (IL-8) gene promoter in stressed human bronchial epithelial cells, suggesting that CHOP may also contribute directly to transcriptional activation of cytokine gene expression [171].

6.3 The UPR and inhibition of autophagic flux is a key driver of NASH

Autophagy is often thought of as a cell survival pathway that directs damaged organelles and misfolded proteins for degradation in lysosomes [172]. However, autophagy can also play a direct role in cell death, and recent studies have suggested that there are two main processes: (1) type II autophagic cell death, which consists of cell death accompanied by accumulation of large secondary vacuoles, and (2) autosis, which is characterized by a disappearance of the ER and general self-eating [173]. Our studies suggest that saturated FFAs induce neither type II cell death nor autosis, as autophagy is a key driver in hepatocellular death without the appearance of secondary lysosomes (Fig 4-7 and 4-11). A key feature of our study is the localization of IBTKα to ERES through a complex that includes LC3b, SEC16A, and SEC31A (Fig 4-14). When the hepatocytes were exposed to palmitate, LC3b-II was retained at the ER with IBTKα, suggesting either a defect in phagophore elongation or trafficking from the ERES to the lysosome. These findings suggest that saturated FFAs induce a novel form of autophagic cell death, perhaps a subset of autosis, which allows for the lipidation of LC3b but interferes with LC3b trafficking from the ER to lysosomes. Importantly, this block in autophagic flux is coincident with increased inflammation and TNFα signaling, thereby linking key features of NASH pathogenesis in a linked signaling cascade (Fig 4-21). While it is possible that this form of cell death is unique to metabolic stress, it is also likely to be a driver in other diseases states or even drug-induced liver injury in which hepatocellular death and inflammation or prominent pathologies.

Induction of the UPR and a block in autophagic flux were also supported by our analysis of human liver biopsy samples, which indicated that levels of IBTKα and CHOP, as well as total and phosphorylated P65 were increased in both simple steatosis and in NASH (Fig 4-18). Importantly, levels of LC3b-II and P62 were significantly elevated in NASH, which were strongly associated with hepatocellular injury markers, such as

ballooning. Therefore, we identified biomarkers suggested to be specific for NASH, as well as others associated with general NAFLD. Furthermore, analyses of the liver biopsy samples indicate that our in vitro model correlates well with the events occurring in NAFLD. Our principal component analysis combining protein quantification, histology, and serum analysis indicates that key factors and pathways described herein will provide new insight into the progression of simple steatosis to NASH.

In summary, we identified IBTKα as a new member of the UPR that is transcriptionally and translationally expressed during metabolic stress. IBTKα plays a role in both phagophore initiation and formation of transport vesicles at the ERES, linking autophagy and secretion to the pathogensis of NASH. Furthermore, our study indicates that aberrant autophagy and the consequent inhibition of autophagic flux is a key driver in the pathogensis of NASH at both the cellular level and as a correlative biomarker in patient samples. At present, no approved therapies exist to treat NASH, and there is a need for better mechanistic understanding of cellular targets that repress the associated pathologies and progression of NASH. The ability to target both hepatocellular death and inflammation through IBTKα in the treatment in simple steatosis and/or NASH could have therapeutic benefit, and further work in the validation of this target is warranted.

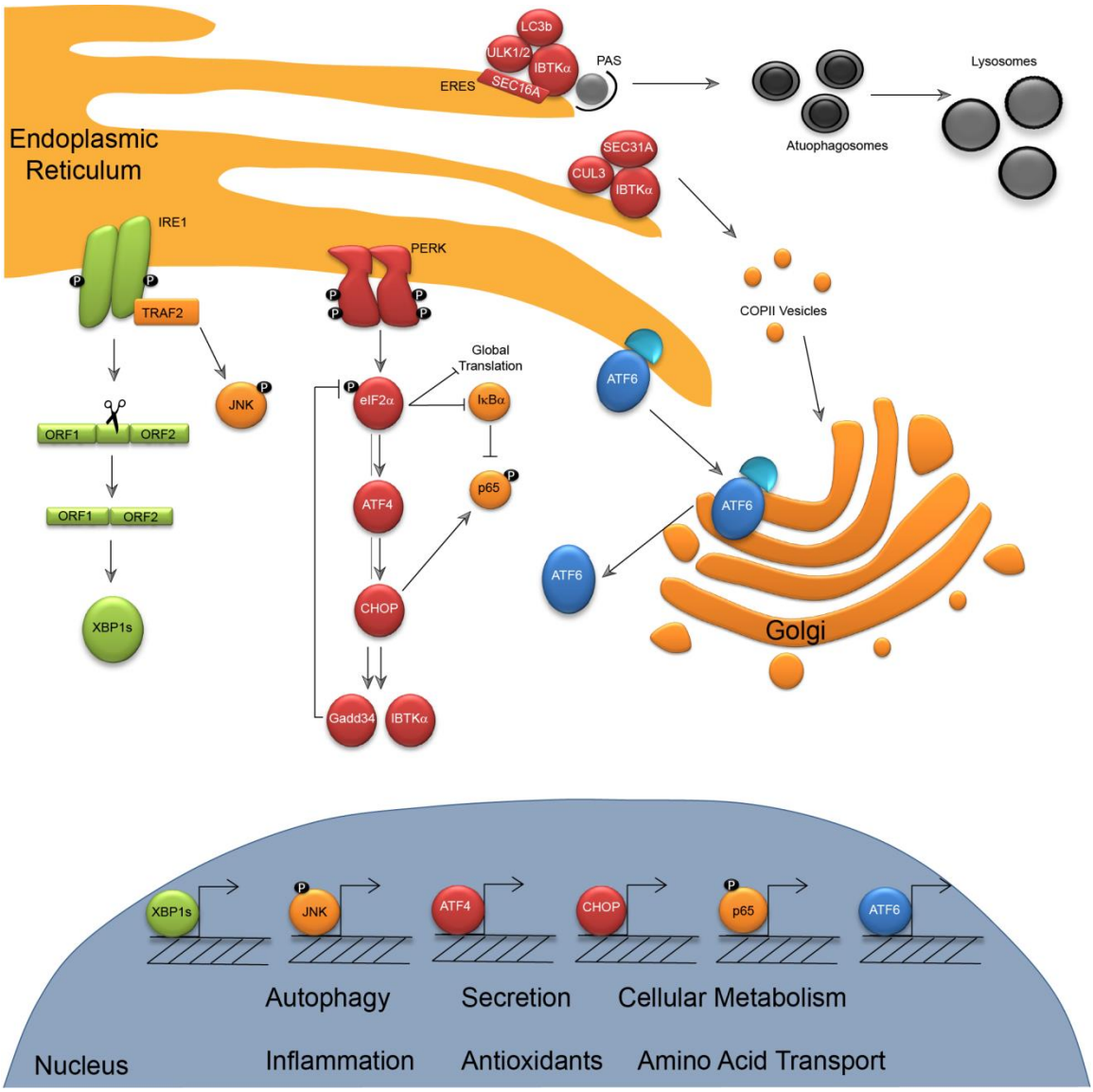

Figure 6-1. The UPR in hepatocellular autophagy and inflammation. Model describing the roles of activation UPR and key transcription factors in the pathogenesis of NASH.

6.4 CHOP and NF-κB coordinately regulate gene expression

Both inhibition of autophagic flux and hepatocellular inflammation, such as the secretion of TNFα, are key drivers in the lipotoxicity associated with palmitate. Our studies indicate that not only is CHOP required for phosphorylation of p65, but that CHOP and NF-κB coordinately regulate global gene expression responses in hepatocytes (Fig 3-12, 5-4, and 5-6). Furthermore, we found that although CHOP and NF-κB result in the co-regulation of global gene expression, many biological pathways are controlled by direct promoter binding of only ~10% of those genes induced or repressed following palmitate exposure. This finding suggests that CHOP and NF-κB regulate discrete nodes in gene expression networks, which together have large scale effects on the global transcriptome and consequent biological expression.

A key feature of NASH is inhibition of autophagic flux, which we determined triggers activation of the proteasome through NRF2 (Fig 5-7). CHOP and NF-κB contribute to increased NRF2 expression in hepatocytes treated with palmitate. Additionally, we suggest that inhibition of autophagic flux results in an accumulation of p62, which binds to KEAP1, resulting in NRF2 nuclear localization and enhanced expression gene encoding proteasome subunits, such as *PSMB5* (Fig 5-7 and 5-8). Additionally, we showed that enhanced proteasome activity was an adaptive response to inhibition of autophagic flux in hepatocytes. These investigations suggest that although depletion of CHOP and NF-κB is cytoprotective in response to palmitate exposure, these transcription factors play dynamic roles to co-regulate biological processes that participate in both pro-death and pro-survival depending on the context and timing of the ER stress conditions.

6.5 UPR in NASH and model systems

Studies on rodent dietary models of NASH and inflammation suggest distinct differences from humans [142, 143]. Our results suggest that there are critical signaling differences in the hepatocyte from these different species (Fig 3-21). Whereas both human and mouse hepatocytes showed induction of the UPR and *CHOP* expression in response to saturated FFA, only human liver cells showed activation of NF-κB and increased expression of key cytokines, such as TNFα, which triggered cell death and inflammation. An underlying contributor to human CHOP activation of NF-κB is p65 phosphorylation at serine-536 by a signaling pathway featuring IRAK2. In mouse primary hepatocytes, there was no induction of p65 phosphorylation in response to palmitate and there was minimal IRAK2 expression (Fig 3-18). Furthermore, expression of TNFα and murine homologue KC were not significantly elevated in mouse cells treated with saturated FFA as observed in human hepatocytes (Fig 3-18). Rodent models of NASH are often lacking in their ability to mimic the human disease [142, 143]. These results suggest that phenotypic deficiencies of mouse dietary models of NASH are due to the absence of key portions of UPR signaling through IRAK2/NF-κB, resulting in lowered hepatotoxicity and macrophage recruitment in response saturated FFA.

Interestingly, both rodent models of NASH and human liver biopsy samples from patients with NASH exhibit UPR induction preceding inhibition of autophagic flux, suggesting a strong correlation between these biological pathways and liver injury [50, 174, 175]. Furthermore, addition of recombinant TNFα in the presence of palmitate to HepG2 cells depleted for IBTKα and CHOP resulted in cell death, but not to the full extent of wild type cells, which have the autophagic pathway intact (Fig 4-17). These results suggest that both an inhibition and autophagic flux and the secretion of CHOP-dependent secreted factors, such as TNFα, are required for lipotoxicity during the pathogensis of NASH. We showed that IBTKα not only plays a role in both the induction

of autophagy, but also the formation of COPII vesicles and consequent secretion of cytokines such as TNFα (Fig 4-11 and 4-17). Furthermore, IBTKα is upregulated in NASH patients coincident with an inhibition of autophagic flux and secretion of TNFα (Fig 4-18 and 4-19), suggesting that depletion of this CHOP-dependent factor could have therapeutic potential to alleviate both hepatoxicity and inflammation observed in NASH.

In summary, we describe new mechanisms that link chronic activation of the UPR with cell death and inflammation, two critical components of progression from hepatic steatosis to NASH. While it is well known that liver-related complications due to NASH are on the rise, there are no FDA approved therapeutic interventions to control the progression of NAFLD to NASH. Furthermore, there is a need for improved prognostic biomarkers and an understanding of genetic susceptibility to NASH. It is noteworthy that there are genetic polymorphisms in *IRAK2* that significantly alter NF-κB activation [150-153], and our study suggests that these genetic alterations will alter CHOP signaling in response to saturated FFA and will affect induction of secreted factors in hepatocytes that trigger inflammation and death. UPR signaling events will also offer new strategies for the diagnosis and treatment of NASH.

6.6 Biomarkers for monitoring the pathogenesis of NAFLD

While the current standard for differentiating patients with simple steatosis from non-alcoholic steatohepatitis involves the characterization of liver biopsy samples, there is a great need for the development of non-invasive biomarkers to assess NAFLD progression [176]. Currently, physicians suggest that there are two key transitions in which biomarkers would be helpful for diagnosis of liver pathologies: (1) simple steatosis from NASH and (2) the onset of fibrosis. Recent studies have suggested that biomarkers that predict hepatocelluar death, such as caspase cleaved cytokeratin 18, and

inflammation, such as TNFα and adipokines, may be useful to differentiate NASH from simple steatosis [177, 178]. Our results indicate that CHOP regulates the secretion of cytokines such as TNFα and IL-8 through both the expression of IBTKα and consequent activation of NF-κB (Fig 4-21). While we did not look for the expression of and release of novel biomarkers of cellular injury and inflammation due to palmitate exposure, we did see a global reduction in secretion due to repression of IBTKα coincident with a reduction in palmitate-induced cell death in IBTKα depleted HepG2 cells (Fig 4-9 and 4-17), suggesting that the CHOP-IBTKα pathway is responsible for the secretion of other biomarkers involved in NASH.

Although the vast majority of publications in the field focus on discovering non-invasive biomarkers to monitor the onset of NASH and fibrosis, the identification of biomarkers which appropriately identifies obese individuals with and without simple steasosis would be of significant value. Our principle component analysis revealed that we have a robust *in vitro* assay in correlation with *in vivo* NASH, but few markers correlated with simple steatosis alone (Fig 4-20). In order to better monitor the progression of NAFLD in the clinic, including the potential reversibility, it will be necessary to both develop robust models and identify biomarkers for simple steatosis.

6.7 Therapeutic landscape for NASH

Currently the standard of care for reversal of both simple steatosis and NASH is lifestyle modifications, including caloric restriction and exercise, and sometimes the need for bariatric surgery or liver transplantation in severe cases of liver disease. While the current belief is that pharmacological intervention is not necessary for the reversal of simple steatosis, there is growing consensus that patients with NASH can benefit from pharmaceutical intervention [179]. Unfortunately, there are currently no FDA-approved therapies for NASH, although pharmacologic agents have been investigated pre-

clinically focus on weight loss, decreased lipid accumulation, as well as enhanced insulin sensitivity. However, the clinical relevance and efficacy of many of these biological targets have not yet been fully tested [180, 181]. Our studies indicate that inhibition of autophagic flux coincident and the consequent secretion of TNFα is a key molecular event driving hepatocellular injury during the pathogenesis of NASH both *in vitro* and in human liver biopsy samples. Furthermore, both the UPR and NF-κB regulate the induction of autophagy and secretion of cytokines through IBTKα (Fig 4-18 and 5-1). Inhibition of the induction of autophagy reduces the secretion of TNFα and rescues hepatocytes from palmitate-induced lipotoxicity, suggesting that this pathway might be a viable therapeutic target for NASH.

6.8 Closing remarks

The UPR and inhibition of autophagic flux have been associated with NASH in both rodent and human liver biopsy samples, and a major goal of this investigation was to establish the role of the UPR in the pathogenesis of NASH through mechanistic studies using human hepatocytes. We show that palmitate directly localizes to the ER wherein it can activate PERK, resulting in activation of the UPR and eIF2α~P, which induces CHOP expression. Deletion of *CHOP* not only prevented the induction of autophagy and palmitate-induced lipotoxicity, but also prevented phosphorylation and nuclear localization of the p65 subunit of NF-κB, and consequent secretion of cytokines, such as TNFα and IL-8. The idea that CHOP regulates NF-κB and secretion is a new concept with regards to UPR signaling. While we present insight about the coordinated regulation of secreted biomarkers by CHOP and NF-κB following hepatoceullar lipotoxicity, the full extent of how the secretome is modified is an important topic for future study. Additionally, a better understanding of how CHOP and NF-κB regulate

global secretion in response to lipotoxicity, including the extracellular release of lipids and non-coding RNAs, will be important for the development of future sera-based biomarkers for NASH.

While the idea that inhibition of autophagic flux has been associated with NASH [50], we showed that a block in autophagic flux is a key driver in the hepatocellular injury during lipotoxicity, providing insight into the intracellular pathway regulating cell injury during the pathogenesis of NASH. Furthermore, we identified IBTKα as a novel UPR member that is essential for inducing autophagy through the formation of a multi-subunit complex at the ERES. Not only is IBTKα essential for the induction of autophagy, but we also showed that IBTKα is critical for secretion of cytokines, such as TNFα. Because NASH is associated with both an inhibition of autophagic flux and hepatocellular inflammation, the ability to target a biological node responsible for both adverse pathways could prove the most beneficial.

A final goal of this investigation was to utilize next generation sequencing to understand the extent of co-regulated networks by CHOP and NF-κB following lipotoxicity. We found that both CHOP and NF-κB coordinately regulate global gene expression, and that each transcription factor binds to a subset of promoters to control critical biological networks, such as inflammation and autophagy. Furthermore, we discovered that in response to an inhibition of autophagic flux, hepatocytes enhance proteasome activity through NRF2 activity, through a pathway involving both CHOP and NF-κB. The utility of an NRF2 activator for the treatment of NASH remains questionable. Although activation of proteasomes would presumably enhance the ability of the hepatocyte to degrade misfolded proteins, the proteasome is incapable of degrading damaged organelles, such as the ER and mitochondria. Similarly, long-term inhibition of autophagy through inhibiting IBTKα might provide a short-term survival advantage, but

might not be a feasible target for a chronic disease state as cells rely upon autophagy for survival. Hence, a greater understanding of networks regulated by CHOP and NF-κB in response to palmitate will be essential to fully appreciate the impact of the UPR with regards to cell injury and potential therapeutic benefit for NAFLD.

Appendix 1. Top 350 proteins identified in pull-downs with IBTKα by using mass spectrometry and MudPIT.

					IBTKα affinity purifications				Normal IgG controls			
Protein Name	IBTK_Fold_Change_A	IBTK_Fold_Change_B	IBTK SAINT Probability	IBTK iREF Known Interaction (0=no;1=yes)	#PSMs IBTK_VEH	# PSMs IBTK_Tg	#PSMs IBTK_PA	#PSMs IBTK_CQ	#PSMs IgG_VEH	#PSMs IgG_TG	#PSMs IgG_PA	#PSMs IgG_CQ
SEC16A	288.58	250.71	1	0	391	68	159	716	0	0	0	0
IGF2BP1	94.53	69.41	1	0	35	164	58	196	0	1	0	0
SEC31A	70.45	59.18	1	0	105	64	29	176	0	1	0	0
PRRC2C	56.02	49.46	1	0	47	13	71	98	0	0	0	0
DOCK4	45.78	45.41	1	0	39	23	38	89	0	0	0	0
IBTK	48.37	40.56	1	1	30	35	59	30	0	0	0	0
PABPC1	52.11	34.95	1	0	115	21	119	569	2	3	0	1
FKBP15	40.12	34.49	1	0	60	10	24	67	0	0	0	0
DHRS2	52.35	33.58	1	0	204	305	114	203	0	4	10	1
IGF2BP3	29.74	26.54	1	0	18	24	25	121	0	1	0	0
EIF3A	26.01	25.86	1	0	20	12	20	62	0	0	0	0
PABPC4	32.22	24.78	1	0	41	14	60	207	0	1	0	1
NUFIP2	24.01	22.75	1	0	18	7	24	57	0	0	0	0
IGF2BP2	25.2	22.19	1	0	20	21	14	106	0	1	0	0
PRRC2B	27.44	21.83	1	0	29	4	35	34	0	0	0	0
RPS24	23.16	21.38	1	0	14	13	28	26	0	0	0	0
EIF4A1	23.66	19.07	1	0	27	23	46	170	1	3	1	0
RPS3	23.98	18.72	1	0	4	10	16	111	0	0	0	0
RPS3A	19.54	18.36	1	0	17	5	17	48	0	0	0	0
KIAA1217	22.83	18.19	1	0	33	3	12	53	0	0	0	0
RPS17	21.28	17.55	1	0	18	21	13	11	0	0	0	0
RPS18	28.8	17.48	1	0	4	3	28	146	0	0	0	0
EIF3B	18.23	17.04	1	0	11	6	22	35	0	0	0	0
RPS7	20.58	16.39	1	0	17	20	41	133	0	3	1	0
GNB2L1	18.51	15.65	1	0	15	25	16	75	0	0	3	0
RPP25L	18.37	14.97	1	0	11	3	10	84	0	0	0	0
RPS16	17.51	13.55	1	0	5	15	11	92	0	1	0	0
RPS10	15.43	12.72	1	0	28	16	26	104	0	4	1	0
HSBP1	14.07	11.92	1	0	18	4	13	11	0	0	0	0
RPL26	15.52	11.57	1	0	6	4	19	84	0	1	0	0
RPLP1	13.49	11.17	1	0	7	15	9	8	0	0	0	0
DNM1L	12.34	10.9	1	0	14	3	12	14	0	0	0	0
ELMO2	12.43	10.75	1	0	3	13	7	24	0	0	0	0
RUVBL1	11.51	10.01	1	0	12	7	9	6	0	0	0	0
TJP1	11.69	9.72	1	0	12	3	14	8	0	0	0	0
ELAVL1	9.92	9.14	1	0	10	4	9	9	0	0	0	0
DDX6	11.45	9.02	1	0	8	5	16	4	0	0	0	0
SEC13	8.83	8.8	1	0	6	4	6	20	0	0	0	0
CBL	10.14	8.79	1	0	15	3	5	12	0	0	0	0
RPS27	8.69	8.32	1	0	6	6	3	20	0	0	0	0
LSM12	8.69	7.97	1	0	4	6	9	8	0	0	0	0
EIF4G2	8.35	7.39	1	0	3	7	8	7	0	0	0	0
SYNCRIP	9.06	7.1	1	0	10	20	13	31	1	3	1	0
DDX3X	6.29	5.4	1	0	10	6	6	23	0	2	1	0
PKP2	5.32	5.12	1	0	3	4	3	6	0	0	0	0
RPS8	7.15	5.11	1	0	10	33	15	38	1	4	4	1

RPS21	6.7	4.87	1	0	8	14	8	8	0	1	0	1
SCAF4	20.02	16.1	0.99	0	17	2	15	70	0	0	0	0
WNK1	18.59	15.05	0.99	0	22	2	12	51	0	0	0	0
RPS15	21.08	13.86	0.99	0	21	19	15	2	0	0	0	0
ATXN2L	15.77	11.55	0.99	0	8	2	28	19	0	0	0	0
TJP2	14.09	11.44	0.99	0	21	2	9	22	0	0	0	0
ZNF512B	11.8	9.29	0.99	0	18	2	9	10	0	0	0	0
RPS27L	9.78	8.74	0.99	0	7	6	2	30	0	0	0	0
PEG10	12.78	8.06	0.99	0	6	4	24	2	0	0	0	0
HNRNPR	8.57	7.86	0.99	0	6	3	9	25	1	0	0	0
TPX2	10.06	7.31	0.99	0	12	2	12	3	0	0	0	0
RUVBL2	7.98	7.06	0.99	0	6	2	10	8	0	0	0	0
MDC1	7.4	5.23	0.99	0	13	3	2	2	0	0	0	0
RPL14	8.29	6.7	0.98	0	6	8	11	54	0	1	3	0
RPS23	40.09	15.32	0.97	0	13	359	57	264	0	1	9	3
G3BP1	7.55	5.73	0.97	0	5	2	14	6	1	0	0	0
RPS2	5.69	4.57	0.97	0	2	4	9	5	0	0	1	0
NONO	5.23	3.92	0.96	0	4	2	10	3	0	1	0	0
ARL6IP4	4.78	3.44	0.96	0	7	18	7	37	0	0	0	4
STAU1	7.48	5.99	0.95	0	9	5	18	23	2	0	3	0
RPS4X	3.43	2.91	0.95	0	2	3	3	16	0	0	0	1
YBX1	7.74	5.59	0.9	0	20	3	16	51	0	3	0	1
FAU	9.3	5.08	0.89	0	3	24	2	41	0	0	1	1
EIF3I	4.54	3.95	0.89	0	2	4	4	16	0	0	2	0
RPL23	3.96	3.26	0.87	0	5	5	7	9	0	0	5	0
S100P	3.63	2.74	0.85	0	8	2	3	3	0	2	0	0
RPSA	5.69	3.74	0.82	0	4	22	11	25	0	3	3	1
HNRNPA1	3.67	2.8	0.76	0	9	3	11	14	2	3	3	0
PRRC2A	21.26	14.76	0.75	0	14	1	30	49	0	0	0	0
DNM2	28.44	13.35	0.75	0	52	0	19	38	0	0	0	0
MYO18A	20.99	12.08	0.75	0	40	1	15	14	0	0	0	0
ZNF318	13.82	8.88	0.75	0	6	1	27	14	0	0	0	0
ARHGAP21	11.27	8.6	0.75	0	14	1	4	36	0	0	0	0
EIF3D	13.04	8.3	0.75	0	15	0	12	29	0	0	0	0
WNK2	12.7	7.62	0.75	0	16	0	5	44	0	0	0	0
UPF1	8.11	6.9	0.75	0	6	1	10	13	0	0	0	0
DPY30	9.92	6.55	0.75	0	10	4	12	0	0	0	0	0
ZCCHC2	15.53	6.54	0.75	0	32	0	11	4	0	0	0	0
SRRM2	11.85	6.52	0.75	0	9	0	21	9	0	0	0	0
EIF4A3	10.86	6.01	0.75	0	11	0	17	6	0	0	0	0
PNN	10.08	5.61	0.75	0	16	0	10	5	0	0	0	0
EIF3C	7.57	5.46	0.75	0	8	0	7	15	0	0	0	0
YLPM1	11.92	5.41	0.75	0	26	0	6	4	0	0	0	0
RANBP3	8.65	5.22	0.75	0	16	0	4	10	0	0	0	0
RPL28	8.45	5.12	0.75	0	9	0	12	5	0	0	0	0
POLR2A	6.04	4.1	0.75	0	6	0	8	4	0	0	0	0
HNRNPU	7.18	3.97	0.75	0	11	0	11	4	0	0	1	0
SPATS2L	6.15	3.95	0.75	0	3	0	11	5	0	0	0	0
PPP1CA	6.37	3.89	0.75	1	3	0	12	4	0	0	0	0
EIF4G1	5.5	3.87	0.75	0	9	1	12	12	1	2	0	0

RPL38	6.42	3.82	0.75	0	8	0	13	16	0	1	1	0
RPS20	4.94	3.8	0.75	0	5	0	5	6	0	0	0	0
EIF3F	4.73	3.66	0.75	0	3	0	6	7	0	0	0	0
MTSS1L	5.26	3.48	0.75	0	9	0	3	3	0	0	0	0
RPS13	4.72	3.43	0.75	0	7	0	3	4	0	0	0	0
HNRNPH1	3.92	3.07	0.75	0	0	3	4	3	0	0	0	0
RPL12	3.96	3.05	0.75	0	3	0	5	3	0	0	0	0
NCL	4.3	2.98	0.75	0	23	75	75	87	8	25	18	6
H2AFX	5.25	2.94	0.75	0	23	0	19	43	4	2	4	1
SOGA2	3.41	2.86	0.75	0	3	0	3	4	0	0	0	0
H2AFZ	4.07	2.39	0.75	0	15	0	17	44	4	3	4	1
NOLC1	11.94	5.72	0.74	0	3	7	27	0	1	0	0	0
RBBP7	6.56	5.57	0.74	0	1	2	6	22	0	0	0	0
EIF3J	7.75	4.8	0.74	0	14	2	4	0	0	0	0	0
KIF18B	9.09	4.6	0.74	0	17	0	7	2	0	0	0	0
SEC23A	7.55	4.39	0.74	0	15	0	2	9	0	0	0	0
FLJ45252	5.24	4.33	0.74	0	6	2	4	1	0	0	0	0
REPS1	8.1	4.2	0.74	0	16	0	5	2	0	0	0	0
RPL5	4.59	4.08	0.74	0	6	1	2	5	0	0	0	0
LARP1	6.47	3.96	0.74	0	7	0	9	2	0	0	0	0
EIF3G	5.27	3.95	0.74	0	6	0	2	15	0	0	0	0
KPNA4	5.14	3.68	0.74	0	2	2	8	0	0	0	0	0
DDX41	5.49	3.61	0.74	0	7	0	6	2	0	0	0	0
HNRNPC	6.52	3.52	0.74	0	14	0	10	7	3	0	0	0
RNPS1	5.48	3.5	0.74	0	9	0	4	2	0	0	0	0
MYCBP2	5.59	3.37	0.74	0	11	0	2	3	0	0	0	0
RPS11	3.93	3.29	0.74	0	0	2	3	10	0	0	0	0
PPP1CB	4.95	3.22	0.74	1	2	0	9	3	0	0	0	0
MYH10	4.26	3.16	0.74	0	3	0	6	9	1	0	0	0
TNRC6A	3.74	3.13	0.74	0	2	0	3	10	0	0	0	0
DLAT	3.38	3.11	0.74	0	3	2	1	2	0	0	0	0
HIST2H2AC	3.92	3.06	0.74	0	30	6	23	50	10	9	4	1
HNRNPF	3.71	3.06	0.74	0	0	2	4	5	0	0	0	0
EIF1AY	3.58	2.99	0.74	0	2	3	2	0	0	0	0	0
EIF3E	3.27	2.84	0.74	0	0	2	2	7	0	0	0	0
CSTF2T	3.52	2.76	0.74	0	3	0	4	2	0	0	0	0
ARHGEF17	3.08	2.7	0.74	0	2	0	2	7	0	0	0	0
MLLT4	3.19	2.55	0.74	0	2	0	4	2	0	0	0	0
RPL15	2.86	2.41	0.74	0	3	0	2	2	0	0	0	0
RPL7A	4.44	2.4	0.74	0	15	0	8	21	2	1	4	0
MYH9	2.71	2.13	0.74	0	3	0	3	5	0	1	0	0
RPLP0	2.4	2.03	0.74	0	7	3	5	13	1	1	2	2
FAM133B	7.46	3.75	0.73	0	1	4	6	95	0	0	2	1
CSTF2	2.53	2.23	0.73	0	2	0	2	2	0	0	0	0
EIF2S1	3.58	2.73	0.72	0	0	2	5	6	1	0	0	0
MYL12A	2.72	2.1	0.72	0	2	1	6	4	0	0	0	1
RPS12	2.86	2.55	0.71	0	3	2	1	5	0	1	0	0
RPL3	5.04	2.47	0.71	0	4	0	16	4	0	2	0	0
RPL13	4.73	3.06	0.7	0	5	1	13	40	0	0	4	1
DDX3Y	3.76	2.91	0.68	0	3	3	1	22	0	2	0	0

PRPF40A	2.75	2.11	0.68	0	2	0	4	2	1	0	0	0
MAPRE1	2.28	1.94	0.68	0	2	0	2	3	1	0	0	0
PTBP1	3.24	1.9	0.65	0	8	0	4	2	0	2	0	0
RPL17	4	2.45	0.64	0	10	1	8	2	0	3	0	0
RPL35	3.03	1.96	0.63	0	7	0	2	3	0	0	2	0
CAPRIN1	3.07	2.17	0.62	0	2	1	9	13	1	1	0	1
RPS19	4.97	3.48	0.61	0	5	10	19	71	1	4	9	0
NAP1L4	3.12	2.06	0.6	0	12	1	3	9	1	4	0	0
RPS6	2.48	1.77	0.6	0	2	0	2	15	0	2	0	0
RPL22	5.8	3.1	0.56	0	4	1	7	81	1	0	6	0
RPL11	3.29	2.33	0.56	0	2	1	6	26	0	3	1	0
RPL27	3.07	1.46	0.56	0	2	0	6	48	0	2	0	2
DDX5	1.71	1.05	0.54	0	3	0	7	7	0	3	2	1
TCOF1	3.33	2.15	0.52	0	15	4	23	13	4	0	13	1
MYL6	3.37	2.01	0.52	0	13	2	13	4	2	5	2	0
SSB	1.92	1.56	0.52	0	2	0	2	2	2	0	0	0
RPS26	3.58	1.43	0.52	0	0	15	2	4	0	1	2	1
DHX15	1.59	1.25	0.52	0	2	0	2	2	0	2	0	0
ALYREF	1.49	0.84	0.52	0	4	0	11	15	2	1	1	5
RPL21	15.13	5.37	0.5	0	18	0	25	0	0	0	0	0
MATR3	6.79	4.74	0.5	0	7	1	9	1	0	0	0	0
FXR1	6.36	4.02	0.5	0	4	1	11	0	0	0	0	0
AAK1	6.34	4.02	0.5	0	11	1	4	0	0	0	0	0
RAVER1	6.37	3.5	0.5	0	4	0	12	1	0	0	0	0
CTNNB1	5.48	3.48	0.5	0	10	0	1	8	0	0	0	0
PSRC1	5.15	3.4	0.5	0	9	0	1	8	0	0	0	0
DCP1A	5.38	3.38	0.5	0	6	0	7	1	0	0	0	0
SRRM1	4.29	3.04	0.5	0	1	0	7	6	0	0	0	0
ILF3	4.29	3.04	0.5	0	1	0	7	6	0	0	0	0
PPP1CC	5.28	2.89	0.5	1	3	0	10	0	0	0	0	0
SNRPD1	4.62	2.83	0.5	0	4	0	7	0	0	0	0	0
CASC3	3.63	2.82	0.5	0	1	0	5	6	0	0	0	0
NKAP	4.73	2.81	0.5	0	0	0	8	10	0	0	0	0
BCLAF1	5.5	2.71	0.5	0	0	0	12	5	0	0	0	0
SCAF1	4.18	2.61	0.5	0	0	0	7	8	0	0	0	0
KIF18A	3.41	2.58	0.5	0	3	0	4	1	0	0	0	0
RBM33	3.41	2.58	0.5	0	3	0	4	1	0	0	0	0
FMR1	4.95	2.45	0.5	0	0	0	11	3	0	0	0	0
ACIN1	4.4	2.44	0.5	0	0	0	9	4	0	0	0	0
CARM1	4.38	2.44	0.5	0	9	0	0	4	0	0	0	0
PHRF1	3.52	2.31	0.5	0	0	0	6	5	0	0	0	0
EIF3L	3.2	2.22	0.5	0	0	0	5	5	0	0	0	0
DNAJA1	2.97	2.22	0.5	0	3	0	3	0	0	0	0	0
PDHA1	3.4	2.22	0.5	0	6	0	0	4	0	0	0	0
NOS1AP	2.97	2.18	0.5	0	4	0	0	6	0	0	0	0
DLST	2.64	2.06	0.5	0	3	0	0	6	0	0	0	0
SRCAP	2.65	1.95	0.5	0	0	0	4	3	0	0	0	0
KCTD3	2.43	1.92	0.5	0	0	0	3	4	0	0	0	0
RPL18	2.56	1.68	0.5	0	0	0	5	4	0	0	1	0
RPL31	4.25	1.51	0.5	0	0	19	5	2	0	1	3	1

TRAP1	2.19	0.58	0.5	0	0	24	0	62	2	5	4	7
SAP18	6.89	2.99	0.49	0	16	0	2	0	0	0	0	0
ELMSAN1	3.73	2.93	0.49	0	2	1	5	0	0	0	0	0
PPP1R10	5.5	2.92	0.49	0	1	0	12	2	0	0	0	0
DLD	3.49	2.82	0.49	0	1	2	0	12	0	0	0	0
SRSF3	3.41	2.74	0.49	0	1	0	2	13	0	0	0	0
LUZP1	3.19	2.64	0.49	0	2	0	1	11	0	0	0	0
RPLP2	3.84	2.58	0.49	0	13	25	12	164	3	13	6	5
SRSF7	3.19	2.39	0.49	0	1	0	5	2	0	0	0	0
MYO9A	2.86	2.28	0.49	0	4	0	1	2	0	0	0	0
ASPSCR1	2.86	2.28	0.49	0	4	0	1	2	0	0	0	0
TRIM71	2.86	2.28	0.49	0	1	0	4	2	0	0	0	0
EIF5	2.42	2.19	0.49	0	1	0	2	4	0	0	0	0
MYCBP	2.42	2.19	0.49	0	1	0	2	4	0	0	0	0
RPL6	2.42	2.19	0.49	0	2	0	1	4	0	0	0	0
CAP1	2.61	2.19	0.49	0	2	2	0	1	0	0	0	0
CHORDC1	2.41	2.18	0.49	0	2	1	0	3	0	0	0	0
SKP1	2.97	2.18	0.49	0	4	0	2	0	0	0	0	0
ATXN2	2.41	2.18	0.49	0	0	1	2	3	0	0	0	0
EPS8L2	2.53	2.15	0.49	0	3	0	1	2	0	0	0	0
SEC24C	2.53	2.15	0.49	0	1	0	3	2	0	0	0	0
ATXN10	3.2	2.02	0.49	0	0	0	6	2	0	0	0	0
RBM12	2.21	1.99	0.49	0	1	0	2	2	0	0	0	0
RPS9	2.2	1.99	0.49	0	2	0	1	2	0	0	0	0
FAM195A	2.43	1.96	0.49	0	0	0	2	7	0	0	0	0
AGO2	2.31	1.9	0.49	0	2	0	0	6	0	0	0	0
OLA1	2.53	1.85	0.49	0	4	0	0	2	0	0	0	0
FILIP1L	2.09	1.78	0.49	0	2	0	0	4	0	0	0	0
ERH	2.21	1.75	0.49	0	0	0	3	2	0	0	0	0
KPNA3	2.21	1.75	0.49	0	0	0	3	2	0	0	0	0
OTUD4	2.2	1.74	0.49	0	3	0	0	2	0	0	0	0
PPP1R13L	2.2	1.74	0.49	0	3	0	0	2	0	0	0	0
RPL37A	1.99	1.7	0.49	0	0	0	2	3	0	0	0	0
MTSS1	1.98	1.7	0.49	0	2	0	0	3	0	0	0	0
RPL10A	2.07	1.69	0.49	0	0	2	0	2	0	0	0	0
DHX29	1.88	1.62	0.49	0	0	0	2	2	0	0	0	0
RPL36AL	1.88	1.62	0.49	0	0	0	2	2	0	0	0	0
SLAIN2	1.88	1.62	0.49	0	0	0	2	2	0	0	0	0
PDZD11	1.88	1.62	0.49	0	0	0	2	2	0	0	0	0
ASCC3	1.87	1.61	0.49	0	2	0	0	2	0	0	0	0
HNRNPM	2.2	1.61	0.49	0	1	0	4	6	0	1	1	0
RPL36	5.44	3.13	0.48	0	1	5	1	46	0	0	3	0
H3F3B	3.33	2.1	0.48	0	4	0	6	1	2	0	0	0
RPS14	2.82	2.09	0.48	0	7	10	7	7	1	1	8	1
RPL23A	1.34	0.76	0.48	0	0	2	8	18	2	3	0	4
SFPQ	4.36	2.81	0.47	0	1	1	10	2	0	0	1	0
TUBA1C	2.61	1.83	0.47	0	40	61	22	83	5	34	12	11
RBM8A	2.38	1.71	0.47	0	2	0	4	1	0	1	0	0
GPI	2.2	1.64	0.47	0	4	0	1	2	0	1	0	0
MTUS1	2.28	1.7	0.46	0	3	0	2	0	1	0	0	0

SSBP1	1.86	1.4	0.46	0	2	0	3	6	3	1	0	0
PDAP1	1.7	1.25	0.46	0	0	0	3	2	0	1	0	0
DDX17	1.46	0.96	0.46	0	2	0	5	8	0	2	3	1
DEK	1.46	1.09	0.44	0	3	0	1	3	1	0	0	1
RBMS1	1.56	1.27	0.43	0	0	0	2	2	0	0	1	0
RPS28	3.24	1.55	0.41	0	3	13	6	154	3	7	0	7
SRSF1	1.74	1.15	0.41	0	0	0	4	2	1	1	0	0
XRCC5	1.69	1.11	0.41	0	0	0	4	2	0	1	1	0
EIF5A2	1.59	1.03	0.41	0	4	0	0	2	0	2	0	0
EIF3K	1.92	1.51	0.39	0	3	0	1	2	2	0	0	0
ZYX	1.7	1.32	0.39	0	2	0	1	7	0	0	3	0
SNRNP200	1.81	1.28	0.39	0	3	0	2	0	1	1	0	0
RPL9	1.25	0.95	0.39	0	0	0	2	3	0	2	0	0
POLDIP3	1.39	0.81	0.39	0	4	0	5	1	2	1	0	2
CCT2	1.56	1.29	0.36	0	2	2	1	4	0	3	1	0
EIF3H	1.77	1.26	0.35	0	0	1	4	3	2	0	2	0
PCBP2	1.38	0.88	0.35	0	0	0	4	3	2	2	0	0
RPL24	3.17	1.64	0.34	0	6	2	6	110	1	2	3	5
SERBP1	1.64	0.91	0.34	0	6	0	9	7	0	9	2	0
EEF2	1.41	0.68	0.34	0	3	0	15	20	0	15	5	0
HIST1H1C	2.57	1.69	0.31	0	7	2	19	7	5	5	2	1
HIST1H2BK	3.23	0.97	0.31	0	36	0	17	3	17	7	0	0
RPL8	2.63	0.88	0.29	0	26	0	7	2	0	0	11	2
RPL18A	1.22	0.87	0.29	0	2	0	2	0	0	3	0	0
UBB	1.21	0.63	0.29	1	9	0	11	23	6	4	0	8
RPS25	6.96	2.31	0.28	0	5	1	6	203	4	7	1	0
RPL27A	6.04	1.61	0.28	0	1	0	3	121	1	2	4	0
RPL34	1.56	1.02	0.28	0	0	4	3	8	0	3	5	0
HNRNPD	1.2	0.63	0.28	0	0	0	2	19	0	2	1	2
PDHX	3.5	2.87	0.25	0	5	1	1	1	0	0	0	0
PFKL	6.56	2.67	0.25	0	16	0	1	0	0	0	0	0
TK1	6.67	2.4	0.25	0	17	0	0	1	0	0	0	0
C4B	3.62	2.2	0.25	0	7	0	1	0	0	0	0	0
SLIRP	3.45	2.16	0.25	0	1	5	0	0	0	0	0	0
THRAP3	4.4	2.13	0.25	0	0	0	10	1	0	0	0	0
ATRX	2.3	2.11	0.25	0	0	1	1	5	0	0	0	0
RSBN1L	5.61	2.1	0.25	0	0	0	14	0	0	0	0	0
HELZ	2.19	2.03	0.25	0	1	1	0	4	0	0	0	0
SEC16B	2.2	2.03	0.25	0	1	0	1	5	0	0	0	0
SETX	2.08	1.95	0.25	0	1	1	0	3	0	0	0	0
DIAPH1	3.07	1.89	0.25	0	6	0	0	1	0	0	0	0
RPL19	3.09	1.89	0.25	0	0	0	6	1	0	0	0	0
ZC3HAV1	1.99	1.88	0.25	0	1	0	1	3	0	0	0	0
IGHG1	6.78	1.87	0.25	0	23	153	7	9	20	3	8	7
SF3B2	2.32	1.84	0.25	0	1	0	3	0	0	0	0	0
TMPO	2.32	1.84	0.25	0	1	0	3	0	0	0	0	0
RSBN1	2.32	1.84	0.25	0	1	0	3	0	0	0	0	0
YEATS2	2.32	1.84	0.25	0	1	0	3	0	0	0	0	0
NCOR1	2.32	1.84	0.25	0	1	0	3	0	0	0	0	0
ZCCHC3	2.76	1.82	0.25	0	0	0	5	1	0	0	0	0

RPL30	2.76	1.82	0.25	0	0	0	5	1	0	0	0	0
RABL6	3.29	1.79	0.25	0	7	0	0	0	0	0	0	0
HSPA8	2.24	1.76	0.25	0	80	71	47	412	39	44	27	41
DNTTIP1	2.98	1.73	0.25	0	0	0	6	0	0	0	0	0
DIDO1	2.98	1.73	0.25	0	0	0	6	0	0	0	0	0
DDX21	2.43	1.73	0.25	0	0	0	4	1	0	0	0	0
CKAP2	2.42	1.73	0.25	0	4	0	0	1	0	0	0	0
SSRP1	2.98	1.73	0.25	0	0	0	6	0	0	0	0	0
IQSEC1	2.96	1.72	0.25	0	6	0	0	0	0	0	0	0
WASF2	1.99	1.7	0.25	0	0	0	1	6	0	0	0	0
ANKHD1	1.99	1.7	0.25	0	0	0	1	6	0	0	0	0
SRSF10	2.65	1.66	0.25	0	0	0	5	0	0	0	0	0
SUPT16H	2.65	1.66	0.25	0	0	0	5	0	0	0	0	0
CNN3	1.77	1.59	0.25	0	0	0	1	4	0	0	0	0
FAM195B	1.77	1.59	0.25	0	1	0	0	4	0	0	0	0
KNCN	1.77	1.59	0.25	0	1	0	0	4	0	0	0	0
R13AX	1.77	1.59	0.25	0	0	0	1	4	0	0	0	0
H1FX	2.32	1.58	0.25	0	0	0	4	0	0	0	0	0
YTHDF1	2.32	1.58	0.25	0	0	0	4	0	0	0	0	0
DALRD3	2.31	1.58	0.25	0	4	0	0	0	0	0	0	0
TOX4	2.32	1.58	0.25	0	0	0	4	0	0	0	0	0
EDC3	1.66	1.52	0.25	0	0	0	1	3	0	0	0	0
EML3	1.66	1.52	0.25	0	0	0	1	3	0	0	0	0
RTCB	1.66	1.52	0.25	0	0	0	1	3	0	0	0	0
CYFIP2	1.66	1.52	0.25	0	1	0	0	3	0	0	0	0
ANKRD17	2.1	1.52	0.25	0	0	0	0	10	0	0	0	0
AGO1	1.66	1.52	0.25	0	1	0	0	3	0	0	0	0
RALBP1	1.98	1.49	0.25	0	3	0	0	0	0	0	0	0
RPL36A	1.99	1.49	0.25	0	0	0	3	0	0	0	0	0
DIAPH3	1.98	1.49	0.25	0	3	0	0	0	0	0	0	0
CSTF3	1.99	1.49	0.25	0	0	0	3	0	0	0	0	0
HAUS8	1.98	1.49	0.25	0	3	0	0	0	0	0	0	0
MAP7D2	1.98	1.49	0.25	0	3	0	0	0	0	0	0	0
RPL32	1.99	1.49	0.25	0	0	0	3	0	0	0	0	0
SDHA	1.98	1.49	0.25	0	3	0	0	0	0	0	0	0
POLR2E	1.88	1.46	0.25	0	0	0	0	8	0	0	0	0
HSPA1A	1.87	1.44	0.25	0	22	17	24	148	18	29	7	11
CLTC	1.62	1.4	0.25	0	1	0	1	4	0	1	0	0
MEF2B	1.55	1.34	0.25	0	0	0	0	5	0	0	0	0
CALD1	1.55	1.34	0.25	0	0	0	0	5	0	0	0	0
MKI67	1.44	1.29	0.25	0	0	0	0	4	0	0	0	0
TDRD3	1.44	1.29	0.25	0	0	0	0	4	0	0	0	0
FBXO45	1.44	1.29	0.25	0	0	0	0	4	0	0	0	0
ALDOA	1.55	1.27	0.25	0	4	6	3	23	3	6	4	2
COL3A1	1.33	1.23	0.25	0	0	0	0	3	0	0	0	0
PDLIM5	1.33	1.23	0.25	0	0	0	0	3	0	0	0	0
DHX9	1.33	1.23	0.25	0	0	0	0	3	0	0	0	0
PRKRA	1.33	1.23	0.25	0	0	0	0	3	0	0	0	0
ABCE1	1.33	1.23	0.25	0	0	0	0	3	0	0	0	0
PHLDB2	1.33	1.23	0.25	0	0	0	0	3	0	0	0	0

Appendix 2. List of CHOP and P~p65 target genes that have binding peaks near TSS of annotated gene.

Overlap	Symbol	Chromosome	CHOP Peak Start	CHOP Peak End	CHOP dTSS	P~p65 Peak Start	P~p65 Peak End	P~p65 dTSS
Common	ACP6	chr1	147141401	147143999	-66	147142281	147143391	-202
Common	ACSM2B	chr16	20586801	20588999	-205	20547377	20548487	39763
Common	ANGPTL7	chr1	11248001	11249999	-346	11248312	11249422	-479
Common	ANKRD23	chr2	97501801	97504599	6558	97502306	97503416	6897
Common	ATP2A2	chr12	110717001	110720199	-432	110718030	110719140	-447
Common	CACTIN	chr19	3626401	3627999	-387	3626187	3627297	71
Common	CCDC97	chr19	41813201	41817599	-694	41814722	41815832	-817
Common	CETN3	chr5	89704601	89706399	103	89705120	89706230	-72
Common	CTTN	chr11	70312601	70315199	69288	70313251	70314361	69194
Common	CYP21A2	chr6	32005001	32006799	-193	31970023	31971133	-2781
Common	DNAH14	chr1	225117001	225117599	-56	225212269	225213379	95461
Common	DYRK3	chr1	206808001	206809799	19	206807812	206808922	-514
Common	ERCC6-PGBD3	chr10	50747201	50748999	-516	50746841	50747951	188
Common	EXOC5	chr14	57734801	57736999	-283	57735620	57736730	-558
Common	FAM13C	chr10	61121801	61123599	-39	61122089	61123199	17
Common	FAM200B	chr4	15682801	15683999	48	15692032	15693142	9235
Common	FAM208B	chr10	5725401	5726399	-901	5725438	5726548	-808
Common	FOXJ3	chr1	42800001	42801599	86	42800774	42801884	219
Common	GLDC	chr9	6644201	6648799	-808	6645348	6646458	-211
Common	GMPPB	chr3	49761001	49762599	-393	49761599	49762709	-747
Common	GUF1	chr4	44679201	44680999	-333	44679778	44680888	-100
Common	HNRNPA2B1	chr7	26239001	26242199	-187	26227087	26228197	12771
Common	HNRNPDL	chr4	83349801	83352799	78	83350694	83351804	129
Common	HYKK	chr15	78797801	78801199	-406	78793257	78794367	-6094
Common	IBTK	chr6	15482601	15483799	920	82800671	82801781	245
Common	IL1RAP	chr3	190230601	190232199	-440	190369550	190370660	138265
Common	IL4I1	chr19	50409001	50411199	-9953	50400223	50401333	-631
Common	KLHDC7A	chr1	18805801	18807599	-724	18705255	18706365	-101614
Common	NFE2L2	chr2	178128001	178130799	459	104067050	104068160	500
Common	MAD2L1	chr4	120987601	120989799	-687	120979452	120980562	8006
Common	MCC	chr5	112630201	112632399	-688	112824154	112825264	-182
Common	METTL20	chr12	31822201	31823399	10191	31811881	31812991	-173
Common	MTHFD2L	chr4	75023001	75024799	71	75022831	75023941	-443
Common	NUDT9	chr4	88342401	88344199	-428	88393426	88394536	50232
Common	PET100	chr19	7693401	7695799	-71	7694037	7695147	-79
Common	PHYHIPL	chr10	60936201	60937599	-327	60936091	60937201	298
Common	PIFO	chr1	111887801	111888599	-982	111862537	111863647	-26090
Common	PKHD1L1	chr8	110373801	110375399	-106	110373176	110374286	-975
Common	PPIP5K2	chr5	102455201	102456799	42	102455700	102456810	297
Common	PRKCZ	chr1	2033801	2037199	-655	2035293	2036403	-307
Common	PRSS12	chr4	119273801	119275799	-878	119273723	119274833	-356
Common	RAB3IP	chr12	70132001	70133599	334	70132504	70133614	-111
Common	RABAC1	chr19	42462601	42464399	28	42463254	42464364	-281
Common	RASA1	chr5	86563001	86564599	-270	86563529	86564639	14
Common	RFXANK	chr19	19302201	19303999	92	19292199	19293309	-10254
Common	SAMD1	chr19	14201601	14202799	-968	111334931	111336041	-808
Common	SH3D21	chr1	36770201	36772199	-794	36771033	36772143	-406
Common	SLC22A25	chr11	63013801	63015199	-17376	63013178	63014288	-16609
Common	SLC25A46	chr5	110073801	110075199	-254	110073412	110074522	-787
Common	SNX24	chr5	122179401	122182399	-260	122169850	122170960	-10755
Common	SUGT1	chr13	53226001	53227599	-31	53225726	53226836	-550
Common	THAP5	chr7	108208601	108210599	297	108209217	108210327	125
Common	TMEM102	chr17	7337601	7339399	-262	7338196	7339306	-11
Common	TMX3	chr18	66340201	66340399	42053	66339896	66341006	41902
Common	TPCN2	chr11	68814601	68817799	-150	68815324	68816434	-471
Common	TRIM24	chr7	138143401	138146199	-279	138143535	138144645	-989
Common	TTC21B	chr2	166809801	166810999	-52	166804824	166805934	4969
Common	UBE2J1	chr6	90062001	90064199	-481	90062615	90063725	-551
Common	WDR5B	chr3	122133601	122136199	-18	122133653	122134763	674
Common	ZNF446	chr19	58985601	58987999	-995	58985218	58986328	-2022
Common	ZNF79	chr9	130184801	130187599	-453	130185992	130187102	-106
Common	ZNF837	chr19	58891801	58893199	-111	58892475	58893585	-641

Overlap	Symbol	Chromosome	P~p65 Peak Start	P~p65 Peak End	P~p65 dTSS
P~p65	ABHD14B	chr3	52007902	52009012	189
P~p65	ACACB	chr12	109576361	109577471	-286
P~p65	ACTA1	chr1	229575870	229576980	-6582
P~p65	ACTA2	chr10	90751285	90752395	-693
P~p65	ACVR1	chr2	158730969	158732079	99
P~p65	ADAM22	chr7	87562485	87563595	-526
P~p65	ADAP2	chr17	29247325	29248435	-874
P~p65	ADIPOR2	chr12	1798858	1799968	-834
P~p65	ADORA2A	chr22	24818639	24819749	-371
P~p65	ADRA2C	chr4	3770696	3771806	2955
P~p65	AHCYL2	chr7	129007426	129008536	17
P~p65	AK9	chr6	110011559	110012669	301
P~p65	AKAP13	chr15	85922835	85923945	-457
P~p65	ALKBH4	chr7	102103856	102104966	910
P~p65	AMIGO1	chr1	110051989	110053099	-208
P~p65	ANGPTL3	chr1	63072277	63073387	9674
P~p65	ANKAR	chr2	190539489	190540599	-667
P~p65	ANKRD28	chr3	15900409	15901519	89
P~p65	ANKRD49	chr11	94226813	94227923	215
P~p65	AP1S2	chrX	15873325	15874435	-743
P~p65	APAF1	chr12	99129461	99130571	90938
P~p65	APIP	chr11	34938214	34939324	-811
P~p65	APOA5	chr11	116663021	116664131	-440
P~p65	APOBEC3B	chr22	39377367	39378477	-482
P~p65	ARAP1	chr11	72463387	72464497	-508
P~p65	ARGLU1	chr13	107220377	107221487	-418
P~p65	ARHGAP18	chr6	129896977	129898087	133838
P~p65	ARHGAP20	chr11	110584094	110585204	-737
P~p65	ARHGAP20	chr11	110446357	110447467	135861
P~p65	ARHGEF3	chr3	57109469	57110579	3312
P~p65	ARID3C	chr9	34628102	34629212	-646
P~p65	ARL3	chr10	104472958	104474068	677
P~p65	ARMC1	chr8	66514033	66515143	31864
P~p65	ARMC9	chr2	232062432	232063542	-273
P~p65	ARMCX4	chrX	100771964	100773074	29488
P~p65	ARNTL2	chr12	27484800	27485910	-432
P~p65	ARTN	chr1	44402426	44403536	3989
P~p65	ASIC2	chr17	32495617	32496727	-12347
P~p65	ASTN2	chr9	119372108	119373218	76831
P~p65	ATAD1	chr10	89577207	89578317	155
P~p65	ATG13	chr11	46638479	46639589	208
P~p65	ATG14	chr14	55832547	55833657	45474
P~p65	ATHL1	chr11	287653	288763	-930
P~p65	ATP5S	chr14	50779284	50780394	792
P~p65	ATXN7L3B	chr12	74931095	74932205	99
P~p65	AVEN	chr15	34331118	34332228	-370
P~p65	AWAT1	chrX	69460651	69461761	6701
P~p65	BARX1	chr9	96712495	96713605	4558
P~p65	BBIP1	chr10	112677939	112679049	200
P~p65	BBS10	chr12	76744097	76745207	-2430
P~p65	BCL11B	chr14	99738348	99739458	-853
P~p65	BCL2L12	chr19	50167775	50168885	-69
P~p65	BCO2	chr11	112045782	112046892	129
P~p65	BIRC3	chr11	102104082	102105192	-83544
P~p65	BLZF1	chr1	169336178	169337288	-461
P~p65	BTF3L4	chr1	52556612	52557722	35310
P~p65	BTN3A1	chr6	26394854	26395964	-7056

Overlap	Symbol	Chromosome	P~p65 Peak Start	P~p65 Peak End	P~p65 dTSS
P~p65	BUB1B	chr15	40452514	40453624	-141
P~p65	CALML3	chr10	5565961	5567071	-336
P~p65	CAP2	chr6	17393260	17394370	79
P~p65	CARD9	chr9	139267644	139268754	-66
P~p65	CAV1	chr7	116202317	116203427	36460
P~p65	CBLB	chr3	105587631	105588741	-299
P~p65	CBLC	chr19	45280261	45281371	-310
P~p65	CCDC34	chr11	27359102	27360212	25138
P~p65	CCDC39	chr3	180396878	180397988	-150
P~p65	CCDC90B	chr11	82959623	82960733	37272
P~p65	CCRN4L	chr4	139966806	139967916	30448
P~p65	CD34	chr1	208194762	208195872	-110634
P~p65	CD69	chr12	9904044	9905154	8898
P~p65	CDC42EP3	chr2	37898985	37900095	138
P~p65	CDKL5	chrX	18442191	18443301	-979
P~p65	CDKN2AIPNL	chr5	133737164	133738274	9879
P~p65	CEACAM20	chr19	45033536	45034646	-543
P~p65	CECR6	chr22	17601749	17602859	-47
P~p65	CENPH	chr5	68484592	68485702	-228
P~p65	CEP164	chr11	117197883	117198993	-133
P~p65	CEP192	chr18	12990053	12991163	-753
P~p65	CGA	chr6	87794456	87795566	9854
P~p65	CHRNA5	chr15	78857303	78858413	-4
P~p65	CIB4	chr2	26863556	26864666	100
P~p65	CLDN16	chr3	190129483	190130593	24377
P~p65	CLEC18C	chr16	70206918	70208028	-455
P~p65	CLUL1	chr18	615549	616659	-596
P~p65	COMMD2	chr3	149469788	149470898	-57
P~p65	COX7A2	chr6	75953561	75954671	-472
P~p65	COX7B2	chr4	46911426	46912536	-729
P~p65	CPE	chr4	166299315	166300425	-227
P~p65	CPED1	chr7	120628066	120629176	-130
P~p65	CREBZF	chr11	85376270	85377380	-643
P~p65	CRMP1	chr4	5821321	5822431	67664
P~p65	CRYBG3	chr3	97520324	97521434	-20005
P~p65	CSMD3	chr8	114389085	114390195	-258
P~p65	CSN3	chr4	71117066	71118176	9288
P~p65	CSTF2	chrX	100097541	100098651	22748
P~p65	CTTNBP2	chr7	117513001	117514111	5
P~p65	CTXN1	chr19	7990294	7991404	202
P~p65	CXCL8	chr4	74604790	74605900	-878
P~p65	CXXC4	chr4	105416054	105417164	-551
P~p65	CYB5R1	chr1	202936828	202937938	-979
P~p65	CYP2D6	chr22	42526725	42527835	-397
P~p65	CYP4F12	chr19	15782618	15783728	-655
P~p65	DARS	chr2	136743228	136744338	-529
P~p65	DCAF17	chr2	172289480	172290590	-726
P~p65	DCAF4	chr14	73391867	73392977	-618
P~p65	DCLRE1A	chr10	115593686	115594796	19734
P~p65	DCTN3	chr9	34620076	34621186	-111
P~p65	DCUN1D5	chr11	102962672	102963782	-283
P~p65	DDO	chr6	110712863	110713973	23335
P~p65	DEAF1	chr11	695573	696683	-374
P~p65	DEGS2	chr14	100611507	100612617	13950
P~p65	DFFA	chr1	10532758	10533868	-700
P~p65	DFNB59	chr2	179326374	179327484	10766
P~p65	DGCR2	chr22	19109792	19110902	-380
P~p65	DHFRL1	chr3	93781870	93782980	-358
P~p65	DMD	chrX	31285307	31286417	-838
P~p65	DMTF1	chr7	86780476	86781586	-646

Overlap	Symbol	Chromosome	P~p65 Peak Start	P~p65 Peak End	P~p65 dTSS
P~p65	DNAJB14	chr4	100844375	100845485	22953
P~p65	DNAJC19	chr3	180707197	180708307	-190
P~p65	DNAJC24	chr11	31390948	31392058	126
P~p65	DNAJC24	chr11	31452732	31453842	61910
P~p65	DNM1	chr9	130964158	130965268	-921
P~p65	DNPH1	chr6	43196929	43198039	-273
P~p65	DONSON	chr21	34948724	34949834	11735
P~p65	DOPEY2	chr21	37535929	37537039	-355
P~p65	DPY19L4	chr8	95731371	95732481	-177
P~p65	DTWD2	chr5	118324078	118325188	-393
P~p65	DUOX1	chr15	45422005	45423115	368
P~p65	DZIP1L	chr3	137832438	137833548	-671
P~p65	EEFSEC	chr3	127870776	127871886	-982
P~p65	EFCAB11	chr14	90260233	90261343	160113
P~p65	EGR3	chr8	22550706	22551816	-446
P~p65	ELF5	chr11	34499846	34500956	32945
P~p65	EOGT	chr3	69062703	69063813	-213
P~p65	EPB41L5	chr2	120864101	120865211	93871
P~p65	EPHA6	chr3	96532352	96533462	-518
P~p65	EPPK1	chr8	144938014	144939124	14063
P~p65	ERCC6L2	chr9	98636928	98638038	-417
P~p65	ESD	chr13	47318757	47319867	52055
P~p65	ESPL1	chr12	53660902	53662012	-626
P~p65	ETV1	chr7	14029272	14030382	-185
P~p65	FABP2	chr4	120243751	120244861	-990
P~p65	FAHD2B	chr2	97760875	97761985	-848
P~p65	FAM105A	chr5	14581043	14582153	-293
P~p65	FAM160A2	chr11	6255477	6256587	-91
P~p65	FAM166B	chr9	35564037	35565147	-696
P~p65	FAM174A	chr5	99869878	99870988	-691
P~p65	FAM217B	chr20	58515678	58516788	789
P~p65	FAM229B	chr6	112407873	112408983	-246
P~p65	FAM43B	chr1	20878017	20879127	-360
P~p65	FAM83G	chr17	18923885	18924995	-16380
P~p65	FANCI	chr15	89785981	89787091	-658
P~p65	FASLG	chr1	172581088	172582198	-46542
P~p65	FBXW7	chr4	153273811	153274921	-256
P~p65	FDX1	chr11	110299471	110300581	-635
P~p65	FMN1	chr15	33359581	33360691	97
P~p65	FOXD4L6	chr9	69203090	69204200	-1441
P~p65	FOXL2NB	chr3	138672483	138673593	6962
P~p65	FRZB	chr2	183731414	183732524	-471
P~p65	FUCA1	chr1	24194722	24195832	-418
P~p65	FZD8	chr10	35930068	35931178	-261
P~p65	GALNT5	chr2	158113116	158114226	-669
P~p65	GAN	chr16	81347083	81348193	-933
P~p65	GANC	chr15	42566136	42567246	325
P~p65	GAREM	chr18	30050656	30051766	-764
P~p65	GAST	chr17	39867029	39868139	-994
P~p65	GBA	chr1	155211088	155212198	-574
P~p65	GFRAL	chr6	55266713	55267823	75001
P~p65	GGTLC2	chr22	22990138	22991248	1911
P~p65	GJA3	chr13	20665724	20666834	68904
P~p65	GJB1	chrX	70434564	70435674	57
P~p65	GKN2	chr2	69171066	69172176	8481
P~p65	GLE1	chr9	131266042	131267152	-374
P~p65	GNA14	chr9	80263289	80264399	-612
P~p65	GNAT3	chr7	80086737	80087847	53950
P~p65	GOLGA8M	chr15	28942728	28943838	14284
P~p65	GOLGA8N	chr15	32884188	32885298	-914

Overlap	Symbol	Chromosome	P~p65 Peak Start	P~p65 Peak End	P~p65 dTSS
P~p65	GORASP2	chr2	171846339	171847449	61858
P~p65	GPIHBP1	chr8	144299452	144300562	4939
P~p65	GPR107	chr9	132815122	132816232	-308
P~p65	GPR156	chr3	119962983	119964093	-396
P~p65	GPR161	chr1	168045407	168046517	59712
P~p65	GPR19	chr12	12848814	12849924	-248
P~p65	GRAMD1B	chr11	123395186	123396296	-603
P~p65	GS1-259H13.2	chr7	99194413	99195523	-934
P~p65	GSTCD	chr4	106629808	106630918	422
P~p65	GTDC1	chr2	145051648	145052758	-143
P~p65	GUF1	chr4	44702082	44703192	22204
P~p65	HAPLN4	chr19	19373093	19374203	-52
P~p65	HAUS3	chr4	2243979	2245089	-674
P~p65	HEY1	chr8	80678848	80679958	-693
P~p65	HKR1	chr19	37824487	37825597	-538
P~p65	HMGCR	chr5	74632026	74633136	-412
P~p65	HNRNPU	chr1	245027435	245028545	-163
P~p65	HRSP12	chr8	99113354	99114464	15509
P~p65	HTN3	chr4	70893350	70894460	-225
P~p65	IARS	chr9	95055198	95056308	285
P~p65	IFNL3	chr19	39735665	39736775	-609
P~p65	IKBKE	chr1	206629771	206630881	-13260
P~p65	IL18BP	chr11	71709144	71710254	-259
P~p65	IL36RN	chr2	113815717	113816827	57
P~p65	INPP5B	chr1	38412733	38413843	-559
P~p65	INSL6	chr9	5185400	5186510	-337
P~p65	IRAK1BP1	chr6	79575905	79577015	-801
P~p65	ISY1	chr3	128880201	128881311	-683
P~p65	JMY	chr5	78623293	78624403	91923
P~p65	KALRN	chr3	124302999	124304109	48
P~p65	KANK1	chr9	469450	470560	-289
P~p65	KATNA1	chr6	149978169	149979279	-8784
P~p65	KCNN3	chr1	154832366	154833476	-583
P~p65	KIAA0513	chr16	85060364	85061474	-438
P~p65	KIAA1024L	chr5	129074060	129075170	-9269
P~p65	KIAA1324L	chr7	86669367	86670477	-372
P~p65	KLHL22	chr22	20849645	20850755	-30
P~p65	KLHL7	chr7	23165070	23166180	19708
P~p65	KLK4	chr19	51408782	51409892	4657
P~p65	KLLN	chr10	89605169	89606279	17470
P~p65	KPNA4	chr3	160283358	160284468	-537
P~p65	KRT6A	chr12	52880288	52881398	6338
P~p65	LARS2	chr3	45428869	45429979	-651
P~p65	LCTL	chr15	66857444	66858554	-164
P~p65	LGI3	chr8	22014434	22015544	-645
P~p65	LINGO1	chr15	77903867	77904977	20447
P~p65	LIPM	chr10	90561175	90562285	-757
P~p65	LLPH	chr12	66529970	66531080	-5992
P~p65	LMBR1L	chr12	49504449	49505559	-321
P~p65	LMO7	chr13	76193522	76194632	-493
P~p65	LMOD2	chr7	123321426	123322536	26120
P~p65	LPPR5	chr1	99470093	99471203	-199
P~p65	LRIG1	chr3	66550499	66551609	-209
P~p65	LRRD1	chr7	91794142	91795252	-107
P~p65	LRRFIP2	chr3	37216788	37217898	508
P~p65	LTN1	chr21	30365434	30366544	-712
P~p65	LXN	chr3	158413526	158414636	-23599
P~p65	LY75-CD302	chr2	160801053	160802163	-40341
P~p65	LYRM9	chr17	26219755	26220865	99
P~p65	LYSMD1	chr1	151137840	151138950	-25

Overlap	Symbol	Chromosome	P~p65 Peak Start	P~p65 Peak End	P~p65 dTSS
P~p65	MAD1L1	chr7	2272431	2273541	-403
P~p65	MAGOHB	chr12	10765103	10766213	-81
P~p65	MAL2	chr8	120257766	120258876	37711
P~p65	MAP6D1	chr3	183530836	183531946	12002
P~p65	MAPKBP1	chr15	42065212	42066322	-865
P~p65	MAST1	chr19	12948141	12949251	-563
P~p65	MBD6	chr12	57923318	57924428	7214
P~p65	MBIP	chr14	36789880	36790990	-553
P~p65	MBLAC1	chr7	99722722	99723832	-1043
P~p65	MCC	chr5	112629962	112631072	95
P~p65	MCM2	chr3	127316616	127317726	-29
P~p65	MCTS1	chrX	119736394	119737504	-795
P~p65	MED27	chr9	134954775	134955885	-56
P~p65	MEF2B	chr19	19281267	19282377	-724
P~p65	MFAP4	chr17	19290895	19292005	-918
P~p65	MFSD5	chr12	53644100	53645210	-715
P~p65	MIOX	chr22	50924174	50925284	-484
P~p65	MIS18BP1	chr14	45671483	45672593	50567
P~p65	MLNR	chr13	49783618	49784728	-10301
P~p65	MMP15	chr16	58080227	58081337	21500
P~p65	MNAT1	chr14	61200980	61202090	76
P~p65	MROH5	chr8	142516871	142517981	-96
P~p65	MRPL28	chr16	419282	420392	732
P~p65	MRPL34	chr19	17414993	17416103	-929
P~p65	MTBP	chr8	121456545	121457655	-538
P~p65	MTR	chr1	236957162	236958272	-864
P~p65	MTRNR2L2	chr5	79946477	79947587	-178
P~p65	MTRNR2L8	chr11	10530374	10531484	-206
P~p65	MUTYH	chr1	45806142	45807252	-555
P~p65	MYBBP1A	chr17	4441602	4442712	16524
P~p65	MYBL1	chr8	67541033	67542143	-16104
P~p65	MYOZ1	chr10	75403311	75404421	-2351
P~p65	NAA30	chr14	57856157	57857267	-559
P~p65	NASP	chr1	46048815	46049925	-290
P~p65	NAT1	chr8	18066800	18067910	-257
P~p65	NAT1	chr8	18027399	18028509	-17
P~p65	NCAPD3	chr11	134021658	134022768	72213
P~p65	NDUFAB1	chr16	23607056	23608166	28
P~p65	NDUFAF4	chr6	97345825	97346935	-613
P~p65	NDUFAF7	chr2	37476565	37477675	18346
P~p65	NEIL3	chr4	178229966	178231076	-470
P~p65	NEK11	chr3	130744514	130745624	-625
P~p65	NGRN	chr15	90807906	90809016	-434
P~p65	NICN1	chr3	49466308	49467418	-106
P~p65	NIPSNAP3B	chr9	107525569	107526679	-327
P~p65	NIT2	chr3	100043904	100045014	-9103
P~p65	NKTR	chr3	42641322	42642432	-270
P~p65	NOL8	chr9	95087521	95088631	-200
P~p65	NPFF	chr12	53901427	53902537	-560
P~p65	NPR3	chr5	32709986	32711096	-202
P~p65	NR3C2	chr4	149363143	149364253	-26
P~p65	NR4A3	chr9	102595917	102597027	12335
P~p65	NSUN4	chr1	46831083	46832193	24788
P~p65	NUS1	chr6	118031795	118032905	35733
P~p65	NUTM2A	chr10	88997389	88998499	12739
P~p65	NXPE4	chr11	114466654	114467764	-725
P~p65	OGFOD1	chr16	56485217	56486327	348
P~p65	OR2A12	chr7	143793371	143794481	1725
P~p65	OR4C3	chr11	48347267	48348377	1329
P~p65	OR4K17	chr14	20586271	20587381	1260

Overlap	Symbol	Chromosome	P~p65 Peak Start	P~p65 Peak End	P~p65 dTSS
P~p65	OR5AS1	chr11	55798601	55799711	1261
P~p65	OR5W2	chr11	55680102	55681212	1401
P~p65	OR6C1	chr12	55712988	55714098	-841
P~p65	PAMR1	chr11	35551301	35552411	-8
P~p65	PAPD4	chr5	78907639	78908749	-49
P~p65	PARP12	chr7	139783855	139784965	-20889
P~p65	PAWR	chr12	80084785	80085895	-550
P~p65	PBOV1	chr6	138540000	138541110	-928
P~p65	PCDHA13	chr5	140263628	140264738	2329
P~p65	PCSK9	chr1	55530838	55531948	25498
P~p65	PDCD6IP	chr3	33839077	33840187	-431
P~p65	PDE11A	chr2	178937105	178938215	-178
P~p65	PDE12	chr3	57556428	57557538	15002
P~p65	PDGFC	chr4	157892236	157893346	-245
P~p65	PDPN	chr1	13944292	13945402	32880
P~p65	PDX1	chr13	28493194	28494304	-419
P~p65	PES1	chr22	30987331	30988441	41
P~p65	PGBD4	chr15	34394459	34395569	740
P~p65	PHF3	chr6	64396556	64397666	40680
P~p65	PIGV	chr1	27124522	27125632	10398
P~p65	PKD2L1	chr10	102089748	102090858	-60
P~p65	PLD6	chr17	17114622	17115732	-5531
P~p65	PLXNA1	chr3	126679516	126680626	-27366
P~p65	POLR2J2	chr7	102312283	102313393	-662
P~p65	POP4	chr19	30095779	30096889	-836
P~p65	POU5F1B	chr8	128454432	128455542	27130
P~p65	POU6F1	chr12	51611859	51612969	-937
P~p65	PPAP2A	chr5	54830783	54831893	-432
P~p65	PPIAL4E	chr1	148805246	148806356	-214
P~p65	PPP1R3C	chr10	93393223	93394333	-920
P~p65	PPP2R5A	chr1	212473970	212475080	-623
P~p65	PRDM15	chr21	43283486	43284596	-630
P~p65	PRDX1	chr1	45988256	45989366	-249
P~p65	PRG2	chr11	57173298	57174408	-15723
P~p65	PRRC2C	chr1	171454175	171455285	64
P~p65	PSMB7	chr9	127177566	127178676	-369
P~p65	PSMC6	chr14	53173242	53174352	-99
P~p65	PSMG1	chr21	40546529	40547639	8356
P~p65	PSPC1	chr13	20357130	20358240	-526
P~p65	PTBP2	chr1	97281048	97282158	93409
P~p65	PTPN18	chr2	131133119	131134229	20094
P~p65	PTPN9	chr15	75889792	75890902	-18715
P~p65	PURG	chr8	30891372	30892482	-696
P~p65	PXDC1	chr6	3721822	3722932	29869
P~p65	RAB11FIP2	chr10	119805184	119806294	375
P~p65	RAB32	chr6	146863750	146864860	-523
P~p65	RAB4B	chr19	41283171	41284281	-398
P~p65	RALBP1	chr18	9473977	9475087	-998
P~p65	RASA4	chr7	102257399	102258509	-749
P~p65	RASAL1	chr12	113573611	113574721	-122
P~p65	RASSF6	chr4	74486500	74487610	-707
P~p65	RGS2	chr1	192776947	192778057	-667
P~p65	RIN3	chr14	92967513	92968623	-12057
P~p65	RMDN2	chr2	38150931	38152041	-976
P~p65	RNASEK	chr17	6915772	6916882	591
P~p65	RNF144A	chr2	7038059	7039169	-18909
P~p65	RNF215	chr22	30783484	30784594	-737
P~p65	RNF25	chr2	219536600	219537710	-374
P~p65	RNLS	chr10	90342540	90343650	-13
P~p65	ROBO4	chr11	124767880	124768990	-604

Overlap	Symbol	Chromosome	P~p65 Peak Start	P~p65 Peak End	P~p65 dTSS
P~p65	RPS6KA5	chr14	91527300	91528410	-862
P~p65	RPUSD1	chr16	833514	834624	4314
P~p65	RSBN1	chr1	114354836	114355946	-321
P~p65	SAMD1	chr19	14201737	14202847	-1060
P~p65	SCYL3	chr1	169821419	169822529	41126
P~p65	SEC14L4	chr22	30920199	30921309	-19056
P~p65	SECISBP2L	chr15	49339063	49340173	-858
P~p65	SEPW1	chr19	48281220	48282330	-67
P~p65	SERTAD3	chr19	40950324	40951434	-597
P~p65	SESN3	chr11	94964209	94965319	-518
P~p65	SHFM1	chr7	96338847	96339957	-199
P~p65	SHPK	chr17	3538523	3539633	538
P~p65	SIRT1	chr10	69677777	69678887	33393
P~p65	SLC25A26	chr3	66270381	66271491	-232
P~p65	SLC35A1	chr6	88222754	88223864	40666
P~p65	SLC35G1	chr10	95652779	95653889	-396
P~p65	SLC6A20	chr3	45837386	45838496	94
P~p65	SLC6A3	chr5	1460161	1461271	-15173
P~p65	SLC7A13	chr8	87225423	87226533	16626
P~p65	SLN	chr11	107577312	107578422	4920
P~p65	SLURP1	chr8	143820888	143821998	2386
P~p65	SMC2	chr9	106856157	106857267	-119
P~p65	SMC4	chr3	160117318	160118428	-474
P~p65	SMLR1	chr6	131159730	131160840	11740
P~p65	SMPDL3A	chr6	123105044	123106154	-4595
P~p65	SNAPC4	chr9	139292559	139293669	-225
P~p65	SNRK	chr3	43326770	43327880	-679
P~p65	SNX16	chr8	82754659	82755769	-693
P~p65	SON	chr21	34914821	34915931	32
P~p65	SOX5	chr12	24102882	24103992	529
P~p65	SP3	chr2	174770242	174771352	58150
P~p65	SPEG	chr2	220324051	220325161	-928
P~p65	SPN	chr16	29672828	29673938	-888
P~p65	SPON2	chr4	1167154	1168264	-710
P~p65	SQRDL	chr15	45983063	45984173	56680
P~p65	SS18	chr18	23670996	23672106	-940
P~p65	SSBP2	chr5	81047398	81048508	-881
P~p65	ST8SIA5	chr18	44394341	44395451	-57857
P~p65	STARD13	chr13	33676536	33677646	83125
P~p65	STARD13	chr13	33690800	33691910	68861
P~p65	STX3	chr11	59521316	59522426	-661
P~p65	SYCE3	chr22	51006274	51007384	-5501
P~p65	SYNPO2	chr4	119808996	119810106	-445
P~p65	SYT1	chr12	79438084	79439194	-794
P~p65	TAAR2	chr6	132939403	132940513	-726
P~p65	TAF6L	chr11	62537406	62538516	-814
P~p65	TALDO1	chr11	727484	728594	-19393
P~p65	TAS2R43	chr12	11244478	11245588	-121
P~p65	TBCEL	chr11	120894108	120895218	-140
P~p65	TC2N	chr14	92302553	92303663	-238
P~p65	TDRD3	chr13	60970210	60971320	174
P~p65	TFF1	chr21	43786193	43787303	-104
P~p65	TFPT	chr19	54619246	54620356	-746
P~p65	TGFBR1	chr9	101866127	101867237	-730
P~p65	THAP10	chr15	71183645	71184755	572
P~p65	THG1L	chr5	157157410	157158520	-358
P~p65	TIGD2	chr4	90032619	90033729	-794
P~p65	TLR1	chr4	38805962	38807072	-105
P~p65	TMEM132B	chr12	126147169	126148279	40726
P~p65	TMEM150B	chr19	55823740	55824850	12413

Overlap	Symbol	Chromosome	P~p65 Peak Start	P~p65 Peak End	P~p65 dTSS
P~p65	TMEM173	chr5	138862014	138863124	-226
P~p65	TMEM18	chr2	667119	668229	9765
P~p65	TMEM38B	chr9	108455458	108456568	-793
P~p65	TMEM40	chr3	12801084	12802194	-831
P~p65	TMEM5	chr12	64172830	64173940	-198
P~p65	TMEM69	chr1	46152904	46154014	-388
P~p65	TMEM74	chr8	109799404	109800514	-189
P~p65	TMEM9	chr1	201123215	201124325	-87
P~p65	TOR1B	chr9	132564560	132565670	-317
P~p65	TOR4A	chr9	140171474	140172584	-251
P~p65	TOX3	chr16	52581911	52583021	-752
P~p65	TRIM49D1	chr11	89650623	89651733	-300
P~p65	TRIM50	chr7	72739108	72740218	-84
P~p65	TRIOBP	chr22	38155511	38156621	13825
P~p65	TSC22D1	chr13	45010724	45011834	111
P~p65	TSPAN14	chr10	82212618	82213728	-865
P~p65	TSPY10	chrY	9367763	9368873	2810
P~p65	TSR2	chrX	54466004	54467114	-294
P~p65	TTK	chr6	80713132	80714242	-635
P~p65	TYRO3	chr15	41850128	41851238	-537
P~p65	UBE2D1	chr10	60093401	60094511	-783
P~p65	UBE2Q1	chr1	154531286	154532396	-721
P~p65	UGGT1	chr2	128953638	128954748	105411
P~p65	UNC5A	chr5	176236448	176237558	-557
P~p65	USF1	chr1	161015578	161016688	-364
P~p65	USP17L29	chr4	9325674	9326784	-662
P~p65	VIP	chr6	153071092	153072202	-285
P~p65	VWC2L	chr2	215275456	215276566	-450
P~p65	WASL	chr7	123389265	123390375	-695
P~p65	WDR13	chrX	48455548	48456658	-121
P~p65	WDR18	chr19	983312	984422	-461
P~p65	WDR72	chr15	53832747	53833857	-2
P~p65	WDR73	chr15	85196932	85198042	34
P~p65	WIPF1	chr2	175548059	175549169	-987
P~p65	WNT2B	chr1	113064203	113065313	13388
P~p65	XPC	chr3	14219284	14220394	333
P~p65	YAP1	chr11	101979899	101981009	-738
P~p65	ZAP70	chr2	98356582	98357692	6268
P~p65	ZC2HC1A	chr8	79577198	79578308	-529
P~p65	ZC3H8	chr2	112971995	112973105	40114
P~p65	ZDHHC20	chr13	22033376	22034486	-422
P~p65	ZFP14	chr19	36869714	36870824	-164
P~p65	ZFP37	chr9	115818858	115819968	-342
P~p65	ZFYVE27	chr10	99496150	99497260	-173
P~p65	ZMPSTE24	chr1	40722487	40723597	-680
P~p65	ZNF195	chr11	3400527	3401637	-630
P~p65	ZNF211	chr19	58143319	58144429	-661
P~p65	ZNF326	chr1	90460730	90461840	607
P~p65	ZNF347	chr19	53662172	53663282	-405
P~p65	ZNF407	chr18	72516438	72517548	174074
P~p65	ZNF428	chr19	44123510	44124620	-51
P~p65	ZNF43	chr19	22019406	22020516	-951
P~p65	ZNF438	chr10	31287850	31288960	41
P~p65	ZNF493	chr19	21571218	21572328	-8148
P~p65	ZNF597	chr16	3485123	3486233	7812
P~p65	ZNF610	chr19	52829299	52830409	-9644
P~p65	ZNF641	chr12	48744115	48745225	4
P~p65	ZNF660	chr3	44625324	44626434	-577
P~p65	ZNF706	chr8	102208033	102209143	9372
P~p65	ZNF71	chr19	57105358	57106468	-751
P~p65	ZNF80	chr3	113952835	113953945	3035
P~p65	ZNF883	chr9	115774418	115775528	-501
P~p65	ZNF90	chr19	20232342	20233452	44094
P~p65	ZNF98	chr19	22572787	22573897	31806
P~p65	ZP3	chr7	76071434	76072544	17717
P~p65	ZSCAN9	chr6	28200908	28202018	8434

Overlap	Symbol	Chromosome	CHOP Peak Start	CHOP Peak End	CHOP dTSS
CHOP only	ABCA2	chr9	139923601	139925599	-1226
CHOP only	ABCC4	chr13	95951401	95955999	-13
CHOP only	ABHD16B	chr20	62483601	62501599	34
CHOP only	ABHD17A	chr19	1875001	1877199	9418
CHOP only	ABHD3	chr18	19283401	19287399	-634
CHOP only	ABHD5	chr3	43731401	43733399	25
CHOP only	ABTB1	chr3	127390801	127391999	-381
CHOP only	ACAD10	chr12	112124001	112125399	843
CHOP only	ACE	chr17	61575201	61578199	14522
CHOP only	ACOT7	chr1	6453401	6454799	-274
CHOP only	ACSL1	chr4	185726601	185727799	-258
CHOP only	ACSS3	chr12	81470601	81472999	-9
CHOP only	ACTN4	chr19	39127201	39128399	-10467
CHOP only	ACY3	chr11	67416801	67419999	-270
CHOP only	ADAL	chr15	43620401	43623199	-754
CHOP only	ADAM10	chr15	59040801	59044399	-423
CHOP only	ADAM19	chr5	157001401	157004199	31
CHOP only	ADAM23	chr2	207306801	207307999	-968
CHOP only	ADAM8	chr10	135090801	135091999	-993
CHOP only	ADAMTS1	chr9	136270201	136272999	-7859
CHOP only	ADAMTS3	chr4	73433601	73435599	-84
CHOP only	ADAMTS7	chr15	79103201	79105199	-427
CHOP only	ADAMTSL	chr19	1511601	1515799	-512
CHOP only	ADAT3	chr19	1902201	1906999	-771
CHOP only	ADPGK	chr15	73075201	73078599	-774
CHOP only	ADPRHL2	chr1	36553201	36556399	347
CHOP only	ADRA2A	chr10	112835601	112837199	-390
CHOP only	AFF3	chr2	100721601	100723399	-455
CHOP only	AGBL3	chr7	134670801	134671799	41
CHOP only	AGER	chr6	32151601	32152399	99
CHOP only	AGO3	chr1	36395801	36397599	17
CHOP only	AGPAT9	chr4	84456001	84458199	33
CHOP only	AHDC1	chr1	27929601	27931199	-395
CHOP only	AHSG	chr3	186328201	186333599	50
CHOP only	AIM1	chr6	106957201	106960799	-730
CHOP only	AK3	chr9	4740401	4743399	-101
CHOP only	AK4	chr1	65611001	65616399	-150
CHOP only	AKAP11	chr13	42845201	42846799	-289
CHOP only	AKAP17A	chrX	1708401	1710799	-886
CHOP only	AKAP9	chr7	91569001	91570799	-289
CHOP only	ALG12	chr22	50294601	50297199	16206
CHOP only	ALG14	chr1	95538001	95538999	7
CHOP only	ALG3	chr3	183966401	183968199	13
CHOP only	ALKBH1	chr14	78137401	78138799	36256
CHOP only	ALKBH3	chr11	43901601	43902799	-157
CHOP only	ALKBH8	chr11	107435601	107437399	-39
CHOP only	ALS2	chr2	202644601	202647399	-105
CHOP only	AMBP	chr9	116819801	116823199	19252
CHOP only	AMD1	chr6	111194401	111197599	13
CHOP only	AMDHD1	chr12	96336001	96338799	329
CHOP only	AMOTL2	chr3	134090801	134095999	27
CHOP only	ANAPC10	chr4	146053601	146054199	-34207
CHOP only	ANGPTL1	chr1	178817201	178818199	22515
CHOP only	ANGPTL4	chr19	8437401	8440599	9989
CHOP only	ANKIB1	chr7	91874601	91876399	-48
CHOP only	ANKRA2	chr5	72860001	72862199	411
CHOP only	ANKRD1	chr10	92680601	92681999	-268
CHOP only	ANKRD1	chr10	92671001	92671799	9632
CHOP only	ANKRD13I	chr11	67055001	67058199	-162

Overlap	Symbol	Chromosome	CHOP Peak Start	CHOP Peak End	CHOP dTSS
CHOP only	ANKRD20A2	chr9	43133001	43135199	-556
CHOP only	ANKRD29	chr18	21241801	21243999	-51
CHOP only	ANKRD32	chr5	93953601	93955999	409
CHOP only	ANKRD36	chr2	97778201	97779799	-233
CHOP only	ANKRD52	chr12	56650401	56653999	-57
CHOP only	ANKS1B	chr12	100379001	100379799	-968
CHOP only	ANKS3	chr16	4784001	4786599	-922
CHOP only	ANO6	chr12	45607801	45610399	-670
CHOP only	ANO7	chr2	242134601	242136599	7676
CHOP only	ANP32B	chr9	100744601	100745999	-189
CHOP only	ANXA2	chr15	60711001	60711399	-21015
CHOP only	ANXA2R	chr5	43038601	43043799	-753
CHOP only	AP4B1	chr1	114445601	114449199	125
CHOP only	AP5B1	chr11	65547001	65549999	-438
CHOP only	APBB3	chr5	139943001	139944799	289
CHOP only	APEH	chr3	49707201	49712199	-1735
CHOP only	AQP6	chr12	50381201	50383799	15880
CHOP only	AQP7	chr9	33402001	33404399	-683
CHOP only	ARCN1	chr11	118441601	118444199	-202
CHOP only	ARF4	chr3	57581601	57584999	-85
CHOP only	ARF6	chr14	50356801	50360999	-836
CHOP only	ARFGAP2	chr11	47196601	47200199	276
CHOP only	ARFIP2	chr11	6500801	6506399	-891
CHOP only	ARG2	chr14	68084401	68087399	-679
CHOP only	ARHGAP22	chr10	49863801	49864799	10
CHOP only	ARHGEF1	chr19	42386401	42389399	-546
CHOP only	ARHGEF12	chr11	120205601	120208799	-418
CHOP only	ARHGEF16	chr1	3369801	3370999	-747
CHOP only	ARHGEF2	chr1	155946801	155948999	66
CHOP only	ARHGEF26	chr3	153837401	153839599	-292
CHOP only	ARHGEF28	chr5	72920201	72922999	-383
CHOP only	ARID4A	chr14	58764201	58766799	278
CHOP only	ARL6IP4	chr12	123464601	123466399	893
CHOP only	ARPC5L	chr9	127628601	127632599	-884
CHOP only	ARPIN	chr15	90454201	90457799	-81
CHOP only	ARRDC2	chr19	18122801	18127199	6023
CHOP only	ASAP3	chr1	23808601	23813199	-150
CHOP only	ASB1	chr2	239360801	239362799	26174
CHOP only	ASB13	chr10	5707801	5709999	-342
CHOP only	ASB6	chr9	132396001	132397599	7648
CHOP only	ASCC3	chr6	101328401	101329999	48
CHOP only	ASNS	chr7	97501201	97502199	154
CHOP only	ASPHD1	chr16	29909401	29913399	-747
CHOP only	ASTE1	chr3	130745201	130746799	-302
CHOP only	ATAD2	chr8	124406801	124410999	-195
CHOP only	ATAD3A	chr1	1445601	1448599	-423
CHOP only	ATAD3B	chr1	1405801	1407399	-564
CHOP only	ATE1	chr10	123686401	123688799	-22
CHOP only	ATF3	chr1	212779601	212782799	-770
CHOP only	ATG12	chr5	115175801	115178599	348
CHOP only	ATG9B	chr7	150707601	150708999	13286
CHOP only	ATG9B	chr7	150721601	150722599	-514
CHOP only	ATL2	chr2	38603201	38605999	-168
CHOP only	ATN1	chr12	7036001	7036999	-980
CHOP only	ATP10D	chr4	47487001	47487999	90
CHOP only	ATP5C1	chr10	7829401	7831799	507
CHOP only	ATP5SL	chr19	41944801	41946999	-57
CHOP only	ATP6V0A2	chr12	124193801	124199799	-65
CHOP only	ATP6V0E1	chr5	172409201	172411399	-463
CHOP only	ATP6V1G1	chr9	117348001	117351399	-294

Overlap	Symbol	Chromosome	CHOP Peak Start	CHOP Peak End	CHOP dTSS
CHOP only	ATP7B	chr13	52585401	52586399	-270
CHOP only	ATP8B2	chr1	154296601	154298599	-436
CHOP only	ATP8B3	chr19	1809801	1815199	-225
CHOP only	ATP9B	chr18	76828601	76829999	-97
CHOP only	ATR	chr3	142297001	142298199	68
CHOP only	ATXN7	chr3	63849201	63850799	-233
CHOP only	ATXN7L1	chr7	105516201	105517999	-69
CHOP only	AVPI1	chr10	99436401	99437999	9815
CHOP only	AXL	chr19	41731601	41732799	-460
CHOP only	B3GNT9	chr16	67182001	67187999	-98
CHOP only	B4GALT4	chr3	118958001	118961599	-48
CHOP only	B4GALT6	chr18	29264401	29265999	-514
CHOP only	BAHD1	chr15	40729801	40732999	-520
CHOP only	BANP	chr16	87992001	87993399	-777
CHOP only	BATF3	chr1	212872601	212874999	-473
CHOP only	BAZ1B	chr7	72934401	72938999	-85
CHOP only	BAZ2B	chr2	160548601	160549399	19946
CHOP only	BBC3	chr19	47735201	47736799	23
CHOP only	BCAP29	chr7	107219201	107221399	-122
CHOP only	BCAR3	chr1	94312401	94313999	-494
CHOP only	BCKDHA	chr19	41902601	41905399	306
CHOP only	BCL9L	chr11	118779001	118784999	-387
CHOP only	BCR	chr22	23520601	23522599	-952
CHOP only	BDH1	chr3	197235201	197237199	46658
CHOP only	BLM	chr15	91259801	91261199	-58
CHOP only	BMP1	chr8	22021001	22022999	-653
CHOP only	BMP10	chr2	69053201	69054599	44749
CHOP only	BMP2	chr20	6747001	6750399	-45
CHOP only	BMPR2	chr2	203238401	203242799	-450
CHOP only	BORA	chr13	73300001	73302199	-787
CHOP only	BRCA2	chr13	32888601	32890199	-217
CHOP only	BRF2	chr8	37705801	37709799	-369
CHOP only	BSCL2	chr11	62473201	62474599	-113
CHOP only	BTAF1	chr10	93682601	93683999	-436
CHOP only	BTBD10	chr11	13484401	13485199	44
CHOP only	BTBD8	chr1	92544801	92546599	-162
CHOP only	BTG1	chr12	92539201	92540599	-227
CHOP only	BUD31	chr7	99005201	99008799	399
CHOP only	CA12	chr15	63673801	63676199	-691
CHOP only	CAB39L	chr13	50016201	50019999	162
CHOP only	CACNG6	chr19	54492201	54494599	-1003
CHOP only	CAMK1	chr3	9811201	9812199	-32
CHOP only	CAPZA1	chr1	113161201	113163199	125
CHOP only	CASC4	chr15	44580001	44581999	91
CHOP only	CBR3	chr21	37512001	37514599	6037
CHOP only	CBS	chr21	44472401	44473999	22840
CHOP only	CBX5	chr12	54673001	54673999	415
CHOP only	CCAR2	chr8	22461201	22463799	-39
CHOP only	CCDC108	chr2	219906201	219907199	-427
CHOP only	CCDC112	chr5	114631401	114632999	-213
CHOP only	CCDC116	chr22	21985401	21986799	-986
CHOP only	CCDC124	chr19	18042201	18044599	-424
CHOP only	CCDC127	chr5	217001	219199	197
CHOP only	CCDC136	chr7	128430001	128431799	-564
CHOP only	CCDC169	chr13	36871201	36872999	-108
CHOP only	CCDC53	chr12	102456201	102457599	-998
CHOP only	CCDC62	chr12	123255401	123256999	-2856
CHOP only	CCDC69	chr5	150603201	150604399	-146
CHOP only	CCNC	chr6	100015801	100017599	-10
CHOP only	CCND1	chr11	69469201	69469999	13727

Overlap	Symbol	Chromosome	CHOP Peak Start	CHOP Peak End	CHOP dTSS
CHOP only	CCNDBP1	chr15	43477201	43478399	334
CHOP only	CCNE2	chr8	95905601	95909199	82
CHOP only	CCNG2	chr4	78077601	78078999	-57
CHOP only	CCNK	chr14	99947201	99948799	261
CHOP only	CCNL1	chr3	156877001	156880799	-418
CHOP only	CCS	chr11	66360601	66362399	810
CHOP only	CCSER2	chr10	86086801	86087999	-945
CHOP only	CD207	chr2	71054401	71058599	6453
CHOP only	CD276	chr15	73974401	73977799	-522
CHOP only	CD300LD	chr17	72588801	72589799	-930
CHOP only	CD3D	chr11	118212201	118215599	-441
CHOP only	CD47	chr3	107808201	107812399	-365
CHOP only	CD7	chr17	80276801	80280399	-3120
CHOP only	CD79B	chr17	62004401	62006199	4404
CHOP only	CDA	chr1	20913601	20916999	-144
CHOP only	CDAN1	chr15	43028001	43030999	-83
CHOP only	CDC14A	chr1	100816601	100818999	-223
CHOP only	CDC20	chr1	43821801	43827399	-26
CHOP only	CDC42	chr1	22417401	22418399	38780
CHOP only	CDC42EP1	chr22	37964801	37966999	9429
CHOP only	CDH22	chr20	44937201	44937999	-463
CHOP only	CDH7	chr18	63416601	63418799	212
CHOP only	CDHR2	chr5	175975001	175977399	-143
CHOP only	CDIP1	chr16	4585601	4591399	-29
CHOP only	CDK13	chr7	39987601	39990999	-659
CHOP only	CDK19	chr6	111136001	111137199	-81
CHOP only	CDK6	chr7	92461801	92466599	-969
CHOP only	CDK8	chr13	26827601	26829799	-56
CHOP only	CDK9	chr9	130548201	130550199	895
CHOP only	CDKL3	chr5	133702201	133703999	-335
CHOP only	CDKN2A	chr9	21973801	21975999	-74
CHOP only	CDKN2C	chr1	51433601	51436199	533
CHOP only	CDKN3	chr14	54862401	54863799	-573
CHOP only	CDPF1	chr22	46644801	46647799	-107
CHOP only	CDRT15	chr17	14111601	14114199	27250
CHOP only	CELA2B	chr1	15815601	15818599	14504
CHOP only	CEMIP	chr15	81069801	81073599	16
CHOP only	CEP290	chr12	88535201	88536799	-7
CHOP only	CEP350	chr1	179922201	179924399	-608
CHOP only	CEP44	chr4	175204201	175205599	72
CHOP only	CEP72	chr5	611401	614199	395
CHOP only	CFAP69	chr7	89872801	89875999	-88
CHOP only	CFB	chr6	31911601	31914799	-521
CHOP only	CGGBP1	chr3	88107001	88109399	-54
CHOP only	CHD1L	chr1	146712601	146715399	-291
CHOP only	CHD4	chr12	6714801	6716599	-83
CHOP only	CHID1	chr11	909401	912199	74
CHOP only	CHKA	chr11	67889001	67890199	-742
CHOP only	CHMP1B	chr18	11849001	11852199	-789
CHOP only	CHMP4C	chr8	82644001	82645199	-88
CHOP only	CHN2	chr7	29521601	29524199	-532
CHOP only	CHN2	chr7	29233401	29234799	-21
CHOP only	CHRNA2	chr8	27316401	27318799	19213
CHOP only	CHRNB2	chr1	154539601	154540999	43
CHOP only	CHRNG	chr2	233401001	233403599	-2137
CHOP only	CHST14	chr15	40762001	40764199	-60
CHOP only	CHST15	chr10	125849801	125854199	-60
CHOP only	CIART	chr1	150253001	150254199	-1343
CHOP only	CIRBP	chr19	1265601	1267999	-2465
CHOP only	CIZ1	chr9	130953201	130954999	-232

Overlap	Symbol	Chromosome	CHOP Peak Start	CHOP Peak End	CHOP dTSS
CHOP only	CKAP4	chr12	106642001	106643199	-887
CHOP only	CLASRP	chr19	45540001	45544399	-98
CHOP only	CLOCK	chr4	56412801	56413599	-124
CHOP only	CLYBL	chr13	100257401	100259199	-618
CHOP only	CMTM7	chr3	32432201	32433599	-263
CHOP only	CNIH1	chr14	54887201	54888199	20448
CHOP only	CNTN5	chr11	98891001	98891999	-206
CHOP only	COA7	chr1	53150801	53152599	12338
CHOP only	COBLL1	chr2	165697201	165698999	-172
CHOP only	COL27A1	chr9	116917201	116917999	-631
CHOP only	COL4A3BP	chr5	74806201	74808799	-46
CHOP only	COL6A1	chr21	47400001	47401399	-963
CHOP only	COMTD1	chr10	76995001	76997999	-730
CHOP only	COPS2	chr15	49446801	49448399	254
CHOP only	CORIN	chr4	47838801	47841399	23
CHOP only	CORO7	chr16	4466401	4468199	-338
CHOP only	COX18	chr4	73934801	73935999	76
CHOP only	CPA1	chr7	130018001	130020599	-990
CHOP only	CPA6	chr8	68658201	68659799	-380
CHOP only	CPSF2	chr14	92587801	92590199	702
CHOP only	CPT1A	chr11	68609001	68611599	-901
CHOP only	CRB3	chr19	6462201	6465999	-160
CHOP only	CRCP	chr7	65577001	65581799	-405
CHOP only	CREB3L3	chr19	4152401	4154799	2
CHOP only	CREBL2	chr12	12762601	12766599	-167
CHOP only	CREBRF	chr5	172482001	172484799	45
CHOP only	CRLF3	chr17	29151001	29153199	-322
CHOP only	CSHL1	chr17	61986201	61987799	1618
CHOP only	CTC1	chr17	8150601	8153399	-587
CHOP only	CTNND1	chr11	57527601	57530199	-334
CHOP only	CTNS	chr17	3539201	3540799	238
CHOP only	CTRL	chr16	67962601	67964599	2178
CHOP only	CUL3	chr2	225450201	225450999	-486
CHOP only	CWC15	chr11	94706001	94707199	176
CHOP only	CXXC5	chr5	139025601	139030599	-201
CHOP only	CYB561D1	chr1	110042201	110043999	6399
CHOP only	CYCS	chr7	25156401	25158399	7580
CHOP only	CYP11A1	chr15	74657001	74659999	53
CHOP only	CYP26A1	chr10	94831801	94834999	168
CHOP only	CYP2F1	chr19	41633001	41635599	13947
CHOP only	CYP2W1	chr7	1021001	1024599	-35
CHOP only	CYSRT1	chr9	140117001	140119599	-787
CHOP only	DAND5	chr19	13079201	13081799	68
CHOP only	DAP3	chr1	155658201	155660999	715
CHOP only	DARS2	chr1	173792801	173795199	203
CHOP only	DAZAP1	chr19	1406401	1407399	-668
CHOP only	DBNDD1	chr16	90060001	90066599	13229
CHOP only	DCAF6	chr1	167904401	167906999	-97
CHOP only	DCDC1	chr11	31390601	31391599	257
CHOP only	DCLK2	chr4	151177601	151180199	179474
CHOP only	DCP1B	chr12	2113001	2114399	-23
CHOP only	DCTD	chr4	183838601	183840399	-870
CHOP only	DCUN1D2	chr13	114142601	114147399	23
CHOP only	DDHD1	chr14	53618201	53620799	546
CHOP only	DDX17	chr22	38900801	38904199	-155
CHOP only	DDX19A	chr16	70406401	70408199	26476
CHOP only	DDX24	chr14	94546601	94548199	158
CHOP only	DDX59	chr1	200638401	200639799	26
CHOP only	DEF8	chr16	90013401	90017199	161
CHOP only	DENND1B	chr1	197744201	197745599	-277

Overlap	Symbol	Chromosome	CHOP Peak Start	CHOP Peak End	CHOP dTSS
CHOP only	DENR	chr12	123234801	123238999	-471
CHOP only	DEPDC5	chr22	32148201	32151799	-9
CHOP only	DEPDC5	chr22	32210801	32214999	62052
CHOP only	DERL2	chr17	5387601	5390999	194
CHOP only	DGKD	chr2	234261801	234262999	-753
CHOP only	DHPS	chr19	12791601	12792999	-275
CHOP only	DHRS3	chr1	12676201	12680599	-663
CHOP only	DHRS7B	chr17	21029201	21031399	59
CHOP only	DHX15	chr4	24585401	24587399	-216
CHOP only	DIAPH3	chr13	60737401	60738999	-81
CHOP only	DIP2A	chr21	47876201	47879999	-762
CHOP only	DISP1	chr1	222987401	222989199	-131
CHOP only	DLG4	chr17	7121601	7125199	-31
CHOP only	DLG5	chr10	79685201	79686199	648
CHOP only	DMTN	chr8	21909401	21912399	-181
CHOP only	DNAJB5	chr9	34988601	34991399	-267
CHOP only	DNAJC13	chr3	132135001	132137399	-353
CHOP only	DNAJC18	chr5	138773801	138776799	-86
CHOP only	DNAJC4	chr11	63992201	64001799	-753
CHOP only	DNAJC6	chr1	65774401	65775999	-18
CHOP only	DNAJC8	chr1	28559401	28560799	-558
CHOP only	DNER	chr2	230578801	230580799	-514
CHOP only	DNLZ	chr9	139258001	139259399	-437
CHOP only	DOC2B	chr17	31801	33799	-1379
CHOP only	DOCK6	chr19	11371801	11374599	-32
CHOP only	DOK1	chr2	74784601	74785599	3588
CHOP only	DPEP2	chr16	68032801	68034399	-179
CHOP only	DPF3	chr14	73358601	73361999	524
CHOP only	DPM3	chr1	155112201	155113999	-104
CHOP only	DPYSL2	chr8	26433601	26435399	-840
CHOP only	DR1	chr1	93811001	93812599	322
CHOP only	DRAM2	chr1	111682401	111683599	-162
CHOP only	DSCC1	chr8	120867401	120870399	-730
CHOP only	DTL	chr1	212208201	212209399	-95
CHOP only	DTYMK	chr2	242613401	242615399	11983
CHOP only	DUOX2	chr15	45383001	45384799	22459
CHOP only	DUSP5	chr10	112270801	112271799	13675
CHOP only	DYNLRB2	chr16	80574401	80575399	46
CHOP only	E2F8	chr11	19262001	19264599	-98
CHOP only	EBAG9	chr8	110551201	110553799	196
CHOP only	ECH1	chr19	39318801	39326799	-303
CHOP only	EEA1	chr12	93322201	93323999	7
CHOP only	EEF1D	chr8	144678601	144679799	358
CHOP only	EFCAB7	chr1	63988601	63989799	187
CHOP only	EFTUD1	chr15	82554401	82555799	4
CHOP only	EGR1	chr5	137800001	137801599	-381
CHOP only	EHBP1L1	chr11	65341801	65344199	-509
CHOP only	EIF1B	chr3	40350001	40351999	-173
CHOP only	EIF4G3	chr1	21503201	21504799	-619
CHOP only	EIF4H	chr7	73587201	73589399	-406
CHOP only	EIF5A2	chr3	170625401	170627399	26
CHOP only	ELAC1	chr18	48493201	48495199	-187
CHOP only	ELF3	chr1	201974601	201977599	-3590
CHOP only	ELMOD2	chr4	141444201	141445799	-312
CHOP only	ELOF1	chr19	11669201	11672399	-749
CHOP only	ELOVL3	chr10	103984201	103986599	-635
CHOP only	ELOVL5	chr6	53212001	53215799	77
CHOP only	ELOVL6	chr4	111116801	111124399	-780
CHOP only	ELOVL7	chr5	60139201	60142199	-599
CHOP only	ELP2	chr18	33708201	33711199	-137

Overlap	Symbol	Chromosome	CHOP Peak Start	CHOP Peak End	CHOP dTSS
CHOP only	EMC1	chr1	19577601	19578399	53
CHOP only	EMG1	chr12	7084801	7086199	5556
CHOP only	EMILIN3	chr20	39987801	39991799	5698
CHOP only	EMILIN3	chr20	40029201	40031199	-34702
CHOP only	EML4	chr2	42395601	42395999	-690
CHOP only	EMP1	chr12	13347801	13350799	-302
CHOP only	ENAH	chr1	225839601	225842999	-455
CHOP only	ENDOG	chr9	131579801	131581799	21
CHOP only	ENHO	chr9	34522401	34523999	-163
CHOP only	ENO4	chr10	118606601	118609999	-723
CHOP only	ENTPD2	chr9	139948001	139950599	-797
CHOP only	EPHA1	chr7	143105401	143107599	-515
CHOP only	EPHA2	chr1	16481601	16483799	-118
CHOP only	EPHX1	chr1	226032001	226033999	19998
CHOP only	EPHX1	chr1	225996201	225997599	-876
CHOP only	EPN1	chr19	56186601	56188199	-591
CHOP only	ERBB4	chr2	213400801	213405999	-48
CHOP only	ERICH1	chr8	680601	682799	-474
CHOP only	ERLIN1	chr10	101945001	101947599	-486
CHOP only	ERRFI1	chr1	8085201	8088199	-307
CHOP only	ESR2	chr14	64760401	64762399	-272
CHOP only	ESR2	chr14	64805001	64807399	-932
CHOP only	ETF1	chr5	137877601	137880599	-111
CHOP only	ETNK1	chr12	22776601	22778999	-276
CHOP only	ETV7	chr6	36332801	36335199	21568
CHOP only	EVA1C	chr21	33783601	33785999	55
CHOP only	EXD2	chr14	69657601	69658999	106
CHOP only	EXOC3L4	chr14	103563601	103568599	-381
CHOP only	EXOSC4	chr8	145131201	145135399	-222
CHOP only	FAHD1	chr16	1877001	1878399	475
CHOP only	FAHD2A	chr2	96066201	96070599	-48
CHOP only	FAM102A	chr9	130742801	130744599	-888
CHOP only	FAM103A1	chr15	83653801	83654999	-555
CHOP only	FAM107B	chr10	14613801	14615599	-328
CHOP only	FAM114A2	chr5	153417801	153419199	-3
CHOP only	FAM118A	chr22	45704201	45705999	19
CHOP only	FAM131A	chr3	184051601	184054399	-717
CHOP only	FAM131A	chr3	184063001	184065399	8924
CHOP only	FAM132B	chr2	239060401	239063399	-5749
CHOP only	FAM132B	chr2	239078001	239079599	11151
CHOP only	FAM162B	chr6	117086001	117087799	-14
CHOP only	FAM167A	chr8	11324201	11325799	-724
CHOP only	FAM171A1	chr10	15413401	15414399	-842
CHOP only	FAM173A	chr16	769401	772199	-342
CHOP only	FAM19A4	chr3	68981601	68983399	-739
CHOP only	FAM214B	chr9	35114601	35117599	-207
CHOP only	FAM219B	chr15	75198601	75200799	-238
CHOP only	FAM43A	chr3	194405801	194406999	-222
CHOP only	FAM46A	chr6	82460401	82465599	-572
CHOP only	FAM53A	chr4	1693801	1694999	-8360
CHOP only	FAM60A	chr12	31478601	31480599	-441
CHOP only	FAM65B	chr6	24935801	24937799	-520
CHOP only	FAM65B	chr6	24877001	24877999	93
CHOP only	FAM8A1	chr6	17598001	17602599	-218
CHOP only	FAM90A1	chr12	8380001	8381599	-586
CHOP only	FANCD2	chr3	10067001	10069799	287
CHOP only	FASTK	chr7	150777801	150778999	-430
CHOP only	FASTKD2	chr2	207628601	207630999	-312
CHOP only	FBXL3	chr13	77600401	77602799	-269
CHOP only	FBXO11	chr2	48131401	48134799	-168

Overlap	Symbol	Chromosome	CHOP Peak Start	CHOP Peak End	CHOP dTSS
CHOP only	FBXO27	chr19	39523201	39524399	-602
CHOP only	FBXO34	chr14	55737801	55738999	379
CHOP only	FBXO38	chr5	147763001	147764399	202
CHOP only	FCF1	chr14	75179401	75181199	450
CHOP only	FCHO2	chr5	72250201	72252599	-408
CHOP only	FDX1L	chr19	10425401	10427599	191
CHOP only	FEM1A	chr19	4790201	4792799	-228
CHOP only	FGD3	chr9	95709001	95710399	99
CHOP only	FGF17	chr8	21893401	21896999	-5228
CHOP only	FGF18	chr5	170845401	170846799	-567
CHOP only	FGFR3	chr4	1811401	1813799	17561
CHOP only	FGFR4	chr5	176510201	176516199	-673
CHOP only	FICD	chr12	108907001	108909199	-951
CHOP only	FILIP1L	chr3	99594601	99595399	47
CHOP only	FIP1L1	chr4	54242401	54244599	-320
CHOP only	FIS1	chr7	100887201	100889799	-129
CHOP only	FIZ1	chr19	56109401	56113199	-407
CHOP only	FNBP1	chr9	132804201	132807199	-227
CHOP only	FNDC5	chr1	33336801	33339399	-7
CHOP only	FNIP1	chr5	131132201	131133399	-44
CHOP only	FOXO3	chr6	108881001	108883199	31
CHOP only	FPGS	chr9	130564601	130566199	-60
CHOP only	FRAS1	chr4	78975201	78980999	-624
CHOP only	FRYL	chr4	48781001	48783599	16
CHOP only	FUT8	chr14	65878401	65880799	152
CHOP only	FXYD3	chr19	35605001	35606799	-832
CHOP only	FYCO1	chr3	46036401	46039199	-484
CHOP only	FZR1	chr19	3503401	3508199	-495
CHOP only	GABBR1	chr6	29599601	29603199	-438
CHOP only	GAL3ST4	chr7	99764401	99769399	-527
CHOP only	GALNT16	chr14	69724401	69728199	-381
CHOP only	GALNT6	chr12	51785001	51786799	-700
CHOP only	GAPVD1	chr9	128198001	128199599	137631
CHOP only	GATA4	chr8	11560401	11562599	-217
CHOP only	GBF1	chr10	104004001	104006199	-155
CHOP only	GCDH	chr19	13000801	13002199	-443
CHOP only	GDAP2	chr1	118471601	118472999	2
CHOP only	GDF7	chr2	20863801	20868999	-24
CHOP only	GDNF	chr5	37839001	37840399	82
CHOP only	GET4	chr7	914401	916199	-891
CHOP only	GGNBP2	chr17	34898201	34902199	-537
CHOP only	GGPS1	chr1	235489801	235493799	47
CHOP only	GGT1	chr22	24979201	24981999	882
CHOP only	GHRL	chr3	10333601	10336399	-369
CHOP only	GKN1	chr2	69200801	69202799	95
CHOP only	GLB1L	chr2	220100401	220102599	6853
CHOP only	GLMN	chr1	92764001	92765199	-34
CHOP only	GLS	chr2	191744001	191746999	-47
CHOP only	GLTPD2	chr17	4690001	4694399	-54
CHOP only	GLTSCR2	chr19	48246401	48249999	-593
CHOP only	GMNC	chr3	190580201	190580999	-135
CHOP only	GMPR	chr6	16294801	16296799	56989
CHOP only	GNAI2	chr3	50283201	50285199	-126
CHOP only	GNAI3	chr1	110089401	110091999	-486
CHOP only	GNAT1	chr3	50226401	50227599	-2043
CHOP only	GNB1L	chr22	19841601	19844799	-738
CHOP only	GNG4	chr1	235813801	235815999	-846
CHOP only	GNG7	chr19	2703001	2704199	-854
CHOP only	GNPTG	chr16	1412801	1414399	11700
CHOP only	GNRH1	chr8	25276001	25276999	6056

Overlap	Symbol	Chromosome	CHOP Peak Start	CHOP Peak End	CHOP dTSS
CHOP only	GNS	chr12	65153001	65154199	-374
CHOP only	GOLPH3	chr5	32174201	32175599	-475
CHOP only	GPHA2	chr11	64701601	64703799	660
CHOP only	GPR179	chr17	36476401	36482399	20293
CHOP only	GPR37L1	chr1	202090001	202092199	-929
CHOP only	GPT	chr8	145724801	145730199	-1965
CHOP only	GPX4	chr19	1102001	1104399	-725
CHOP only	GRB14	chr2	165477001	165479799	-40
CHOP only	GSDMD	chr8	144646601	144648199	6923
CHOP only	GSE1	chr16	85642601	85647199	-129
CHOP only	GSR	chr8	30584001	30586799	86
CHOP only	GSTA1	chr6	52655201	52656199	12964
CHOP only	GSTK1	chr7	142959201	142961199	-322
CHOP only	GTF2A2	chr15	59949201	59950999	-363
CHOP only	GTPBP1	chr22	39099801	39103599	-107
CHOP only	GTPBP2	chr6	43592601	43599999	683
CHOP only	GUK1	chr1	228325201	228328999	-685
CHOP only	GULP1	chr2	189155801	189157799	404
CHOP only	GZMM	chr19	549001	551399	6166
CHOP only	H1F0	chr22	38172401	38173799	-28014
CHOP only	HAMP	chr19	35770601	35772199	-2010
CHOP only	HAPLN3	chr15	89440001	89441999	-2230
CHOP only	HARS2	chr5	140069001	140071399	-811
CHOP only	HEATR2	chr7	764601	766399	-838
CHOP only	HECTD4	chr12	112818401	112821199	96
CHOP only	HEMK1	chr3	50604801	50608399	-309
CHOP only	HERC3	chr4	89512201	89514599	-174
CHOP only	HERPUD2	chr7	35733401	35736599	-228
CHOP only	HES3	chr1	6306001	6308799	3148
CHOP only	HHEX	chr10	94446001	94451799	-781
CHOP only	HHLA3	chr1	70820401	70822199	807
CHOP only	HIC1	chr17	1957801	1958599	-193
CHOP only	HIF1A	chr14	62160001	62162999	-619
CHOP only	HIGD1B	chr17	42927201	42928199	2430
CHOP only	HIST1H2AC	chr6	26121801	26126999	27
CHOP only	HIST1H2BL	chr6	27774201	27776599	309
CHOP only	HIST1H2BO	chr6	27859601	27864199	697
CHOP only	HIST1H4B	chr6	26026401	26028399	80
CHOP only	HIST2H2BE	chr1	149854801	149861399	132
CHOP only	HLA-C	chr6	31235201	31237399	3613
CHOP only	HMCES	chr3	128996201	128999199	16
CHOP only	HMGA2	chr12	66216801	66218999	-340
CHOP only	HMGB2	chr4	174254001	174256999	9
CHOP only	HNRNPA0	chr5	137088401	137091599	39
CHOP only	HNRNPH1	chr5	179050201	179052799	-778
CHOP only	HNRNPH3	chr10	70090201	70092799	-268
CHOP only	HNRNPUL1	chr19	41767401	41769599	119
CHOP only	HOGA1	chr10	99343001	99344999	-102
CHOP only	HOMER1	chr5	78808601	78810599	59
CHOP only	HOXA4	chr7	27169401	27171599	-101
CHOP only	HOXB5	chr17	46670401	46672199	-197
CHOP only	HOXB6	chr17	46683201	46684599	-1566
CHOP only	HOXC5	chr12	54425201	54427599	-432
CHOP only	HPD	chr12	122294601	122299199	-131
CHOP only	HPS1	chr10	100206401	100208599	-796
CHOP only	HPS4	chr22	26877401	26881999	129
CHOP only	HPX	chr11	6461801	6462999	-146
CHOP only	HRASLS2	chr11	63330601	63332199	-545
CHOP only	HS2ST1	chr1	87379201	87381599	65
CHOP only	HS3ST3B1	chr17	14199601	14209599	94

Overlap	Symbol	Chromosome	CHOP Peak Start	CHOP Peak End	CHOP dTSS
CHOP only	HSD17B14	chr19	49338801	49340199	434
CHOP only	HSD17B4	chr5	118787201	118789199	8
CHOP only	HSP90AA1	chr14	102552801	102554999	-388
CHOP only	HSPA12A	chr10	118501401	118503399	-315
CHOP only	HSPA4L	chr4	128701401	128704799	-353
CHOP only	HSPA6	chr1	161493201	161494599	-136
CHOP only	HSPB1	chr7	75954601	75956199	23525
CHOP only	HSPB7	chr1	16338201	16340999	5685
CHOP only	HSPBP1	chr19	55790401	55794199	-549
CHOP only	HSPD1	chr2	198363201	198367199	-202
CHOP only	HTT	chr4	3074201	3076399	-937
CHOP only	HVCN1	chr12	111126401	111129799	-483
CHOP only	ID3	chr1	23876801	23891999	1885
CHOP only	IER5L	chr9	131934801	131939599	3340
CHOP only	IFIT3	chr10	91090601	91092999	-436
CHOP only	IFRD2	chr3	50328401	50330599	526
CHOP only	IGF2	chr11	2158201	2160399	-782
CHOP only	IGFALS	chr16	1844401	1845599	-91
CHOP only	IGFBP1	chr7	45933201	45935199	6241
CHOP only	IGHMBP2	chr11	68670401	68673599	681
CHOP only	IGSF3	chr1	117210001	117211399	-323
CHOP only	IL12RB1	chr19	18167801	18171399	28213
CHOP only	IL32	chr16	3113401	3116199	-513
CHOP only	INAFM1	chr19	47776001	47777599	-859
CHOP only	ING1	chr13	111363401	111364999	-770
CHOP only	INO80D	chr2	206951001	206951399	-294
CHOP only	INPP5A	chr10	134350001	134350999	-853
CHOP only	INPP5E	chr9	139333601	139335599	-344
CHOP only	INTS12	chr4	106629401	106630199	81
CHOP only	IP6K1	chr3	49824201	49825399	-827
CHOP only	IPO8	chr12	30848401	30849999	-271
CHOP only	IPP	chr1	46215001	46217799	85
CHOP only	IQCF1	chr3	51937001	51938999	-614
CHOP only	IQGAP3	chr1	156542001	156543199	-204
CHOP only	IRF2BP1	chr19	46388401	46391599	-624
CHOP only	IRF7	chr11	611601	613599	3128
CHOP only	ISX	chr22	35460001	35464199	-30
CHOP only	ITIH4	chr3	52864801	52866599	-983
CHOP only	ITM2B	chr13	48806201	48808399	26
CHOP only	ITPKA	chr15	41782001	41790199	44
CHOP only	ITPRIP	chr10	106088601	106088999	-50
CHOP only	JUNB	chr19	12897201	12905599	-910
CHOP only	KAT6A	chr8	41908201	41911599	-395
CHOP only	KCNJ5	chr11	128760801	128761799	-13
CHOP only	KCTD1	chr18	24128201	24130599	-1
CHOP only	KCTD11	chr17	7251601	7256999	-908
CHOP only	KHDRBS1	chr1	32477401	32479199	-995
CHOP only	KIAA0020	chr9	2843401	2844999	-70
CHOP only	KIAA0040	chr1	175161201	175163199	29
CHOP only	KIAA0196	chr8	126103001	126104599	261
CHOP only	KIAA0319	chr6	24645801	24647599	-317
CHOP only	KIAA0319L	chr1	36020601	36024399	537
CHOP only	KIAA1217	chr10	24495801	24499199	-220
CHOP only	KIAA1257	chr3	128689001	128689799	23586
CHOP only	KIAA1467	chr12	13196601	13197799	-115
CHOP only	KIAA1958	chr9	115247801	115249999	-348
CHOP only	KIF14	chr1	200589601	200591999	-938
CHOP only	KIF5A	chr12	57942801	57943999	-447
CHOP only	KISS1R	chr19	915401	917399	-942
CHOP only	KLF6	chr10	3816201	3819799	9473

Overlap	Symbol	Chromosome	CHOP Peak Start	CHOP Peak End	CHOP dTSS
CHOP only	KLHL20	chr1	173682801	173684799	-280
CHOP only	KMT2B	chr19	36207201	36208599	-1021
CHOP only	KPTN	chr19	47985801	47988399	421
CHOP only	KRBOX4	chrX	46305201	46306999	-524
CHOP only	KREMEN2	chr16	3012801	3014999	-317
CHOP only	KRT13	chr17	39655601	39657199	5465
CHOP only	KRT16	chr17	39764401	39766599	3579
CHOP only	KRT20	chr17	39042001	39042799	-905
CHOP only	KRT24	chr17	38852601	38853999	6702
CHOP only	LACE1	chr6	108615201	108616599	-198
CHOP only	LAMB2	chr3	49169201	49171999	-1
CHOP only	LAMC1	chr1	182990801	182993599	-395
CHOP only	LAMP1	chr13	113949601	113952599	-369
CHOP only	LAMP3	chr3	182879601	182881599	67
CHOP only	LARGE	chr22	34317001	34317599	-884
CHOP only	LCAT	chr16	67974801	67979199	1015
CHOP only	LCK	chr1	32712801	32717199	-1840
CHOP only	LCN8	chr9	139652601	139653599	-369
CHOP only	LCOR	chr10	98590401	98593799	83
CHOP only	LDB1	chr10	103873401	103876199	-77
CHOP only	LDB1	chr10	103880201	103881199	-490
CHOP only	LEF1	chr4	109089601	109091199	-288
CHOP only	LEPROTL1	chr8	29951001	29953599	-622
CHOP only	LETM1	chr4	1857201	1859599	-426
CHOP only	LETMD1	chr12	51441001	51442999	-82
CHOP only	LGR5	chr12	71829001	71836599	-750
CHOP only	LHB	chr19	49520001	49522199	-753
CHOP only	LHX9	chr1	197883401	197888599	-517
CHOP only	LIF	chr22	30642801	30644799	-960
CHOP only	LIMA1	chr12	50720001	50721599	-43447
CHOP only	LIN9	chr1	226497401	226498599	-551
CHOP only	LMBR1	chr7	156684801	156687999	-498
CHOP only	LMBRD2	chr5	36150801	36153199	15
CHOP only	LMF1	chr16	1019201	1023399	-316
CHOP only	LMNB1	chr5	126111201	126113799	185
CHOP only	LMTK3	chr19	49016001	49017199	-154
CHOP only	LRCH1	chr13	47125601	47126999	-996
CHOP only	LRCH4	chr7	100182201	100183799	811
CHOP only	LRG1	chr19	4539401	4541999	-664
CHOP only	LRIG2	chr1	113666601	113667999	51469
CHOP only	LRP3	chr19	33665401	33669199	-18299
CHOP only	LRPAP1	chr4	3532801	3535999	-176
CHOP only	LRRC27	chr10	134149401	134150599	-611
CHOP only	LRRC56	chr11	536001	537399	-822
CHOP only	LRRC71	chr1	156889801	156891199	76
CHOP only	LRRC8A	chr9	131643601	131646599	319
CHOP only	LRRIQ4	chr3	169538201	169540399	-410
CHOP only	LRTM2	chr12	1899401	1901199	-29133
CHOP only	LSM14A	chr19	34660601	34665199	-452
CHOP only	LST1	chr6	31557001	31558199	2623
CHOP only	LTBR	chr12	6492201	6494199	1
CHOP only	LTK	chr15	41807801	41810199	-2915
CHOP only	LUC7L3	chr17	48795601	48797599	-326
CHOP only	LUZP1	chr1	23495001	23496599	-449
CHOP only	LUZP2	chr11	24517801	24519199	-16
CHOP only	LYSMD4	chr15	100272601	100274999	-151
CHOP only	LYST	chr1	236029201	236031999	-373
CHOP only	MACROD1	chr11	63932601	63935199	-315
CHOP only	MAF1	chr8	145159401	145160599	695
CHOP only	MAFF	chr22	38611201	38615799	14473

Overlap	Symbol	Chromosome	CHOP Peak Start	CHOP Peak End	CHOP dTSS
CHOP only	MAGOH	chr1	53703401	53705399	-118
CHOP only	MALT1	chr18	56336801	56339399	-518
CHOP only	MANBA	chr4	103681001	103683599	-149
CHOP only	MAP2K3	chr17	21188201	21193199	-648
CHOP only	MAP4K1	chr19	39108201	39109199	-25
CHOP only	MAPK8IP1	chr11	45905801	45907599	-347
CHOP only	MARK2	chr11	63654001	63657599	-187
CHOP only	MARVELD1	chr10	99477801	99478799	4835
CHOP only	MATR3	chr5	138627401	138630599	-333
CHOP only	MAX	chr14	65568601	65571399	-587
CHOP only	MBL2	chr10	54524201	54524799	6960
CHOP only	MBOAT4	chr8	29994201	29996799	6700
CHOP only	MBOAT4	chr8	30001801	30003199	-300
CHOP only	MCCC1	chr3	182816801	182817599	-169
CHOP only	MCHR1	chr22	41072601	41075999	-882
CHOP only	MCM7	chr7	99698001	99700799	163
CHOP only	MCRS1	chr12	49959801	49965199	-572
CHOP only	MDH2	chr7	75694001	75700599	19963
CHOP only	MDK	chr11	46399001	46405999	-118
CHOP only	MDM2	chr12	69200401	69202599	-452
CHOP only	MED26	chr19	16738401	16740999	-685
CHOP only	MED31	chr17	6554001	6555999	-46
CHOP only	METRNL	chr17	81036201	81037199	-867
CHOP only	MFAP1	chr15	44115001	44119599	-349
CHOP only	MFI2	chr3	196754601	196759399	-313
CHOP only	MFN1	chr3	179063201	179065999	-880
CHOP only	MFNG	chr22	37882201	37883399	-322
CHOP only	MFSD2A	chr1	40419601	40421999	16
CHOP only	MGAT1	chr5	180236401	180239399	-763
CHOP only	MGRN1	chr16	4672601	4675999	-525
CHOP only	MGST2	chr4	140661201	140663199	75278
CHOP only	MICALL1	chr22	38301201	38301999	-555
CHOP only	MIDN	chr19	1247601	1249599	48
CHOP only	MIER1	chr1	67390601	67391999	722
CHOP only	MIOS	chr7	7605801	7607199	-116
CHOP only	MIS18A	chr21	33649801	33652999	-24
CHOP only	MKNK2	chr19	2036201	2038799	13743
CHOP only	MLLT1	chr19	6279401	6281799	-641
CHOP only	MLST8	chr16	2254601	2256599	-132
CHOP only	MLYCD	chr16	83949801	83950799	17570
CHOP only	MOB3C	chr1	47080401	47083199	763
CHOP only	MOB4	chr2	198379001	198381799	105
CHOP only	MOGAT3	chr7	100842601	100846799	-398
CHOP only	MOK	chr14	102770601	102772399	37
CHOP only	MORN1	chr1	2322401	2323199	390
CHOP only	MPC1	chr6	166795201	166797999	-99
CHOP only	MPHOSPH1	chr2	71377001	71378999	20556
CHOP only	MPI	chr15	75181601	75183199	48
CHOP only	MPND	chr19	4341401	4345199	-224
CHOP only	MPP3	chr17	41908801	41912999	-353
CHOP only	MPP6	chr7	24611801	24612799	-785
CHOP only	MRPL11	chr11	66204201	66208399	19
CHOP only	MRPL32	chr7	42971201	42973599	461
CHOP only	MRPL4	chr19	10369001	10372399	8060
CHOP only	MRPL48	chr11	73497001	73500199	-317
CHOP only	MRPL55	chr1	228295601	228299599	-587
CHOP only	MRPS11	chr15	89009801	89013399	916
CHOP only	MRPS12	chr19	39423201	39425199	2606
CHOP only	MRPS21	chr1	150264201	150267799	-262
CHOP only	MRPS22	chr3	139061401	139063999	-161

Overlap	Symbol	Chromosome	CHOP Peak Start	CHOP Peak End	CHOP dTSS
CHOP only	MRPS30	chr5	44808801	44809999	373
CHOP only	MRPS34	chr16	1821401	1824399	240
CHOP only	MRS2	chr6	24425001	24425399	22064
CHOP only	MTCL1	chr18	8716001	8717799	-469
CHOP only	MTERF3	chr8	97272001	97274999	341
CHOP only	MTFP1	chr22	30812201	30814599	-8211
CHOP only	MTFR1	chr8	66555201	66557999	-288
CHOP only	MTG1	chr10	135206201	135208399	-321
CHOP only	MTIF3	chr13	28022401	28026399	-66
CHOP only	MXI1	chr10	111965801	111967199	-863
CHOP only	MXI1	chr10	111984801	111985599	-562
CHOP only	MYADM	chr19	54366801	54369199	-838
CHOP only	MYADM	chr19	54369801	54371399	-519
CHOP only	MYADML2	chr17	79904601	79906599	-491
CHOP only	MYBPC2	chr19	50934401	50936399	-760
CHOP only	MYCBP2	chr13	77900601	77901599	77
CHOP only	MYCL	chr1	40363601	40366999	2387
CHOP only	MYEOV2	chr2	241068201	241071599	5847
CHOP only	MYL4	chr17	45285401	45287399	-28
CHOP only	MYNN	chr3	169489601	169491799	-153
CHOP only	MYO1F	chr19	8644001	8646199	-2769
CHOP only	NAA38	chr17	7760201	7762799	-328
CHOP only	NAA38	chr17	7764401	7766599	-4328
CHOP only	NADK2	chr5	36241201	36243399	81
CHOP only	NAF1	chr4	164087201	164088799	73
CHOP only	NAPA	chr19	48022001	48024199	-4585
CHOP only	NARS	chr18	55288801	55290999	-723
CHOP only	NAT14	chr19	55995801	55997399	43
CHOP only	NBEAL1	chr2	203877601	203880599	-502
CHOP only	NCOA7	chr6	126101201	126102599	-407
CHOP only	NCOR1	chr17	16117601	16121199	-526
CHOP only	NDFIP1	chr5	141534001	141535399	46376
CHOP only	NDST3	chr4	118954401	118955799	-400
CHOP only	NDUFA11	chr19	5887401	5893799	13424
CHOP only	NDUFA2	chr5	140024801	140027999	970
CHOP only	NDUFA5	chr7	123197201	123198399	25
CHOP only	NDUFAF3	chr3	49054201	49061399	-108
CHOP only	NDUFS6	chr5	1800001	1801999	-496
CHOP only	NDUFS7	chr19	1381801	1384799	-583
CHOP only	NDUFV2	chr18	9101201	9103199	-428
CHOP only	NEDD4	chr15	56286201	56287199	-756
CHOP only	NEK6	chr9	127019001	127019999	-385
CHOP only	NEK8	chr17	27053601	27057199	-432
CHOP only	NEK9	chr14	75593001	75595599	-522
CHOP only	NEMF	chr14	50318801	50320999	-361
CHOP only	NEU4	chr2	242748801	242750999	-260
CHOP only	NEU4	chr2	242743801	242744999	-5760
CHOP only	NEURL2	chr20	44525601	44527199	-6474
CHOP only	NFIA	chr1	61543801	61549799	-734
CHOP only	NFKB2	chr10	104152001	104156599	-35
CHOP only	NFKBID	chr19	36391401	36392799	-548
CHOP only	NHEJ1	chr2	220024001	220027999	-413
CHOP only	NIPA1	chr15	23086601	23087599	-257
CHOP only	NIPA2	chr15	23033801	23035999	-473
CHOP only	NIPAL1	chr4	48017601	48019799	-91
CHOP only	NKAIN2	chr6	124123601	124124599	-891
CHOP only	NKX2-5	chr5	172661201	172663999	-285
CHOP only	NLK	chr17	26367001	26370399	-988
CHOP only	NLN	chr5	65017001	65019199	77
CHOP only	NOC3L	chr10	96122201	96124399	-617

Overlap	Symbol	Chromosome	CHOP Peak Start	CHOP Peak End	CHOP dTSS
CHOP only	NOL3	chr16	67208001	67213199	2844
CHOP only	NOL4	chr18	31801801	31805599	-185
CHOP only	NOP14	chr4	2964401	2965799	133
CHOP only	NOXA1	chr9	140316801	140320599	853
CHOP only	NPAS1	chr19	47508401	47509799	-15043
CHOP only	NPC1L1	chr7	44579801	44583799	-886
CHOP only	NPM2	chr8	21880401	21882199	-321
CHOP only	NR1I2	chr3	119499601	119502199	-657
CHOP only	NR2E3	chr15	72075401	72077999	-26188
CHOP only	NR2F2	chr15	96872601	96874199	-711
CHOP only	NR3C1	chr5	142781401	142785599	-246
CHOP only	NR4A1	chr12	52442801	52446799	-386
CHOP only	NR5A1	chr9	127242001	127243999	26699
CHOP only	NRD1	chr1	52343601	52345999	-191
CHOP only	NREP	chr5	111092401	111095199	-7
CHOP only	NRIP1	chr21	16437401	16438599	-874
CHOP only	NRN1L	chr16	67917201	67920999	319
CHOP only	NSMF	chr9	140352601	140354399	286
CHOP only	NSUN5	chr7	72721801	72723799	64
CHOP only	NT5DC3	chr12	104234201	104236599	-425
CHOP only	NTNG2	chr9	135117601	135118999	80966
CHOP only	NTRK1	chr1	156829001	156830999	-671
CHOP only	NTSR2	chr2	11797201	11799399	12029
CHOP only	NUAK2	chr1	205290601	205292199	-517
CHOP only	NUBP2	chr16	1832201	1834799	576
CHOP only	NUCKS1	chr1	205717401	205721399	-28
CHOP only	NUDCD1	chr8	110345801	110346999	-50
CHOP only	NUDT16L1	chr16	4742401	4744599	-194
CHOP only	NUDT2	chr9	34328401	34331199	296
CHOP only	NUP107	chr12	69080201	69081199	-31
CHOP only	NUP210	chr3	13462201	13463199	-881
CHOP only	NUP214	chr9	133998601	134003199	-48
CHOP only	NUPL1	chr13	25873801	25876199	-666
CHOP only	NUSAP1	chr15	41623801	41627199	608
CHOP only	NXPH4	chr12	57607001	57608399	-2878
CHOP only	OAZ1	chr19	2273201	2275199	4715
CHOP only	OAZ2	chr15	64978001	64978799	17080
CHOP only	ODF2	chr9	131216401	131219399	-385
CHOP only	OMG	chr17	29620001	29621399	3680
CHOP only	OPHN1	chrX	67652401	67654399	-101
CHOP only	OPLAH	chr8	145115201	145116399	-194
CHOP only	OPN1SW	chr7	128415201	128417399	-456
CHOP only	OR1F1	chr16	3252801	3254199	-747
CHOP only	ORAOV1	chr11	69489801	69490999	-235
CHOP only	ORC1	chr1	52869401	52870599	143
CHOP only	OSBP2	chr22	31089601	31091599	-193
CHOP only	OSTM1	chr6	108394801	108398599	-759
CHOP only	OTOF	chr2	26677201	26682799	20910
CHOP only	OTUD6B	chr8	92082001	92083999	576
CHOP only	OTULIN	chr5	14663201	14664799	-783
CHOP only	OXER1	chr2	42983801	42985799	6601
CHOP only	P2RX7	chr12	121570001	121571399	69
CHOP only	PABPC1	chr8	101734001	101735199	-285
CHOP only	PACRG	chr6	163148401	163149799	98
CHOP only	PAK2	chr3	196465801	196467799	72
CHOP only	PAN2	chr12	56726601	56729599	-263
CHOP only	PAQR3	chr4	79860201	79862399	-718
CHOP only	PAQR8	chr6	52224401	52228599	-426
CHOP only	PARP9	chr3	122281401	122284799	47
CHOP only	PCF11	chr11	82866601	82869599	-37

Overlap	Symbol	Chromosome	CHOP Peak Start	CHOP Peak End	CHOP dTSS
CHOP only	PCMT1	chr6	150067201	150073799	-331
CHOP only	PDCD4	chr10	112629601	112632799	-353
CHOP only	PDCL	chr9	125614601	125616199	-24465
CHOP only	PDDC1	chr11	764601	765999	12187
CHOP only	PDE3B	chr11	14663801	14666799	31
CHOP only	PDE4A	chr19	10526201	10527799	-449
CHOP only	PDE4D	chr5	58335801	58336599	-861
CHOP only	PDGFB	chr22	39636001	39639799	-986
CHOP only	PDHB	chr3	58418001	58421599	-221
CHOP only	PDIA3	chr15	44038201	44038999	10
CHOP only	PDK2	chr17	48170201	48173599	-201
CHOP only	PDK2	chr17	48167801	48169599	-3401
CHOP only	PDLIM1	chr10	97049001	97053199	-195
CHOP only	PDLIM3	chr4	186455601	186457799	12
CHOP only	PDSS1	chr10	26985201	26986599	-695
CHOP only	PEAK1	chr15	77711001	77713999	-54
CHOP only	PELP1	chr17	4605801	4610599	-568
CHOP only	PEX10	chr1	2342401	2346399	-390
CHOP only	PFDN1	chr5	139623601	139625199	58289
CHOP only	PFKFB4	chr3	48592601	48597199	-673
CHOP only	PGAM5	chr12	133285601	133287199	-993
CHOP only	PGAP2	chr11	3817601	3821199	211
CHOP only	PGM3	chr6	83906601	83907799	-3545
CHOP only	PGP	chr16	2264401	2266799	-778
CHOP only	PHC2	chr1	33815801	33816799	-801
CHOP only	PHF11	chr13	50068601	50071599	299
CHOP only	PHLDA1	chr12	76424801	76426599	-144
CHOP only	PHLDA2	chr11	2949601	2952599	-450
CHOP only	PHLDA3	chr1	201437201	201439599	-101
CHOP only	PHOX2A	chr11	71948801	71951999	4820
CHOP only	PHPT1	chr9	139741801	139743399	-668
CHOP only	PIGB	chr15	55609201	55612599	-233
CHOP only	PIGC	chr1	172412801	172413799	-70
CHOP only	PIGY	chr4	89444001	89445999	-48
CHOP only	PIK3R1	chr5	67583401	67585199	48
CHOP only	PILRA	chr7	99997001	99998799	26832
CHOP only	PIP4K2A	chr10	23002801	23004599	-197
CHOP only	PIP5K1C	chr19	3700601	3701799	-710
CHOP only	PJA2	chr5	108744601	108746999	-125
CHOP only	PKM	chr15	72518001	72527599	-737
CHOP only	PLA2G12A	chr4	110650201	110652199	42
CHOP only	PLCB3	chr11	64017201	64020799	5
CHOP only	PLEC	chr8	145016201	145017799	-308
CHOP only	PLEC	chr8	145013601	145015599	-842
CHOP only	PLEKHA1	chr10	124132601	124134799	-394
CHOP only	PLEKHB2	chr2	131907401	131908399	45480
CHOP only	PLEKHG6	chr12	6417601	6420999	-302
CHOP only	PLEKHH2	chr2	43862201	43865399	-639
CHOP only	PLEKHN1	chr1	900401	902999	-177
CHOP only	PLEKHO2	chr15	65132801	65135199	-82
CHOP only	PLIN4	chr19	4520801	4523599	-4484
CHOP only	PLOD2	chr3	145878001	145881399	-418
CHOP only	PLXNB2	chr22	50745601	50747599	-599
CHOP only	PMEL	chr12	56358001	56361999	-154
CHOP only	PMEPA1	chr20	56285001	56288599	-208
CHOP only	PMM1	chr22	41991601	41994799	-7329
CHOP only	PMVK	chr1	154914601	154917799	-6716
CHOP only	PNRC1	chr6	89794601	89796199	4971
CHOP only	POC1B	chr12	89918201	89920199	144
CHOP only	POLA2	chr11	65028201	65029799	-432

Overlap	Symbol	Chromosome	CHOP Peak Start	CHOP Peak End	CHOP dTSS
CHOP only	POLD2	chr7	44161801	44164599	-31
CHOP only	POLR3A	chr10	79787401	79791999	-402
CHOP only	POTEF	chr2	130885801	130887599	95
CHOP only	POU2F1	chr1	167189001	167189999	-566
CHOP only	PPA1	chr10	72012801	72015399	-20910
CHOP only	PPID	chr4	159643401	159647199	-748
CHOP only	PPM1A	chr14	60715001	60715799	-566
CHOP only	PPM1J	chr1	113257401	113259999	-750
CHOP only	PPP1CA	chr11	67167801	67171399	-224
CHOP only	PPP1R14B	chr11	64012201	64016599	13
CHOP only	PPP1R27	chr17	79798801	79802599	-7774
CHOP only	PPP1R42	chr8	67940601	67942199	-614
CHOP only	PPP2R1A	chr19	52691801	52693199	-555
CHOP only	PPP2R2A	chr8	26147601	26149599	-407
CHOP only	PPP2R3A	chr3	135683201	135685599	-115
CHOP only	PPP2R4	chr9	131871601	131875399	-93
CHOP only	PRDM10	chr11	129872201	129874999	-870
CHOP only	PRDM9	chr5	23506001	23508399	-524
CHOP only	PRDX2	chr19	12912201	12913599	-176
CHOP only	PRELID1	chr5	176730601	176731799	437
CHOP only	PRIMA1	chr14	94253401	94257999	-934
CHOP only	PRKCSH	chr19	11545001	11548799	339
CHOP only	PRKG2	chr4	82074801	82075799	11
CHOP only	PRMT1	chr19	50179201	50181799	91
CHOP only	PROCA1	chr17	27028801	27030799	9072
CHOP only	PROM1	chr4	16084201	16086799	94
CHOP only	PROSER1	chr13	39611601	39612999	-87
CHOP only	PROZ	chr13	113812401	113812999	-268
CHOP only	PRR18	chr6	166721401	166722399	-29
CHOP only	PRR19	chr19	42804801	42807799	16
CHOP only	PRR19	chr19	42800001	42801399	-5584
CHOP only	PRR7	chr5	176881601	176885399	8174
CHOP only	PRRC2B	chr9	134303801	134305799	-677
CHOP only	PRSS27	chr16	2758001	2760799	11152
CHOP only	PSCA	chr8	143750801	143752599	-26
CHOP only	PSIP1	chr9	15510001	15511599	203
CHOP only	PSMA1	chr11	14541201	14543399	-309
CHOP only	PSMA4	chr15	78831201	78833799	-247
CHOP only	PSMA5	chr1	109968401	109969599	70
CHOP only	PSMB2	chr1	36106401	36109999	-755
CHOP only	PSMC3IP	chr17	40728201	40731599	-51
CHOP only	PSMD2	chr3	184015401	184018399	14
CHOP only	PSMD8	chr19	38863001	38865799	-790
CHOP only	PSORS1C2	chr6	31109201	31110599	-2773
CHOP only	PSTK	chr10	124738201	124738999	-956
CHOP only	PTH2R	chr2	209270601	209272599	45
CHOP only	PUF60	chr8	144910201	144913399	-244
CHOP only	PURB	chr7	44924201	44925599	84
CHOP only	PVR	chr19	45146001	45148199	2
CHOP only	PVRL3	chr3	110789601	110791999	194
CHOP only	PXYLP1	chr3	140866801	140868199	-83167
CHOP only	PYDC1	chr16	31226601	31229999	95
CHOP only	PYGL	chr14	51409801	51412799	-52
CHOP only	QRICH1	chr3	49130601	49133399	-496
CHOP only	R3HCC1	chr8	23144801	23146199	-112
CHOP only	R3HCC1	chr8	23153801	23155199	8888
CHOP only	RAB11A	chr15	66159801	66162999	-397
CHOP only	RAB24	chr5	176727201	176728799	2745
CHOP only	RAB3D	chr19	11449801	11451599	-356
CHOP only	RAB40B	chr17	80656201	80657999	-502

Overlap	Symbol	Chromosome	CHOP Peak Start	CHOP Peak End	CHOP dTSS
CHOP only	RAB43	chr3	128839801	128843199	-507
CHOP only	RABL3	chr3	120460201	120460999	784
CHOP only	RAD17	chr5	68664801	68666599	61
CHOP only	RAD51AP1	chr12	4647201	4648399	-150
CHOP only	RAD9A	chr11	67158201	67159199	-723
CHOP only	RADIL	chr7	4923201	4924199	-365
CHOP only	RANGRF	chr17	8189601	8193199	-569
CHOP only	RAPGEF6	chr5	130970401	130971999	-271
CHOP only	RARG	chr12	53626201	53627399	-760
CHOP only	RARS	chr5	167912601	167913999	-163
CHOP only	RASA2	chr3	141205001	141206799	-26
CHOP only	RASGEF1B	chr4	82392201	82394399	-218
CHOP only	RBBP8	chr18	20513001	20514999	161
CHOP only	RBM12B	chr8	94752401	94753999	24
CHOP only	RBM15B	chr3	51431401	51435199	4601
CHOP only	RBM26	chr13	79978601	79981199	456
CHOP only	RBM48	chr7	92156801	92160399	513
CHOP only	RBPJ	chr4	26319801	26323799	468
CHOP only	RCL1	chr9	4791601	4793999	-34
CHOP only	REN	chr1	204135601	204136399	-535
CHOP only	REXO1	chr19	1846601	1850999	-348
CHOP only	RFC2	chr7	73667601	73669999	-12
CHOP only	RFC5	chr12	118452601	118455799	-306
CHOP only	RFFL	chr17	33388401	33393199	-41
CHOP only	RFPL2	chr22	32600601	32601599	-382
CHOP only	RFWD2	chr1	176175601	176177599	-220
CHOP only	RGL2	chr6	33264801	33269199	165
CHOP only	RGS9BP	chr19	33165201	33168199	387
CHOP only	RHOBTB1	chr10	62760001	62761999	198
CHOP only	RIBC2	chr22	45809401	45810799	528
CHOP only	RIC1	chr9	5627401	5629999	-419
CHOP only	RICTOR	chr5	39074401	39075399	-390
CHOP only	RIOK2	chr5	96518001	96520199	-95
CHOP only	RIPK4	chr21	43185001	43189999	-251
CHOP only	RITA1	chr12	113621801	113625599	369
CHOP only	RMDN1	chr8	87520401	87521599	9
CHOP only	RMND5B	chr5	177556001	177559999	38
CHOP only	RNASEH2C	chr11	65485601	65488999	1109
CHOP only	RND3	chr2	151344201	151345599	-691
CHOP only	RNF113A	chrX	119005401	119006599	-209
CHOP only	RNF121	chr11	71638201	71641999	332
CHOP only	RNF126	chr19	660601	665799	33
CHOP only	RNF145	chr5	158635001	158636199	-460
CHOP only	RNF151	chr16	2014001	2018199	-775
CHOP only	RNF185	chr22	31555801	31556999	262
CHOP only	RNF19A	chr8	101321601	101322999	94
CHOP only	RNF2	chr1	185013601	185015399	-51
CHOP only	RNF207	chr1	6279801	6282199	14811
CHOP only	RNPEP	chr1	201950401	201952199	-466
CHOP only	RORC	chr1	151803001	151806799	-552
CHOP only	RPA1	chr17	1732001	1734799	127
CHOP only	RPL24	chr3	101404601	101406799	-137
CHOP only	RPL32	chr3	12881401	12884999	-119
CHOP only	RPL34	chr4	109541201	109543399	551
CHOP only	RPL36	chr19	5687201	5690599	-1372
CHOP only	RPL36	chr19	5691201	5692399	1454
CHOP only	RPL37	chr5	40835401	40836599	-613
CHOP only	RPRM	chr2	154333001	154334199	1722
CHOP only	RPS19BP1	chr22	39928401	39931199	-940
CHOP only	RPS20	chr8	56986001	56988599	-160

Overlap	Symbol	Chromosome	CHOP Peak Start	CHOP Peak End	CHOP dTSS
CHOP only	RPS24	chr10	79792801	79794399	82
CHOP only	RPS6	chr9	19374601	19376599	4635
CHOP only	RPS6KB2	chr11	67193801	67197199	-435
CHOP only	RRAGC	chr1	39323201	39327799	-5
CHOP only	RRM2B	chr8	103250601	103251199	159
CHOP only	RRP15	chr1	218458201	218459199	71
CHOP only	RRP9	chr3	51973801	51977799	157
CHOP only	RTBDN	chr19	12945001	12947799	-158
CHOP only	RTCB	chr22	32808001	32809799	-626
CHOP only	RTF1	chr15	41707601	41709999	-502
CHOP only	RTN4RL1	chr17	1927601	1929399	-322
CHOP only	RTN4RL2	chr11	57251001	57252799	23890
CHOP only	RUNDC3A	chr17	42385601	42387199	473
CHOP only	RUNDC3B	chr7	87256201	87258999	-129
CHOP only	RUNX1	chr21	36259401	36263999	-713
CHOP only	RWDD4	chr4	184579201	184580999	231
CHOP only	S100A10	chr1	151966001	151967399	14
CHOP only	S1PR2	chr19	10341201	10342999	-152
CHOP only	SAC3D1	chr11	64807001	64810199	224
CHOP only	SAMD15	chr14	77843801	77844799	538
CHOP only	SAMD4A	chr14	55033001	55035199	-230
CHOP only	SATB2	chr2	200335601	200336799	-211
CHOP only	SBDS	chr7	66459401	66461999	-112
CHOP only	SBDS	chr7	66451601	66452399	8588
CHOP only	SBF2	chr11	10315001	10316599	-46
CHOP only	SBK2	chr19	56039401	56041199	8135
CHOP only	SC5D	chr11	121162801	121164199	-77
CHOP only	SCAF11	chr12	46383201	46386199	-299
CHOP only	SCML4	chr6	108053601	108055199	-800
CHOP only	SCO1	chr17	10599401	10601399	485
CHOP only	SEC11A	chr15	85258801	85261199	-309
CHOP only	SEC14L2	chr22	30792001	30793999	70
CHOP only	SEC16A	chr9	139376001	139380399	11
CHOP only	SEC22B	chr1	145095601	145097199	-7
CHOP only	SEC63	chr6	108279601	108280799	-718
CHOP only	SELENBP1	chr1	151343801	151346599	10
CHOP only	SELM	chr22	31503201	31504999	-549
CHOP only	SERINC2	chr1	31882601	31889399	37
CHOP only	SERP1	chr3	150263201	150264999	328
CHOP only	SERPINA10	chr14	94757401	94761599	108
CHOP only	SERPINE1	chr7	100763801	100776399	-270
CHOP only	SERPINF2	chr17	1644801	1646399	-530
CHOP only	SET	chr9	131446201	131447599	-465
CHOP only	SETD1B	chr12	122240801	122244399	-38
CHOP only	SFR1	chr10	105881001	105882199	-216
CHOP only	SFTA2	chr6	30893001	30895399	5752
CHOP only	SFXN4	chr10	120925001	120927199	-896
CHOP only	SFXN4	chr10	120898601	120900399	25704
CHOP only	SGMS1	chr10	52381601	52386599	-363
CHOP only	SGOL1	chr3	20227401	20229399	-676
CHOP only	SGPP1	chr14	64193801	64195799	-44
CHOP only	SH2D5	chr1	21059001	21060599	-667
CHOP only	SH3BGRL2	chr6	80340201	80341799	0
CHOP only	SH3BGRL3	chr1	26605201	26607799	287
CHOP only	SH3BP1	chr22	38028401	38030799	-6084
CHOP only	SH3BP5	chr3	15373801	15375399	-464
CHOP only	SH3GLB1	chr1	87169401	87170799	-153
CHOP only	SH3GLB2	chr9	131768001	131770399	21432
CHOP only	SH3RF3	chr2	109744201	109745999	-897
CHOP only	SHD	chr19	4277201	4279199	-398

Overlap	Symbol	Chromosome	CHOP Peak Start	CHOP Peak End	CHOP dTSS
CHOP only	SHF	chr15	45457201	45459399	15105
CHOP only	SHISA5	chr3	48513201	48516199	42
CHOP only	SHMT2	chr12	57619801	57627799	-28
CHOP only	SIAH2	chr3	150481401	150481999	-437
CHOP only	SIGMAR1	chr9	34636801	34639399	-277
CHOP only	SIK2	chr11	111471601	111473999	-370
CHOP only	SIPA1	chr11	65405201	65406399	222
CHOP only	SIRT5	chr6	13572601	13576399	-261
CHOP only	SKIDA1	chr10	21813401	21816599	-389
CHOP only	SKP1	chr5	133511601	133514999	-576
CHOP only	SLC11A2	chr12	51416801	51423799	-101
CHOP only	SLC15A4	chr12	129308201	129310799	-959
CHOP only	SLC16A11	chr17	6941801	6944999	3842
CHOP only	SLC16A11	chr17	6945601	6948799	42
CHOP only	SLC16A3	chr17	80192201	80193799	225
CHOP only	SLC17A2	chr6	25929801	25932399	-146
CHOP only	SLC17A5	chr6	74362801	74364599	37
CHOP only	SLC18B1	chr6	133119401	133121599	-753
CHOP only	SLC19A3	chr2	228582001	228583599	-55
CHOP only	SLC1A7	chr1	53607201	53609799	-196
CHOP only	SLC22A15	chr1	116518001	116519999	-119
CHOP only	SLC22A20	chr11	64992601	64994799	12389
CHOP only	SLC22A4	chr5	131628801	131630999	-245
CHOP only	SLC24A1	chr15	65902201	65906199	457
CHOP only	SLC25A1	chr22	19166401	19167599	-624
CHOP only	SLC25A22	chr11	796001	797199	-337
CHOP only	SLC25A3	chr12	98985801	98988599	-203
CHOP only	SLC25A39	chr17	42399601	42406599	-883
CHOP only	SLC25A39	chr17	42394401	42398399	5817
CHOP only	SLC25A45	chr11	65148201	65154399	-128
CHOP only	SLC26A1	chr4	985601	988799	28
CHOP only	SLC26A11	chr17	78192401	78195999	0
CHOP only	SLC26A6	chr3	48671401	48675799	-674
CHOP only	SLC27A5	chr19	59022001	59025999	-568
CHOP only	SLC2A13	chr12	40499201	40500999	-439
CHOP only	SLC2A7	chr1	9086001	9088799	-996
CHOP only	SLC30A7	chr1	101360401	101362599	-132
CHOP only	SLC35D2	chr9	99145401	99147199	-308
CHOP only	SLC37A4	chr11	118913401	118914399	-12284
CHOP only	SLC38A1	chr12	46661401	46663799	608
CHOP only	SLC38A2	chr12	46765001	46769399	-555
CHOP only	SLC38A3	chr3	50242201	50243199	21
CHOP only	SLC39A13	chr11	47437401	47438799	8054
CHOP only	SLC4A2	chr7	150753001	150757799	101
CHOP only	SLC52A2	chr8	145582201	145583199	424
CHOP only	SLC5A5	chr19	17980801	17982999	-882
CHOP only	SLC7A1	chr13	30168401	30171199	25
CHOP only	SLC7A9	chr19	33359201	33362599	-217
CHOP only	SLC9A1	chr1	27423001	27426999	56621
CHOP only	SLMAP	chr3	57742001	57743999	-174
CHOP only	SLTM	chr15	59224401	59227399	-48
CHOP only	SMAD6	chr15	66992201	66995799	-674
CHOP only	SMAD9	chr13	37493001	37496799	-491
CHOP only	SMARCA4	chr19	11092601	11095199	-928
CHOP only	SMIM1	chr1	3692001	3694599	3949
CHOP only	SMIM1	chr1	3686401	3689999	-1125
CHOP only	SMIM19	chr8	42395001	42397199	-198
CHOP only	SMIM24	chr19	3480001	3482199	-560
CHOP only	SMIM5	chr17	73627201	73630799	-514
CHOP only	SMIM8	chr6	88030601	88033199	-406

Overlap	Symbol	Chromosome	CHOP Peak Start	CHOP Peak End	CHOP dTSS
CHOP only	SMKR1	chr7	129140201	129143399	-520
CHOP only	SMOC1	chr14	70342601	70348199	-714
CHOP only	SNRNP35	chr12	123943201	123944199	-551
CHOP only	SNRNP35	chr12	123957601	123958199	13649
CHOP only	SNRPD2	chr19	46192201	46197999	343
CHOP only	SNX13	chr7	17979401	17980799	31
CHOP only	SNX22	chr15	64442201	64444399	-616
CHOP only	SNX30	chr9	115512001	115512799	-734
CHOP only	SNX33	chr15	75938601	75942999	-548
CHOP only	SNX8	chr7	2353201	2355799	-401
CHOP only	SOCS2	chr12	93962001	93966399	25
CHOP only	SOCS2	chr12	93957801	93959399	-4998
CHOP only	SOD2	chr6	160112801	160117799	-947
CHOP only	SORBS3	chr8	22406201	22411599	-351
CHOP only	SORL1	chr11	121504601	121505999	182388
CHOP only	SORT1	chr1	109940801	109941799	-737
CHOP only	SOWAHC	chr2	110370601	110373999	389
CHOP only	SP7	chr12	53736201	53740799	77
CHOP only	SPA17	chr11	124542801	124543599	-540
CHOP only	SPDYA	chr2	29025601	29027399	-7200
CHOP only	SPECC1	chr17	19911401	19912599	-649
CHOP only	SPG11	chr15	44954401	44957199	76
CHOP only	SPHK2	chr19	49121601	49124599	310
CHOP only	SPHK2	chr19	49132601	49134999	5591
CHOP only	SPIRE2	chr16	89892401	89896999	-207
CHOP only	SPOCK2	chr10	73847401	73850199	-10
CHOP only	SPPL2A	chr15	51057201	51058599	10
CHOP only	SPR	chr2	73109801	73118199	-512
CHOP only	SPRED1	chr15	38543401	38545999	-352
CHOP only	SPRED2	chr2	65536801	65538599	56231
CHOP only	SPRY1	chr4	124317601	124321199	-141
CHOP only	SQSTM1	chr5	179262601	179265399	16158
CHOP only	SREBF1	chr17	17738601	17743999	-975
CHOP only	SRP19	chr5	112195801	112197199	-385
CHOP only	SRP68	chr17	74068001	74069199	7
CHOP only	SRRM1	chr1	24966801	24970599	-894
CHOP only	SRRT	chr7	100470801	100474399	-101
CHOP only	SRSF10	chr1	24306201	24307999	-147
CHOP only	SSC5D	chr19	56015001	56016399	15830
CHOP only	SSNA1	chr9	140080601	140084799	-354
CHOP only	ST3GAL4	chr11	126292201	126294199	17123
CHOP only	STAG1	chr3	136470001	136472399	45
CHOP only	STAR	chr8	38007001	38011799	-800
CHOP only	STARD4	chr5	110847201	110849599	-243
CHOP only	STIL	chr1	47779401	47781199	-481
CHOP only	STK11	chr19	1204201	1205999	-698
CHOP only	STK35	chr20	2126201	2132199	46672
CHOP only	STOX1	chr10	70586001	70587199	-694
CHOP only	STPG2	chr4	99063401	99065599	-109
CHOP only	STX18	chr4	4542401	4544799	175
CHOP only	SUCLA2	chr13	48574801	48577399	-638
CHOP only	SUCLA2	chr13	48515001	48516799	59562
CHOP only	SUGP1	chr19	19429601	19432999	21
CHOP only	SUN1	chr7	853401	855799	-594
CHOP only	SUN2	chr22	39128401	39131799	21367
CHOP only	SURF6	chr9	136202401	136203599	47
CHOP only	SUV39H2	chr10	14920201	14921599	1
CHOP only	SYNCRIP	chr6	86351401	86353999	-60
CHOP only	SYNE4	chr19	36499201	36500199	-5
CHOP only	SYNGR2	chr17	76162601	76166199	-271

Overlap	Symbol	Chromosome	CHOP Peak Start	CHOP Peak End	CHOP dTSS
CHOP only	SZRD1	chr1	16691801	16694799	-225
CHOP only	TACR1	chr2	75426001	75427199	45
CHOP only	TAF2	chr8	120844201	120846199	-126
CHOP only	TAF5L	chr1	229760201	229762599	394
CHOP only	TAGLN	chr11	117064801	117066799	-4240
CHOP only	TARSL2	chr15	102263401	102265999	-55
CHOP only	TBC1D1	chr4	38110401	38113199	-2
CHOP only	TBC1D14	chr4	6909601	6911399	-671
CHOP only	TBC1D22A	chr22	47156801	47160399	86
CHOP only	TBCCD1	chr3	186284601	186285999	-157
CHOP only	TBL2	chr7	72991001	72995599	-287
CHOP only	TBRG1	chr11	124492201	124493199	-42
CHOP only	TBX10	chr11	67407001	67408999	-969
CHOP only	TBXA2R	chr19	3605801	3608199	-169
CHOP only	TCEA1	chr8	54933601	54936999	-284
CHOP only	TCERG1	chr5	145825401	145827999	-173
CHOP only	TCF7L1	chr2	85359001	85360199	-983
CHOP only	TCIRG1	chr11	67802801	67808599	-762
CHOP only	TCP1	chr6	160208001	160212999	235
CHOP only	TDRP	chr8	495401	496999	-419
CHOP only	TEAD2	chr19	49864401	49867799	-386
CHOP only	TEF	chr22	41775601	41780199	-33
CHOP only	TESK1	chr9	35603401	35605199	-981
CHOP only	TEX10	chr9	103114201	103115599	-47
CHOP only	TEX22	chr14	105864001	105866799	480
CHOP only	TEX264	chr3	51702801	51706799	-391
CHOP only	TEX40	chr11	64066801	64069199	137
CHOP only	TFDP2	chr3	141867601	141869399	-114
CHOP only	TFR2	chr7	100238601	100240999	-627
CHOP only	TGDS	chr13	95247801	95249199	11
CHOP only	TGFB1	chr19	41858401	41861799	-262
CHOP only	TGIF1	chr18	3457201	3459599	4628
CHOP only	TGIF1	chr18	3450601	3451999	-103
CHOP only	THAP3	chr1	6684001	6686199	-110
CHOP only	THAP3	chr1	6693401	6695399	9190
CHOP only	THAP6	chr4	76438801	76440599	46
CHOP only	THBS1	chr15	39872201	39873599	-380
CHOP only	THEM6	chr8	143805601	143811799	79
CHOP only	THNSL1	chr10	25305001	25306599	292
CHOP only	THOC3	chr5	175395001	175395599	18
CHOP only	THPO	chr3	184087601	184090599	6896
CHOP only	TIGD5	chr8	144684401	144686399	5326
CHOP only	TIPARP	chr3	156391401	156393999	-15
CHOP only	TJP1	chr15	30114201	30116399	-594
CHOP only	TJP3	chr19	3705401	3710199	-535
CHOP only	TJP3	chr19	3721001	3722199	-97
CHOP only	TLE3	chr15	70388601	70392199	-144
CHOP only	TM2D3	chr15	102191401	102193799	-6
CHOP only	TM4SF1	chr3	149095001	149096999	-432
CHOP only	TM4SF5	chr17	4672401	4677399	-287
CHOP only	TM9SF2	chr13	100152801	100154599	72
CHOP only	TMBIM6	chr12	50133601	50136199	-393
CHOP only	TMCC2	chr1	205195801	205199199	462
CHOP only	TMCO6	chr5	140017401	140020199	-212
CHOP only	TMED5	chr1	93644401	93647599	246
CHOP only	TMEM135	chr11	86747601	86749799	-186
CHOP only	TMEM136	chr11	120195001	120196599	-38
CHOP only	TMEM140	chr7	134832001	134833399	-66
CHOP only	TMEM143	chr19	48866601	48868199	-214
CHOP only	TMEM151A	chr11	66064001	66065999	5627

Overlap	Symbol	Chromosome	CHOP Peak Start	CHOP Peak End	CHOP dTSS
CHOP only	TMEM151B	chr6	44246201	44248999	9120
CHOP only	TMEM156	chr4	39034201	39035599	-859
CHOP only	TMEM161A	chr19	19248001	19251799	-590
CHOP only	TMEM170B	chr6	11537401	11539399	-60
CHOP only	TMEM184A	chr7	1595201	1596999	-34
CHOP only	TMEM2	chr9	74297601	74298199	85900
CHOP only	TMEM39A	chr3	119181401	119183799	-71
CHOP only	TMEM45A	chr3	100210001	100211799	-563
CHOP only	TMEM52B	chr12	10345001	10345799	13843
CHOP only	TMEM53	chr1	45138401	45141999	80
CHOP only	TMEM56	chr1	95581601	95583399	-394
CHOP only	TMEM59L	chr19	18722001	18724199	-582
CHOP only	TMTC2	chr12	83079601	83080399	-934
CHOP only	TMUB1	chr7	150779801	150781799	-180
CHOP only	TMX1	chr14	51705201	51707599	-486
CHOP only	TNFAIP1	chr17	26671801	26674399	10552
CHOP only	TNFRSF10B	chr8	22926001	22928199	-400
CHOP only	TNFRSF6B	chr20	62329401	62331399	2396
CHOP only	TNFSF9	chr19	6534801	6537199	4990
CHOP only	TNIP1	chr5	150466001	150467599	-53
CHOP only	TNNT1	chr19	55661001	55664399	-1978
CHOP only	TNPO3	chr7	128694201	128696199	27
CHOP only	TOMM40	chr19	45392601	45395799	-277
CHOP only	TOMM70A	chr3	100119601	100120799	42
CHOP only	TONSL	chr8	145668601	145671399	-188
CHOP only	TOP3B	chr22	22336601	22337999	-60
CHOP only	TP53	chr17	7588601	7593399	-132
CHOP only	TP53BP1	chr15	43800201	43805399	-93
CHOP only	TP53BP2	chr1	224033401	224035799	-926
CHOP only	TPBG	chr6	83072401	83074599	-461
CHOP only	TPP2	chr13	103248201	103249999	-186
CHOP only	TPRA1	chr3	127309801	127310999	-798
CHOP only	TPRG1L	chr1	3540001	3542399	-356
CHOP only	TRADD	chr16	67189201	67196799	812
CHOP only	TRAIP	chr3	49893801	49895199	-508
CHOP only	TRAP1	chr16	3767001	3769799	-802
CHOP only	TRAPPC10	chr21	45431001	45433399	-6
CHOP only	TRAPPC13	chr5	64919401	64921599	-58
CHOP only	TRAPPC3	chr1	36621801	36623399	-946
CHOP only	TRAPPC6A	chr19	45679201	45683199	301
CHOP only	TREX1	chr3	48506601	48507799	281
CHOP only	TRIAP1	chr12	120883001	120884799	315
CHOP only	TRIM11	chr1	228594001	228595799	-383
CHOP only	TRIM3	chr11	6494801	6497399	-411
CHOP only	TRIM36	chr5	114504801	114507199	-340
CHOP only	TRIM56	chr7	100701201	100703799	-26286
CHOP only	TRIM7	chr5	180628601	180629999	-1370
CHOP only	TRIP10	chr19	6748801	6755799	12607
CHOP only	TRMT112	chr11	64081801	64086199	1556
CHOP only	TRMT13	chr1	100598401	100599599	294
CHOP only	TRNT1	chr3	3166601	3168799	-900
CHOP only	TRPV1	chr17	3510801	3512399	1105
CHOP only	TRRAP	chr7	98473401	98476999	-913
CHOP only	TSGA10	chr2	99757001	99758599	237
CHOP only	TSHZ1	chr18	73002201	73003399	80090
CHOP only	TSPAN10	chr17	79607601	79610199	-431
CHOP only	TSPAN4	chr11	842201	843399	-24
CHOP only	TSSC4	chr11	2418801	2422999	-818
CHOP only	TTBK2	chr15	43213001	43213999	-493
CHOP only	TTC21A	chr3	39136801	39139599	-10952

Overlap	Symbol	Chromosome	CHOP Peak Start	CHOP Peak End	CHOP dTSS
CHOP only	TTC23L	chr5	34836201	34840399	-969
CHOP only	TTC24	chr1	156548001	156550399	-319
CHOP only	TTC33	chr5	40755201	40757399	-228
CHOP only	TTC9C	chr11	62505601	62507199	10448
CHOP only	TTI2	chr8	33370201	33372599	-697
CHOP only	TTLL10	chr1	1107401	1109399	-886
CHOP only	TTLL10	chr1	1121001	1121799	6323
CHOP only	TTLL7	chr1	84464001	84466199	-267
CHOP only	TUBA8	chr22	18591601	18593599	-853
CHOP only	TUBAL3	chr10	5433201	5435399	12493
CHOP only	TUBB4B	chr9	140129201	140133799	-4211
CHOP only	TUBB4B	chr9	140137201	140138999	2389
CHOP only	TUBB4B	chr9	140134601	140136399	-211
CHOP only	TUBB6	chr18	12327601	12329199	20143
CHOP only	TUBGCP6	chr22	50682601	50685599	-700
CHOP only	TULP3	chr12	2998801	3000599	-333
CHOP only	TUSC2	chr3	50365001	50366399	-31
CHOP only	TXNDC12	chr1	52520001	52522399	643
CHOP only	TXNRD3	chr3	126373601	126374999	-333
CHOP only	TYMS	chr18	654001	660999	-104
CHOP only	TYW3	chr1	75197201	75200599	38
CHOP only	UBAC2	chr13	99852401	99854199	137
CHOP only	UBB	chr17	16285401	16286999	1421
CHOP only	UBE2B	chr5	133707001	133707999	633
CHOP only	UBE2G2	chr21	46219801	46223199	251
CHOP only	UBE2L6	chr11	57333001	57337399	-20
CHOP only	UBE2S	chr19	55918801	55920599	-375
CHOP only	UBL5	chr19	9936601	9939799	-356
CHOP only	UBN1	chr16	4896201	4899199	68
CHOP only	UBP1	chr3	33480801	33484799	-903
CHOP only	UBTD1	chr10	99257201	99261199	561
CHOP only	UBTD2	chr5	171711401	171711799	-805
CHOP only	UBXN2B	chr8	59322201	59324199	-623
CHOP only	UBXN4	chr2	136496401	136500399	-789
CHOP only	UBXN6	chr19	4457601	4459599	-809
CHOP only	UCKL1	chr20	62584801	62591399	-300
CHOP only	UCN2	chr3	48598001	48599999	2201
CHOP only	UFSP1	chr7	100486801	100488199	-161
CHOP only	UGGT2	chr13	96705001	96707199	-364
CHOP only	UHRF1	chr19	4908601	4912199	21
CHOP only	UNC13B	chr9	35160401	35162799	-389
CHOP only	UNC13D	chr17	73821801	73823599	18098
CHOP only	UPF2	chr10	12083601	12086599	69
CHOP only	UQCR11	chr19	1604601	1607399	-517
CHOP only	UQCRC1	chr3	48646201	48648399	-202
CHOP only	URB1	chr21	33763801	33765199	812
CHOP only	URI1	chr19	30431401	30433199	-846
CHOP only	URM1	chr9	131124001	131125399	-8898
CHOP only	USE1	chr19	17330001	17332399	5045
CHOP only	USMG5	chr10	105154801	105157399	170
CHOP only	USP1	chr1	62899601	62903599	-375
CHOP only	USP15	chr12	62653201	62654999	-21
CHOP only	USP20	chr9	132597001	132599999	804
CHOP only	USP35	chr11	77924001	77927799	26042
CHOP only	USP49	chr6	41870601	41874599	-9501
CHOP only	USP53	chr4	120133201	120134199	-82
CHOP only	UST	chr6	149067201	149069399	29
CHOP only	UTP3	chr4	71552801	71555199	-196
CHOP only	VAMP1	chr12	6579401	6581199	-235
CHOP only	VEGFA	chr6	43754201	43755599	15178

Overlap	Symbol	Chromosome	CHOP Peak Start	CHOP Peak End	CHOP dTSS
CHOP only	VGF	chr7	100813201	100814399	-4948
CHOP only	VGLL4	chr3	11761801	11762599	42
CHOP only	VNN2	chr6	133089201	133090599	-5302
CHOP only	VOPP1	chr7	55640401	55641599	-800
CHOP only	VPRBP	chr3	51532401	51537199	-782
CHOP only	VPS18	chr15	41183001	41189399	-428
CHOP only	VPS26A	chr10	70882001	70884799	-508
CHOP only	VPS37A	chr8	17103601	17106199	499
CHOP only	VPS54	chr2	64246601	64247199	-686
CHOP only	VSTM2L	chr20	36529401	36532799	-399
CHOP only	VSTM2L	chr20	36500401	36500999	-30799
CHOP only	VTI1A	chr10	114205801	114208399	344
CHOP only	VTN	chr17	26696801	26698999	-527
CHOP only	VWA1	chr1	1368601	1371999	-603
CHOP only	VWA5B1	chr1	20684201	20686999	68188
CHOP only	VWA7	chr6	31742401	31746999	408
CHOP only	WBSCR27	chr7	73256001	73258399	-345
CHOP only	WDR24	chr16	739601	741599	-200
CHOP only	WDR31	chr9	116102201	116104199	-580
CHOP only	WDR38	chr9	127618401	127620199	3604
CHOP only	WDR38	chr9	127615001	127616399	4
CHOP only	WDR81	chr17	1626001	1629399	-134
CHOP only	WDR83	chr19	12776401	12778999	82
CHOP only	WDR83	chr19	12780001	12780999	-17
CHOP only	WDR90	chr16	698001	699999	-363
CHOP only	WFIKKN1	chr16	678601	682199	-612
CHOP only	WNK1	chr12	860401	862399	-689
CHOP only	WNT5B	chr12	1736401	1739199	-612
CHOP only	WTAP	chr6	160147401	160149399	-132
CHOP only	XPO7	chr8	21776401	21777799	-80
CHOP only	XRCC3	chr14	104180801	104182199	323
CHOP only	XYLB	chr3	38387001	38389399	-51
CHOP only	YIF1A	chr11	66054201	66059199	-62
CHOP only	YWHAH	chr22	32302201	32303999	-37379
CHOP only	YWHAZ	chr8	101962401	101965999	157
CHOP only	ZACN	chr17	74074201	74078799	1237
CHOP only	ZBTB42	chr14	105265601	105266599	-833
CHOP only	ZBTB45	chr19	59029601	59033399	-579
CHOP only	ZBTB48	chr1	6638001	6642199	49
CHOP only	ZBTB48	chr1	6649601	6651799	10649
CHOP only	ZBTB49	chr4	4291001	4293199	176
CHOP only	ZC3H14	chr14	89028201	89029999	-153
CHOP only	ZCCHC2	chr18	60189601	60190199	-758
CHOP only	ZCCHC6	chr9	88968801	88970799	-398
CHOP only	ZCCHC9	chr5	80595801	80599199	98
CHOP only	ZCWPW1	chr7	100025001	100028599	-369
CHOP only	ZDHHC12	chr9	131485201	131487799	-92
CHOP only	ZEB1	chr10	31607001	31610999	899
CHOP only	ZFAND5	chr9	74979201	74981999	-437
CHOP only	ZFP30	chr19	38145601	38147399	-187
CHOP only	ZMAT2	chr5	140077801	140080599	-832
CHOP only	ZMYM4	chr1	35733801	35735199	-68
CHOP only	ZMYM5	chr13	20437401	20439599	-724
CHOP only	ZNF106	chr15	42781601	42784999	95
CHOP only	ZNF131	chr5	43120201	43122199	197
CHOP only	ZNF142	chr2	219501801	219503399	21663
CHOP only	ZNF165	chr6	28045001	28050399	-782
CHOP only	ZNF213	chr16	3193001	3194399	8566
CHOP only	ZNF213	chr16	3185201	3185999	466
CHOP only	ZNF24	chr18	32910401	32912199	13126

CHOP only	ZNF248	chr10	38146001	38148199	-88
CHOP only	ZNF25	chr10	38265001	38265999	-47
CHOP only	ZNF26	chr12	133562201	133563599	-34
CHOP only	ZNF276	chr16	89784201	89789599	124
CHOP only	ZNF324	chr19	58976801	58978799	-612
CHOP only	ZNF33B	chr10	43133201	43135599	-408
CHOP only	ZNF385C	chr17	40189401	40191599	-456
CHOP only	ZNF395	chr8	28244001	28245399	-723
CHOP only	ZNF425	chr7	148822601	148823599	338
CHOP only	ZNF426	chr19	9648801	9650599	-379
CHOP only	ZNF445	chr3	44518801	44520799	-638
CHOP only	ZNF461	chr19	37156601	37159599	-345
CHOP only	ZNF511	chr10	135120601	135122599	-823
CHOP only	ZNF516	chr18	74206801	74207799	-154
CHOP only	ZNF527	chr19	37860201	37862399	-759
CHOP only	ZNF564	chr19	12661801	12663999	-544
CHOP only	ZNF594	chr17	5093801	5095999	278
CHOP only	ZNF600	chr19	53289601	53290399	34
CHOP only	ZNF609	chr15	64747801	64748599	-43419
CHOP only	ZNF620	chr3	40545801	40547799	-730
CHOP only	ZNF629	chr16	30785201	30791399	10223
CHOP only	ZNF649	chr19	52407201	52409799	-195
CHOP only	ZNF669	chr1	247262601	247263799	4474
CHOP only	ZNF680	chr7	64022801	64025199	-495
CHOP only	ZNF701	chr19	53072201	53073399	-726
CHOP only	ZNF721	chr4	491001	493599	660
CHOP only	ZNF747	chr16	30536601	30548399	3694
CHOP only	ZNF765	chr19	53896601	53899799	-197
CHOP only	ZNF77	chr19	2944401	2945599	-31
CHOP only	ZNF777	chr7	149157801	149158599	-147
CHOP only	ZNF778	chr16	89332601	89333999	49189
CHOP only	ZNF844	chr19	12174601	12175799	-346
CHOP only	ZNF852	chr3	44551801	44553399	-468
CHOP only	ZNF860	chr3	32021401	32023399	-866
CHOP only	ZNHIT2	chr11	64877601	64891599	570
CHOP only	ZSCAN21	chr7	99645801	99648399	-317
CHOP only	ZZEF1	chr17	4045401	4047199	-47
CHOP only	ZZZ3	chr1	78147401	78149399	-57

Appendix 3. List of top 450 induced genes following palmitate treatment identified through RNA-seq.

Gene Symbol	Description	WT Palmitate	RELA-KO Vehicle	RELA-KO Palmitate	CHOP-KO Vehicle	CHOP-KO Palmitate
KLHDC7B	kelch domain containing 7B	6.4	2.9	-0.8	-3.2	2.2
C11orf96	chromosome 11 open reading frame 96	6.3	8.5	6.2	5.1	8.4
LINC01564	long intergenic non-protein coding RNA 1564	5.4	-4.7	-3.8	-4.5	-4.8
ATP6V0D2	ATPase, H+ transporting, lysosomal 38kDa, V0 subunit d2	5.4	0.1	-0.4	1.4	2.1
HSPA6	heat shock protein family A (Hsp70) member 6	4.7	2.2	2.6	2.4	2.4
DRD5P1	dopamine receptor D5 pseudogene 1	4.5	4.0	1.0	1.3	5.2
P2RX1	purinergic receptor P2X, ligand gated ion channel, 1	4.3	1.6	-0.2	-0.9	-0.1
GEM	GTP binding protein overexpressed in skeletal muscle	4.0	3.8	2.7	2.6	4.3
HSPA7	heat shock protein family A (Hsp70) member 7	4.0	1.9	2.3	2.3	2.3
FOS	FBJ murine osteosarcoma viral oncogene homolog	3.9	3.0	1.0	0.3	3.0
SPX	spexin hormone	3.9	4.3	3.3	2.5	4.8
KLF4	Kruppel-like factor 4 (gut)	3.9	3.3	2.3	2.3	3.6
RAB39B	RAB39B, member RAS oncogene family	3.5	4.3	2.5	2.5	5.1
EID3	EP300 interacting inhibitor of differentiation 3	3.4	-1.3	-0.2	-0.7	0.3
AMZ1	archaelysin family metallopeptidase 1	3.4	-2.1	-3.3	-3.1	-1.8
DUSP1	dual specificity phosphatase 1	3.3	2.7	1.9	1.2	2.4
ATF3	activating transcription factor 3	3.3	3.3	1.3	1.3	3.7
DDIT3	DNA damage inducible transcript 3	3.3	1.6	-0.8	-0.6	2.0
DRD5P2	dopamine receptor D5 pseudogene 2	3.3	3.2	-0.4	0.8	4.4
ALPK3	alpha kinase 3	3.2	0.6	0.2	0.7	0.2
IFIT2	interferon induced protein with tetratricopeptide repeats 2	3.2	-0.1	-0.3	-1.4	-1.2
BEX2	brain expressed X-linked 2	3.1	9.0	8.6	7.6	8.6
GPR83	G protein-coupled receptor 83	3.1	1.6	1.2	1.7	1.9
IGFBP1	insulin like growth factor binding protein 1	3.1	-12.7	-11.6	-11.5	-12.2
IL21R	interleukin 21 receptor	3.1	-0.8	-3.0	-3.2	-0.8
LVRN	laeverin	3.1	0.1	-0.8	0.5	2.5
KLF2	Kruppel-like factor 2	3.1	2.4	1.8	2.6	3.1
SCG5	secretogranin V	3.0	0.8	0.8	1.1	1.6
GYS2	glycogen synthase 2	3.0	3.4	2.9	2.3	4.0
IL21R-AS1	IL21R antisense RNA 1	3.0	-1.5	-3.1	-4.2	-1.0
FAM129A	family with sequence similarity 129 member A	3.0	7.7	6.5	6.4	7.9
LINC00942	long intergenic non-protein coding RNA 942	3.0	0.3	2.0	-0.9	1.6
FUT1	fucosyltransferase 1 (H blood group)	2.9	5.7	1.3	1.7	6.9
CXCL8	chemokine (C-X-C motif) ligand 8	2.9	-8.9	-10.0	-8.4	-5.8
TMEM154	transmembrane protein 154	2.9	3.4	1.5	-0.6	3.1
C5AR1	complement component 5a receptor 1	2.9	0.8	0.6	0.5	0.3
TRIM54	tripartite motif containing 54	2.9	-2.6	-2.7	-2.9	-1.6
PPP1R15A	protein phosphatase 1 regulatory subunit 15A	2.9	0.7	-0.8	-0.7	1.0
TTLL6	tubulin tyrosine ligase like 6	2.9	-0.2	0.3	0.2	1.2
CD44	CD44 molecule (Indian blood group)	2.8	6.0	5.2	2.0	3.7
IGFN1	immunoglobulin-like and fibronectin type III domain containing 1	2.8	1.2	0.5	-1.9	-1.2
FOSB	FBJ murine osteosarcoma viral oncogene homolog B	2.8	2.9	1.9	0.6	2.6
LURAP1L	leucine rich adaptor protein 1-like	2.8	-1.5	-2.9	-3.0	-1.2
LUCAT1	lung cancer associated transcript 1 (non-protein coding)	2.8	-4.0	-4.7	-5.1	-4.0
ZSCAN12P1	zinc finger and SCAN domain containing 12 pseudogene 1	2.8	0.3	0.2	0.3	0.7
DNAJB9	DnaJ heat shock protein family (Hsp40) member B9	2.8	0.3	-1.2	-0.9	0.6
FGF21	fibroblast growth factor 21	2.8	5.2	1.3	1.8	6.6
SKAP1	src kinase associated phosphoprotein 1	2.8	-2.1	-2.2	-1.3	-0.8
BACH2	BTB and CNC homology 1, basic leucine zipper transcription factor 2	2.7	7.0	6.3	6.2	7.1
PDK4	pyruvate dehydrogenase kinase 4	2.7	2.7	2.6	2.4	3.0
ZNF165	zinc finger protein 165	2.7	0.5	-0.3	-0.2	0.3
PLIN2	perilipin 2	2.7	-9.5	-9.6	-9.0	-9.0
C3orf80	chromosome 3 open reading frame 80	2.7	6.7	6.4	6.3	6.7
F2RL2	coagulation factor II (thrombin) receptor-like 2	2.6	5.1	3.7	1.9	4.5
SLC7A11-AS1	SLC7A11 antisense RNA 1	2.6	1.3	-0.9	0.1	1.9
TRIB3	tribbles pseudokinase 3	2.6	-0.6	-2.6	-2.7	-0.1
ERN1	endoplasmic reticulum to nucleus signaling 1	2.6	0.1	-0.6	-0.6	0.2
SLC22A15	solute carrier family 22 member 15	2.6	2.3	1.9	1.8	2.7
TNFRSF9	tumor necrosis factor receptor superfamily member 9	2.6	0.4	-2.0	-1.0	2.6
CYTH4	cytohesin 4	2.6	-3.6	-3.6	-3.0	-2.9
HRK	harakiri, BCL2 interacting protein	2.5	5.4	5.0	4.6	5.6
OASL	2'-5'-oligoadenylate synthetase-like	2.5	-3.6	-3.7	-3.6	-4.0
GCLC	glutamate-cysteine ligase, catalytic subunit	2.5	-0.7	-0.9	-0.7	-0.4
SLC7A11	solute carrier family 7 (anionic amino acid transporter light chain, xc- system), member 11	2.5	1.6	-1.2	-0.2	2.3
RASGEF1B	RasGEF domain family member 1B	2.5	4.5	4.3	4.2	4.6
PTPRH	protein tyrosine phosphatase, receptor type H	2.5	-5.3	-6.3	-6.9	-6.0
EGR1	early growth response 1	2.5	-0.6	-2.1	-3.1	-0.4
HERPUD1	homocysteine-inducible, endoplasmic reticulum stress-inducible, ubiquitin-like domain member 1	2.5	0.2	-2.4	-1.9	0.3
LINC00346	long intergenic non-protein coding RNA 346	2.5	0.4	-2.9	-2.7	0.9
PAPPA2	pappalysin 2	2.4	3.2	2.1	1.4	3.8
OSGIN1	oxidative stress induced growth inhibitor 1	2.4	-6.2	-6.3	-7.0	-5.7
THSD7A	thrombospondin type 1 domain containing 7A	2.4	1.1	1.2	1.7	1.8
DIO2	deiodinase, iodothyronine, type II	2.4	3.4	3.3	3.8	4.1
RND1	Rho family GTPase 1	2.4	-0.5	-0.1	-0.5	-0.9

CTH	cystathionine gamma-lyase	2.4	3.0	0.8	0.5	3.8
BHLHA15	basic helix-loop-helix family member a15	2.4	-1.5	-3.1	-3.1	-1.5
RCAN3AS	RCAN3 antisense	2.4	1.0	1.9	2.4	2.4
RRAD	Ras-related associated with diabetes	2.4	-4.7	-4.5	-4.3	-5.0
MUC12	mucin 12, cell surface associated	2.4	-1.5	-2.8	-3.7	-3.7
CEBPB	CCAAT/enhancer binding protein beta	2.4	-0.1	-1.5	-1.5	0.3
CBR3	carbonyl reductase 3	2.4	6.3	6.4	6.3	5.9
FABP5P9	fatty acid binding protein 5 pseudogene 9	2.3	0.4	1.0	-0.4	0.9
MMP10	matrix metallopeptidase 10	2.3	1.7	0.2	-0.5	1.4
ADGRF4	adhesion G protein-coupled receptor F4	2.3	2.0	1.5	0.0	1.8
GULP1	GULP, engulfment adaptor PTB domain containing 1	2.3	5.3	5.5	5.7	5.5
INHBE	inhibin beta E	2.3	-0.8	-4.1	-3.6	0.3
BEST1	bestrophin 1	2.3	4.6	1.2	1.0	5.0
NALCN-AS1	NALCN antisense RNA 1	2.3	3.1	3.3	2.8	3.2
TXNRD1	thioredoxin reductase 1	2.2	0.0	-0.1	0.0	0.2
AMPD3	adenosine monophosphate deaminase 3	2.2	-2.0	-1.9	-2.4	-2.1
SQSTM1	sequestosome 1	2.2	-0.9	-1.2	-1.9	-1.7
HIST1H1E	histone cluster 1, H1e	2.2	-0.4	-0.1	-0.6	-0.5
COX5BP4	cytochrome c oxidase subunit Vb pseudogene 4	2.2	1.3	0.8	1.3	2.0
FCGR2A	Fc fragment of IgG receptor IIa	2.2	5.0	4.5	4.5	4.4
GLT1D1	glycosyltransferase 1 domain containing 1	2.2	0.9	-0.2	1.2	1.0
TRAF1	TNF receptor associated factor 1	2.2	-1.0	-1.3	-1.1	-0.3
TSC22D3	TSC22 domain family member 3	2.2	5.3	4.4	4.5	6.1
LIPG	lipase, endothelial	2.2	-0.5	-1.0	-0.5	0.0
RNU6-16P	RNA, U6 small nuclear 16, pseudogene	2.2	1.3	1.7	2.3	2.4
UNC5B	unc-5 netrin receptor B	2.2	6.5	5.6	5.8	7.1
CHAC1	ChaC glutathione-specific gamma-glutamylcyclotransferase 1	2.2	7.5	4.3	5.4	8.8
TEX21P	testis expressed 21, pseudogene	2.2	3.3	2.9	3.4	3.1
PTGER4P2-CDK2AP2P2	PTGER4P2-CDK2AP2P2 readthrough transcribed pseudogene	2.2	4.3	4.3	4.7	4.8
HMX3	H6 family homeobox 3	2.1	1.3	0.8	-1.0	2.1
METRNL	meteorin, glial cell differentiation regulator-like	2.1	0.6	0.9	1.5	1.2
BHLHE40	basic helix-loop-helix family member e40	2.1	-0.4	-1.3	-1.8	-0.7
HKDC1	hexokinase domain containing 1	2.1	-6.5	-7.5	-7.6	-7.2
SNHG17	small nucleolar RNA host gene 17	2.1	1.7	1.1	1.1	2.0
MXD1	MAX dimerization protein 1	2.1	0.1	-0.4	-0.7	-0.1
TMEM236	transmembrane protein 236	2.1	0.6	-0.1	1.3	0.7
FBLL1	fibrillarin-like 1	2.1	2.2	0.0	0.2	2.9
MIR616	microRNA 616	2.1	-0.7	-1.1	0.2	-0.6
DDIT4	DNA damage inducible transcript 4	2.1	1.3	-0.3	0.6	2.5
PYY2	peptide YY, 2 (pseudogene)	2.0	2.3	2.1	2.2	2.0
TCP11L2	t-complex 11, testis-specific-like 2	2.0	-2.0	-2.4	-2.6	-1.8
HDAC9	histone deacetylase 9	2.0	3.5	3.3	3.5	3.9
GRIK1-AS2	GRIK1 antisense RNA 2	2.0	2.1	2.7	2.3	3.0
GABARAPL1	GABA(A) receptor-associated protein like 1	2.0	0.6	-0.2	-0.3	0.7
GPR158	G protein-coupled receptor 158	2.0	2.8	3.1	1.6	2.5
HIST1H4I	histone cluster 1, H4i	2.0	2.4	3.4	3.3	2.4
HSPB7	heat shock protein family B (small) member 7	2.0	0.6	1.0	-0.3	-0.7
C5orf45	chromosome 5 open reading frame 45	2.0	-0.2	-0.3	-0.8	-0.9
AQP3	aquaporin 3 (Gill blood group)	2.0	-0.6	-0.6	-0.8	-1.3
VLDLR-AS1	VLDLR antisense RNA 1	2.0	2.1	0.0	-0.2	3.2
ZNF474	zinc finger protein 474	2.0	2.2	0.6	1.7	2.2
GAREM1	GRB2 associated regulator of MAPK1 subtype 1	2.0	1.3	1.3	1.3	1.2
DAND5	DAN domain family member 5, BMP antagonist	2.0	3.0	2.8	2.0	2.3
PPP4R1L	protein phosphatase 4 regulatory subunit 1 like (pseudogene)	2.0	0.5	0.3	0.2	0.5
GCLM	glutamate-cysteine ligase, modifier subunit	2.0	0.2	0.0	0.3	0.5
LRRC69	leucine rich repeat containing 69	2.0	4.4	4.9	4.5	3.9
IRS2	insulin receptor substrate 2	1.9	7.6	7.1	6.9	7.8
LSMEM1	leucine-rich single-pass membrane protein 1	1.9	-0.8	-0.9	-0.6	-0.1
ZFP36	ZFP36 ring finger protein	1.9	-3.2	-3.7	-4.0	-3.4
NFIL3	nuclear factor, interleukin 3 regulated	1.9	-1.3	-2.1	-1.7	-0.5
MEI1	meiotic double-stranded break formation protein 1	1.9	-1.9	-2.4	-2.1	-2.1
HSD17B7P2	hydroxysteroid (17-beta) dehydrogenase 7 pseudogene 2	1.9	-0.7	-1.4	-1.1	-0.5
ARHGDIG	Rho GDP dissociation inhibitor (GDI) gamma	1.9	6.7	6.8	7.1	6.9
PIM1	Pim-1 proto-oncogene, serine/threonine kinase	1.9	-0.8	-1.0	-0.7	-0.6
KRTAP5-2	keratin associated protein 5-2	1.9	0.6	-0.5	-2.6	0.4
MB	myoglobin	1.9	1.6	2.2	-0.3	0.3
HOXB9	homeobox B9	1.9	12.0	11.7	11.8	12.3
SYT16	synaptotagmin 16	1.9	3.6	3.7	3.0	2.8
KYNU	kynureninase	1.9	-6.0	-6.4	-5.8	-5.7
SESN2	sestrin 2	1.9	2.8	0.8	1.3	3.8
WNT11	wingless-type MMTV integration site family member 11	1.9	0.1	0.5	0.9	0.2
LGSN	lengsin, lens protein with glutamine synthetase domain	1.9	1.3	1.9	0.8	0.9
HIST1H4B	histone cluster 1, H4b	1.9	1.5	1.7	2.0	0.3
AGTR1	angiotensin II receptor type 1	1.9	1.4	1.5	1.3	1.7
ADM2	adrenomedullin 2	1.9	-1.2	-4.5	-3.4	0.8

SLC25A51P1	solute carrier family 25, member 51 pseudogene 1	1.9	0.7	0.1	1.4	-0.3
GDF15	growth differentiation factor 15	1.9	-7.0	-9.3	-8.9	-6.7
FAM167A	family with sequence similarity 167 member A	1.9	4.7	3.6	3.7	5.5
ARHGEF2	Rho/Rac guanine nucleotide exchange factor 2	1.9	2.0	1.1	1.1	2.1
DDR2	discoidin domain receptor tyrosine kinase 2	1.9	3.9	1.9	1.6	4.5
MTHFD2P5	methylenetetrahydrofolate dehydrogenase (NADP+ dependent) 2, methenyltetrahydrofolate cyclohydrolase pseudogene 5	1.8	0.6	0.9	0.3	1.3
SNAI2	snail family zinc finger 2	1.8	4.5	3.8	2.9	4.4
PTHLH	parathyroid hormone-like hormone	1.8	1.7	1.2	0.8	1.5
BHLHE40-AS1	BHLHE40 antisense RNA 1	1.8	-1.1	-1.2	-1.5	-1.3
COX6B2	cytochrome c oxidase subunit VIb polypeptide 2 (testis)	1.8	1.3	1.6	1.1	1.5
RASD1	RAS, dexamethasone-induced 1	1.8	-6.5	-6.5	-6.7	-6.4
GPAT3	glycerol-3-phosphate acyltransferase 3	1.8	0.3	-0.2	-0.2	0.8
SNHG12	small nucleolar RNA host gene 12	1.8	1.4	0.7	1.0	1.6
N4BP3	NEDD4 binding protein 3	1.8	3.0	2.6	2.0	2.3
TMEM71	transmembrane protein 71	1.8	-2.9	-2.9	-2.9	-2.3
HCAR2	hydroxycarboxylic acid receptor 2	1.8	-5.0	-3.4	-5.0	-3.3
ISG20	interferon stimulated exonuclease gene 20kDa	1.8	-1.2	-2.0	-1.4	-0.7
RPS6P16	ribosomal protein S6 pseudogene 16	1.8	-0.8	-0.7	-0.8	-0.2
DNAAF1	dynein, axonemal, assembly factor 1	1.8	-0.1	0.5	0.6	0.9
SLC3A2	solute carrier family 3 (amino acid transporter heavy chain), member 2	1.8	0.7	-0.7	-0.7	1.0
MYC	v-myc avian myelocytomatosis viral oncogene homolog	1.8	0.3	0.3	0.5	0.6
SLC16A12	solute carrier family 16 member 12	1.8	0.5	-0.3	-1.2	-0.1
ELMSAN1	ELM2 and Myb/SANT-like domain containing 1	1.8	0.5	0.2	0.3	0.3
FOXD1	forkhead box D1	1.8	4.8	5.0	4.5	4.5
RFTN2	raftlin family member 2	1.8	2.3	2.0	1.9	2.1
ZNF807	zinc finger protein 807	1.8	1.3	0.7	2.1	2.0
TNS1	tensin 1	1.8	-4.0	-3.9	-4.1	-4.9
CLEC4A	C-type lectin domain family 4 member A	1.8	2.1	2.5	2.4	2.7
SRXN1	sulfiredoxin 1	1.8	-0.7	-0.7	-0.6	-0.7
FAM220CP	family with sequence similarity 220 member C, pseudogene	1.8	2.0	2.6	2.5	3.1
SLC1A2	solute carrier family 1 (glial high affinity glutamate transporter), member 2	1.8	-2.1	-2.8	-4.2	-3.1
JMY	junction mediating and regulatory protein, p53 cofactor	1.8	1.3	1.0	0.4	0.9
FICD	FIC domain containing	1.8	0.3	-0.8	-0.4	0.5
EREG	epiregulin	1.8	-6.3	-6.8	-6.5	-6.9
TBC1D30	TBC1 domain family member 30	1.8	5.0	5.2	4.9	4.9
HIST1H2BN	histone cluster 1, H2bn	1.7	-0.6	-1.3	-1.2	-1.2
ALOXE3	arachidonate lipoxygenase 3	1.7	2.0	0.9	2.4	2.8
PALLD	palladin, cytoskeletal associated protein	1.7	0.3	0.2	0.2	0.2
MAFK	v-maf avian musculoaponeurotic fibrosarcoma oncogene homolog K	1.7	-1.0	-1.2	-1.3	-1.4
KLF6	Kruppel-like factor 6	1.7	-1.5	-2.6	-2.4	-1.1
LDLR	low density lipoprotein receptor	1.7	-1.5	-1.5	-1.4	-1.7
TUSC3	tumor suppressor candidate 3	1.7	7.1	6.9	6.8	7.0
RPS9P1	ribosomal protein S9 pseudogene 1	1.7	1.9	1.9	0.5	1.7
ALDH1L2	aldehyde dehydrogenase 1 family member L2	1.7	1.5	-0.2	1.1	3.9
SPI1	Spi-1 proto-oncogene	1.7	1.0	1.2	2.3	1.5
KCND3	potassium channel, voltage gated Shal related subfamily D, member 3	1.7	3.5	4.0	0.4	1.1
LILRA6	leukocyte immunoglobulin like receptor A6	1.7	4.0	3.5	3.5	2.5
DNM1P46	dynamin 1 pseudogene 46	1.7	2.1	1.3	2.3	3.0
KRTAP5-AS1	KRTAP5-1/KRTAP5-2 antisense RNA 1	1.7	0.5	-1.1	-2.0	0.2
RPL18AP11	ribosomal protein L18a pseudogene 11	1.7	1.2	1.8	1.4	1.1
LRRC75A	leucine rich repeat containing 75A	1.7	3.2	2.8	2.8	3.4
HIVEP2	human immunodeficiency virus type I enhancer binding protein 2	1.7	0.5	0.1	0.1	0.4
JUN	jun proto-oncogene	1.7	2.2	1.3	1.2	2.3
PTGR1	prostaglandin reductase 1	1.7	-3.5	-3.6	-2.3	-2.1
GCKR	glucokinase (hexokinase 4) regulator	1.7	-6.2	-7.1	-6.9	-7.2
GP6	glycoprotein VI platelet	1.7	2.7	3.2	2.7	2.5
ZMIZ1-AS1	ZMIZ1 antisense RNA 1	1.7	-4.7	-5.1	-5.1	-5.6
MAFA	v-maf avian musculoaponeurotic fibrosarcoma oncogene homolog A	1.7	3.7	4.2	4.8	4.3
MTHFD2	methylenetetrahydrofolate dehydrogenase (NADP+ dependent) 2, methenyltetrahydrofolate cyclohydrolase	1.7	1.3	0.4	0.7	2.0
TMEM88	transmembrane protein 88	1.7	-1.7	-2.6	-2.3	-1.2
GTPBP2	GTP binding protein 2	1.7	0.8	-0.1	-0.1	0.8
EPB41L4A-AS1	EPB41L4A antisense RNA 1	1.7	0.9	0.4	0.3	1.1
ETV7	ets variant 7	1.7	5.9	5.2	3.7	5.4
LINC01484	long intergenic non-protein coding RNA 1484	1.7	-6.3	-6.3	-6.3	-6.3
RPLP1P7	ribosomal protein, large, P1 pseudogene 7	1.7	2.4	3.7	4.0	3.4
IL23A	interleukin 23 subunit alpha	1.6	-0.7	-1.3	-1.3	-0.5
FAM223B	family with sequence similarity 223 member B (non-protein coding)	1.6	-2.6	-3.7	-1.0	-2.5
ZBTB10	zinc finger and BTB domain containing 10	1.6	1.2	0.8	0.7	1.3
BEND6	BEN domain containing 6	1.6	4.7	4.1	4.5	5.7
ZFAS1	ZNFX1 antisense RNA 1	1.6	-0.3	-0.6	-0.6	0.0
MAFF	v-maf avian musculoaponeurotic fibrosarcoma oncogene homolog F	1.6	-3.0	-4.1	-4.4	-2.8
NEURL3	neuralized E3 ubiquitin protein ligase 3	1.6	-5.4	-5.3	-6.4	-6.5
DAPK2	death-associated protein kinase 2	1.6	0.4	0.1	0.9	1.1
WT1-AS	WT1 antisense RNA	1.6	-1.0	0.5	0.6	1.0
PINLYP	phospholipase A2 inhibitor and LY6/PLAUR domain containing	1.6	1.4	0.7	1.0	1.0

TRL-TAA4-1	transfer RNA-Leu (TAA) 4-1	1.6	2.6	3.1	3.0	2.2
AQP8	aquaporin 8	1.6	-3.0	-3.4	-3.5	-3.0
CCDC13	coiled-coil domain containing 13	1.6	1.8	1.7	1.5	1.6
TMEM150B	transmembrane protein 150B	1.6	-1.2	-2.1	-2.5	-1.4
NCF2	neutrophil cytosolic factor 2	1.6	-7.0	-7.5	-7.5	-7.5
CSRNP1	cysteine-serine-rich nuclear protein 1	1.6	-0.1	-1.1	-2.0	-0.8
SEPT7-AS1	SEPT7 antisense RNA 1 (head to head)	1.6	1.0	1.7	1.4	2.5
TMEM151B	transmembrane protein 151B	1.6	3.0	3.2	3.4	3.3
DOCK11P1	dedicator of cytokinesis 11 pseudogene 1	1.6	3.4	3.5	3.5	3.9
C2orf27B	chromosome 2 open reading frame 27B	1.6	1.6	1.5	1.7	2.0
CPT1A	carnitine palmitoyltransferase 1A (liver)	1.6	-0.9	-2.1	-2.0	-0.7
AKR1C2	aldo-keto reductase family 1, member C2	1.6	-7.4	-7.7	-8.8	-8.1
PTGES	prostaglandin E synthase	1.6	0.0	1.0	0.6	-0.6
JAG1	jagged 1	1.6	-2.4	-2.8	-2.9	-2.2
KDM6B	lysine (K)-specific demethylase 6B	1.6	0.5	-0.4	-0.4	0.3
SPATA41	spermatogenesis associated 41 (non-protein coding)	1.6	1.4	1.5	2.7	3.2
SLC25A25	solute carrier family 25 (mitochondrial carrier; phosphate carrier), member 25	1.6	1.2	0.6	0.3	1.1
AKR1C1	aldo-keto reductase family 1, member C1	1.6	-8.6	-8.7	-9.5	-8.4
IL11	interleukin 11	1.6	-6.5	-7.3	-6.9	-6.3
AKR1B10	aldo-keto reductase family 1, member B10 (aldose reductase)	1.6	-7.3	-8.0	-7.0	-6.3
GK	glycerol kinase	1.6	-1.3	-1.2	-1.4	-1.2
STX1A	syntaxin 1A	1.6	-0.1	-0.3	-0.3	-0.3
RNF152	ring finger protein 152	1.6	4.8	5.3	5.6	5.2
BBC3	BCL2 binding component 3	1.6	0.7	0.0	0.3	1.2
GFPT2	glutamine-fructose-6-phosphate transaminase 2	1.6	4.1	4.5	4.4	4.1
TNFSF9	tumor necrosis factor superfamily member 9	1.6	1.9	2.1	2.3	2.1
ZBTB21	zinc finger and BTB domain containing 21	1.6	2.5	1.9	1.9	2.5
GOLGA7B	golgin A7 family member B	1.6	2.4	2.2	1.2	1.9
FAM47E-STBD1	FAM47E-STBD1 readthrough	1.6	-3.0	-3.1	-3.4	-3.1
FAM189A2	family with sequence similarity 189 member A2	1.5	3.4	2.7	2.8	3.5
TCEAL7	transcription elongation factor A (SII)-like 7	1.5	4.1	3.5	3.4	4.4
ASNS	asparagine synthetase (glutamine-hydrolyzing)	1.5	2.5	0.5	0.8	3.4
BTG1	B-cell translocation gene 1, anti-proliferative	1.5	1.2	0.8	1.0	1.5
MIR22	microRNA 22	1.5	-3.0	-3.2	-3.4	-3.8
UBE2NL	ubiquitin conjugating enzyme E2N-like (gene/pseudogene)	1.5	0.6	1.1	1.4	0.6
RAB33A	RAB33A, member RAS oncogene family	1.5	0.3	-0.6	0.0	-0.8
MIR3191	microRNA 3191	1.5	-2.0	-1.7	-1.1	-0.7
CPEB4	cytoplasmic polyadenylation element binding protein 4	1.5	0.0	-0.3	-1.1	-0.8
MIR3945HG	MIR3945 host gene	1.5	-2.2	-2.5	-3.6	-2.8
THSD4	thrombospondin type 1 domain containing 4	1.5	3.8	2.9	3.0	3.9
CREB5	cAMP responsive element binding protein 5	1.5	1.9	1.1	1.2	2.1
STBD1	starch binding domain 1	1.5	-3.0	-3.3	-3.5	-3.1
TTLL9	tubulin tyrosine ligase like 9	1.5	1.6	1.9	0.9	1.8
LRRC49	leucine rich repeat containing 49	1.5	3.0	3.0	3.0	3.5
MIR3190	microRNA 3190	1.5	-2.0	-1.6	-1.1	-0.8
RPL29P9	ribosomal protein L29 pseudogene 9	1.5	1.0	2.3	1.5	1.3
RFPL2	ret finger protein-like 2	1.5	2.7	2.8	2.4	2.4
LINC00899	long intergenic non-protein coding RNA 899	1.5	1.5	2.6	1.3	1.8
LRIT3	leucine-rich repeat, immunoglobulin-like and transmembrane domains 3	1.5	3.3	3.9	4.8	4.1
ABI3BP	ABI family member 3 binding protein	1.5	2.6	3.2	2.0	1.0
SHC4	SHC (Src homology 2 domain containing) family member 4	1.5	2.4	2.6	2.3	3.1
IFRD1	interferon-related developmental regulator 1	1.5	1.3	0.3	0.3	1.9
GNA13	guanine nucleotide binding protein (G protein), alpha 13	1.5	-0.3	-0.3	-0.1	0.0
PLA2G4C	phospholipase A2 group IVC	1.5	-0.9	-2.2	-2.6	-0.9
SOWAHC	sosondowah ankyrin repeat domain family member C	1.5	-2.4	-2.3	-2.0	-1.9
AKR1B15	aldo-keto reductase family 1, member B15	1.5	-5.4	-5.6	-5.7	-5.7
SMOX	spermine oxidase	1.5	-2.9	-3.5	-3.4	-2.1
UNC5B-AS1	UNC5B antisense RNA 1	1.5	1.8	0.3	0.8	2.2
SERPINB8	serpin peptidase inhibitor, clade B (ovalbumin), member 8	1.5	-2.0	-3.0	-4.6	-3.2
CHORDC2P	cysteine and histidine rich domain containing 2, pseudogene	1.5	-0.2	0.8	0.9	0.3
CSF1	colony stimulating factor 1	1.5	-2.0	-2.2	-1.7	-1.5
DUSP5	dual specificity phosphatase 5	1.5	-1.1	-1.1	-1.1	-1.1
FRMD4B	FERM domain containing 4B	1.5	1.8	1.8	0.7	0.5
MATN1-AS1	MATN1 antisense RNA 1	1.5	2.6	1.8	2.0	3.2
RPL27P7	ribosomal protein L27 pseudogene 7	1.5	-0.5	1.8	1.0	0.6
IL15RA	interleukin 15 receptor subunit alpha	1.5	0.7	0.5	1.4	1.8
GK3P	glycerol kinase 3 pseudogene	1.5	-1.9	-1.6	-2.0	-1.4
TMEM151A	transmembrane protein 151A	1.5	-1.4	-1.7	-1.5	-1.0
PELI2	pellino E3 ubiquitin protein ligase family member 2	1.5	6.6	6.6	6.7	6.7
MARK2P9	MAP/microtubule affinity-regulating kinase 2 pseudogene 9	1.5	1.2	2.5	2.8	2.3
AREG	amphiregulin	1.5	-6.3	-6.7	-7.1	-5.4
NXPH4	neurexophilin 4	1.5	6.1	6.3	5.8	5.6
PAEP	progestagen-associated endometrial protein	1.5	-3.6	-4.7	-4.6	-4.5
KLF11	Kruppel-like factor 11	1.5	0.5	0.0	0.5	0.9
MAP1LC3B	microtubule associated protein 1 light chain 3 beta	1.4	-1.2	-1.3	-1.5	-1.2

DUSP8	dual specificity phosphatase 8	1.4	0.4	-0.6	-1.0	0.5
RELB	v-rel avian reticuloendotheliosis viral oncogene homolog B	1.4	-3.4	-3.6	-4.2	-3.3
DIRC3	disrupted in renal carcinoma 3	1.4	-3.0	-2.6	-2.7	-1.6
VCX3A	variable charge, X-linked 3A	1.4	3.0	2.8	2.3	2.4
CYP51A1P2	cytochrome P450 family 51 subfamily A member 1 pseudogene 2	1.4	-0.5	-0.6	-0.3	-0.2
HAMP	hepcidin antimicrobial peptide	1.4	-9.6	-9.6	-10.3	-9.3
LCN2	lipocalin 2	1.4	-3.4	-3.7	-3.5	-3.9
DAGLA	diacylglycerol lipase, alpha	1.4	-0.2	-0.5	-0.6	-0.6
HID1	HID1 domain containing	1.4	-0.6	-0.8	-1.3	-1.2
FAM132B	family with sequence similarity 132 member B	1.4	7.4	6.6	7.1	8.1
KCNE5	potassium channel, voltage gated subfamily E regulatory beta subunit 5	1.4	-1.8	-2.0	-1.2	-1.2
MAP1LC3B2	microtubule associated protein 1 light chain 3 beta 2	1.4	-1.1	-1.1	-1.3	-1.2
TPPP3	tubulin polymerization-promoting protein family member 3	1.4	1.5	0.9	1.2	1.7
PCK1	phosphoenolpyruvate carboxykinase 1	1.4	-1.1	-0.7	-2.0	-0.3
CREB3L3	cAMP responsive element binding protein 3-like 3	1.4	-6.5	-7.2	-7.6	-7.4
FAM223A	family with sequence similarity 223 member A (non-protein coding)	1.4	-2.7	-3.5	-1.8	-2.4
LPIN1	lipin 1	1.4	1.0	0.4	0.6	1.3
OR2A9P	olfactory receptor family 2 subfamily A member 9 pseudogene	1.4	-2.1	-3.1	-2.9	-2.1
FOXF2	forkhead box F2	1.4	8.5	8.8	9.2	8.9
LINC01433	long intergenic non-protein coding RNA 1433	1.4	-3.4	-3.4	-1.7	-2.2
CSGALNACT2	chondroitin sulfate N-acetylgalactosaminyltransferase 2	1.4	0.1	-0.3	-0.3	0.3
HEY1	hes-related family bHLH transcription factor with YRPW motif 1	1.4	5.7	5.5	5.4	5.7
JUNB	jun B proto-oncogene	1.4	0.0	-0.1	-0.9	-0.2
HDAC5	histone deacetylase 5	1.4	0.6	-0.2	-0.3	0.5
RASGRP3	RAS guanyl releasing protein 3	1.4	-0.2	0.3	-0.4	-0.8
SBF1P1	SET binding factor 1 pseudogene 1	1.4	1.5	0.3	1.3	1.3
PER2	period circadian clock 2	1.4	-1.0	-1.2	-1.4	-0.9
HECA	hdc homolog, cell cycle regulator	1.4	3.5	3.2	3.2	3.6
KLHL24	kelch like family member 24	1.4	1.3	0.7	0.6	1.2
KLHL31	kelch like family member 31	1.4	-0.8	-0.6	-0.8	-0.5
RNF217-AS1	RNF217 antisense RNA 1 (head to head)	1.4	2.7	2.4	2.5	3.1
TNF	tumor necrosis factor	1.4	-2.4	-3.8	-2.3	-1.4
BRINP2	bone morphogenetic protein/retinoic acid inducible neural-specific 2	1.4	2.1	1.8	-1.0	0.1
H2AFB3	H2A histone family member B3	1.4	-0.3	2.2	1.3	1.4
LMOD1	leiomodin 1	1.4	5.5	5.6	4.9	4.7
HCAR3	hydroxycarboxylic acid receptor 3	1.4	-6.6	-6.0	-6.4	-4.9
FST	follistatin	1.4	-6.7	-6.5	-6.7	-6.4
PTPDC1	protein tyrosine phosphatase domain containing 1	1.4	0.9	0.3	0.3	1.2
FOXE1	forkhead box E1	1.4	5.1	4.9	5.7	6.3
H2AFB2	H2A histone family member B2	1.4	-0.6	1.6	1.0	0.7
MAP3K14	mitogen-activated protein kinase kinase kinase 14	1.4	0.2	-0.5	-0.3	0.2
MID2	midline 2	1.4	5.1	4.9	5.1	5.4
MIR22HG	MIR22 host gene	1.4	-2.4	-2.8	-3.0	-3.0
KPNA7	karyopherin alpha 7 (importin alpha 8)	1.4	-4.0	-4.9	-4.5	-4.6
AKR1C4	aldo-keto reductase family 1, member C4	1.4	-4.7	-5.2	-5.1	-4.9
HSPB8	heat shock protein family B (small) member 8	1.4	-2.6	-3.9	-5.7	-4.1
NRROS	negative regulator of reactive oxygen species	1.4	4.4	4.5	4.1	4.3
PNPLA8	patatin like phospholipase domain containing 8	1.4	0.5	0.0	-0.2	0.6
IL12A	interleukin 12A	1.4	3.0	2.8	2.3	3.2
RORA	RAR-related orphan receptor A	1.4	-0.7	-0.9	-0.4	-0.4
NAGS	N-acetylglutamate synthase	1.4	-2.4	-2.2	-2.3	-2.4
GADD45A	growth arrest and DNA damage inducible alpha	1.4	0.2	-1.0	-0.9	0.9
SNHG8	small nucleolar RNA host gene 8	1.3	0.9	1.0	0.8	0.6
ZSWIM6	zinc finger, SWIM-type containing 6	1.3	2.8	2.5	2.0	2.0
FAM134B	family with sequence similarity 134 member B	1.3	4.7	4.7	4.7	5.0
ODF3L1	outer dense fiber of sperm tails 3-like 1	1.3	1.4	0.1	-0.1	1.2
SPATA6L	spermatogenesis associated 6 like	1.3	-1.5	-2.3	-3.3	-1.3
OSCAR	osteoclast associated, immunoglobulin-like receptor	1.3	-4.5	-4.9	-4.7	-4.6
TAT	tyrosine aminotransferase	1.3	-5.2	-5.7	-5.7	-5.3
KLRC2	killer cell lectin like receptor C2	1.3	-1.5	-1.2	-3.3	-2.7
NPPA	natriuretic peptide A	1.3	-2.1	-0.7	-0.3	-0.9
PNRC1	proline rich nuclear receptor coactivator 1	1.3	-0.2	-0.5	-0.5	-0.1
CREBRF	CREB3 regulatory factor	1.3	0.2	-0.5	-1.6	-0.5
SLC35G2	solute carrier family 35 member G2	1.3	1.4	0.7	-0.2	1.2
MAFG	v-maf avian musculoaponeurotic fibrosarcoma oncogene homolog G	1.3	-0.4	-1.1	-1.0	-0.3
SCN4A	sodium channel, voltage gated, type IV alpha subunit	1.3	3.5	3.2	2.9	4.2
SLC26A4-AS1	SLC26A4 antisense RNA 1	1.3	2.3	2.4	3.4	3.5
MSX2P1	msh homeobox 2 pseudogene 1	1.3	4.1	3.8	3.3	4.2
UBC	ubiquitin C	1.3	0.3	-0.3	-0.2	0.5
FMNL1	formin like 1	1.3	-0.9	-1.4	-1.3	-0.8
POR	P450 (cytochrome) oxidoreductase	1.3	-1.6	-1.6	-1.6	-1.7
DUSP2	dual specificity phosphatase 2	1.3	3.1	3.9	2.3	1.6
PRSS27	protease, serine 27	1.3	3.0	2.0	2.5	3.6
MGARP	mitochondria localized glutamic acid rich protein	1.3	3.3	4.0	4.6	3.7
RPL5P22	ribosomal protein L5 pseudogene 22	1.3	1.5	2.3	2.1	1.8

CYP51A1	cytochrome P450 family 51 subfamily A member 1	1.3	0.0	-0.2	0.0	0.2
PAK1	p21 protein (Cdc42/Rac)-activated kinase 1	1.3	3.1	3.1	3.1	3.1
ARHGEF4	Rho guanine nucleotide exchange factor 4	1.3	4.4	4.8	4.9	4.1
LYG1	lysozyme g1	1.3	0.2	0.0	1.3	1.1
C4orf36	chromosome 4 open reading frame 36	1.3	0.0	-0.2	0.3	0.9
KRT8P46	keratin 8 pseudogene 46	1.3	0.3	-0.5	-0.4	0.3
TAT-AS1	TAT antisense RNA 1	1.3	-1.3	-1.8	-1.2	-1.2
RASL10A	RAS-like family 10 member A	1.3	3.8	3.3	2.2	2.9
ERO1B	endoplasmic reticulum oxidoreductase beta	1.3	2.4	2.0	1.8	2.5
VEGFA	vascular endothelial growth factor A	1.3	0.2	-1.2	-0.6	1.0
ELF3	E74-like factor 3 (ets domain transcription factor, epithelial-specific)	1.3	-8.0	-7.9	-8.6	-7.7
ZNF663P	zinc finger protein 663, pseudogene	1.3	-3.2	-2.9	-0.7	-0.1
FAM181B	family with sequence similarity 181 member B	1.3	6.1	6.3	6.5	6.5
SNORD15A	small nucleolar RNA, C/D box 15A	1.3	-0.1	-0.1	0.6	-1.1
EGR3	early growth response 3	1.3	-0.2	-0.5	-0.9	0.4
NRBF2P3	nuclear receptor binding factor 2 pseudogene 3	1.3	-0.3	0.1	0.0	-0.3
RIPK2	receptor interacting serine/threonine kinase 2	1.3	0.3	0.1	0.1	0.7
AKNA	AT-hook transcription factor	1.3	0.5	-0.7	-1.0	0.6
ARL9	ADP ribosylation factor like GTPase 9	1.3	0.0	0.6	1.5	3.0
SNORA84	small nucleolar RNA, H/ACA box 84	1.3	0.6	-0.3	0.0	0.8
RPL38P3	ribosomal protein L38 pseudogene 3	1.3	1.3	1.4	1.8	0.8
HSPA13	heat shock protein family A (Hsp70) member 13	1.3	1.3	0.5	0.5	1.6
NOCT	nocturnin	1.3	0.9	1.0	0.9	1.0
ZNF697	zinc finger protein 697	1.3	0.1	-0.4	-0.5	0.4
ZFAND1	zinc finger, AN1-type domain 1	1.3	1.2	0.7	0.6	1.7
PRPH	peripherin	1.3	2.3	2.2	2.6	2.3
ULK1	unc-51 like autophagy activating kinase 1	1.3	0.4	0.0	0.2	0.3
S100P	S100 calcium binding protein P	1.3	-5.9	-8.5	-7.2	-3.2
CLK1	CDC like kinase 1	1.3	0.0	-0.4	-0.6	0.0
TRIB1	tribbles pseudokinase 1	1.3	-0.6	-1.0	-0.4	0.1
MIR4749	microRNA 4749	1.3	0.8	1.4	0.8	-0.6
C15orf65	chromosome 15 open reading frame 65	1.3	2.0	2.5	2.5	2.5
NPC1L1	NPC1-like 1	1.3	-4.3	-4.4	-4.8	-4.7
IRAK2	interleukin 1 receptor associated kinase 2	1.3	-2.8	-2.5	-3.5	-3.4
RASSF1	Ras association (RalGDS/AF-6) domain family member 1	1.3	1.6	0.5	0.2	1.9
SH2B3	SH2B adaptor protein 3	1.3	-0.6	-1.3	-1.0	0.2
ACSL3	acyl-CoA synthetase long-chain family member 3	1.3	-0.1	-0.2	0.0	0.3
STX11	syntaxin 11	1.3	0.4	0.1	0.1	0.9
MIR4315-2	microRNA 4315-2	1.3	-1.6	-1.8	-1.5	-1.3
SLC43A3	solute carrier family 43 member 3	1.3	-1.2	-2.4	-1.7	-2.3
VIMP	VCP interacting membrane selenoprotein	1.3	1.3	0.8	1.1	1.9
LONRF3	LON peptidase N-terminal domain and ring finger 3	1.3	1.7	1.4	1.6	2.0
MIR4750	microRNA 4750	1.2	-1.4	-1.1	-1.3	-1.0
TNXA	tenascin XA (pseudogene)	1.2	-3.5	-2.5	-2.8	-2.3
TCTEX1D4	Tctex1 domain containing 4	1.2	-3.2	-3.9	-3.9	-3.2
DLX3	distal-less homeobox 3	1.2	-0.1	0.5	0.6	0.0
IL6R	interleukin 6 receptor	1.2	-1.9	-2.8	-2.9	-2.2
ZBTB43	zinc finger and BTB domain containing 43	1.2	0.2	0.1	0.3	0.5
ACSL1	acyl-CoA synthetase long-chain family member 1	1.2	-1.1	-1.0	-1.0	-1.0
CXCL3	chemokine (C-X-C motif) ligand 3	1.2	-0.2	-0.4	0.1	0.5
RDXP1	radixin pseudogene 1	1.2	0.4	0.0	0.7	0.6
ATF4P3	activating transcription factor 4 pseudogene 3	1.2	1.0	0.2	0.7	1.3
PTMAP3	prothymosin, alpha pseudogene 3	1.2	0.8	1.5	1.2	0.6
CBR3-AS1	CBR3 antisense RNA 1	1.2	0.8	0.8	0.2	0.6
GAB2	GRB2 associated binding protein 2	1.2	-0.8	-1.5	-1.6	-0.9
SNAI1	snail family zinc finger 1	1.2	-0.3	-0.1	0.0	-0.5
SOD2	superoxide dismutase 2, mitochondrial	1.2	-1.0	-0.8	-0.8	-1.1
PLAC8L1	PLAC8-like 1	1.2	2.5	2.3	2.7	2.7
GADD45G	growth arrest and DNA damage inducible gamma	1.2	3.3	3.0	2.8	3.5
MEIS1-AS3	MEIS1 antisense RNA 3	1.2	3.1	3.0	4.4	4.6
NFATC1	nuclear factor of activated T-cells, cytoplasmic, calcineurin-dependent 1	1.2	4.8	5.0	4.7	4.6
BVES-AS1	BVES antisense RNA 1	1.2	2.2	2.4	3.3	3.0
TAF1D	TATA-box binding protein associated factor, RNA polymerase I, D	1.2	-0.4	-0.6	-0.3	-0.1
MIR4258	microRNA 4258	1.2	-0.3	-0.7	0.6	1.3
RRH	retinal pigment epithelium-derived rhodopsin homolog	1.2	2.6	2.4	2.8	2.1
CLCN6	chloride channel, voltage-sensitive 6	1.2	-1.1	-1.1	-0.6	-0.7
NCAN	neurocan	1.2	2.0	2.2	0.5	1.1
LARP6	La ribonucleoprotein domain family member 6	1.2	1.8	1.0	1.2	2.3
TSC22D2	TSC22 domain family member 2	1.2	1.3	0.9	0.5	0.7
PTGIS	prostaglandin I2 (prostacyclin) synthase	1.2	3.6	2.5	4.8	4.8
DNAJB4	DnaJ heat shock protein family (Hsp40) member B4	1.2	0.2	0.3	0.4	0.4
STARD5	StAR related lipid transfer domain containing 5	1.2	1.0	1.3	1.3	1.3
RNU11	RNA, U11 small nuclear	1.2	1.4	1.1	1.5	1.6
TMEM39A	transmembrane protein 39A	1.2	0.4	-0.1	-0.5	0.4
RUNDC3A	RUN domain containing 3A	1.2	1.9	1.8	1.0	1.6

Appendix 4. List of top 450 repressed genes following palmitate treatment identified through RNA-seq.

Gene Symbol	Description	WT Palmitate	RELA-KO Vehicle	RELA-KO Palmitate	CHOP-KO Vehicle	CHOP-KO Palmitate
TLR5	toll-like receptor 5	-2.5	3.2	3.2	3.3	3.1
CCNI2	cyclin I family member 2	-2.5	-0.3	0.1	-0.8	0.0
NPM1P21	nucleophosmin 1 (nucleolar phosphoprotein B23, numatrin) pseudogene 21	-2.4	-1.3	0.3	0.4	-0.5
PRSS35	protease, serine 35	-2.4	1.0	1.8	1.7	1.0
CLDN18	claudin 18	-2.3	0.4	0.0	1.4	0.6
PLEK	pleckstrin	-2.3	-1.8	-0.4	-1.4	-0.4
LUM	lumican	-2.2	1.5	1.1	-1.0	1.9
RPS2P33	ribosomal protein S2 pseudogene 33	-2.2	-0.3	0.5	1.0	0.6
MESP1	mesoderm posterior bHLH transcription factor 1	-2.2	5.7	5.4	6.4	6.7
DKK1	dickkopf WNT signaling pathway inhibitor 1	-2.2	-7.8	-7.4	-7.2	-7.8
GRIN3A	glutamate receptor, ionotropic, N-methyl-D-aspartate 3A	-2.2	0.7	1.6	1.8	1.6
NAP1L3	nucleosome assembly protein 1-like 3	-2.2	4.1	4.2	3.2	3.3
LDB3	LIM domain binding 3	-2.1	2.4	1.4	2.0	2.2
LINC00950	long intergenic non-protein coding RNA 950	-2.1	2.6	1.9	2.1	2.7
MLNR	motilin receptor	-2.1	-1.9	-2.8	-3.5	-4.2
DRICH1	aspartate-rich 1	-2.1	-1.6	-1.7	0.0	0.3
CCRL1P1	chemokine (C-C motif) receptor-like 1 pseudogene	-2.1	0.7	-0.1	-0.7	-0.2
TNS4	tensin 4	-2.0	-8.9	-9.7	-9.4	-9.5
TRR-CCT3-1	transfer RNA-Arg (CCT) 3-1	-2.0	0.0	0.1	0.0	-0.6
SRD5A3-AS1	SRD5A3 antisense RNA 1	-2.0	-0.6	-1.2	0.2	-0.1
RNU5A-1	RNA, U5A small nuclear 1	-2.0	-0.6	1.3	-0.1	0.0
LINC00896	long intergenic non-protein coding RNA 896	-2.0	5.3	5.4	5.7	5.2
RPL39P	ribosomal protein L39 pseudogene	-2.0	-3.0	-3.6	-1.8	-3.2
FAIM2	Fas apoptotic inhibitory molecule 2	-2.0	-2.1	-3.8	-4.0	-3.5
NHLH1	nescient helix-loop-helix 1	-2.0	2.8	2.7	3.2	2.7
WBP2NL	WBP2 N-terminal like	-1.9	8.2	8.2	8.2	8.0
DNAH2	dynein, axonemal, heavy chain 2	-1.9	0.0	0.7	0.7	0.6
SNORD51	small nucleolar RNA, C/D box 51	-1.9	-3.1	-0.7	-0.9	-0.9
LINC00327	long intergenic non-protein coding RNA 327	-1.9	-0.6	-0.6	0.6	0.0
ZNF488	zinc finger protein 488	-1.9	0.5	1.1	1.3	0.1
OCLM	oculomedin	-1.9	-1.2	-0.8	0.5	-0.6
CLEC2L	C-type lectin domain family 2 member L	-1.8	-4.2	-4.6	-4.9	-4.9
SLC24A2	solute carrier family 24 (sodium/potassium/calcium exchanger), member 2	-1.8	1.8	2.5	0.6	1.2
C8orf48	chromosome 8 open reading frame 48	-1.7	2.7	3.1	3.4	3.1
LCE1E	late cornified envelope 1E	-1.7	-5.6	-4.0	-6.3	-5.7
GSTTP2	glutathione S-transferase theta pseudogene 2	-1.7	-5.2	-5.8	-5.8	-5.8
CD247	CD247 molecule	-1.7	2.1	2.6	-0.8	-0.3
KRTAP3-1	keratin associated protein 3-1	-1.7	-10.8	-10.5	-10.5	-10.8
KRT81	keratin 81, type II	-1.7	-5.3	-5.6	-6.4	-6.9
RPS2P51	ribosomal protein S2 pseudogene 51	-1.7	0.7	0.7	0.1	0.1
LRRC26	leucine rich repeat containing 26	-1.7	0.1	0.2	0.2	-0.4
SNORD54	small nucleolar RNA, C/D box 54	-1.7	-2.4	-1.5	-0.9	-1.4
CHST4	carbohydrate (N-acetylglucosamine 6-O) sulfotransferase 4	-1.7	4.1	4.6	2.5	2.1
APOBR	apolipoprotein B receptor	-1.7	-2.5	-4.0	-3.5	-2.8
WDR93	WD repeat domain 93	-1.6	-0.1	0.2	-0.1	0.4
DLEU2L	deleted in lymphocytic leukemia 2-like	-1.6	-2.1	-1.5	-1.0	-1.6
SCUBE2	signal peptide, CUB domain, EGF-like 2	-1.6	0.1	0.9	1.1	0.6
FAM19A2	family with sequence similarity 19 (chemokine (C-C motif)-like), member A2	-1.6	1.3	1.5	0.7	1.4
MIRLET7BHG	MIRLET7B host gene	-1.6	-0.8	-1.4	0.1	-1.0
OLFM1	olfactomedin 1	-1.6	2.8	2.8	0.7	1.0
GAPDHP14	glyceraldehyde-3-phosphate dehydrogenase pseudogene 14	-1.6	-5.0	-3.9	-4.8	-4.6
SCARNA22	small Cajal body-specific RNA 22	-1.6	-1.1	0.1	0.5	0.4
SNORA59B	small nucleolar RNA, H/ACA box 59B	-1.6	-0.7	-0.1	0.9	0.8
SIGLEC14	sialic acid binding Ig-like lectin 14	-1.6	-4.7	-4.9	-4.8	-5.2
LINC00842	long intergenic non-protein coding RNA 842	-1.6	-3.8	-2.6	-1.3	-3.6
OLFML2B	olfactomedin like 2B	-1.6	0.8	1.0	0.8	0.8
OR56B4	olfactory receptor family 56 subfamily B member 4	-1.6	-1.5	-0.3	-1.7	0.2
GMCL1P1	germ cell-less, spermatogenesis associated 1 pseudogene 1	-1.5	-1.1	-1.5	-1.1	-1.3
CXCR6	chemokine (C-X-C motif) receptor 6	-1.5	-0.6	0.2	-0.9	-0.4
MTRNR2L4	MT-RNR2-like 4	-1.5	-0.2	-1.2	-0.7	0.1
FAT2	FAT atypical cadherin 2	-1.5	0.7	1.1	0.8	-1.1
GRAMD1B	GRAM domain containing 1B	-1.5	2.1	1.9	1.8	1.6
MIR4697HG	MIR4697 host gene	-1.5	6.6	6.9	6.8	6.4
PRDM13	PR domain containing 13	-1.5	7.6	7.6	8.2	8.1
APOBEC3H	apolipoprotein B mRNA editing enzyme catalytic polypeptide like 3H	-1.5	0.3	1.0	0.3	-0.4
ADAM21	ADAM metallopeptidase domain 21	-1.5	4.2	4.6	3.2	2.8
ARHGDIB	Rho GDP dissociation inhibitor (GDI) beta	-1.5	-2.0	-2.2	-3.3	-2.7
NAP1L2	nucleosome assembly protein 1-like 2	-1.5	1.7	2.4	-0.7	-1.1
EFCAB13	EF-hand calcium binding domain 13	-1.5	-2.3	-2.1	-1.7	-1.3
ACTG2	actin, gamma 2, smooth muscle, enteric	-1.5	-3.2	-1.9	-3.3	-3.6
DDX18P6	DEAD-box helicase 18 pseudogene 6	-1.5	-0.6	-0.1	0.2	-1.1
HIST1H2AH	histone cluster 1, H2ah	-1.5	2.3	3.0	2.5	1.6
KRTAP2-2	keratin associated protein 2-2	-1.5	-4.8	-4.8	-4.8	-4.5
PAGE4	PAGE family member 4	-1.5	-3.0	-3.3	-4.7	-5.0

C22orf24	chromosome 22 open reading frame 24	-1.5	0.1	-0.2	0.2	-0.6
TSPY26P	testis specific protein, Y-linked 26, pseudogene	-1.5	-0.4	0.5	0.7	0.2
SNAP25-AS1	SNAP25 antisense RNA 1	-1.5	-4.3	-3.7	-4.3	-4.7
FAM92A1P1	family with sequence similarity 92 member A1 pseudogene 1	-1.5	-0.2	0.1	0.0	0.5
RPL12P25	ribosomal protein L12 pseudogene 25	-1.5	-1.1	-1.0	0.0	-0.5
STARD8	StAR related lipid transfer domain containing 8	-1.4	0.3	1.1	0.9	0.3
ADAM19	ADAM metallopeptidase domain 19	-1.4	-1.8	-1.8	-2.9	-3.0
MYL7	myosin light chain 7	-1.4	-5.9	-6.7	-6.7	-6.6
CDC42P3	cell division cycle 42 pseudogene 3	-1.4	-0.9	-0.8	-1.0	-1.2
GRK5-IT1	GRK5 intronic transcript 1	-1.4	-3.8	-2.2	-3.3	-3.6
SNORD98	small nucleolar RNA, C/D box 98	-1.4	-2.5	-0.8	-2.3	-0.5
PTPN7	protein tyrosine phosphatase, non-receptor type 7	-1.4	1.3	1.0	-0.5	0.1
FAM183A	family with sequence similarity 183 member A	-1.4	-2.0	-1.5	-1.8	-2.1
CXCR2	chemokine (C-X-C motif) receptor 2	-1.4	1.8	-0.6	-1.2	1.5
CEND1	cell cycle exit and neuronal differentiation 1	-1.4	4.4	4.1	4.6	4.8
PRR15L	proline rich 15 like	-1.4	-4.6	-3.9	-4.5	-4.9
C11orf45	chromosome 11 open reading frame 45	-1.4	3.3	3.5	3.4	2.8
PLCB2	phospholipase C beta 2	-1.4	1.7	2.0	1.5	0.4
SOX11	SRY-box 11	-1.4	11.7	11.0	11.3	12.3
LINC00577	long intergenic non-protein coding RNA 577	-1.4	-3.8	-2.8	-4.0	-3.8
MIR762	microRNA 762	-1.4	-1.8	-0.8	-1.3	-1.5
MYL9	myosin light chain 9	-1.4	-8.6	-10.1	-10.1	-10.3
SLC7A10	solute carrier family 7 (neutral amino acid transporter light chain, asc system), member 10	-1.4	1.0	1.7	1.4	0.6
GPR45	G protein-coupled receptor 45	-1.4	2.0	1.7	2.8	2.3
CNGA1	cyclic nucleotide gated channel alpha 1	-1.4	-0.3	-0.1	0.0	-0.7
ZNF252P-AS1	ZNF252P antisense RNA 1	-1.4	-2.9	-1.6	-1.4	-1.6
TAGLN	transgelin	-1.4	-8.8	-8.7	-8.8	-9.1
SEMA3C	semaphorin 3C	-1.4	1.5	1.1	1.0	1.5
UBXN10	UBX domain protein 10	-1.4	-5.5	-4.4	-4.7	-5.9
MYEOV	myeloma overexpressed	-1.4	-4.4	-3.6	-4.2	-4.9
GGT6	gamma-glutamyltransferase 6	-1.4	-4.9	-5.0	-5.0	-4.9
EDN1	endothelin 1	-1.3	-8.2	-9.1	-7.3	-7.3
HIST1H4D	histone cluster 1, H4d	-1.3	0.8	1.0	1.1	-0.2
PCYT1B	phosphate cytidylyltransferase 1, choline, beta	-1.3	-3.2	-3.7	-3.9	-3.2
MKRN2OS	MKRN2 opposite strand	-1.3	-0.9	-0.3	-0.7	-0.5
KRTAP2-4	keratin associated protein 2-4	-1.3	-5.5	-5.5	-5.5	-5.2
MIR3648-1	microRNA 3648-1	-1.3	-2.0	-1.3	-2.0	-2.0
SNORA66	small nucleolar RNA, H/ACA box 66	-1.3	-0.6	-0.3	0.1	-0.5
NANOG	Nanog homeobox	-1.3	-5.7	-6.1	-6.1	-6.1
DNALI1	dynein, axonemal, light intermediate chain 1	-1.3	-1.3	-1.3	-2.4	-1.5
MUC19	mucin 19, oligomeric	-1.3	1.2	-0.2	0.7	1.1
RPRM	reprimo, TP53 dependent G2 arrest mediator candidate	-1.3	10.1	10.1	7.7	8.4
CUBN	cubilin	-1.3	1.3	1.4	2.0	2.3
C9orf173-AS1	C9orf173 antisense RNA 1	-1.3	-1.0	-2.2	-1.0	-1.3
KLHL33	kelch like family member 33	-1.3	-3.7	-3.5	-4.6	-3.4
ASB4	ankyrin repeat and SOCS box containing 4	-1.3	-6.2	-6.6	-6.6	-7.6
NANOGNBP3	NANOGNB pseudogene 3	-1.3	0.9	1.7	1.3	1.6
LRRC4	leucine rich repeat containing 4	-1.3	7.8	7.9	7.8	7.5
ACTBP9	actin, beta pseudogene 9	-1.3	-2.4	-2.0	-1.6	-2.1
HACD4	3-hydroxyacyl-CoA dehydratase 4	-1.3	0.8	1.3	1.5	0.8
SYNPR	synaptoporin	-1.3	-4.1	-4.1	-4.8	-4.8
MIR1469	microRNA 1469	-1.3	1.2	1.8	2.5	2.2
RHOH	ras homolog family member H	-1.3	1.8	0.5	0.5	1.5
MSX2	msh homeobox 2	-1.3	10.9	10.8	10.8	10.9
SNORD1B	small nucleolar RNA, C/D box 1B	-1.3	-1.6	-1.0	0.3	-1.5
NEURL1B	neuralized E3 ubiquitin protein ligase 1B	-1.3	-1.8	-1.2	-2.2	-3.1
LINC00618	long intergenic non-protein coding RNA 618	-1.3	0.8	0.5	1.8	2.1
MRGPRX4	MAS related GPR family member X4	-1.3	-6.9	-7.0	-7.0	-7.0
FGD2	FYVE, RhoGEF and PH domain containing 2	-1.3	-0.2	-0.6	-1.9	-1.8
GPR55	G protein-coupled receptor 55	-1.3	-4.0	-3.9	-4.3	-3.8
APOD	apolipoprotein D	-1.3	-0.7	-1.0	-2.7	-2.9
ODAM	odontogenic, ameloblast asssociated	-1.3	-9.1	-10.0	-10.1	-9.9
RPL7AP10	ribosomal protein L7a pseudogene 10	-1.3	-2.1	-1.5	-0.9	-1.1
S100A4	S100 calcium binding protein A4	-1.2	-5.3	-4.9	-4.4	-5.9
PAIP2B	poly(A) binding protein interacting protein 2B	-1.2	4.3	4.3	4.3	4.1
LINC00326	long intergenic non-protein coding RNA 326	-1.2	-5.9	-6.1	-5.6	-6.1
RAB9B	RAB9B, member RAS oncogene family	-1.2	2.7	2.5	2.6	2.7
MEIS3P1	Meis homeobox 3 pseudogene 1	-1.2	0.6	0.8	-0.2	-0.1
TNNC2	troponin C type 2 (fast)	-1.2	-2.3	-2.8	-3.1	-2.8
BNIPL	BCL2/adenovirus E1B 19kD interacting protein like	-1.2	0.7	-0.3	0.9	0.2
LINC00649	long intergenic non-protein coding RNA 649	-1.2	5.0	4.8	3.9	4.2
C1QL3	complement component 1, q subcomponent-like 3	-1.2	-1.2	-1.6	-0.5	-1.1
TSPAN11	tetraspanin 11	-1.2	0.4	0.0	0.5	0.0
ZCCHC12	zinc finger, CCHC domain containing 12	-1.2	6.3	6.1	4.9	5.4
TFDP1P	transcription factor Dp-1 pseudogene	-1.2	-1.8	-1.2	0.5	-0.5

ATP5G1P5	ATP synthase, H+ transporting, mitochondrial Fo complex subunit C1 (subunit 9) pseudogene 5	-1.2	-0.1	0.9	0.8	-0.7
DKKL1	dickkopf-like 1	-1.2	-0.3	-0.8	-0.3	-0.7
PSCA	prostate stem cell antigen	-1.2	0.1	-1.2	-0.2	0.7
HCST	hematopoietic cell signal transducer	-1.2	-2.3	-2.3	-2.3	-1.8
RIBC2	RIB43A domain with coiled-coils 2	-1.2	1.2	1.1	2.1	2.7
SLC34A2	solute carrier family 34 (type II sodium/phosphate cotransporter), member 2	-1.2	-2.7	-4.0	-4.6	-2.3
RPL23P2	ribosomal protein L23 pseudogene 2	-1.2	0.9	0.3	0.5	1.0
KRTAP2-3	keratin associated protein 2-3	-1.2	-7.1	-7.2	-7.2	-6.4
KCNJ4	potassium channel, inwardly rectifying subfamily J, member 4	-1.2	2.1	2.3	2.1	1.9
HILS1	histone linker H1 domain, spermatid-specific 1 (pseudogene)	-1.2	-6.6	-6.7	-6.7	-6.3
MSMB	microseminoprotein, beta-	-1.2	-5.5	-5.5	-5.5	-5.4
SLC2A3P2	solute carrier family 2 (facilitated glucose transporter), member 3 pseudogene 2	-1.2	-3.6	-5.1	-3.9	-3.2
DRAXIN	dorsal inhibitory axon guidance protein	-1.2	3.2	2.4	3.0	2.7
ACTA1	actin, alpha 1, skeletal muscle	-1.2	-6.6	-6.2	-5.9	-6.4
CFAP57	cilia and flagella associated protein 57	-1.2	-1.4	-1.2	-1.3	-1.4
S100A2	S100 calcium binding protein A2	-1.2	-3.7	-3.7	-4.0	-4.8
SNORD45A	small nucleolar RNA, C/D box 45A	-1.2	-1.7	-2.0	0.0	-1.5
SLC2A3	solute carrier family 2 (facilitated glucose transporter), member 3	-1.2	-8.4	-8.7	-9.6	-9.0
FRMPD2	FERM and PDZ domain containing 2	-1.2	-1.0	-2.0	-2.4	-1.8
C6orf141	chromosome 6 open reading frame 141	-1.2	4.2	3.2	3.6	5.1
LYPD6	LY6/PLAUR domain containing 6	-1.2	3.3	3.4	3.5	3.2
TACSTD2	tumor-associated calcium signal transducer 2	-1.2	-4.4	-3.2	-3.9	-4.3
FAM99A	family with sequence similarity 99 member A (non-protein coding)	-1.2	-5.0	-4.7	-5.0	-5.0
SPEF1	sperm flagellar 1	-1.2	-0.8	-0.6	-1.3	-1.3
TNFSF15	tumor necrosis factor superfamily member 15	-1.2	0.8	1.0	-0.4	-2.1
C20orf144	chromosome 20 open reading frame 144	-1.2	-0.7	-1.9	-0.8	-1.1
CHP2	calcineurin-like EF-hand protein 2	-1.2	-1.2	-1.1	-1.8	-3.2
NGFR	nerve growth factor receptor	-1.2	-4.3	-4.6	-5.4	-4.9
KIAA0825	KIAA0825	-1.2	-0.2	-0.7	0.1	-0.6
CCNB1IP1P1	cyclin B1 interacting protein 1 pseudogene 1	-1.2	-4.0	-3.4	-2.3	-2.3
CD8B	CD8b molecule	-1.2	-5.4	-5.4	-5.3	-5.5
PRR5L	proline rich 5 like	-1.2	1.7	1.9	1.9	1.9
KCNH1	potassium channel, voltage gated eag related subfamily H, member 1	-1.2	0.2	0.2	-0.7	-0.2
IKZF3	IKAROS family zinc finger 3	-1.2	5.4	5.5	5.6	5.6
BEX4	brain expressed X-linked 4	-1.2	10.2	9.9	9.6	10.1
LINC00479	long intergenic non-protein coding RNA 479	-1.2	-5.7	-6.4	-6.4	-6.1
CDRT15P1	CMT1A duplicated region transcript 15 pseudogene 1	-1.2	-0.9	0.1	0.4	-0.5
SNORA69	small nucleolar RNA, H/ACA box 69	-1.1	1.3	1.1	1.4	1.5
CASS4	Cas scaffolding protein family member 4	-1.1	-2.8	-3.4	-2.3	-2.0
CCDC148	coiled-coil domain containing 148	-1.1	-2.6	-2.3	-2.6	-1.8
TMSB4X	thymosin beta 4, X-linked	-1.1	-1.4	-1.5	-1.5	-0.9
SNORA72	small nucleolar RNA, H/ACA box 72	-1.1	-1.2	-1.4	-0.2	-0.3
SMC1B	structural maintenance of chromosomes 1B	-1.1	-0.6	0.6	0.2	1.3
LZTS1	leucine zipper, putative tumor suppressor 1	-1.1	4.2	4.5	4.9	4.6
TTPA	tocopherol (alpha) transfer protein	-1.1	-4.4	-4.1	-4.3	-4.9
ACTL8	actin like 8	-1.1	0.4	1.1	0.8	0.2
HES5	hes family bHLH transcription factor 5	-1.1	2.7	2.8	2.9	2.9
TRK-TTT2-1	transfer RNA-Lys (TTT) 2-1	-1.1	0.1	2.4	1.5	0.4
TMEM31	transmembrane protein 31	-1.1	3.5	3.9	3.8	3.3
GATA6-AS1	GATA6 antisense RNA 1 (head to head)	-1.1	0.4	1.1	1.1	0.3
KLHDC7A	kelch domain containing 7A	-1.1	-6.3	-7.1	-7.5	-7.1
PDE7B	phosphodiesterase 7B	-1.1	3.1	3.7	2.1	3.4
KCNIP4	Kv channel interacting protein 4	-1.1	0.6	0.3	1.3	1.3
RACGAP1P	Rac GTPase activating protein 1 pseudogene	-1.1	0.0	0.2	0.3	-0.1
IL9R	interleukin 9 receptor	-1.1	3.1	3.3	3.8	3.6
KRT37	keratin 37, type I	-1.1	-5.3	-6.1	-5.9	-5.4
LINC01488	long intergenic non-protein coding RNA 1488	-1.1	-6.3	-6.6	-6.5	-6.7
CELF3	CUGBP, Elav-like family member 3	-1.1	1.4	1.4	0.7	0.8
TRD-GTC2-4	transfer RNA-Asp (GTC) 2-4	-1.1	0.3	1.2	1.6	0.4
TRD-GTC2-2	transfer RNA-Asp (GTC) 2-2	-1.1	0.3	1.2	1.6	0.4
TRD-GTC2-6	transfer RNA-Asp (GTC) 2-6	-1.1	0.2	1.2	1.6	0.7
TRD-GTC2-3	transfer RNA-Asp (GTC) 2-3	-1.1	0.3	1.2	1.6	0.4
LRRIQ1	leucine-rich repeats and IQ motif containing 1	-1.1	2.4	2.0	2.1	2.7
HES2	hes family bHLH transcription factor 2	-1.1	-1.9	-2.3	-2.7	-2.7
PRF1	perforin 1 (pore forming protein)	-1.1	-6.5	-8.0	-7.5	-7.5
MIR3176	microRNA 3176	-1.1	0.3	1.2	1.8	0.7
HAPLN3	hyaluronan and proteoglycan link protein 3	-1.1	5.0	5.3	5.2	4.9
KLHL3	kelch like family member 3	-1.1	2.6	2.0	2.1	2.8
TRAM1L1	translocation associated membrane protein 1-like 1	-1.1	1.1	1.3	1.6	1.6
LAMB2P1	laminin subunit beta 2 pseudogene 1	-1.1	1.6	1.4	1.1	2.3
BCYRN1	brain cytoplasmic RNA 1	-1.1	5.2	5.1	4.6	4.6
FSTL1	follistatin like 1	-1.1	8.3	8.1	8.4	8.5
FLG2	filaggrin family member 2	-1.1	1.0	0.9	0.2	1.5
HRCT1	histidine rich carboxyl terminus 1	-1.1	-6.7	-5.9	-6.2	-6.8
CD207	CD207 molecule	-1.1	-2.0	-2.3	-1.9	-1.3

SLC2A3P4	solute carrier family 2 (facilitated glucose transporter), member 3 pseudogene 4	-1.1	-3.5	-2.5	-2.6	-4.4
DEGS2	delta(4)-desaturase, sphingolipid 2	-1.1	-2.1	-1.7	-1.1	-2.2
MESP2	mesoderm posterior bHLH transcription factor 2	-1.1	1.9	1.7	3.0	3.3
AQP6	aquaporin 6	-1.1	-1.5	-1.2	-1.1	-1.3
ZBTB8OSP1	zinc finger and BTB domain containing 8 opposite strand pseudogene 1	-1.1	-2.3	-1.3	-0.5	-1.4
TRIM45	tripartite motif containing 45	-1.1	0.9	0.7	1.2	1.2
ATP5G1P2	ATP synthase, H+ transporting, mitochondrial Fo complex subunit C1 (subunit 9) pseudogene 2	-1.1	0.4	1.3	1.2	-0.4
BCYRN1P1	brain cytoplasmic RNA 1, pseudogene 1	-1.1	5.3	5.1	4.7	4.6
ARSI	arylsulfatase family member I	-1.1	-11.1	-11.0	-11.4	-11.6
DDX11L9	DEAD/H-box helicase 11 like 9	-1.1	1.1	1.4	0.0	0.3
KITLG	KIT ligand	-1.1	-1.6	-1.6	-1.7	-1.6
HIST2H2BA	histone cluster 2, H2ba (pseudogene)	-1.1	0.2	-0.1	0.0	-0.5
EPHB3	EPH receptor B3	-1.1	3.8	3.8	3.2	2.7
TMSB15A	thymosin beta 15a	-1.1	7.6	8.1	7.7	7.3
CD14	CD14 molecule	-1.1	-3.2	-2.6	-2.8	-3.4
CHEK2P2	checkpoint kinase 2 pseudogene 2	-1.0	-1.1	-0.9	0.4	-1.2
APCDD1	adenomatosis polyposis coli down-regulated 1	-1.0	3.0	2.6	3.1	3.4
KCNN4	potassium channel, calcium activated intermediate/small conductance subfamily N alpha, member 4	-1.0	-4.3	-4.1	-3.3	-2.9
PDE3A	phosphodiesterase 3A	-1.0	1.0	1.2	0.9	1.1
C1QL4	complement component 1, q subcomponent-like 4	-1.0	3.2	3.5	4.2	3.6
MAGI1-IT1	MAGI1 intronic transcript 1	-1.0	-5.3	-3.8	-3.6	-4.1
FBXL7	F-box and leucine-rich repeat protein 7	-1.0	3.1	3.1	1.6	2.3
ZNF618	zinc finger protein 618	-1.0	4.7	4.9	5.2	4.8
MRPS17P1	mitochondrial ribosomal protein S17 pseudogene 1	-1.0	-1.1	1.0	1.2	-0.1
TMEM27	transmembrane protein 27	-1.0	-2.5	-3.5	-3.8	-2.7
GAPDHP2	glyceraldehyde-3-phosphate dehydrogenase pseudogene 2	-1.0	-1.0	-0.5	-1.4	-1.7
C10orf25	chromosome 10 open reading frame 25	-1.0	1.4	1.2	2.4	2.9
KCTD12	potassium channel tetramerization domain containing 12	-1.0	10.1	10.5	10.0	9.2
DYNC1I1	dynein, cytoplasmic 1, intermediate chain 1	-1.0	2.9	3.2	3.3	2.5
JAKMIP2-AS1	JAKMIP2 antisense RNA 1	-1.0	6.9	7.1	6.1	6.4
CA7	carbonic anhydrase VII	-1.0	1.3	2.7	1.6	1.5
CD248	CD248 molecule	-1.0	-7.3	-7.9	-6.2	-8.2
UCA1	urothelial cancer associated 1 (non-protein coding)	-1.0	-6.0	-6.2	-6.5	-6.6
LRRN4	leucine rich repeat neuronal 4	-1.0	-6.6	-6.9	-7.5	-7.7
RNF43	ring finger protein 43	-1.0	-3.1	-2.9	-3.1	-3.8
ABCG1	ATP binding cassette subfamily G member 1	-1.0	2.7	3.4	2.6	1.8
TPM1	tropomyosin 1 (alpha)	-1.0	-2.8	-2.5	-2.3	-2.9
ZBTB8B	zinc finger and BTB domain containing 8B	-1.0	3.0	3.1	3.3	3.1
GINS2	GINS complex subunit 2 (Psf2 homolog)	-1.0	0.3	0.5	0.5	0.2
SNORD27	small nucleolar RNA, C/D box 27	-1.0	-0.2	0.1	0.6	0.0
HSPB9	heat shock protein family B (small) member 9	-1.0	0.9	0.1	1.3	1.2
KCNK10	potassium channel, two pore domain subfamily K, member 10	-1.0	3.3	2.5	-0.4	2.6
GFY	golgi associated olfactory signaling regulator	-1.0	3.2	2.8	1.3	1.7
ZNF890P	zinc finger protein 890, pseudogene	-1.0	-0.1	0.1	0.4	-0.5
FOXO6	forkhead box O6	-1.0	3.6	4.1	4.3	4.0
HSPG2	heparan sulfate proteoglycan 2	-1.0	-4.4	-4.8	-4.8	-4.9
LDLRAD2	low density lipoprotein receptor class A domain containing 2	-1.0	-4.9	-5.2	-4.8	-5.0
HIST1H2BH	histone cluster 1, H2bh	-1.0	-1.3	-0.8	-1.4	-2.0
CLDN24	claudin 24	-1.0	-3.5	-2.8	-1.4	-2.6
KCNJ10	potassium channel, inwardly rectifying subfamily J, member 10	-1.0	-6.7	-6.8	-6.5	-7.1
C3orf70	chromosome 3 open reading frame 70	-1.0	-1.9	-1.9	-1.3	-1.7
ENDOD1	endonuclease domain containing 1	-1.0	-0.3	-0.5	-0.4	-0.2
RFPL3	ret finger protein-like 3	-1.0	2.5	1.9	2.8	2.6
CDC20B	cell division cycle 20B	-1.0	2.0	1.8	0.1	1.8
LY6D	lymphocyte antigen 6 complex, locus D	-1.0	-6.9	-7.4	-7.4	-7.2
GRHL3	grainyhead like transcription factor 3	-1.0	2.6	2.3	2.6	2.5
NFE2	nuclear factor, erythroid 2	-1.0	-6.1	-4.8	-6.0	-6.0
VDAC1P8	voltage dependent anion channel 1 pseudogene 8	-1.0	-0.6	0.2	0.2	-0.8
TLR4	toll-like receptor 4	-1.0	-7.4	-7.4	-7.5	-7.8
GLDC	glycine dehydrogenase (decarboxylating)	-1.0	-1.2	-0.9	-1.1	-1.5
NTN3	netrin 3	-1.0	-1.4	-1.7	-1.1	-1.2
TGM2	transglutaminase 2	-1.0	-5.9	-5.6	-6.6	-7.5
SYT1	synaptotagmin 1	-1.0	2.1	1.8	2.0	2.7
HTR7P1	5-hydroxytryptamine (serotonin) receptor 7 pseudogene 1	-1.0	0.5	0.7	0.8	0.5
TMEM17	transmembrane protein 17	-1.0	2.8	2.8	2.7	3.4
SCARNA17	small Cajal body-specific RNA 17	-1.0	-1.1	-0.9	-1.6	-0.2
FAM78B	family with sequence similarity 78 member B	-1.0	0.3	0.6	-1.0	-1.1
ZNF638-IT1	ZNF638 intronic transcript 1	-1.0	-3.0	-2.9	-1.0	-1.5
HIPK4	homeodomain interacting protein kinase 4	-1.0	-0.1	1.2	1.0	0.2
SNORD47	small nucleolar RNA, C/D box 47	-1.0	-1.1	-0.3	0.5	-0.3
MIR3198-2	microRNA 3198-2	-1.0	0.4	0.5	0.3	0.3
SKP2	S-phase kinase-associated protein 2, E3 ubiquitin protein ligase	-1.0	1.1	1.3	1.5	1.3
ART5	ADP-ribosyltransferase 5	-1.0	2.9	3.2	2.4	1.8
HOXC-AS1	HOXC cluster antisense RNA 1	-1.0	3.4	4.0	4.1	3.4
RPL6P1	ribosomal protein L6 pseudogene 1	-1.0	0.4	0.8	0.0	-0.3

SRY	sex determining region Y	-1.0	-8.0	-8.0	-8.0	-8.0
UHRF1	ubiquitin-like with PHD and ring finger domains 1	-1.0	1.4	1.5	1.6	1.5
PKDCC	protein kinase domain containing, cytoplasmic	-1.0	-3.0	-2.9	-2.1	-2.2
SNORA81	small nucleolar RNA, H/ACA box 81	-1.0	-1.3	-1.5	-0.6	-1.1
KIAA1755	KIAA1755	-1.0	-5.0	-5.1	-5.1	-5.1
JAKMIP2	janus kinase and microtubule interacting protein 2	-1.0	5.4	5.4	4.6	4.8
C2orf54	chromosome 2 open reading frame 54	-1.0	-6.3	-7.5	-7.0	-7.4
NRGN	neurogranin	-1.0	2.4	2.9	2.9	2.1
HOXC13	homeobox C13	-1.0	6.4	6.8	7.0	6.2
HIST1H3C	histone cluster 1, H3c	-1.0	-3.5	-3.6	-2.9	-4.5
LINC00260	long intergenic non-protein coding RNA 260	-1.0	1.3	1.6	1.3	1.3
NPPB	natriuretic peptide B	-1.0	-5.8	-5.7	-6.0	-5.4
CCDC39	coiled-coil domain containing 39	-1.0	-1.8	-1.5	-0.7	-1.9
SNORD56	small nucleolar RNA, C/D box 56	-1.0	-1.7	-1.1	-0.5	-1.0
RNF224	ring finger protein 224	-1.0	-1.2	-2.0	-0.6	-0.3
COTL1	coactosin-like F-actin binding protein 1	-1.0	0.0	0.3	-0.1	-0.3
PVRL1	poliovirus receptor-related 1 (herpesvirus entry mediator C)	-1.0	-1.5	-1.4	-1.3	-1.8
PSD2	pleckstrin and Sec7 domain containing 2	-1.0	-0.6	-0.6	-0.6	-0.5
API5P2	apoptosis inhibitor 5 pseudogene 2	-1.0	-1.8	-0.5	-0.3	-0.6
PCED1B	PC-esterase domain containing 1B	-1.0	-3.6	-3.5	-4.4	-4.4
MRAP2	melanocortin 2 receptor accessory protein 2	-1.0	2.3	2.7	2.1	1.7
CORO1A	coronin 1A	-1.0	-0.6	-0.5	-1.0	-0.9
LINC00853	long intergenic non-protein coding RNA 853	-1.0	-0.2	-0.2	-0.6	-0.8
CLDN6	claudin 6	-1.0	-10.7	-10.3	-9.3	-9.4
ATP5J2P5	ATP synthase, H+ transporting, mitochondrial Fo complex subunit F2 pseudogene 5	-1.0	-0.9	-0.4	0.5	-1.5
DLX5	distal-less homeobox 5	-1.0	4.4	5.5	5.9	4.7
PLCL2	phospholipase C like 2	-1.0	6.5	6.6	6.4	6.3
KRT8P48	keratin 8 pseudogene 48	-1.0	-6.7	-6.1	-6.1	-6.4
SPC24	SPC24, NDC80 kinetochore complex component	-1.0	1.7	2.0	1.8	1.5
SNORD77	small nucleolar RNA, C/D box 77	-0.9	-1.9	0.0	0.2	-0.5
LINC00612	long intergenic non-protein coding RNA 612	-0.9	-3.9	-3.7	-3.0	-3.7
SSBP3-AS1	SSBP3 antisense RNA 1	-0.9	0.0	0.4	0.7	-0.2
FAM198B	family with sequence similarity 198 member B	-0.9	-10.3	-10.7	-10.6	-10.7
PDZK1IP1	PDZK1 interacting protein 1	-0.9	-5.5	-5.5	-5.3	-5.0
AATBC	apoptosis associated transcript in bladder cancer	-0.9	-1.4	-1.0	-1.3	-1.7
ESRRG	estrogen related receptor gamma	-0.9	4.7	5.2	5.1	4.6
GDA	guanine deaminase	-0.9	-4.4	-5.4	-4.8	-5.2
RXFP4	relaxin/insulin-like family peptide receptor 4	-0.9	-6.3	-6.6	-5.9	-6.3
PLXNC1	plexin C1	-0.9	-3.8	-3.8	-3.9	-4.0
RASSF2	Ras association (RalGDS/AF-6) domain family member 2	-0.9	-1.4	-1.0	-0.5	-1.4
AKAP5	A-kinase anchoring protein 5	-0.9	0.9	1.6	1.9	1.2
LDOC1	leucine zipper, down-regulated in cancer 1	-0.9	6.9	7.2	7.0	6.3
DCBLD1	discoidin, CUB and LCCL domain containing 1	-0.9	-2.4	-2.4	-2.3	-2.1
GLOD5	glyoxalase domain containing 5	-0.9	-5.1	-5.8	-5.5	-5.9
MIR631	microRNA 631	-0.9	-0.9	-1.1	0.4	0.3
C14orf105	chromosome 14 open reading frame 105	-0.9	-5.4	-6.0	-5.8	-5.8
MIR600	microRNA 600	-0.9	-0.8	-0.5	0.1	-0.4
ZNF815P	zinc finger protein 815, pseudogene	-0.9	0.4	0.9	1.0	0.4
CHAD	chondroadherin	-0.9	-4.0	-4.0	-2.3	-3.1
PRSS23	protease, serine 23	-0.9	1.8	1.0	0.3	1.6
ENHO	energy homeostasis associated	-0.9	4.0	4.3	4.4	4.0
POLR2L	polymerase (RNA) II (DNA directed) polypeptide L, 7.6kDa	-0.9	0.7	1.1	0.9	0.0
SNORA11D	small nucleolar RNA, H/ACA box 11D	-0.9	-3.5	-4.6	-3.1	-2.7
UGT2B10	UDP glucuronosyltransferase 2 family, polypeptide B10	-0.9	-9.0	-9.7	-9.6	-9.6
KCNJ8	potassium channel, inwardly rectifying subfamily J, member 8	-0.9	7.0	7.5	7.3	6.6
POM121L1P	POM121 transmembrane nucleoporin like 1, pseudogene	-0.9	-1.8	-0.4	0.0	-2.1
PLPPR1	phospholipid phosphatase related 1	-0.9	-6.0	-5.7	-7.5	-7.3
DCTN1-AS1	DCTN1 antisense RNA 1	-0.9	-0.7	-0.4	-0.8	-0.4
FAM167B	family with sequence similarity 167 member B	-0.9	-4.6	-4.4	-4.6	-5.4
SCIMP	SLP adaptor and CSK interacting membrane protein	-0.9	1.0	0.9	1.4	1.2
SNORA11	small nucleolar RNA, H/ACA box 11	-0.9	-1.4	-2.1	-1.8	-2.8
CALB2	calbindin 2	-0.9	-4.0	-4.2	-4.7	-4.0
SDPR	serum deprivation response	-0.9	-10.5	-11.1	-11.9	-11.6
SOWAHA	sosondowah ankyrin repeat domain family member A	-0.9	2.0	1.9	1.7	1.6
RPL7AP63	ribosomal protein L7a pseudogene 63	-0.9	-0.9	0.0	1.0	0.8
SNORD5	small nucleolar RNA, C/D box 5	-0.9	-3.1	-3.0	-1.3	-1.6
SCN1A	sodium channel, voltage gated, type I alpha subunit	-0.9	-5.3	-6.1	-6.1	-6.1
RLBP1	retinaldehyde binding protein 1	-0.9	-4.9	-4.5	-5.1	-5.3
SESN3	sestrin 3	-0.9	1.8	1.6	2.2	2.3
RPL29P3	ribosomal protein L29 pseudogene 3	-0.9	-0.5	0.8	-0.5	-0.4
HOXA9	homeobox A9	-0.9	8.0	8.5	8.6	7.9
PCNA-AS1	PCNA antisense RNA 1	-0.9	-0.2	-0.3	-0.1	-0.2
FAM19A4	family with sequence similarity 19 (chemokine (C-C motif)-like), member A4	-0.9	-2.5	-2.8	-4.9	-5.5
BZRAP1-AS1	BZRAP1 antisense RNA 1	-0.9	-1.7	-1.0	-1.2	-1.9
PEX7	peroxisomal biogenesis factor 7	-0.9	4.9	4.7	4.8	5.2

TSPAN8	tetraspanin 8	-0.9	-5.9	-6.6	-6.4	-6.4
PCNA	proliferating cell nuclear antigen	-0.9	-0.3	-0.4	-0.3	-0.1
MCHR1	melanin concentrating hormone receptor 1	-0.9	-6.1	-5.6	-7.1	-7.1
CYSRT1	cysteine-rich tail protein 1	-0.9	-1.9	-2.0	-1.9	-1.6
EHD3	EH domain containing 3	-0.9	3.9	4.2	4.1	3.7
LINC00634	long intergenic non-protein coding RNA 634	-0.9	4.9	4.6	4.8	5.2
SNORA11E	small nucleolar RNA, H/ACA box 11E	-0.9	-3.5	-4.6	-3.1	-2.7
IGFBP7	insulin like growth factor binding protein 7	-0.9	-5.8	-6.0	-8.0	-7.1
DKK3	dickkopf WNT signaling pathway inhibitor 3	-0.9	0.2	0.4	-0.2	-0.8
UCP3	uncoupling protein 3 (mitochondrial, proton carrier)	-0.9	1.0	0.8	1.6	0.7
ECSCR	endothelial cell surface expressed chemotaxis and apoptosis regulator	-0.9	-4.2	-5.2	-5.0	-5.3
SNORD29	small nucleolar RNA, C/D box 29	-0.9	-0.6	-0.2	0.5	-0.1
CFAP44	cilia and flagella associated protein 44	-0.9	0.4	0.4	0.5	0.5
MYT1	myelin transcription factor 1	-0.9	0.5	0.4	1.2	0.6
CLDN2	claudin 2	-0.9	-6.7	-5.7	-5.1	-5.9
RNU6-48P	RNA, U6 small nuclear 48, pseudogene	-0.9	-0.1	0.7	0.9	0.5
FAM109B	family with sequence similarity 109 member B	-0.9	-0.1	-0.5	1.4	1.4
PEX5L	peroxisomal biogenesis factor 5-like	-0.9	1.2	0.5	0.0	2.4
GMPR	guanosine monophosphate reductase	-0.9	4.9	5.2	4.9	4.4
POM121L8P	POM121 transmembrane nucleoporin like 8, pseudogene	-0.9	3.3	3.3	3.5	3.5
SOD3	superoxide dismutase 3, extracellular	-0.9	-4.2	-5.2	-5.2	-5.2
ITGA9-AS1	ITGA9 antisense RNA 1	-0.9	-2.8	-2.8	-2.4	-3.2
CFLAR-AS1	CFLAR antisense RNA 1	-0.9	-2.9	-3.1	-2.5	-3.0
PCDHB9	protocadherin beta 9	-0.9	-2.9	-2.6	-4.5	-4.6
C8orf46	chromosome 8 open reading frame 46	-0.9	-3.2	-2.4	-1.3	-2.1
CNTNAP2	contactin associated protein-like 2	-0.9	4.1	4.3	4.3	4.1
CST4	cystatin S	-0.9	-5.4	-5.9	-5.6	-5.9
CADM2	cell adhesion molecule 2	-0.9	2.8	2.4	1.5	2.6
KCNK9	potassium channel, two pore domain subfamily K, member 9	-0.9	-1.5	-0.8	-2.8	-3.6
RIMS2	regulating synaptic membrane exocytosis 2	-0.9	1.5	-0.4	1.3	1.4
HEPHL1	hephaestin like 1	-0.9	-5.8	-5.9	-5.9	-5.9
RAB41	RAB41, member RAS oncogene family	-0.9	0.1	0.3	0.6	0.4
IFIT1	interferon induced protein with tetratricopeptide repeats 1	-0.9	-2.1	-0.4	-0.9	-3.7
LIMA1	LIM domain and actin binding 1	-0.9	0.2	0.4	0.3	-0.1
IGFBP4	insulin like growth factor binding protein 4	-0.9	-10.0	-10.3	-8.6	-8.3
WDR34	WD repeat domain 34	-0.9	0.6	0.4	0.6	0.7
SNX19P3	sorting nexin 19 pseudogene 3	-0.9	2.6	2.0	2.3	2.0
ZNF385B	zinc finger protein 385B	-0.9	-1.1	-1.0	-0.9	-0.9
MYOF	myoferlin	-0.9	-4.0	-4.3	-4.4	-4.6
LYPD1	LY6/PLAUR domain containing 1	-0.9	2.9	3.3	4.0	3.8
SNORA6	small nucleolar RNA, H/ACA box 6	-0.9	0.2	0.7	0.6	0.0
SNPH	syntaphilin	-0.9	2.4	2.2	1.8	2.1
HOXA10	homeobox A10	-0.9	5.5	6.1	6.0	5.3
SAMD12	sterile alpha motif domain containing 12	-0.9	3.4	3.6	3.6	3.4
PLAC1	placenta specific 1	-0.9	3.9	3.4	2.8	4.0
TNNC1	troponin C type 1 (slow)	-0.9	-5.7	-5.4	-6.8	-6.3
RAB40A	RAB40A, member RAS oncogene family	-0.9	2.9	2.4	2.6	3.1
RNU6ATAC	RNA, U6atac small nuclear (U12-dependent splicing)	-0.9	-1.0	0.1	0.3	-0.9
ERVMER34-1	endogenous retrovirus group MER34 member 1	-0.9	2.8	3.1	2.8	2.4
EFNB2	ephrin-B2	-0.9	4.7	4.6	4.5	4.6
ACTB	actin, beta	-0.9	-0.7	-0.5	-0.6	-1.2
DCDC2	doublecortin domain containing 2	-0.9	-4.0	-4.0	-4.4	-3.9
PKP2	plakophilin 2	-0.9	-1.3	-0.9	-0.6	-1.3
MORC4	MORC family CW-type zinc finger 4	-0.9	0.0	-0.4	-0.4	0.4
NFE2L3	nuclear factor, erythroid 2 like 3	-0.9	-2.8	-2.3	-2.2	-2.6
TMSB4XP8	thymosin beta 4, X-linked pseudogene 8	-0.9	-1.5	-1.6	-1.4	-1.0
WFIKKN2	WAP, follistatin/kazal, immunoglobulin, kunitz and netrin domain containing 2	-0.9	-3.6	-3.2	-3.0	-3.7
CLUL1	clusterin like 1	-0.9	-0.2	-0.3	0.0	0.6
TRIL	TLR4 interactor with leucine-rich repeats	-0.9	-3.7	-5.2	-5.4	-5.1
TNFRSF19	tumor necrosis factor receptor superfamily member 19	-0.9	-5.7	-5.1	-4.7	-5.2
VSNL1	visinin like 1	-0.9	-5.2	-4.5	-8.1	-8.0
PDE6G	phosphodiesterase 6G	-0.9	-5.2	-5.4	-5.1	-5.3
DUBR	DPPA2 upstream binding RNA	-0.9	2.2	2.4	2.0	1.9
NRIP2	nuclear receptor interacting protein 2	-0.9	1.1	1.3	1.2	0.7
NEXN-AS1	NEXN antisense RNA 1	-0.9	-1.5	-1.7	-1.0	-2.1
ZNF185	zinc finger protein 185 (LIM domain)	-0.9	-0.2	-0.5	-0.3	0.1
TK1	thymidine kinase 1, soluble	-0.9	-0.4	-0.4	-0.7	-0.7
C8orf49	chromosome 8 open reading frame 49	-0.9	-3.9	-2.5	-3.0	-3.7
HMGN5	high mobility group nucleosome binding domain 5	-0.9	5.6	6.0	5.7	5.4
GPR119	G protein-coupled receptor 119	-0.9	-7.6	-7.2	-7.0	-7.8
PCDHB10	protocadherin beta 10	-0.9	-3.5	-3.8	-4.6	-4.5
PRIMA1	proline rich membrane anchor 1	-0.9	-2.3	-2.2	-1.9	-1.9
HOXD10	homeobox D10	-0.9	8.8	8.8	9.1	9.1
SNN	stannin	-0.9	-0.9	-0.1	0.1	-1.2
KIAA1462	KIAA1462	-0.9	4.1	4.6	4.8	3.9

REFERENCES

1. Masuoka, H.C. and N. Chalasani, *Nonalcoholic fatty liver disease: an emerging threat to obese and diabetic individuals.* Ann N Y Acad Sci, 2013. **1281**: p. 106-22.
2. Berlanga, A., E. Guiu-Jurado, J.A. Porras, and T. Auguet, *Molecular pathways in non-alcoholic fatty liver disease.* Clin Exp Gastroenterol, 2014. **7**: p. 221-39.
3. Deurenberg, P., M. Yap, and W.A. van Staveren, *Body mass index and percent body fat: a meta analysis among different ethnic groups.* Int J Obes Relat Metab Disord, 1998. **22**(12): p. 1164-71.
4. Amarapurkar, D., P. Kamani, N. Patel, P. Gupte, P. Kumar, S. Agal, R. Baijal, S. Lala, D. Chaudhary, and A. Deshpande, *Prevalence of non-alcoholic fatty liver disease: population based study.* Ann Hepatol, 2007. **6**(3): p. 161-3.
5. Vernon, G., A. Baranova, and Z.M. Younossi, *Systematic review: the epidemiology and natural history of non-alcoholic fatty liver disease and non-alcoholic steatohepatitis in adults.* Aliment Pharmacol Ther, 2011. **34**(3): p. 274-85.
6. Chalasani, N., Z. Younossi, J.E. Lavine, A.M. Diehl, E.M. Brunt, K. Cusi, M. Charlton, A.J. Sanyal, A. American Gastroenterological, D. American Association for the Study of Liver, and G. American College of, *The diagnosis and management of non-alcoholic fatty liver disease: practice guideline by the American Gastroenterological Association, American Association for the Study of Liver Diseases, and American College of Gastroenterology.* Gastroenterology, 2012. **142**(7): p. 1592-609.
7. Weisberg, S.P., D. McCann, M. Desai, M. Rosenbaum, R.L. Leibel, and A.W. Ferrante, Jr., *Obesity is associated with macrophage accumulation in adipose tissue.* J Clin Invest, 2003. **112**(12): p. 1796-808.

8. Uysal, K.T., S.M. Wiesbrock, M.W. Marino, and G.S. Hotamisligil, *Protection from obesity-induced insulin resistance in mice lacking TNF-alpha function.* Nature, 1997. **389**(6651): p. 610-4.

9. Fu, S., S.M. Watkins, and G.S. Hotamisligil, *The role of endoplasmic reticulum in hepatic lipid homeostasis and stress signaling.* Cell Metab, 2012. **15**(5): p. 623-34.

10. Ricchi, M., M.R. Odoardi, L. Carulli, C. Anzivino, S. Ballestri, A. Pinetti, L.I. Fantoni, F. Marra, M. Bertolotti, S. Banni, A. Lonardo, N. Carulli, and P. Loria, *Differential effect of oleic and palmitic acid on lipid accumulation and apoptosis in cultured hepatocytes.* J Gastroenterol Hepatol, 2009. **24**(5): p. 830-40.

11. Brenner, C., L. Galluzzi, O. Kepp, and G. Kroemer, *Decoding cell death signals in liver inflammation.* J Hepatol, 2013. **59**(3): p. 583-94.

12. Bedossa, P. and K. Patel, *Biopsy and Non-invasive Methods to Assess Progression of Nonalcoholic Fatty Liver Disease.* Gastroenterology, 2016.

13. Kleiner, D.E., E.M. Brunt, M. Van Natta, C. Behling, M.J. Contos, O.W. Cummings, L.D. Ferrell, Y.C. Liu, M.S. Torbenson, A. Unalp-Arida, M. Yeh, A.J. McCullough, A.J. Sanyal, and N. Nonalcoholic Steatohepatitis Clinical Research, *Design and validation of a histological scoring system for nonalcoholic fatty liver disease.* Hepatology, 2005. **41**(6): p. 1313-21.

14. Malik, R., M. Chang, K. Bhaskar, I. Nasser, M. Curry, D. Schuppan, V. Byrnes, and N. Afdhal, *The clinical utility of biomarkers and the nonalcoholic steatohepatitis CRN liver biopsy scoring system in patients with nonalcoholic fatty liver disease.* J Gastroenterol Hepatol, 2009. **24**(4): p. 564-8.

15. Becker, P.P., M. Rau, J. Schmitt, C. Malsch, C. Hammer, H. Bantel, B. Mullhaupt, and A. Geier, *Performance of Serum microRNAs -122, -192 and -21*

as Biomarkers in Patients with Non-Alcoholic Steatohepatitis. PLoS One, 2015. **10**(11): p. e0142661.

16. Jamali, R., A. Arj, M. Razavizade, and M.H. Aarabi, *Prediction of Nonalcoholic Fatty Liver Disease Via a Novel Panel of Serum Adipokines.* Medicine (Baltimore), 2016. **95**(5): p. e2630.
17. Bahcecioglu, I.H., M. Yalniz, H. Ataseven, N. Ilhan, I.H. Ozercan, D. Seckin, and K. Sahin, *Levels of serum hyaluronic acid, TNF-alpha and IL-8 in patients with nonalcoholic steatohepatitis.* Hepatogastroenterology, 2005. **52**(65): p. 1549-53.
18. Promrat, K., D.E. Kleiner, H.M. Niemeier, E. Jackvony, M. Kearns, J.R. Wands, J.L. Fava, and R.R. Wing, *Randomized controlled trial testing the effects of weight loss on nonalcoholic steatohepatitis.* Hepatology, 2010. **51**(1): p. 121-9.
19. Harrison, S.A., W. Fecht, E.M. Brunt, and B.A. Neuschwander-Tetri, *Orlistat for overweight subjects with nonalcoholic steatohepatitis: A randomized, prospective trial.* Hepatology, 2009. **49**(1): p. 80-6.
20. Zhang, Y., J. Nicholatos, J.R. Dreier, S.J. Ricoult, S.B. Widenmaier, G.S. Hotamisligil, D.J. Kwiatkowski, and B.D. Manning, *Coordinated regulation of protein synthesis and degradation by mTORC1.* Nature, 2014. **513**(7518): p. 440-3.
21. Singh, S., A.M. Allen, Z. Wang, L.J. Prokop, M.H. Murad, and R. Loomba, *Fibrosis progression in nonalcoholic fatty liver vs nonalcoholic steatohepatitis: a systematic review and meta-analysis of paired-biopsy studies.* Clin Gastroenterol Hepatol, 2015. **13**(4): p. 643-54 e1-9; quiz e39-40.
22. Malhi, H. and R.J. Kaufman, *Endoplasmic reticulum stress in liver disease.* J Hepatol, 2011. **54**(4): p. 795-809.
23. Walter, P. and D. Ron, *The unfolded protein response: from stress pathway to homeostatic regulation.* Science, 2011. **334**(6059): p. 1081-6.

24. Bertolotti, A., Y. Zhang, L.M. Hendershot, H.P. Harding, and D. Ron, *Dynamic interaction of BiP and ER stress transducers in the unfolded protein response.* Nat Cell Biol, 2000. **2**: p. 326-332.

25. Credle, J.J., J.S. Finer-Moore, F.R. Papa, R.M. Stroud, and P. Walter, *On the mechanism of sensing unfolded protein in the endoplasmic reticulum.* Proc Natl Acad Sci U S A, 2005. **102**(52): p. 18773-84.

26. Ye, J., R.B. Rawson, R. Komuro, X. Chen, U.P. Dave, R. Prywes, M.S. Brown, and J.L. Goldstein, *ER stress induces cleavage of membrane-bound ATF6 by the same proteases that process SREBPs.* Mol Cell, 2000. **6**(6): p. 1355-64.

27. Yoshida, H., T. Okada, K. Haze, H. Yanagi, T. Yura, M. Negishi, and K. Mori, *ATF6 activated by proteolysis binds in the presence of NF-Y (CBF) directly to the cis-acting element responsible for the mammalian unfolded protein response.* Mol Cell Biol, 2000. **20**(18): p. 6755-67.

28. Thuerauf, D.J., M. Marcinko, P.J. Belmont, and C.C. Glembotski, *Effects of the isoform-specific characteristics of ATF6 alpha and ATF6 beta on endoplasmic reticulum stress response gene expression and cell viability.* J Biol Chem, 2007. **282**(31): p. 22865-78.

29. Bertolotti, A., X. Wang, I. Novoa, R. Jungreis, K. Schlessinger, J.H. Cho, A.B. West, and D. Ron, *Increased sensitivity to dextran sodium sulfate colitis in IRE1beta-deficient mice.* J Clin Invest, 2001. **107**(5): p. 585-93.

30. Hetz, C., F. Martinon, D. Rodriguez, and L.H. Glimcher, *The unfolded protein response: integrating stress signals through the stress sensor IRE1alpha.* Physiol Rev, 2011. **91**(4): p. 1219-43.

31. Hetz, C. and L.H. Glimcher, *Fine-tuning of the unfolded protein response: Assembling the IRE1alpha interactome.* Mol Cell, 2009. **35**(5): p. 551-61.

32. Uemura, A., M. Oku, K. Mori, and H. Yoshida, *Unconventional splicing of XBP1 mRNA occurs in the cytoplasm during the mammalian unfolded protein response.* J Cell Sci, 2009. **122**(Pt 16): p. 2877-86.

33. Jurkin, J., T. Henkel, A.F. Nielsen, M. Minnich, J. Popow, T. Kaufmann, K. Heindl, T. Hoffmann, M. Busslinger, and J. Martinez, *The mammalian tRNA ligase complex mediates splicing of XBP1 mRNA and controls antibody secretion in plasma cells.* EMBO J, 2014. **33**(24): p. 2922-36.

34. Hollien, J., J.H. Lin, H. Li, N. Stevens, P. Walter, and J.S. Weissman, *Regulated Ire1-dependent decay of messenger RNAs in mammalian cells.* J Cell Biol, 2009. **186**(3): p. 323-31.

35. Urano, F., X. Wang, A. Bertolotti, Y. Zhang, P. Chung, H.P. Harding, and D. Ron, *Coupling of stress in the ER to activation of JNK protein kinases by transmembrane protein kinase IRE1.* Science, 2000. **287**(5453): p. 664-6.

36. Baird, T.D. and R.C. Wek, *Eukaryotic initiation factor 2 phosphorylation and translational control in metabolism.* Adv Nutr, 2012. **3**(3): p. 307-21.

37. Lee, K., W. Tirasophon, X. Shen, M. Michalak, R. Prywes, T. Okada, H. Yoshida, K. Mori, and R.J. Kaufman, *IRE1-mediated unconventional mRNA splicing and S2P-mediated ATF6 cleavage merge to regulate XBP1 in signaling the unfolded protein response.* Genes Dev, 2002. **16**: p. 452-466.

38. Teske, B.F., S.A. Wek, P. Bunpo, J.K. Cundiff, J.N. McClintick, T.G. Anthony, and R.C. Wek, *The eIF2 kinase PERK and the integrated stress response facilitate activation of ATF6 during endoplasmic reticulum stress.* Mol Biol Cell, 2011. **22**: p. 4390-405.

39. Fusakio, M.E., J.A. Willy, Y. Wang, E.T. Mirek, R.J. Baghdadi, C.M. Adams, T.G. Anthony, and R.C. Wek, *Transcription factor ATF4 directs basal and select*

induced gene expression in the unfolded protein response and cholesterol metabolism in liver. Mol Biol Cell, 2016.

40. Ma, Y., J.W. Brewer, J.A. Diehl, and L.M. Hendershot, *Two distinct stress signaling pathways converge upon the CHOP promoter during the mammalian unfolded protein response.* J Mol Biol, 2002. **318**(5): p. 1351-65.
41. Yamamoto, K., H. Yoshida, K. Kokame, R.J. Kaufman, and K. Mori, *Differential contributions of ATF6 and XBP1 to the activation of endoplasmic reticulum stress-responsive cis-acting elements ERSE, UPRE and ERSE-II.* J Biochem, 2004. **136**(3): p. 343-50.
42. Su, N. and M.S. Kilberg, *C/EBP homology protein (CHOP) interacts with activating transcription factor 4 (ATF4) and negatively regulates the stress-dependent induction of the asparagine synthetase gene.* J Biol Chem, 2008. **283**(50): p. 35106-17.
43. Yamamoto, K., T. Sato, T. Matsui, M. Sato, T. Okada, H. Yoshida, A. Harada, and K. Mori, *Transcriptional induction of mammalian ER quality control proteins is mediated by single or combined action of ATF6alpha and XBP1.* Dev Cell, 2007. **13**(3): p. 365-76.
44. Hoyer-Hansen, M. and M. Jaattela, *Connecting endoplasmic reticulum stress to autophagy by unfolded protein response and calcium.* Cell Death Differ, 2007. **14**(9): p. 1576-82.
45. Harding, H.P., Y. Zhang, H. Zeng, I. Novoa, P.D. Lu, M. Calfon, N. Sadri, C. Yun, B. Popko, R. Paules, D.F. Stojdl, J.C. Bell, T. Hettmann, J.M. Leiden, and D. Ron, *An integrated stress response regulates amino acid metabolism and resistance to oxidative stress.* Mol Cell, 2003. **11**: p. 619-33.
46. Tabas, I. and D. Ron, *Integrating the mechanisms of apoptosis induced by endoplasmic reticulum stress.* Nat Cell Biol, 2011. **13**(3): p. 184-90.

47. Willy, J.A., S.K. Young, J.L. Stevens, H.C. Masuoka, and R.C. Wek, *CHOP Links Endoplasmic Reticulum Stress to NF-kappaB Activation in the Pathogenesis of Nonalcoholic Steatohepatitis.* Mol Biol Cell, 2015.

48. Teske, B.F., M.E. Fusakio, D. Zhou, J. Shan, J.N. McClintick, M.S. Kilberg, and R.C. Wek, *CHOP induces activating transcription factor 5 (ATF5) to trigger apoptosis in response to perturbations in protein homeostasis.* Mol Biol Cell, 2013. **24**(15): p. 2477-90.

49. Lake, A.D., P. Novak, R.N. Hardwick, B. Flores-Keown, F. Zhao, W.T. Klimecki, and N.J. Cherrington, *The adaptive endoplasmic reticulum stress response to lipotoxicity in progressive human nonalcoholic fatty liver disease.* Toxicol Sci, 2014. **137**(1): p. 26-35.

50. Gonzalez-Rodriguez, A., R. Mayoral, N. Agra, M.P. Valdecantos, V. Pardo, M.E. Miquilena-Colina, J. Vargas-Castrillon, O. Lo Iacono, M. Corazzari, G.M. Fimia, M. Piacentini, J. Muntane, L. Bosca, C. Garcia-Monzon, P. Martin-Sanz, and A.M. Valverde, *Impaired autophagic flux is associated with increased endoplasmic reticulum stress during the development of NAFLD.* Cell Death Dis, 2014. **5**: p. e1179.

51. Volmer, R., K. van der Ploeg, and D. Ron, *Membrane lipid saturation activates endoplasmic reticulum unfolded protein response transducers through their transmembrane domains.* Proc Natl Acad Sci U S A, 2013. **110**(12): p. 4628-33.

52. Kitai, Y., H. Ariyama, N. Kono, D. Oikawa, T. Iwawaki, and H. Arai, *Membrane lipid saturation activates IRE1alpha without inducing clustering.* Genes Cells, 2013. **18**(9): p. 798-809.

53. Hetz, C., *The unfolded protein response: controlling cell fate decisions under ER stress and beyond.* Nat Rev Mol Cell Biol, 2012. **13**(2): p. 89-102.

54. Fusakio, M.E., J.A. Willy, Y. Wang, E.T. Mirek, R.J. Al Baghdadi, C.M. Adams, T.G. Anthony, and R.C. Wek, Mol Biol Cell, 2016. **27**(9): p. 1536-51.

55. Barbosa-Tessmann, I.P., C. Chen, C. Zhong, F. Siu, S.M. Schuster, H.S. Nick, and M.S. Kilberg, *Activation of the human asparagine synthetase gene by the amino acid response and the endoplasmic reticulum stress response pathways occurs by common genomic elements.* J Biol Chem, 2000. **275**(35): p. 26976-85.

56. B'Chir, W., A.C. Maurin, V. Carraro, J. Averous, C. Jousse, Y. Muranishi, L. Parry, G. Stepien, P. Fafournoux, and A. Bruhat, *The eIF2alpha/ATF4 pathway is essential for stress-induced autophagy gene expression.* Nucleic Acids Res, 2013. **41**(16): p. 7683-99.

57. Li, J., B. Lee, and A.S. Lee, *Endoplasmic reticulum stress-induced apoptosis: multiple pathways and activation of p53-up-regulated modulator of apoptosis (PUMA) and NOXA by p53.* J Biol Chem, 2006. **281**(11): p. 7260-70.

58. Marciniak, S.J. and D. Ron, *Endoplasmic reticulum stress signaling in disease.* Physiol Rev, 2006. **86**(4): p. 1133-49.

59. Malhi, H., E.M. Kropp, V.F. Clavo, C.R. Kobrossi, J. Han, A.S. Mauer, J. Yong, and R.J. Kaufman, *C/EBP homologous protein-induced macrophage apoptosis protects mice from steatohepatitis.* J Biol Chem, 2013. **288**(26): p. 18624-42.

60. Rahman, S.M., J.M. Schroeder-Gloeckler, R.C. Janssen, H. Jiang, I. Qadri, K.N. Maclean, and J.E. Friedman, *CCAAT/enhancing binding protein beta deletion in mice attenuates inflammation, endoplasmic reticulum stress, and lipid accumulation in diet-induced nonalcoholic steatohepatitis.* Hepatology, 2007. **45**(5): p. 1108-17.

61. Schwanhausser, B., D. Busse, N. Li, G. Dittmar, J. Schuchhardt, J. Wolf, W. Chen, and M. Selbach, *Global quantification of mammalian gene expression control.* Nature, 2011. **473**(7347): p. 337-42.

62. Harding, H.P., I. Novoa, Y. Zhang, H. Zeng, R. Wek, M. Schapira, and D. Ron, *Regulated translation initiation controls stress-induced gene expression in mammalian cells.* Mol Cell, 2000. **6**: p. 1099-108.

63. Hinnebusch, A.G., R.C. Wek, T.E. Dever, A.M. Cigan, F. Feng, and T.F. Donahue, *Regulation of GCN4 expression in yeast. Gene specific translation control by phosphorylation of eIF-2a*, in *Translation Regulation of Gene Expression*, J. Ilan, Editor 1993, Plenum Press: New York. p. pp. 87-115.

64. Dey, S., T.D. Baird, D. Zhou, L.R. Palam, D.F. Spandau, and R.C. Wek, *Both transcriptional regulation and translational control of ATF4 are central to the integrated stress response.* J Biol Chem, 2010. **285**(43): p. 33165-74.

65. Palam, L.R., T.D. Baird, and R.C. Wek, *Phosphorylation of eIF2 facilitates ribosomal bypass of an inhibitory upstream ORF to enhance CHOP translation.* J Biol Chem, 2011. **286**(13): p. 10939-49.

66. Baird, T.D., L.R. Palam, M.E. Fusakio, J.A. Willy, C.M. Davis, J.N. McClintick, T.G. Anthony, and R.C. Wek, *Selective mRNA translation during eIF2 phosphorylation induces expression of IBTKalpha.* Mol Biol Cell, 2014. **25**(10): p. 1686-97.

67. Jin, L., K.B. Pahuja, K.E. Wickliffe, A. Gorur, C. Baumgartel, R. Schekman, and M. Rape, *Ubiquitin-dependent regulation of COPII coat size and function.* Nature, 2012. **482**(7386): p. 495-500.

68. Pisano, A., S. Ceglia, C. Palmieri, E. Vecchio, G. Fiume, A. de Laurentiis, S. Mimmi, C. Falcone, E. Iaccino, A. Scialdone, M. Pontoriero, F.F. Masci, R. Valea, S. Krishnan, M. Gaspari, G. Cuda, G. Scala, and I. Quinto, *CRL3IBTK Regulates the Tumor Suppressor Pdcd4 through Ubiquitylation Coupled to Proteasomal Degradation.* J Biol Chem, 2015. **290**(22): p. 13958-71.

69. Knight, B., V.B. Matthews, B. Akhurst, E.J. Croager, E. Klinken, L.J. Abraham, J.K. Olynyk, and G. Yeoh, *Liver inflammation and cytokine production, but not acute phase protein synthesis, accompany the adult liver progenitor (oval) cell response to chronic liver injury.* Immunol Cell Biol, 2005. **83**(4): p. 364-74.

70. Rao, K.M., *MAP kinase activation in macrophages.* J Leukoc Biol, 2001. **69**(1): p. 3-10.

71. Ip, Y.T. and R.J. Davis, *Signal transduction by the c-Jun N-terminal kinase (JNK)--from inflammation to development.* Curr Opin Cell Biol, 1998. **10**(2): p. 205-19.

72. Lawrence, T., *The nuclear factor NF-kappaB pathway in inflammation.* Cold Spring Harb Perspect Biol, 2009. **1**(6): p. a001651.

73. Igoillo-Esteve, M., L. Marselli, D.A. Cunha, L. Ladriere, F. Ortis, F.A. Grieco, F. Dotta, G.C. Weir, P. Marchetti, D.L. Eizirik, and M. Cnop, *Palmitate induces a pro-inflammatory response in human pancreatic islets that mimics CCL2 expression by beta cells in type 2 diabetes.* Diabetologia, 2010. **53**(7): p. 1395-405.

74. Huang, W., A. Metlakunta, N. Dedousis, P. Zhang, I. Sipula, J.J. Dube, D.K. Scott, and R.M. O'Doherty, *Depletion of liver Kupffer cells prevents the development of diet-induced hepatic steatosis and insulin resistance.* Diabetes, 2010. **59**(2): p. 347-57.

75. Baffy, G., *Kupffer cells in non-alcoholic fatty liver disease: the emerging view.* J Hepatol, 2009. **51**(1): p. 212-23.

76. Xu, C.F., C.H. Yu, Y.M. Li, L. Xu, J. Du, and Z. Shen, *Association of the frequency of peripheral natural killer T cells with nonalcoholic fatty liver disease.* World J Gastroenterol, 2007. **13**(33): p. 4504-8.

77. Kremer, M., I.N. Hines, R.J. Milton, and M.D. Wheeler, *Favored T helper 1 response in a mouse model of hepatosteatosis is associated with enhanced T cell-mediated hepatitis.* Hepatology, 2006. **44**(1): p. 216-27.

78. Garg, A.D., A. Kaczmarek, O. Krysko, P. Vandenabeele, D.V. Krysko, and P. Agostinis, *ER stress-induced inflammation: does it aid or impede disease progression?* Trends Mol Med, 2012. **18**(10): p. 589-98.

79. Hotamisligil, G.S., *Inflammation and metabolic disorders.* Nature, 2006. **444**(7121): p. 860-7.

80. Hummasti, S. and G.S. Hotamisligil, *Endoplasmic reticulum stress and inflammation in obesity and diabetes.* Circ Res, 2010. **107**(5): p. 579-91.

81. Anderson, J.M., A. Rodriguez, and D.T. Chang, *Foreign body reaction to biomaterials.* Semin Immunol, 2008. **20**(2): p. 86-100.

82. Jiang, H.Y., S.A. Wek, B.C. McGrath, D. Scheuner, R.J. Kaufmann, D.R. Cavener, and R.C. Wek, *Phosphorylation of the a subunit of eukaryotic initiation factor 2 is required for activation of NF-kB in response to diverse cellular stress.* Mol Cell Biol, 2003. **23**: p. 5651-63.

83. Davis, R.J., *Signal transduction by the JNK group of MAP kinases.* Cell, 2000. **103**: p. 239-252.

84. Dong, C., R.J. Davis, and R.A. Flavell, *Signaling by the JNK group of MAP kinases. c-jun N-terminal Kinase.* Journal of Clinical Immunology, 2001. **21**: p. 253-257.

85. Weston, C.R. and R.J. Davis, *The JNK signal transduction pathway.* Curr Opin Genet Dev, 2002. **12**(1): p. 14-21.

86. Gilmore, T.D., *Introduction to NF-kappaB: players, pathways, perspectives.* Oncogene, 2006. **25**(51): p. 6680-4.

87. Sasaki, C.Y., T.J. Barberi, P. Ghosh, and D.L. Longo, *Phosphorylation of RelA/p65 on serine 536 defines an I{kappa}B{alpha}-independent NF-{kappa}B pathway.* J Biol Chem, 2005. **280**(41): p. 34538-47.

88. Viatour, P., M.P. Merville, V. Bours, and A. Chariot, *Phosphorylation of NF-kappaB and IkappaB proteins: implications in cancer and inflammation.* Trends Biochem Sci, 2005. **30**(1): p. 43-52.

89. Hommelberg, P.P., J. Plat, R.C. Langen, A.M. Schols, and R.P. Mensink, *Fatty acid-induced NF-kappaB activation and insulin resistance in skeletal muscle are chain length dependent.* Am J Physiol Endocrinol Metab, 2009. **296**(1): p. E114-20.

90. Papa, S., F. Zazzeroni, C.G. Pham, C. Bubici, and G. Franzoso, *Linking JNK signaling to NF-kappaB: a key to survival.* J Cell Sci, 2004. **117**(Pt 22): p. 5197-208.

91. Levine, B. and G. Kroemer, *Autophagy in the pathogenesis of disease.* Cell, 2008. **132**(1): p. 27-42.

92. He, C. and D.J. Klionsky, *Regulation mechanisms and signaling pathways of autophagy.* Annu Rev Genet, 2009. **43**: p. 67-93.

93. Klionsky, D.J., P. Codogno, A.M. Cuervo, V. Deretic, Z. Elazar, J. Fueyo-Margareto, D.A. Gewirtz, G. Kroemer, B. Levine, N. Mizushima, D.C. Rubinsztein, M. Thumm, and S.A. Tooze, *A comprehensive glossary of autophagy-related molecules and processes.* Autophagy, 2010. **6**(4): p. 438-48.

94. Russell, R.C., Y. Tian, H. Yuan, H.W. Park, Y.Y. Chang, J. Kim, H. Kim, T.P. Neufeld, A. Dillin, and K.L. Guan, *ULK1 induces autophagy by phosphorylating Beclin-1 and activating VPS34 lipid kinase.* Nat Cell Biol, 2013. **15**(7): p. 741-50.

95. Satoo, K., N.N. Noda, H. Kumeta, Y. Fujioka, N. Mizushima, Y. Ohsumi, and F. Inagaki, *The structure of Atg4B-LC3 complex reveals the mechanism of LC3 processing and delipidation during autophagy.* EMBO J, 2009. **28**(9): p. 1341-50.

96. Kirisako, T., Y. Ichimura, H. Okada, Y. Kabeya, N. Mizushima, T. Yoshimori, M. Ohsumi, T. Takao, T. Noda, and Y. Ohsumi, *The reversible modification regulates the membrane-binding state of Apg8/Aut7 essential for autophagy and the cytoplasm to vacuole targeting pathway.* J Cell Biol, 2000. **151**(2): p. 263-76.

97. Geng, J. and D.J. Klionsky, *The Atg8 and Atg12 ubiquitin-like conjugation systems in macroautophagy. 'Protein modifications: beyond the usual suspects' review series.* EMBO Rep, 2008. **9**(9): p. 859-64.

98. Ichimura, Y., T. Kumanomidou, Y.S. Sou, T. Mizushima, J. Ezaki, T. Ueno, E. Kominami, T. Yamane, K. Tanaka, and M. Komatsu, *Structural basis for sorting mechanism of p62 in selective autophagy.* J Biol Chem, 2008. **283**(33): p. 22847-57.

99. Noda, N.N., Y. Ohsumi, and F. Inagaki, *Atg8-family interacting motif crucial for selective autophagy.* FEBS Lett, 2010. **584**(7): p. 1379-85.

100. Graef, M., J.R. Friedman, C. Graham, M. Babu, and J. Nunnari, *ER exit sites are physical and functional core autophagosome biogenesis components.* Mol Biol Cell, 2013. **24**(18): p. 2918-31.

101. Ishihara, N., M. Hamasaki, S. Yokota, K. Suzuki, Y. Kamada, A. Kihara, T. Yoshimori, T. Noda, and Y. Ohsumi, *Autophagosome requires specific early Sec proteins for its formation and NSF/SNARE for vacuolar fusion.* Mol Biol Cell, 2001. **12**(11): p. 3690-702.

102. Reggiori, F., C.W. Wang, U. Nair, T. Shintani, H. Abeliovich, and D.J. Klionsky, *Early stages of the secretory pathway, but not endosomes, are required for Cvt*

vesicle and autophagosome assembly in Saccharomyces cerevisiae. Mol Biol Cell, 2004. **15**(5): p. 2189-204.

103. Kouroku, Y., E. Fujita, I. Tanida, T. Ueno, A. Isoai, H. Kumagai, S. Ogawa, R.J. Kaufman, E. Kominami, and T. Momoi, *ER stress (PERK/eIF2alpha phosphorylation) mediates the polyglutamine-induced LC3 conversion, an essential step for autophagy formation.* Cell Death Differ, 2007. **14**(2): p. 230-9.

104. Ding, W.X., H.M. Ni, W. Gao, Y.F. Hou, M.A. Melan, X. Chen, D.B. Stolz, Z.M. Shao, and X.M. Yin, *Differential effects of endoplasmic reticulum stress-induced autophagy on cell survival.* J Biol Chem, 2007. **282**(7): p. 4702-10.

105. Ogata, M., S. Hino, A. Saito, K. Morikawa, S. Kondo, S. Kanemoto, T. Murakami, M. Taniguchi, I. Tanii, K. Yoshinaga, S. Shiosaka, J.A. Hammarback, F. Urano, and K. Imaizumi, *Autophagy is activated for cell survival after endoplasmic reticulum stress.* Mol Cell Biol, 2006. **26**(24): p. 9220-31.

106. Ganley, I.G., P.M. Wong, N. Gammoh, and X. Jiang, *Distinct autophagosomal-lysosomal fusion mechanism revealed by thapsigargin-induced autophagy arrest.* Mol Cell, 2011. **42**(6): p. 731-43.

107. Deretic, V., T. Saitoh, and S. Akira, *Autophagy in infection, inflammation and immunity.* Nat Rev Immunol, 2013. **13**(10): p. 722-37.

108. Green, D.R., L. Galluzzi, and G. Kroemer, *Mitochondria and the autophagy-inflammation-cell death axis in organismal aging.* Science, 2011. **333**(6046): p. 1109-12.

109. Liu, Y. and B. Levine, *Autosis and autophagic cell death: the dark side of autophagy.* Cell Death Differ, 2015. **22**(3): p. 367-376.

110. Goldberg, A.L. and J.F. Dice, *Intracellular protein degradation in mammalian and bacterial cells.* Annu Rev Biochem, 1974. **43**(0): p. 835-69.

111. Scheffner, M., U. Nuber, and J.M. Huibregtse, *Protein ubiquitination involving an E1-E2-E3 enzyme ubiquitin thioester cascade.* Nature, 1995. **373**(6509): p. 81-3.

112. Ravid, T. and M. Hochstrasser, *Diversity of degradation signals in the ubiquitin-proteasome system.* Nat Rev Mol Cell Biol, 2008. **9**(9): p. 679-90.

113. Wilkinson, C.R., M. Seeger, R. Hartmann-Petersen, M. Stone, M. Wallace, C. Semple, and C. Gordon, *Proteins containing the UBA domain are able to bind to multi-ubiquitin chains.* Nat Cell Biol, 2001. **3**(10): p. 939-43.

114. Hershko, A., A. Ciechanover, H. Heller, A.L. Haas, and I.A. Rose, *Proposed role of ATP in protein breakdown: conjugation of protein with multiple chains of the polypeptide of ATP-dependent proteolysis.* Proc Natl Acad Sci U S A, 1980. **77**(4): p. 1783-6.

115. Kisselev, A.F., T.N. Akopian, V. Castillo, and A.L. Goldberg, *Proteasome active sites allosterically regulate each other, suggesting a cyclical bite-chew mechanism for protein breakdown.* Mol Cell, 1999. **4**(3): p. 395-402.

116. Shang, F. and A. Taylor, *Ubiquitin-proteasome pathway and cellular responses to oxidative stress.* Free Radic Biol Med, 2011. **51**(1): p. 5-16.

117. Zhang, D.D., *Mechanistic studies of the Nrf2-Keap1 signaling pathway.* Drug Metab Rev, 2006. **38**(4): p. 769-89.

118. Malhotra, D., R. Thimmulappa, N. Vij, A. Navas-Acien, T. Sussan, S. Merali, L. Zhang, S.G. Kelsen, A. Myers, R. Wise, R. Tuder, and S. Biswal, *Heightened endoplasmic reticulum stress in the lungs of patients with chronic obstructive pulmonary disease: the role of Nrf2-regulated proteasomal activity*. Am J Respir Crit Care Med, 2009. **180**(12): p. 1196-207.

119. Kwak, M.K., N. Wakabayashi, J.L. Greenlaw, M. Yamamoto, and T.W. Kensler, *Antioxidants enhance mammalian proteasome expression through the Keap1-Nrf2 signaling pathway.* Mol Cell Biol, 2003. **23**(23): p. 8786-94.

120. Meakin, P.J., S. Chowdhry, R.S. Sharma, F.B. Ashford, S.V. Walsh, R.J. McCrimmon, A.T. Dinkova-Kostova, J.F. Dillon, J.D. Hayes, and M.L. Ashford, *Susceptibility of Nrf2-null mice to steatohepatitis and cirrhosis upon consumption of a high-fat diet is associated with oxidative stress, perturbation of the unfolded protein response, and disturbance in the expression of metabolic enzymes but not with insulin resistance.* Mol Cell Biol, 2014. **34**(17): p. 3305-20.

121. Oyadomari, S., C. Yun, E.A. Fisher, N. Kreglinger, G. Kreibich, M. Oyadomari, H.P. Harding, A.G. Goodman, H. Harant, J.L. Garrison, J. Taunton, M.G. Katze, and D. Ron, *Cotranslocational degradation protects the stressed endoplasmic reticulum from protein overload.* Cell, 2006. **126**(4): p. 727-39.

122. Vembar, S.S. and J.L. Brodsky, *One step at a time: endoplasmic reticulum-associated degradation.* Nat Rev Mol Cell Biol, 2008. **9**(12): p. 944-57.

123. Cullinan, S.B., D. Zhang, M. Hannink, E. Arvisais, R.J. Kaufman, and J.A. Diehl, *Nrf2 is a direct PERK substrate and effector of PERK-dependent cell survival.* Molecular and Cellular Biology, 2003. **23**: p. 7198-7209.

124. Jemal, A., F. Bray, M.M. Center, J. Ferlay, E. Ward, and D. Forman, *Global cancer statistics.* CA Cancer J Clin, 2011. **61**(2): p. 69-90.

125. El-Serag, H.B., *Hepatocellular carcinoma.* N Engl J Med, 2011. **365**(12): p. 1118-27.

126. Stickel, F. and C. Hellerbrand, *Non-alcoholic fatty liver disease as a risk factor for hepatocellular carcinoma: mechanisms and implications.* Gut, 2010. **59**(10): p. 1303-7.

127. Baffy, G., E.M. Brunt, and S.H. Caldwell, *Hepatocellular carcinoma in non-alcoholic fatty liver disease: an emerging menace.* J Hepatol, 2012. **56**(6): p. 1384-91.

128. Maeda, S., *NF-kappaB, JNK, and TLR Signaling Pathways in Hepatocarcinogenesis.* Gastroenterol Res Pract, 2010. **2010**: p. 367694.

129. Yang, Z.J., C.E. Chee, S. Huang, and F.A. Sinicrope, *The role of autophagy in cancer: therapeutic implications.* Mol Cancer Ther, 2011. **10**(9): p. 1533-41.

130. Pan, H., Z. Wang, L. Jiang, X. Sui, L. You, J. Shou, Z. Jing, J. Xie, W. Ge, X. Cai, W. Huang, and W. Han, *Autophagy inhibition sensitizes hepatocellular carcinoma to the multikinase inhibitor linifanib.* Sci Rep, 2014. **4**: p. 6683.

131. Scaiewicz, V., A. Nahmias, R.T. Chung, T. Mueller, B. Tirosh, and O. Shibolet, *CCAAT/enhancer-binding protein homologous (CHOP) protein promotes carcinogenesis in the DEN-induced hepatocellular carcinoma model.* PLoS One, 2013. **8**(12): p. e81065.

132. Zhang, Y., R. Xue, Z. Zhang, X. Yang, and H. Shi, *Palmitic and linoleic acids induce ER stress and apoptosis in hepatoma cells.* Lipids Health Dis, 2012. **11**: p. 1.

133. Wang, D., Y. Wei, and M.J. Pagliassotti, *Saturated fatty acids promote endoplasmic reticulum stress and liver injury in rats with hepatic steatosis.* Endocrinology, 2006. **147**(2): p. 943-51.

134. Amir, M. and M.J. Czaja, *Autophagy in nonalcoholic steatohepatitis.* Expert Rev Gastroenterol Hepatol, 2011. **5**(2): p. 159-66.

135. Chen, Q., T.W. Jones, P.C. Brown, and J.L. Stevens, *The mechanism of cysteine conjugate cytotoxicity in renal epithelial cells. Covalent binding leads to thiol depletion and lipid peroxidation.* J Biol Chem, 1990. **265**(35): p. 21603-11.

136. Mahadevan, N.R., J. Rodvold, H. Sepulveda, S. Rossi, A.F. Drew, and M. Zanetti, *Transmission of endoplasmic reticulum stress and pro-inflammation from tumor cells to myeloid cells.* Proc Natl Acad Sci U S A, 2011. **108**(16): p. 6561-6.

137. Jandu, N., P.J. Ceponis, S. Kato, J.D. Riff, D.M. McKay, and P.M. Sherman, *Conditioned medium from enterohemorrhagic Escherichia coli-infected T84 cells inhibits signal transducer and activator of transcription 1 activation by gamma interferon.* Infect Immun, 2006. **74**(3): p. 1809-18.

138. Berry, M.N. and D.S. Friend, *High-yield preparation of isolated rat liver parenchymal cells: a biochemical and fine structural study.* J Cell Biol, 1969. **43**(3): p. 506-20.

139. Seglen, P.O., *Preparation of rat liver cells. I. Effect of Ca 2+ on enzymatic dispersion of isolated, perfused liver.* Exp Cell Res, 1972. **74**(2): p. 450-4.

140. Teske, B.F., T.D. Baird, and R.C. Wek, *Methods for analyzing eIF2 kinases and translational control in the unfolded protein response.* Methods Enzymol, 2011. **490**: p. 333-56.

141. Lu, T., S.S. Sathe, S.M. Swiatkowski, C.V. Hampole, and G.R. Stark, *Secretion of cytokines and growth factors as a general cause of constitutive NFkappaB activation in cancer.* Oncogene, 2004. **23**(12): p. 2138-45.

142. Larter, C.Z. and M.M. Yeh, *Animal models of NASH: getting both pathology and metabolic context right.* J Gastroenterol Hepatol, 2008. **23**(11): p. 1635-48.

143. Takahashi, Y., Y. Soejima, and T. Fukusato, *Animal models of nonalcoholic fatty liver disease/nonalcoholic steatohepatitis.* World J Gastroenterol, 2012. **18**(19): p. 2300-8.

144. Charlton, M., A. Krishnan, K. Viker, S. Sanderson, S. Cazanave, A. McConico, H. Masuoko, and G. Gores, *Fast food diet mouse: novel small animal model of NASH with ballooning, progressive fibrosis, and high physiological fidelity to the human condition.* Am J Physiol Gastrointest Liver Physiol, 2011. **301**(5): p. G825-34.

145. Listenberger, L.L., X. Han, S.E. Lewis, S. Cases, R.V. Farese, Jr., D.S. Ory, and J.E. Schaffer, *Triglyceride accumulation protects against fatty acid-induced lipotoxicity.* Proc Natl Acad Sci U S A, 2003. **100**(6): p. 3077-82.

146. Koutsari, C. and M.D. Jensen, *Thematic review series: patient-oriented research. Free fatty acid metabolism in human obesity.* J Lipid Res, 2006. **47**(8): p. 1643-50.

147. Belfort, R., S.A. Harrison, K. Brown, C. Darland, J. Finch, J. Hardies, B. Balas, A. Gastaldelli, F. Tio, J. Pulcini, R. Berria, J.Z. Ma, S. Dwivedi, R. Havranek, C. Fincke, R. DeFronzo, G.A. Bannayan, S. Schenker, and K. Cusi, *A placebo-controlled trial of pioglitazone in subjects with nonalcoholic steatohepatitis.* N Engl J Med, 2006. **355**(22): p. 2297-307.

148. Wek, R.C., H.Y. Jiang, and T.G. Anthony, *Coping with stress: eIF2 kinases and translational control.* Biochem Soc Trans, 2006. **34**(Pt 1): p. 7-11.

149. Napetschnig, J. and H. Wu, *Molecular basis of NF-kappaB signaling.* Annu Rev Biophys, 2013. **42**: p. 443-68.

150. Muzio, M., J. Ni, P. Feng, and V.M. Dixit, *IRAK (Pelle) family member IRAK-2 and MyD88 as proximal mediators of IL-1 signaling.* Science, 1997. **278**(5343): p. 1612-5.

151. Kawagoe, T., S. Sato, K. Matsushita, H. Kato, K. Matsui, Y. Kumagai, T. Saitoh, T. Kawai, O. Takeuchi, and S. Akira, *Sequential control of Toll-like receptor-dependent responses by IRAK1 and IRAK2.* Nat Immunol, 2008. **9**(6): p. 684-91.

152. Wang, H., S.M. Flannery, S. Dickhofer, S. Huhn, J. George, A.V. Kubarenko, J. Lascorz, M. Bevier, J. Willemsen, T. Pichulik, C. Schafmayer, M. Binder, B. Manoury, S.R. Paludan, M. Alarcon-Riquelme, A.G. Bowie, A. Forsti, and A.N. Weber, *A coding IRAK2 protein variant compromises Toll-like receptor (TLR)*

signaling and is associated with colorectal cancer survival. J Biol Chem, 2014. **289**(33): p. 23123-31.

153. Zhang, W., T. He, Q. Wang, X. Li, J. Wei, X. Hou, B. Zhang, L. Huang, and L. Wang, *Interleukin-1 receptor-associated kinase-2 genetic variant rs708035 increases NF-kappaB activity through promoting TRAF6 ubiquitination.* J Biol Chem, 2014. **289**(18): p. 12507-19.

154. Han, J., S.H. Back, J. Hur, Y.H. Lin, R. Gildersleeve, J. Shan, C.L. Yuan, D. Krokowski, S. Wang, M. Hatzoglou, M.S. Kilberg, M.A. Sartor, and R.J. Kaufman, *ER-stress-induced transcriptional regulation increases protein synthesis leading to cell death.* Nat Cell Biol, 2013. **15**(5): p. 481-90.

155. Alkhouri, N., C. Carter-Kent, and A.E. Feldstein, *Apoptosis in nonalcoholic fatty liver disease: diagnostic and therapeutic implications.* Expert Rev Gastroenterol Hepatol, 2011. **5**(2): p. 201-12.

156. Luo, M., Z. Lu, H. Sun, K. Yuan, Q. Zhang, S. Meng, F. Wang, H. Guo, X. Ju, Y. Liu, T. Ye, Z. Lu, and Z. Zhai, *Nuclear entry of active caspase-3 is facilitated by its p3-recognition-based specific cleavage activity.* Cell Res, 2010. **20**(2): p. 211-22.

157. Tooze, S.A. and T. Yoshimori, *The origin of the autophagosomal membrane.* Nat Cell Biol, 2010. **12**(9): p. 831-5.

158. Alemu, E.A., T. Lamark, K.M. Torgersen, A.B. Birgisdottir, K.B. Larsen, A. Jain, H. Olsvik, A. Overvatn, V. Kirkin, and T. Johansen, *ATG8 family proteins act as scaffolds for assembly of the ULK complex: sequence requirements for LC3-interacting region (LIR) motifs.* J Biol Chem, 2012. **287**(47): p. 39275-90.

159. Zanetti, G., K.B. Pahuja, S. Studer, S. Shim, and R. Schekman, *COPII and the regulation of protein sorting in mammals.* Nat Cell Biol, 2012. **14**(1): p. 20-8.

160. Trocoli, A. and M. Djavaheri-Mergny, *The complex interplay between autophagy and NF-kappaB signaling pathways in cancer cells.* Am J Cancer Res, 2011. **1**(5): p. 629-49.

161. Stein, B., P.C. Cogswell, and A.S. Baldwin, Jr., *Functional and physical associations between NF-kappa B and C/EBP family members: a Rel domain-bZIP interaction.* Mol Cell Biol, 1993. **13**(7): p. 3964-74.

162. Chapple, S.J., R.C. Siow, and G.E. Mann, *Crosstalk between Nrf2 and the proteasome: therapeutic potential of Nrf2 inducers in vascular disease and aging.* Int J Biochem Cell Biol, 2012. **44**(8): p. 1315-20.

163. Jang, J., Y. Wang, H.S. Kim, M.A. Lalli, and K.S. Kosik, *Nrf2, a regulator of the proteasome, controls self-renewal and pluripotency in human embryonic stem cells.* Stem Cells, 2014. **32**(10): p. 2616-25.

164. Lee, S., E.G. Hur, I.G. Ryoo, K.A. Jung, J. Kwak, and M.K. Kwak, *Involvement of the Nrf2-proteasome pathway in the endoplasmic reticulum stress response in pancreatic beta-cells.* Toxicol Appl Pharmacol, 2012. **264**(3): p. 431-8.

165. Nguyen, T., P. Nioi, and C.B. Pickett, *The Nrf2-antioxidant response element signaling pathway and its activation by oxidative stress.* J Biol Chem, 2009. **284**(20): p. 13291-5.

166. Nguyen, T., P.J. Sherratt, H.C. Huang, C.S. Yang, and C.B. Pickett, *Increased protein stability as a mechanism that enhances Nrf2-mediated transcriptional activation of the antioxidant response element. Degradation of Nrf2 by the 26 S proteasome.* Journal of Biological Chemistry, 2003. **278**(7): p. 4536-41.

167. Korolchuk, V.I., F.M. Menzies, and D.C. Rubinsztein, *Mechanisms of cross-talk between the ubiquitin-proteasome and autophagy-lysosome systems.* FEBS Lett, 2010. **584**(7): p. 1393-8.

168. Lau, A., X.J. Wang, F. Zhao, N.F. Villeneuve, T. Wu, T. Jiang, Z. Sun, E. White, and D.D. Zhang, *A noncanonical mechanism of Nrf2 activation by autophagy deficiency: direct interaction between Keap1 and p62.* Mol Cell Biol, 2010. **30**(13): p. 3275-85.

169. Sturley, S.L. and M.M. Hussain, *Lipid droplet formation on opposing sides of the endoplasmic reticulum.* J Lipid Res, 2012. **53**(9): p. 1800-10.

170. Ariyama, H., N. Kono, S. Matsuda, T. Inoue, and H. Arai, *Decrease in membrane phospholipid unsaturation induces unfolded protein response.* J Biol Chem, 2010. **285**(29): p. 22027-35.

171. Bezzerri, V., M. Borgatti, A. Finotti, A. Tamanini, R. Gambari, and G. Cabrini, *Mapping the transcriptional machinery of the IL-8 gene in human bronchial epithelial cells.* J Immunol, 2011. **187**(11): p. 6069-81.

172. Green, D.R. and B. Levine, *To be or not to be? How selective autophagy and cell death govern cell fate.* Cell, 2014. **157**(1): p. 65-75.

173. Liu, Y. and B. Levine, *Autosis and autophagic cell death: the dark side of autophagy.* Cell Death Differ, 2015. **22**(3): p. 367-76.

174. Lee, A.H. and L.H. Glimcher, *Intersection of the unfolded protein response and hepatic lipid metabolism.* Cell Mol Life Sci, 2009. **66**(17): p. 2835-50.

175. Zhang, X.Q., C.F. Xu, C.H. Yu, W.X. Chen, and Y.M. Li, *Role of endoplasmic reticulum stress in the pathogenesis of nonalcoholic fatty liver disease.* World J Gastroenterol, 2014. **20**(7): p. 1768-76.

176. Fitzpatrick, E. and A. Dhawan, *Noninvasive biomarkers in non-alcoholic fatty liver disease: current status and a glimpse of the future.* World J Gastroenterol, 2014. **20**(31): p. 10851-63.

177. Wieckowska, A., N.N. Zein, L.M. Yerian, A.R. Lopez, A.J. McCullough, and A.E. Feldstein, *In vivo assessment of liver cell apoptosis as a novel biomarker of*

disease severity in nonalcoholic fatty liver disease. Hepatology, 2006. **44**(1): p. 27-33.

178. Lemoine, M., V. Ratziu, M. Kim, M. Maachi, D. Wendum, F. Paye, J.P. Bastard, R. Poupon, C. Housset, J. Capeau, and L. Serfaty, *Serum adipokine levels predictive of liver injury in non-alcoholic fatty liver disease.* Liver Int, 2009. **29**(9): p. 1431-8.

179. Kadayifci, A., R.B. Merriman, and N.M. Bass, *Medical treatment of non-alcoholic steatohepatitis.* Clin Liver Dis, 2007. **11**(1): p. 119-40, ix.

180. Schuppan, D. and Y.O. Kim, *Evolving therapies for liver fibrosis.* J Clin Invest, 2013. **123**(5): p. 1887-901.

181. Younossi, Z.M., *Review article: current management of non-alcoholic fatty liver disease and non-alcoholic steatohepatitis.* Aliment Pharmacol Ther, 2008. **28**(1): p. 2-12.

CURRICULUM VITAE

JEFFREY ALLEN WILLY

EDUCATION:

Bachelor of Science, Biology: Molecular Genetics, University of Rochester, 2006

Bachelor of Music, Applied Music: Percussion, Eastman School of Music, 2006

Master of Science, Biology, Purdue University, 2010

Ph.D. in Biochemistry & Molecular Biology with Bioinformatics minor**,** IU, 2016

WORK EXPERIENCE:

Mar. 2016-Present **Consultant Toxicologist, Eli Lilly & Company**, Indianapolis, IN

Implementation of gene editing technology to explore target mediated toxicity and identification of novel biomarkers to support the integration of drug discovery and risk assessment.

Mar. 2012-Mar. 2016 **Senior Toxicologist, Eli Lilly & Company,** Indianapolis, IN

Oversaw the development and implementation of innovative *in vitro* models to explore mechanisms of toxicity to support a variety of drug platform teams, and advised project teams on scientific models to ensure accurate data interpretation. Concurrently pursued a Ph.D. in Dr. Ron Wek's lab at Indiana University School of Medicine through the Lilly Graduate Research program.

Nov. 2007-Feb. 2012 **Toxicologist, Eli Lilly & Company,** Indianapolis, IN

Maintained and cultured mammalian cell lines for compound safety assessment and prioritization; developed and validated high content cell-based surrogate models, including the HepG2 and RPH phospholipidosis,

steatosis, and lysotracker assays as well as an *in vitro* Irritation Assay; and guided project teams through utilization of high content imaging data using the Acumen Explorer and Cellomics platforms.

Sept. 2006-Nov. 2007 **Biochemist, Advanced Testing Management Group at Eli Lilly & Company,** Indianapolis, IN

Maintained and cultured mammalian cell lines, developed and validated cell-based assays, and carried out an array of biochemical and molecular assays in Lead Optimization Biology to assess the efficacy of potential drugs.

HONORS AND AWARDS:

1999-2000	Three time Soloist with the Indianapolis Symphony Orchestra
2004	Selected to Perform with Eastman Wind Ensemble for Asia Tour
2005	Selected to perform with Eastman Wind Ensemble at Carnegie Hall
2006	Linda Muise Student Life Award
2006	Phi Mu Alpha Sinfonia Student Leadership Award
2006	Eastman School of Music Performer's Certificate
2006	Phi Mu Alpha Sinfonia Scholastic Award
2009	John L. Emmerson Award for Scientific Excellence at Eli Lilly
2014	FASEB Graduate Student Travel Grant
2014	Jack Davis Award for Best Seminar by a Graduate Student for the 2013-2014 Academic Year
2014	Co-winner for 1st place on Research Talk in the 2014 Biochemistry Research Day
2015	Student Gordon Research Conference Fellowship Grant

2015 Gordon Research Conference Best Poster

2015 AASLD Presidential Poster of Distinction (two posters)

2015 AASLD Basic Science Young Investigators Travel Award

2015 Eli Lilly Innovator Award

2016 Molecular and Systems Biology SOT Specialty Section Graduate Student Research Award

2016 Student Gordon Research Conference Fellowship Grant

2016 Midwest Regional Chapter SOT Young Investigator Award

ACADEMIC APPOINTMENTS:

Sept 2005 - May 2006 Teaching Assistant, University of Rochester

July 2012 - June 2016 Graduate Fellow, Indiana University, School of Medicine

PROFESSIONAL MEMBERSHIPS:

Society of Toxicology, 2015-present

American Association of Liver Disease, 2015-present

PEER-REVIEWED PUBLICATIONS:

Willy J.A., Schulte N.E., Kreklau E.L., Walgren J.L., Renninger M.L., and T.K. Baker. 2016. In Vitro L6 Irritation Assay Predicts Clinical Injection Site Reactions for Small Molecules. *Toxicol. Sci.* In Press.

Fusakio M.E., **Willy J.A.**, Yongping W., Mirek E.T., Al Baghdadi R.J., Adams C.M., Anthony T.G., and R.C. Wek. 2016. Transcription Factor ATF4 Directs Basal and Select Induced Gene Expression in the Unfolded Protein Response and Cholesterol Metabolism in Liver. *Mol. Biol. Cell.* In Press.

Young S.K., **Willy J.A.**, Wu C., Sachs M.S., and R.C. Wek. 2015. Ribosome Reinitiation Directs Gene-Specific Translation and Regulates the Integrated Stress Response. *J. Biol. Chem.* 290(47): 28257-28271. PMID: 26446796

Willy J.A., Young S.K., Stevens J.L., Masuoka H.C., and R.C. Wek. 2015. Chop Links Endoplasmic Reticulum Stress to NF-κB Activation in the Pathogenesis of Nonalcoholic Steatohepatitis. *Mol. Biol. Cell*. 26(12): 2190-204. PMID: 25904325.

Baird T.D., Palam L.R., Fusakio M.E., **Willy J.A.**, Davis C.M., McClintick J.N., Anthony T.G., and R.C. Wek. 2014. Selective mRNA translation during eIF2 phosphorylation induces expression of IBTKα. *Mol. Biol. Cell*. 25(10): 1684-97. PMID: 24648495.

SUBMITTED MANUSCRIPTS:

Willy J.A., Alakhras N.S., Hamlin D.M., Deqin S., Renninger M.L., Johnson R.L., and T.K. Baker. 2016. HMGB1 Regulates Hepatocyte Cell Death and Release of Acute Liver Injury Biomarkers.

Kwon J.J., **Willy J.A.**, Wek R.C., Korc M., Yin X.M., and J. Kota. 2016. Novel Role of miR-29 in Pancreatic Cancer Autophagy and its Therapeutic Potential.

Willy J.A., Young S.K., Mosley A.L., Gawrieh S., Stevens J.L., Masuoka H.C., and R.C. Wek. 2016. IBTKα Facilitates Phagophore Initiation and Protein Secretion during the Pathogenesis of Nonalcoholic Steatohepatitis.

BOOK CHAPTERS:

T.K. Baker, Engle S.K, Halstead B.W., Paisley B.M., Searfoss G.H.,and **J.A. Willy**. 2016. Discover Toxicology: An Early Safety Assessment Approach. Translating Molecules into Medicines: Cross-Functional Integration at the Drug Discovery-Development Interface. Chapter 2. Springer.

INVITED TALKS:

"Role of the UPR in the Pathogenesis of NASH." *University of Texas Southwestern.* May 19, 2016.

"Identification of Novel UPR Member IBTKα: Linking Autophagosome Formation and Secretion to the Pathogenesis of Non-Alcoholic Steatohepatitis." *Gordon Research Seminar on Autophagy*. March 20, 2016.

"How ER Stress Drives the Pathogensis of Liver Disease: Linking Cell Death to Autophagy and Inflammation." *Valparaiso University.* February 5, 2016.

"Chop Links ER Stress to NF-κB Activation in the Pathogensis of Nonalcoholic Steatohepatitis." *Genetics Department, Indiana University School of Medicine*. December 9, 2014.

"Chop Links ER Stress to NF-κB Activation in the Pathogensis of Nonalcoholic Steatohepatitis." *Fatty Liver Research Group, Indiana University School of Medicine*. November 17, 2014.

"Chop Links ER Stress to NF-κB Activation in the Pathogensis of Nonalcoholic Steatohepatitis." *Biochemistry Research Day, Indiana University School of Medicine*. November 4, 2014.

ABSTRACTS AND POSTERS:

Willy J.A., Young S.K., Stevens J.L., Masuoka H.C., and R.C. Wek. 2016. *Identification of Novel UPR Member IBTKα: Linking Autophagy to the Pathogenesis of Non-Alcoholic Steatohepatitis*. Gordon Research Conference. Ventura Beach, CA.

Kwon J.J., **Willy J.A.**, Wek R.C., Korc M., Yin X.M., and J. Kota. 2016. *Novel Role of miR-29 in Pancreatic Cancer Autophagy and its Therapeutic Potential.* Gordon Research Conference. Ventura Beach, CA.

Willy J.A., Young S.K., Stevens J.L., Masuoka H.C., and R.C. Wek. 2016. *Identification of Novel UPR Member IBTKα: Linking Autophagy to the Pathogenesis of Non-Alcoholic Steatohepatitis*. Society of Toxicology International Convention. New Orleans, LA.

Searfoss G.H., **Willy J.A.,** and T.K. Baker. 2016. *Understanding the Role of the Integrated Stress Response in iPSC derived Human Cardiac Myocytes: From Progenitor Cell to Differentiated Cardiac Myocyte*. Society of Toxicology International Convention. New Orleans, LA.

Willy J.A., Stevens J.L., Masuoka H.C., and R.C. Wek. 2015. *CHOP and the Unfolded Protein Response Regulate NF-κB Activity through IRAK2 in the Pathogensis of Non-Alcoholic Steatohepatitis.* AASLD: The Liver Meeting. San Fransisco, CA.

Willy J.A., Masuoka H.C., and R.C. Wek. 2015. *UPR Regulation of Autophagy in the Pathogensis of Non-Alcoholic Steatohepatitis.* AASLD: The Liver Meeting. San Fransisco, CA.

Willy J.A., Stevens J.L., Masuoka H.C., and R.C. Wek. 2015. *CHOP Regulates Autophagy and Inflammation through Activation of NF-κB in the Pathogenesis of Non-Alcoholic Steatohepatitis.* Gordon Conference for Cellular Mechanisms of Toxicity. Andover, NH.

Baird, T.D., Palam L.R., **Willy, J.A**., and Wek, R.C. 2014. *PERK phosphorylation of eIF2a induces a gradient of mRNA translational efficiencies*. Cold Spring Harbor Meeting for Translational Control. Cold Spring Harbor, NY.

Willy, J.A., Baird, T.D., Masuoka, H., Stevens, J.L. and Wek, R.C. 2014. *UPR Regulation of Autophagy in the Pathogensis of Non-Alcoholic Steatohepatitis*. FASEB for Nutrient Sensing and Metabolic Signaling. Big Sky, MT.

Baird, T.D., Palam L.R., **Willy, J.A**., and Wek, R.C. 2014. *Nutrient Stress Signals and Translational Control*. FASEB for Nutrient Sensing and Metabolic Signaling. Big Sky, MT.

Willy J.A., Stevens J.L., Baker T.K. 2012. *Predicting Preclinical Outcomes by Measurement of Lysosomal Dysfunction*. Society of Toxicology International Convention. The Toxicologist 126:441. San Francisco, CA.

Willy J.A., Schulte N., Kreklau E., Walgren J., Stauber A., Stevens J.L., Baker T.K. 2011. *In Vitro Prediction of Injection Site Reactions Using L6 Rat Skeletal Muscle Cells*. Society of Toxicology International Convention. The Toxicologist 120:407. Washington, D.C.

Aburub A., Baker T., Bhattachar S., Frank S., Havel H., Stickelmeyer M., Heinz-Taheny K., Kreklau E., Snehlata M., Schulte N., **Willy J.**, Sanchez-Felix M. 2009. *Development of IV Liposome Formulation to Address Venous Irritation*. Lilly Expo.